



HAL
open science

From gene identification and functional characterization to genome editing approaches for inherited retinal disorders

Elise Orhan Le Gac de Lansalut

► **To cite this version:**

Elise Orhan Le Gac de Lansalut. From gene identification and functional characterization to genome editing approaches for inherited retinal disorders. Genetics. Université Pierre et Marie Curie - Paris VI, 2015. English. NNT : 2015PA066218 . tel-01261327

HAL Id: tel-01261327

<https://theses.hal.science/tel-01261327>

Submitted on 26 Jan 2016

HAL is a multi-disciplinary open access archive for the deposit and dissemination of scientific research documents, whether they are published or not. The documents may come from teaching and research institutions in France or abroad, or from public or private research centers.

L'archive ouverte pluridisciplinaire **HAL**, est destinée au dépôt et à la diffusion de documents scientifiques de niveau recherche, publiés ou non, émanant des établissements d'enseignement et de recherche français ou étrangers, des laboratoires publics ou privés.

Université Pierre et Marie Curie

Ecole doctorale Physiologie, Physiopathologie et Thérapeutique (ED394)

Institut de la Vision, Département de génétique, Equipe S6 Audo-Zeitz

**From gene identification and functional
characterization to genome editing approaches
for inherited retinal disorders**

Par Elise Orhan Le Gac de Lansalut

Thèse de doctorat en génétique

Dirigée par Isabelle Audo et Christina Zeitz

Présentée et soutenue publiquement le 16 septembre 2015

Devant un jury composé de :

Pr José-Alain Sahel, Professeur, Président du jury

Dr Valeria Marigo, Professeur Attaché, Rapporteur

Pr Stephan Neuhauss, Professeur, Rapporteur

Dr Patrick Benoit, Directeur de Projet International, Examineur

Dr Alain Carrié, MCU-PH, Examineur

Dr Christina Zeitz, CR1, Co-directrice de thèse

Dr Isabelle Audo, MCU-PH, Directrice de thèse

A ma famille

Acknowledgments - Remerciements

Since I had the great opportunity to go on a PhD in an outstanding international environment, I would like to address all my best acknowledgements in different languages. Not that I am that polyglot, but just to notify how I loved working on these conditions.

First of all, I would like to warmly thank all the jury members to make me the honour and pleasure to review and evaluate the work of these last past years. I am really happy to have the opportunity to present my work in its - almost - integrity. The fruitful and kind discussions I had with absolutely all of you when I met you helped me a lot and I am really grateful that you accepted to judge my work.

Je voudrais vous adresser mes plus chaleureux remerciements Pr Sahel pour votre accueil à l'Institut de la Vision et votre soutien durant toutes ces années. Les conditions de travail qui nous sont offertes à l'Institut sont exceptionnelles et vos précieux conseils m'ont énormément aidé lors de ma thèse. Je vous remercie donc pour ce cadre motivant et rassurant, mais également de me faire l'honneur de présider mon jury de thèse.

J'aimerais également te remercier Isabelle d'avoir été ma directrice de thèse, faisant de moi ta première doctorante en Sciences! Ton intelligence, ta perspicacité, ton dévouement envers les patients m'ont beaucoup inspirée depuis mon arrivée à l'Institut, et ce n'est probablement pas une coïncidence si je me suis décidée à faire une thèse dans l'équipe A-Z. Merci également de m'avoir accordée une grande autonomie pratiquement dès mon arrivée, de m'avoir toujours permis de me former auprès des spécialistes, de m'avoir permis de communiquer à de nombreuses reprises mes résultats, et de m'avoir laissée gérer dans leur globalité mes multiples projets. Tu m'as permis de me former, personnellement, à devenir « project manager » et c'est probablement l'un des plus beaux cadeaux que tu m'as fait pour ma carrière.

Ich würde gerne auch dir danken Christina, da du meine andere Doktorarbeits Direktorin warst. Merci d'avoir été ma co-directrice et de m'avoir permis de travailler sur ton « hobby », le CSNB, qui est du coup devenu le mien aussi. Merci pour toutes les opportunités de formation, communication, apprentissage de nouvelles techniques que tu m'as donné. Merci également de m'avoir appris à écrire. Tes relectures, critiques constructives sur la façon de formuler les choses lors de la rédaction des articles, grants, abstracts et autres rapports m'ont appris à formuler les choses et me seront tout particulièrement précieux pour mon avenir.

Je voudrais également remercier les membres de mon équipe, en commençant tout naturellement par mes deux super copines Kinga et Marie-Elise ! Merci les filles de m'avoir réservé un tel accueil au labo ! Votre amitié, nos fous-rires, vos conseils, votre bienveillance m'ont été hyper précieux et m'ont immédiatement rendu le labo hyper agréable ! Je suis très heureuse qu'ont ait gardé cela après vos départs, et je voudrais vous remercier pour tout ce que vous m'avez toutes deux apportée, autant au niveau professionnel que personnel. Dziękuję & merci bras !

Un grand merci également à toi Aline pour ton amitié, pour nos sorties Zenzoo-ciné, pour toutes nos conversations qui m'ont permis de m'évader et pour toutes celles qui m'ont rassurée et m'ont permis de m'épanouir. Ton amitié m'est précieuse et j'espère réellement qu'on gardera le contact après ma thèse.

Merci également à tous les autres membres de mon équipe : obrigado Miguel et merci Thomas for your friendships and your helps in mouse phenotyping, xièxie Bingqian, merci à Christelle a été ma partenaire dans les longues manipes de *vivo*, mais aussi à tout les autres membres de l'équipe : Elise, Fiona, Christel, Marion, Cécile mais aussi Aurore, Vanessa, Said.

Je voudrais également te remercier Deniz, pour ton amitié et ta bienveillance. Üstün başarıların, iyi niyetli candan yaklaşımın ve daima pozitif tavrınla sana özenmemek mümkün değil, dostluğun ve desteğin benim için çok değerli. Tekrar teşekkür ederim, iyiki varsın.

Un grand merci également à toi Olivier pour ta bienveillance, ton aide scientifique et technique, et tous tes conseils qui m'ont été particulièrement précieux tout le long de ma thèse. J'ai beaucoup appris à ton contact et je te remercie de m'avoir réservé tout ce temps.

Merci également Kim pour tout tes conseils et ta bienveillance, de m'avoir guidée à de nombreuses reprises, probablement sans même réellement t'en rendre compte.

I would like also to thank you people of the best office ever, for your kindness, support, friendship, and for all the drinks & partys of course! Grazie Stefania & Cataldo! Gracias Marcela & Oriol! Merci Najate, thanks Abhishek! Thanks also to all the 4th floor friends from development department which made the long days easier, and the evenings happier and funnier! Thanks for your friendship & all your invitations to partys & drinks (I am sure you recognized yourself easily on these 2 last words).

Merci également à toutes les personnes qui m'ont aidé à toutes les différentes étapes de ma thèse pour leur bienveillance et gentillesse. Travailler avec vous ou encore juste vous voir au quotidien a été un véritable plaisir. Je pense tout particulièrement à Manu, Julie, Léa, Quenol, André, Stéphane, Valérie, Serge, Thierry, Géraldine, Caroline, Yvrick, Méliissa et Romain.

Enfin, je finis bien évidemment par ceux qui me sont les plus chers : un grand merci à ma famille et mes amis pour avoir été toujours là, et pour m'avoir toujours encouragée. Merci Özlem, Murat, Nâme, Julie, Matthias, Ridwan, Mathilde, Damien, Sabrina, Thomas, Guillaume, Clara, et tout ceux que j'oublie..

Un grand merci à toute ma famille Le Gac de Lansalut pour vos encouragements, et tout spécialement à Yann et mamie qui m'ont poussé à tenter l'aventure.

Un très grand merci à toute la plus formidable et aimante des familles : ma famille Orhan, pour avoir toujours cru en moi, m'avoir encouragée, soutenue, supportée, divertie, et surtout pour votre amour et soutien inconditionnels.

Canım annecim, canım babacım, bütün başarılarımız sizin desteğiniz, fedakarlıklarınız ve sevginiz sayesinde, size ne kadar teşekkür etsem azdır. Canım kardeşlerim Raziye, Selma ve Yasemin, size de aynı şekilde daima yanımda yer aldığınız, sürekli desteklediğiniz, ve tabii ki güzel kalpleriniz ve sevginiz için sonsuz teşekkür ederim. Enişterim İlkan ve Gürhan size de teşekkür ederim. Ve canım bebişlerimiz Kaan ve Can hayatımıza kattığınız renk, getirdiğiniz sevgi, neşe ve gülcükler için size de ayrıca teşekkür ederim.

Enfin, je tiens à remercier celui qui a enduré tout cela, s'est enthousiasmé avec moi, m'a soutenue, conseillée et chouchoutée lorsque c'était nécessaire : mon mari Emmanuel (Manu pour les amis). Merci mon chéri de m'avoir encouragée à faire cette thèse et soutenue dans les moments délicats. Te voir si fier, si impliqué, capable de parler de mon sujet de thèse (et de mes résultats !), et te voir réaliser une véritable veille scientifique autour de mon projet m'ont tout particulièrement portée, merci pour ton implication et ton soutien de tout les jours.

Table of contents

List of figures and tables	4
List of abbreviations	6
Introduction	10
A. Preamble	11
B. Retinal anatomy and physiology	12
1. General considerations about retina and visual process	12
2. Photoreceptors	14
3. Bipolar cells	16
a) Cone pedicle and cone bipolar cells	16
b) Rod spherule	17
4. Diagnostic tools for retinal diseases	18
a) Full-field electroretinogram	18
b) Spectral Domain-Optical Coherence Tomography	19
C. Congenital Stationary Night Blindness	21
1. Clinical manifestations	21
a) Clinical signs	21
b) Different forms of CSNB and their diagnostic	21
2. Genetic & synapse between rod photoreceptor and ON-bipolar cell	23
a) Genes associated with CSNB	23
b) Signaling cascade between rod photoreceptor and ON-bipolar cell	24
3. Animals models for cCSNB	26
D. Rod-Cone Dystrophy or Retinitis Pigmentosa	28
1. Clinical manifestations	28
a) RCD course and associated clinical signs	28
b) Diagnostics	29
c) Genes associated with the disease	31
2. Rhodopsin	32
a) Function	32
b) Rhodopsin mutations	34
c) Dominant negative effect of P23H exchange	35
d) Animal models with <i>RHO</i> mutations	35
(1) Animal models with <i>RHO</i> mutations	36
(2) Animal models to study <i>RHO</i> quantity effect	36
3. Current therapeutic approaches for RCD	36
a) By preventing photoreceptor degeneration	37
(1) Through genetic targeted approaches	37
(a) Viral vectors for retinal gene therapy	37
(b) Gene augmentation	40
(c) Gene silencing	41
(d) By genome editing for dominant mutations	43
(i) Genome editing strategy	43
(ii) Endonucleases	45
(2) By preventing cell death through genetic-independent approaches	49
b) By restoring vision after photoreceptor cell death	51
(1) By optogenetic	51
(2) With retinal implants	52
(3) By stem cell therapy	52

E.	Objectives of the study	54
1.	<i>GPR179</i> identification and functional characterization	54
2.	Genome editing approaches applied to Rhodopsin mutations	54
	Material and methods	56
A.	Preamble	57
B.	<i>GPR179</i> KO first model characterization	58
1.	Animal Care	58
2.	Genotyping	59
a)	Polymerase chain reaction (PCR) genotyping for <i>Gpr179</i>	59
b)	Genotyping for common mutations found in laboratory mouse strains	60
c)	Genotyping for genes with mutations underlying cCSNB	61
3.	ERG	61
4.	SD-OCT	61
5.	Immunohistochemistry	62
a)	Preparation of retinal sections for immunohistochemistry	62
b)	Immunostaining of retinal cryosections	62
c)	Image acquisition	63
6.	Statistical analyses	64
C.	Endonucleases based therapy of Rhodopsin	65
1.	Meganucleases	65
a)	Meganucleases testing in HEK293 cells	65
(1)	Meganucleases design and production	65
(2)	HEK 293 cells transfection with plasmids expressing meganucleases	65
(3)	gDNA extraction, PCR and deep sequencing	66
(4)	Western-blot	67
b)	Meganucleases testing on newborn rat retinal explants	67
(1)	Meganuclease cloning into pCIG vector	67
(2)	Retinal explants electroporation and culture	68
(3)	Cell dissociation and FACS	69
(4)	DNA extraction and Surveyor mutation detection kit assay	69
2.	TALEN	70
a)	TALENs	70
b)	Animals	71
c)	TALENs testing on P23H newborn rat retinal explants	72
d)	TALENs encapsidation	73
e)	TALENs testing on P23H P21 rat retinal explants	73
(1)	TALEN testing by P21 rat retinal explants infection	73
(2)	Immunohistochemistry	74
f)	TALENs testing <i>in vivo</i>	74
(1)	by subretinal injections	75
(a)	P21 subretinal injections	75
(b)	Fluorescence observation	75
(c)	Phenotype monitoring	76
(2)	by systemic injections	76
(a)	P1-old rat systemic injections	76
(b)	Fluorescence observation	76
(c)	Phenotype monitoring	76
g)	TALENs testing <i>in vitro</i> on P23H rat embryonic fibroblats	77
(1)	P23H rat embryonic fibroblasts isolation	77
(2)	Fluorescent marker cloning into TALEN's subunits expressing plasmids ..	77

(3) TALEN nucleofection into P23H REF	78
Results	80
A. GPR179 identification and functional characterization	81
1. Whole exome sequencing identifies mutations in <i>GPR179</i> leading to autosomal recessive complete stationary night blindness	82
2. Further insights into GPR179: expression, localization, and associated pathogenic mechanisms leading to complete congenital stationary night blindness.....	93
3. Complementary ongoing results: <i>GPR179</i> KO first model characterization.....	104
a) Creation and genotyping of the <i>Gpr179</i> KO first mouse model	104
b) Functional characterization by ERG recordings	105
c) Structural characterization by SD-OCT	107
d) Localization of the proteins of the cascade	107
B. Genome editing approaches applied to Rhodopsin mutations	111
1. Genotypic and phenotypic characterization of P23H line 1 rat model	112
2. Complementary ongoing results: Genome editing approach for Rhodopsin mutants	134
a) Meganucleases	134
(1) <i>In vitro</i> on HEK293 cells	134
(2) <i>Ex vivo</i> on rat retinal explant.....	136
b) TALENs	137
(1) <i>Ex vivo</i> on P23H rat retinal explants	137
(2) <i>Ex vivo</i> and <i>in vivo</i> infection with TALENs expressing AAV.....	138
(a) <i>Ex vivo</i> on 21-days-old P23H rat retinal explants	139
(b) <i>In vivo</i> delivery on P23H rats	140
(i) Subretinal injections at P21	140
(ii) Systemic injections at P1	141
(3) <i>In vitro</i> on P23H rat embryonic fibroblasts.....	143
C. Other projects	144
Discussion and perspectives.....	146
A. Motivation	147
B. Accuracy and limitations of our animal models and new insights into retinal physiology	148
1. <i>Gpr179</i> ^{-/-} mouse model.....	148
2. P23H-1 rat model	150
C. Accuracy and limitations of our genome-editing models	152
1. HEK 293 cells	152
2. REFs.....	152
3. Newborn rat retinal explants	153
4. P21 rat retinal explants.....	153
5. P23H-1 rat model	154
a) Subretinal injections at P21	154
b) Systemic injections at P1.....	154
D. The future of genome editing strategies to prevent dominant negative mutations induced diseases	157
Bibliography.....	160

List of figures and tables

Figure 1: Schematic representation of the human eye with an enlargement of the retina	12
Figure 2: Schematic representation of retinal layers	13
Figure 3: Rod and cone schematic structure	14
Figure 4 : Cones and rod densities in the human retina	15
Figure 5 : Organization of the bipolar cells in a mammalian retina.....	16
Figure 6 : Schematic representation of a cone pedicle.....	17
Figure 7: Organization of a rod spherule	18
Figure 8: Schematic representation of ERG recorded under scotopic conditions.....	19
Figure 9: SD-OCT retinal morphology and retinal thickness layers.....	20
Figure 10: Night vision of unaffected person and CSNB patient	21
Figure 11: ERG responses from an unaffected person and from a patient with Riggs-type of CSNB.	22
Figure 12: ERG response from an unaffected person and from patients with complete and incomplete CSNB.....	23
Figure 13: Genes underlying CSNB.....	24
Figure 14: Schematic drawing of proteins involved in signal transmission from rod photoreceptor to ON-bipolar cell.	25
Figure 15: Vision of an unaffected person and tunnel vision of a Rod-Cone Dystrophy patient.	28
Figure 16: Fundi of a healthy individual and a patient with rod-cone dystrophy.	29
Figure 17: Fundus autofluoresce imaging of an unaffected person and a patient with rod-cone dystrophy.....	30
Figure 18: Spectral-Domain Optical Coherence Tomography of an unaffected person and a Rod-Cone Dystrophy patient.....	30
Figure 19: Full-field ERG responses from a healthy individual and from a patient with an early autosomal dominant retinitis pigmentosa.....	31
Figure 20: Genes and their relative contribution to autosomal dominant Rod-Cone Dystrophy	32
Figure 21: Phototransduction cascade.....	33
Figure 22: RHO mutants.	34
Figure 23: Production of recombinant AAV from wild-type AAV	39
Figure 24: Endonuclease-induced gene targeting approaches.	44
Figure 25: I-CreI Meganuclease in complex with a synthetic DNA.....	45
Figure 26: Schematic representation of a TAL	46
Figure 27: Schematic representation of a TALEN.....	47
Figure 28: Naturally occurring and engineered CRISPR-Cas systems.....	49
Figure 29: Construction of the cassette inserted for mutant allele creation.	58
Figure 30: Genotyping of <i>Gpr179</i> ^{+/+} , <i>Gpr179</i> ^{+/-} and <i>Gpr179</i> ^{-/-} mice.....	60
Figure 31: Schematic representation of plasmids coding for TALEN left and right subunits..	71
Figure 32: Delivery modes and used serotype for TALEN <i>in vivo</i> testing.....	75
Figure 33: Schematic representation of the plasmids constructed for TALENs testing in P23H REF.....	78
Figure 34: Scotopic ERG responses.....	105
Figure 35: Photopic ERG responses.....	106
Figure 36: SD-OCT retinal morphology of 3-month-old <i>Gpr179</i> ^{+/+} , <i>Gpr179</i> ^{+/-} and <i>Gpr179</i> ^{-/-} mice.	107
Figure 37: Validation of <i>Gpr179</i> knock-out model..	108

Figure 38: Localization of GRM6, TRPM1 and LRIT3 at the dendritic tips of ON-bipolar cells is independent of <i>Gpr179</i> expression	109
Figure 39: Localization of RGS11, RGS7 and GNB5 at the dendritic tips of ON-bipolar cells is dependent of <i>Gpr179</i> expression	110
Figure 40: Meganucleases targets on human genomic <i>RHO</i>	134
Figure 41: Western-blot evaluating the expression of meganucleases on transfected HEK 293 cells.....	135
Figure 42: Evaluation of NHEJ with Surveyor mutation detection kit induced by meganuclease on newborn rat retina.....	136
Figure 43: Evaluation of NHEJ with Surveyor mutation detection kit induced by TALEN on newborn rat retina.....	138
Figure 44: Evaluation of NHEJ with Surveyor mutation detection kit induced by TALEN on P21 P23H rat retina.	139
Figure 45: Visualization of GFP expression on infected P21 P23H rat retinal explants..	140
Figure 46: Color and micron 3 fundus imaging of GFP fluorescence for AAV8-Y733F infected animal 14 days after subretinal injection.....	140
Figure 47: Scotopic ERG responses.....	141
Figure 48: Color and micron 3 fundus imaging of GFP fluorescence for AAV9-2YF injected animal 14 days after systemic injection.	142
Figure 49: Scotopic ERG phenotype.....	142
Figure 50: Evaluation of NHEJ with Surveyor mutation detection kit induced by TALEN on P23H REF.	143
Figure 51: Schematic drawing of major molecules important for the first visual synapse between photoreceptors and ON-bipolar cells	150
Table 1: Primary antibodies used in immunohistochemistry	63
Table 2: Meganucleases and their target	65
Table 3 : Primers for deep sequencing.....	66
Table 4 : Plasmids used for each electroporation conditions	68
Table 5 : PCR primers for the loci targeted by the meganucleases.....	69
Table 6: TALENs and their recognition site.....	71
Table 7: Plasmids used for each electroporation conditions	72
Table 8: Primers for TALEN testing.....	72
Table 9: Infection of P23H P21 retinal explants	74
Table 10: Subretinal injections of P23H P21 rats right eyes.....	75
Table 11: Systemic injections of P23H P1 rats	76
Table 12: Nucleofection conditions of P23H REF.....	79
Table 13: Percentage of mutation induced by various meganucleases evaluated by deep sequencing.....	135

List of abbreviations

AAV: adeno-associated virus

adRCD: autosomal dominant rod-cone dystrophy

AmpR: ampicillin resistance gene

bp: base pairs

BGHpA: bovine growth hormone polyadenylation

CAPNS1 : calpain small subunit 1

Cas9: clustered regularly interspaced short palindromic repeats Associated Protein 9

cCSNB: complete congenital stationary night blindness

cGMP: cyclic guanosine monophosphate

CNTF: ciliary neurotrophic factor

CRD: cone-rod dystrophy

crRNA: clustered regularly interspaced short palindromic repeats ribonucleic acid

CRISPR: clustered regularly interspaced short palindromic repeats

CSNB: congenital stationary night blindness

C-term: carboxy-terminus

DNA: deoxyribonucleic acid

DSB: double-stranded break

ER: endoplasmic reticulum

ERG: electroretinogram

ESC: embryonic stem cell

FACS: fluorescence-activated cell sorting

FRT: flippase recognition target

GCL: ganglion cell layer

gDNA: genomic deoxyribonucleic acid

GDP: guanosine diphosphate

GNB5: guanine nucleotide-binding protein subunit beta-5

GFP: green fluorescent protein

GPCR: G protein-coupled receptor

gRNA: guide ribonucleic acid
GTP: guanosine triphosphate
HA-tag: human influenza hemagglutinin tag
HEK 293: Human Embryonic Kidney 293
HR: homologous recombination
icCSNB: incomplete congenital stationary night blindness
iGluR: ionotropic glutamate receptor
IMS: Institute for Microelectronics Stuttgart
indels: insertion or deletion mutations
INL: inner nuclear layer
IPL: inner plexiform layer
IRES: internal ribosome entry site
ITR: inverted terminal repeat
LacZ: lactose operon
LCA: Leber Congenital Amaurosis
LoxP: cre recombinase recognition site
LRIT3: leucine-rich-repeat immunoglobulin-like and transmembrane-domain 3
mGluR: metabotropic glutamate receptor
MN: meganuclease
NFL: nerve fiber layer
NLS: nuclear localization signal
NHEJ: non homologous end joining
N-term: amino-terminus
NYX: nyctalopin
ONL: outer nuclear layer
OPL: outer plexiform layer
P23H-1: P23H line 1
P23H REF: rat embryonic fibroblast from P23H rat
pA: polyadenylation site

PAM: protospacer-adjacent motif
pCMV: cytomegalovirus promoter
PCR: polymerase chain reaction
pEF1a1: human elongation factor-1 alpha 1 promoter
PKC α : protein kinase C alpha
pRHO: rhodopsin promoter
PTM: pre messenger ribonucleic acid *trans*-splicing molecule
pUC ori: pUC plasmide's origine of replication
rAAV: recombinant adeno-associated virus
RAG: recombination activating gene
RCD: rod-cone dystrophy
RdCVF: rod-derived cone viability factor
REF: rat embryonic fibroblast
RGS: regulator of G protein signaling
RGS7: regulator of G protein signaling 7
RGS7BP: regulator of G-protein signaling 7 binding protein
RGS9: regulator of G protein signaling 9
RGS9BP: regulator of G protein signaling 9 binding protein
RGS11: regulator of G protein signaling 11
RHO: rhodopsin
RIPA: radioimmunoprecipitation assay
RPE: retinal pigment epithelium
RNA: ribonucleic acid
RNAi: ribonucleic acid interference
RVD: repeat variable diresidue
SA: signal anchor
SD-OCT: spectral-domain-optical coherence tomography
siRNA: short interfering ribonucleic acid
SMaRT: spliceosome-mediated ribonucleic acid *trans*-splicing

S tag: pancreatic ribonuclease A tag

TALE: Transcription Activator-Like Effector

TALEN: Transcription Activator-Like Effector Nuclease

TBS: tris buffer saline

TN: Transcription Activator-Like Effector Nuclease

tracrRNA: transactivating clustered regularly interspaced short palindromic repeats
ribonucleic acid

UPR: unfolded protein response

UPS: ubiquitin-proteasome system

v: volume

vg: viral genome

w: weight

ZF: zinc finger

ZF-ATF: zinc finger artificial transcription factors

Introduction

A. Preamble

The first steps in vision occur in the retina when rod and cone photoreceptors transform light into a biochemical signal, which gets processed by bipolar cells, ganglion cells and finally by the brain. Our group investigates genetic causes and mechanisms involved in inherited stationary and progressive retinal diseases as congenital stationary night blindness (CSNB), and rod-cone dystrophy (RCD), also called retinitis pigmentosa.

Before I became a PhD student, I worked in this group for 2 years as an assistant engineer. My thesis project is an ongoing study focusing on two axes on which I already obtained results during my assistant engineer period. The first part of my thesis project concentrated on the identification and functional characterization of a gene defect underlying CSNB. The second part concentrated on genome editing approaches for Rhodopsin mutations underlying RCD. In the time lapse of three years of PhD, by studying two retinal disorders, I had the opportunity to work on the discovery and functional characterization of one gene, but also on a therapeutic approach for another gene.

To place my PhD project in the context, I will introduce general knowledge about the retina and the visual process and develop more precisely aspects of photoreceptors and bipolar cells as they are implicated in RCD and CSNB, respectively. In a second part, I will describe clinical signs, diagnostic and genetics of CSNB. Subsequently, I will illustrate the knowledge we had of the bipolar cell signaling cascade and animal models developed for complete CSNB at the time we started the study. For the RCD part, the genetics of the disease, implications of Rhodopsin (*RHO*) and its mutations, animal models for *RHO* and therapeutic approaches and considerations about gene therapy will be more developed since we decided to perform genome editing on Rhodopsin.

B. Retinal anatomy and physiology

1. General considerations about retina and visual process

The vertebrate retina is a light-sensitive layer of tissue at the posterior inner surface of the eye. The optics of the eye creates an image on the retina, which leads to the initiation of a cascade of chemical and electrical events that generate nerve impulses transmitted to the brain. The retina is derived from the central nervous system and is composed of a monolayer of epithelial cells, the retinal pigment epithelium (RPE) and the neural retina, a tissue with several layers of neurons interconnected by synapses (Figure 1).

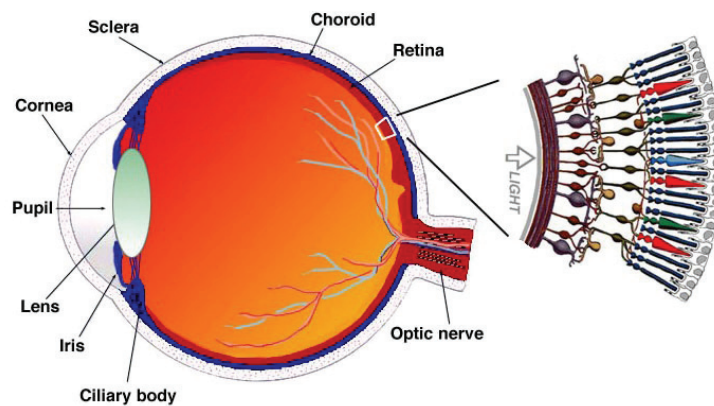


Figure 1: Schematic representation of the human eye with an enlargement of the retina (modified from Webvision)

The visual process in the neural retina can be divided into two essential parts. First, the light signal is captured by rod and cone photoreceptors, which transform light into a chemical signal. Then this chemical signal is transmitted to bipolar cells and ganglion cells, which axons form the optic nerve, driving the information in the visual cortex in the brain. Amacrine and horizontal cells participate to the visual processing by modulating the signal, allowing its better propagation and improving contrast and definition of the visual stimuli. Glial cells, composed of Müller cells, astrocytes and microglial cells, contribute to maintaining the structure and the function of this tissue. Retinal pigment epithelium cells are essential for the survival of the neural retina, in particular since they are implicated in 11-*cis*-retinal recycling through the vitamin A cycle, and in phagocytosis of the damaged photoreceptor outer segments, participate to the blood retinal barrier and ionic and liquid balance in the retina,

provide photoreceptors with nutrients and oxygen, and to some extent absorption of scattered light (Figure 2).

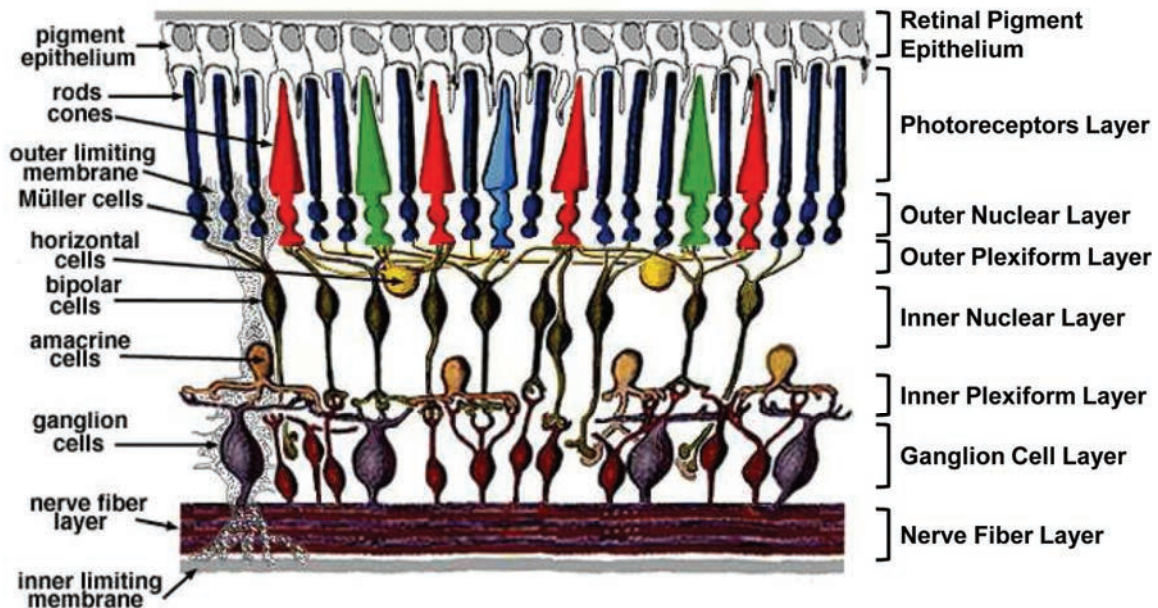


Figure 2: Schematic representation of retinal layers (modified from Webvision)

All these cells are organized in 10 layers (Figure 2), from the inner (vitreous side) towards the outer retina (choroid side):

- The inner limiting membrane, a basal membrane formed by proteins from the extracellular matrix, astrocytes and Müller cell end feet.
- The nerve fiber layer (NFL), constituted of the axons of ganglion cells, which gather to form the optic nerve.
- The ganglion cell layer (GCL), containing ganglion cell bodies.
- The inner plexiform layer (IPL), formed by the synapses between bipolar, amacrine and ganglion cells.
- The inner nuclear layer (INL), containing bipolar, amacrine, horizontal and Müller cell bodies.
- The outer plexiform layer (OPL), formed by the synapses between photoreceptors, bipolar and horizontal cells.
- The outer nuclear layer (ONL), formed by the nuclei of photoreceptors.
- The outer limiting membrane, which is a region of adherence (“zonula adherens”) between photoreceptor inner segments and Müller glial cells.

- The photoreceptor layer, which is actually constituted of inner and outer segments of photoreceptor.
- The RPE composed of cells of the same name.

2. Photoreceptors

Photoreceptors are located in the deeper part of the neural retina and are responsible for the translation of light energy into an electrical signal. Two types of photoreceptors are present in the retina: rods and cones, their name being related to the shape of their outer segment, the part where the phototransduction takes place. Both photoreceptor classes, rods and cones, consist of an outer segment with stacks of discs for rod photoreceptors and invagination of the plasma membrane for cone photoreceptors, a connecting cilium, an inner segment, a cell body with the nucleus and a synaptic terminal connected to bipolar and horizontal cells (Figure 3) (1). The outer segment contain the proteins of the phototransduction cascade, of which opsins are the main and light-sensitive proteins involved in the first step of this phototransduction cascade. The connecting cilium constitutes the bridge between outer and inner segments and is comparable by morphology and composition to primary cilia (2). The inner segment is the place of biosynthesis and endocytosis, and is also rich of mitochondria.

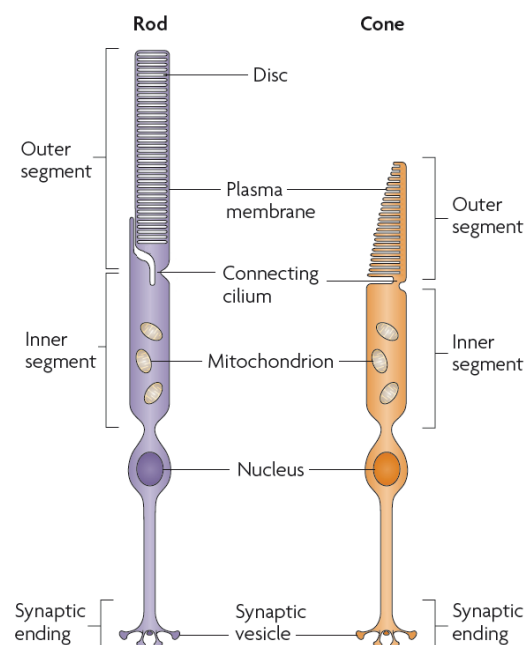


Figure 3: Rod and cone schematic structure (adapted from Wright, A et al., (1))

The entire retina contains about 7 millions cones and 120 millions rods in human (3). Cones and rods are both distributed on the surface of the retina, except in the optic disc and, for humans and other higher primates, in the fovea, which is composed exclusively with cones and represents the regions where the visual acuity is maximal. The optic disc, corresponding to “the blind spot” on visual field since it lacks photoreceptors, is the nasal zone where the optic-nerve fibers leave the eye (Figure 4) (3).

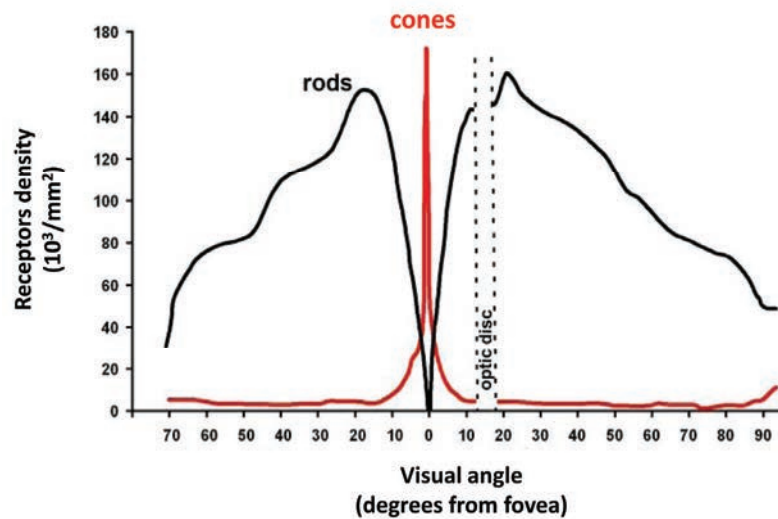


Figure 4: Cones and rod densities in the human retina (adapted from Østerberg, G A et al.,(4))

Rods are responsible for vision under dim light conditions, i.e. scotopic and mesopic, and produce a monochromatic perception. They express Rhodopsin, a photopigment with 507 nm light peak absorption. Human retina comprises 94% rod photoreceptors and 6% cone photoreceptors (3), and mouse retina comprises 97% rod photoreceptors and 3% cone photoreceptors (5). Cones are responsible for vision under bright light conditions, i.e. photopic. Their special arrangement in the fovea allows high spatio-temporal resolution and color vision, which is due to the expression of different opsins dividing cones into 3 categories in normal human retina (6). This classification is defined by the opsin the cones express: short-wavelength sensitive or S-cone (expressing the S-opsin, which absorption peak is at 426 nm), medium-wavelength sensitive or M-cone (expressing the M-opsin, peaking at 530 nm) and long-wavelength sensitive or L-cone (expressing the L-opsin, peaking at 555 nm). Color vision, allowed by these three kinds of opsins, is perceived in the brain after combinatorial analysis of the signal generated by the cone subtypes and processed throughout the retina.

3. Bipolar cells

Bipolar cells transmit signals from the photoreceptors to the ganglion cells. Bipolar cells are so-called since they have a central body from which arise two sets of processes. They can synapse with either rods or cones; they are then defined as rod bipolar cells or cone bipolar cells respectively. In addition, photoreceptors can also signal with horizontal cells. Bipolar cells are classified based on morphology, biochemistry, neurochemistry and functional criteria. Based on morphology, there are nine to thirteen distinct cone bipolar cells in mammals depending on species and only one type of rod bipolar cell. Based on functional criteria, bipolar cells are classified into ON-bipolar cells and OFF-bipolar cells. ON-bipolar cells express the metabotropic glutamate receptor GRM6 (also called mGluR6) (7-9), are depolarized at the onset of light from the signal transmitted by photoreceptor cells and have processes that end in the inner half of the IPL. Rod bipolar cells are exclusively ON-bipolar cells. OFF-bipolar cells express ionotropic glutamate receptors iGluR (10-14), are hyperpolarized at the offset of light from the signal transmitted by cones and have processes that end in the outer half of the IPL (15, 16) (Figure 5).

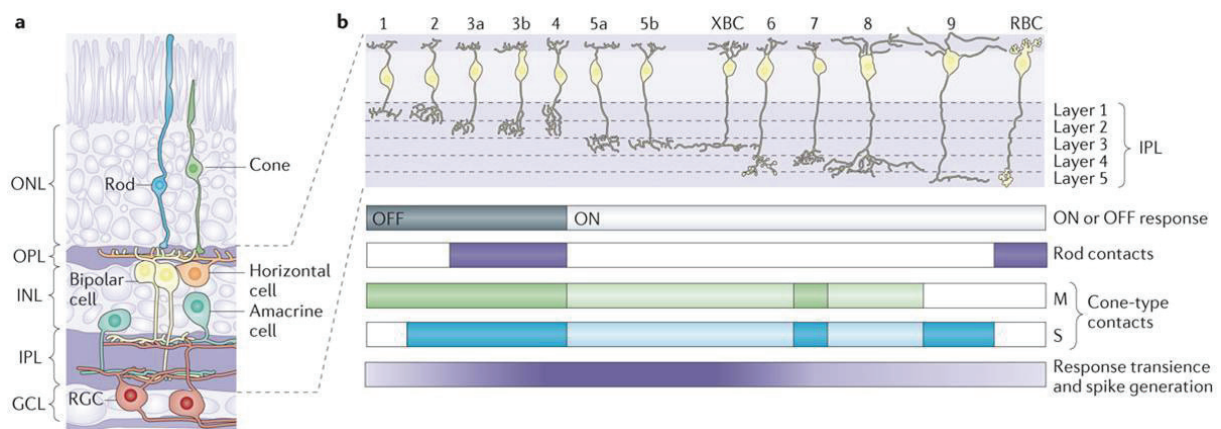


Figure 5: Organization of the bipolar cells in a mammalian retina (adapted from Euler, T et al., (16)) a. Schematic representation of the different retinal cells circuitry in the mammalian retina. b. Morphology of the 12 types of cone bipolar cells and the rod bipolar cell in the mouse, which are arranged according to their IPL stratification level. Some of the functional differences between bipolar cell types are indicated below this schematic drawing.

a) Cone pedicle and cone bipolar cells

The existence of multiple subclasses of cone bipolar cells was initially predicted on structural and molecular characteristics (17). They make synapse at different levels of the IPL, which contains processes of different types of amacrine and ganglion cells. They also express different neurotransmitter receptors and calcium-binding proteins. These structural and

molecular distinctions reflect different modes of intracellular signaling and types of excitatory and inhibitory inputs from other retinal neurons, which give the cells different postsynaptic responses (18).

Cones respond to a light stimulus with a graded hyperpolarization by releasing glutamate at the cone pedicle, their synaptic terminal, at high quantity in darkness and a lower quantity by light (19). The cone pedicle has a particular structure that allows improving the response to a light stimulus. Each cone pedicle contains between 20 and 50 presynaptic ribbons. In the invaginations of these ribbons, horizontal cells of two types and cone ON-bipolar cells of eight types are inserted. OFF-cone bipolar cells contacts take place at the cone pedicle base. Each cone pedicle makes up to five hundred contacts, although the number of postsynaptic cells is smaller because each one receives multiple contacts. The light signal is also distributed into multiple pathways (Figure 6). L- and M-cone pedicles are coupled to their immediate neighbors including the synaptic terminals of rod photoreceptors through gap junctions when S-cone pedicles are only sparsely coupled (16, 19).

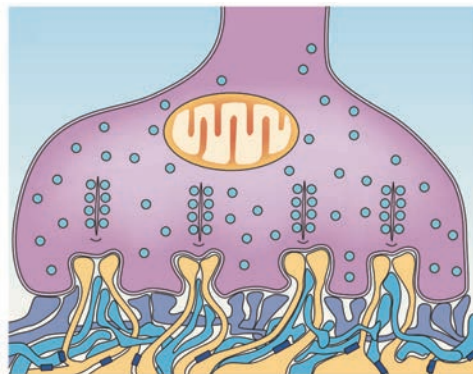


Figure 6: Schematic representation of a cone pedicle (adapted from Wässle, H et al., (19)). Four presynaptic ribbons are opposed to the invaginating dendrites of horizontal cells (yellow) and cone ON-bipolar cells (blue). Cone OFF-bipolar cell dendrites form contacts at the cone pedicle base (purple).

b) Rod spherule

Like cones, rods release glutamate in darkness and this transmitter release is reduced when they are hyperpolarized by light. The rod spherule, which is the synaptic terminal of rod photoreceptors, has also a special structure, containing presynaptic ribbon flanked by synaptic vesicles and opposed to the invaginating processes of horizontal and bipolar cells. In the invagination, two horizontal cell processes take place laterally and one to three rod bipolar cell dendrites occupy a central position. Only one type of rod bipolar cell exists (ON-bipolar cell) in mammals, which is depolarized by a light stimulus (Figure 7). Each ON-bipolar

cell contacts 20–80 rod spherules, and their axons terminate in the inner IPL, close to the ganglion cell layer. However, rod bipolar cells do not send light signals directly into the ganglion cells but instead synapse with AII amacrine cells, which form electrical synapses (gap junctions) onto the axon terminals of cone ON-bipolar cells and inhibitory chemical synapses onto those of cone OFF-bipolar cells. Then, cone bipolar cells synapse with ganglion cells. This processing allows detecting the absorption of a single photon (16, 19).

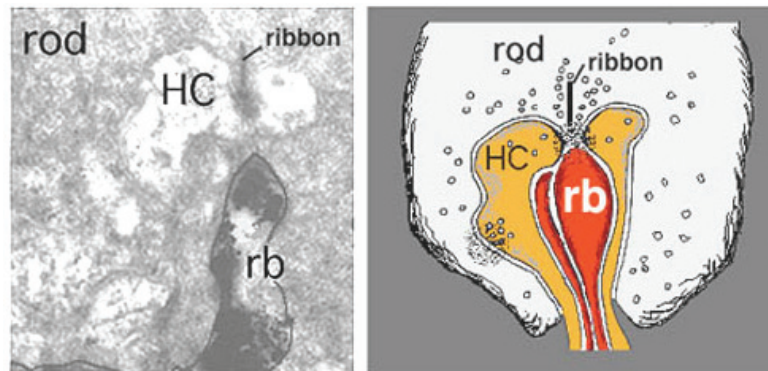


Figure 7: Organization of a rod spherule (adapted from Webvision). Electron micrograph (left) and schematic representation (right) of a rod spherule. The presynaptic ribbon is opposed to the invaginating axons of horizontal cells (HC) and the dendrites of rod bipolar cells (rb).

4. Diagnostic tools for retinal diseases

Many tools are available to document retinal structure and function. We will focus on two of them that are essential and that we used in our experiments: electroretinogram and spectral domain optical coherence tomography that allow investigating respectively function and structure of the retina.

a) Full-field electroretinogram

Full-field electroretinogram (ERG) is a non-invasive technique, which detects, using corneal electrodes, the variation of membrane potentials generated within the retina upon flash stimulation. Electrodes are placed on the cornea and the skin near the eye. During a recording, the patient's eyes are exposed to standardized stimuli and the resulting signal is displayed showing the time course and amplitude of the signal. After the flash, the first negative deflection is called a-wave, and the first positive deflection is called b-wave. The ERG is the summation of membrane potential changes from different retinal cell types, and the stimulus conditions allow specific functional recording of certain cell types. ERG recorded under dark

adapted or, scotopic, conditions allows testing rod pathway function since the dim light stimulation with intensity inferior to 0.01cd.s.m^{-2} is below the cone pathway threshold. A brighter flash, under the same conditions will stimulates both rods and cones but leads to a response dominated by the rods since they outnumber the cones. The negative a-wave reflects photoreceptor hyperpolarization, and the positive b-wave reflects bipolar cell depolarization (20-22) (Figure 8).

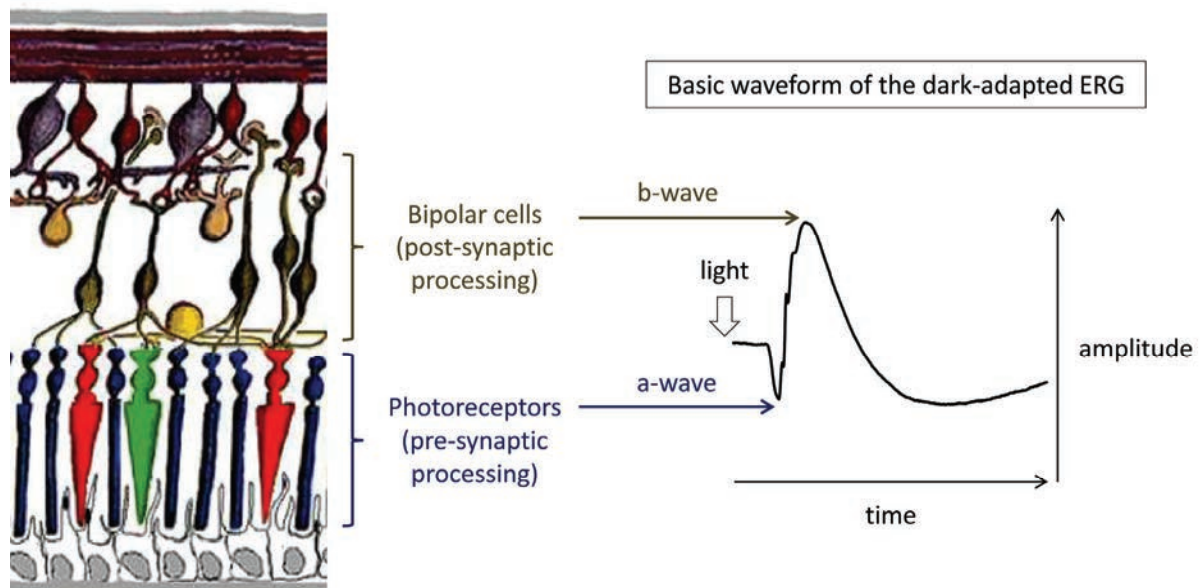


Figure 8: Schematic representation of ERG recorded under scotopic conditions. An illustration of the retina (left, modified from Webvision) and a representative ERG response (right) are shown. In the dark-adapted retina, a light stimulus elicits a presynaptic response from photoreceptor cell hyperpolarization, represented by the a-wave. The subsequent postsynaptic response, mediated largely by bipolar cell depolarization, produces the b-wave.

Photopic ERG performed after light adaptation, which saturates the rod system, allows cone-specific response recordings. The negative a-wave is generated by cone hyperpolarization with an additional contribution of OFF-bipolar cells activity (23, 24), and b-wave reflecting both ON- (ascending segment) and OFF-bipolar cells (descending segment) response (22, 25-27).

b) Spectral Domain-Optical Coherence Tomography

Spectral Domain-Optical Coherence Tomography (SD-OCT) is a non-invasive imaging technique used to evaluate morphology of the retina and also to measure thicknesses of the different retinal layers. This method use low-coherence interferometry to determine echo time delay and magnitude of backscattered light reflected off the retina. It captures images with

very high axial resolution (3 to 15 μm), providing images demonstrating 3D structure (28) (Figure 9).

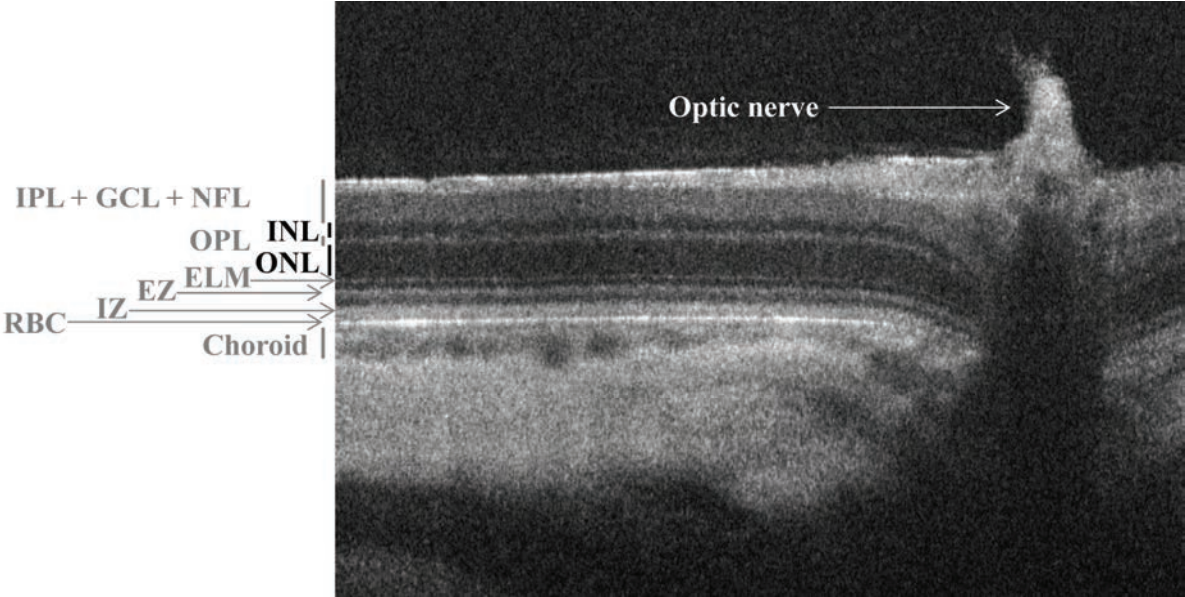


Figure 9: SD-OCT retinal morphology and retinal thickness layers. Optic nerve, outer nuclear layer (ONL), outer plexiform layer (OPL), inner nuclear layer (INL) and a complex comprising inner plexiform layer (IPL), ganglion cell layer (GCL) and nerve fiber layer (NFL) called IPL+GCL+NFL, external limiting membrane (ELM), ellipsoid zone (EZ), interdigitation zone (IZ), retinal pigment epithelium/Bruch's membrane complex (RBC) and choroid are depicted.

C. Congenital Stationary Night Blindness

1. Clinical manifestations

a) Clinical signs

Congenital stationary night blindness (CSNB) refers to a hereditary non progressive group of retinal disorders that predominantly affect signal processing within photoreceptors, retinoid recycling in the retinal pigment epithelium or signal transmission *via* bipolar cells. CSNB is clinically and genetically heterogeneous. Patients often complain of night or dim light vision disturbance or delayed dark adaptation (Figure 10). Poor visual acuity, myopia, nystagmus, strabismus and fundus abnormalities are other ophthalmic signs that can be reported. Vision under dark adaptation is rarely tested routinely and CSNB is likely overlooked by clinicians, underestimating its prevalence (29).



Figure 10: Night vision of unaffected person and CSNB patient (adapted from Retina Swiss)

b) Different forms of CSNB and their diagnostic

CSNB comprises a group of genetically and clinically heterogeneous retinal disorders. The diagnostic is established by performing an ERG, which is critical for functional phenotyping and precise diagnostic (30). Depending on the origin of the gene defect, patients present two types of ERG: Riggs-type for CSNB with photoreceptor dysfunction and Schubert-Bornschein-type for CNSB with bipolar cell dysfunction.

Riggs-type of CSNB shows in scotopic conditions decreased a-wave amplitude, with corresponding b-wave decreased, reflecting the rod dysfunction. There is also a reduced b/a ratio in relation with the photopic hill phenomenon, scotopic responses being dominated by cone responses. Photopic ERGs are preserved, consistent with normal cone system function (31) (Figure 11).

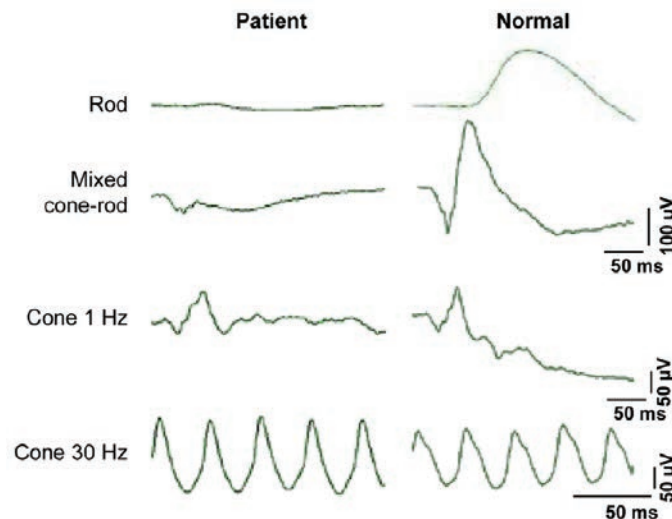


Figure 11: ERG responses from an unaffected person and from a patient with Riggs-type of CSNB (adapted from Manes, G et al., (32)). First column: patient with Riggs-type of CSNB, Second column: unaffected person.

Schubert-Bornschein-type of ERG shows a normal scotopic a-wave and severely reduced b-wave giving rise to an electronegative waveform (33). This ERG phenotype indicates a dysfunction of signal transmission between photoreceptors and bipolar cells. Schubert-Bornschein-type of ERG is the most common type of ERG abnormality associated with CSNB and can be classified into two subgroups: complete (cCSNB) and incomplete form (icCSNB), respectively characterized by ON- or both ON- and OFF-bipolar pathways dysfunction. cCSNB is named complete since, under scotopic conditions there is no detectable ERG to a dim flash. In response to a bright flash under scotopic conditions, the ERG presents normal a-wave and severely reduced b-wave, leading to an electronegative response. Under photopic conditions, the photopic single flash response has an a-wave with normal amplitude but a square-shaped trough, and a b-wave with a sharply rising peak with no oscillatory potentials and a mildly reduced b/a ratio. The photopic 30 Hz flicker response is of normal amplitude but with a mild implicit time shift. icCSNB is named incomplete since, under scotopic conditions the b-wave is present but severely reduced and delayed in response to a dim flash. Under scotopic conditions in response to a bright flash, the ERG responses

show a normal a-wave, confirming normal rod phototransduction, but a reduced b-wave giving an electronegative waveform. Photopic responses are more severely affected than in the complete form: the photopic single flash response presents a markedly subnormal ERG with a profoundly reduced b/a ratio. The photopic 30 Hz flicker response is also markedly subnormal in amplitude and delayed with a distinctive bifid peak (34, 35) (Figure 12).

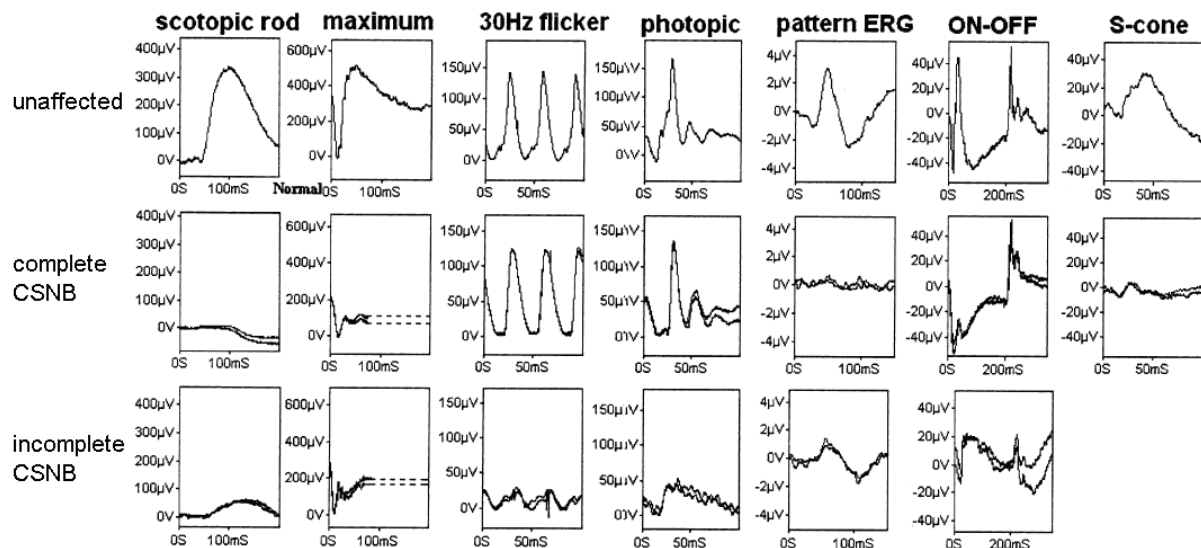


Figure 12: ERG response from an unaffected person and from patients with complete and incomplete CSNB (adapted from Audo, I et al., (36)). First line: unaffected individual, Second line: patient with complete CSNB, Third line: patient with incomplete CSNB.

2. Genetic & synapse between rod photoreceptor and ON-bipolar cell

a) Genes associated with CSNB

At the time we started our study, little was known about gene defects associated with CSNB. The pattern of inheritance may be X-linked, autosomal recessive or autosomal dominant. In 2012, genotyping studies of our CSNB cohort, comprising 160 patients, revealed that in 13% of cases mutations in known genes underlying CSNB were not identified, indicating that mutations in other genes or unscreened regions of known genes remained to be discovered.

Riggs-type of CSNB can be inherited as an autosomal dominant disorder with underlying mutations in *RHO* [MIM180380] (37-41), *GNAT1* [MIM139330] (42-44) and *PDE6B* [MIM180072] (45), or as an autosomal recessive disorder with underlying mutations in *GNAT1* (44), and *SLC24A1* [MIM603617] (46).

Schubert-Bornschein-type of CSNB is subdivided into cCSNB and icCSNB. cCSNB can be inherited as an x-linked trait due to mutation in *NYX* [MIM300278] (47, 48) or as an autosomal recessive disorder with underlying mutations in *GRM6* [MIM604096] (49, 50) and *TRPM1* [MIM603576] (51-53). icCSNB can also be inherited as an x-linked trait due to mutation in *CACNA1F* (54, 55) [MIM300110] or as an autosomal recessive disorder with underlying mutations in *CABP4* [MIM608965] (56) and *CACNA2D4* [MIM608171] (57) (Figure 13).

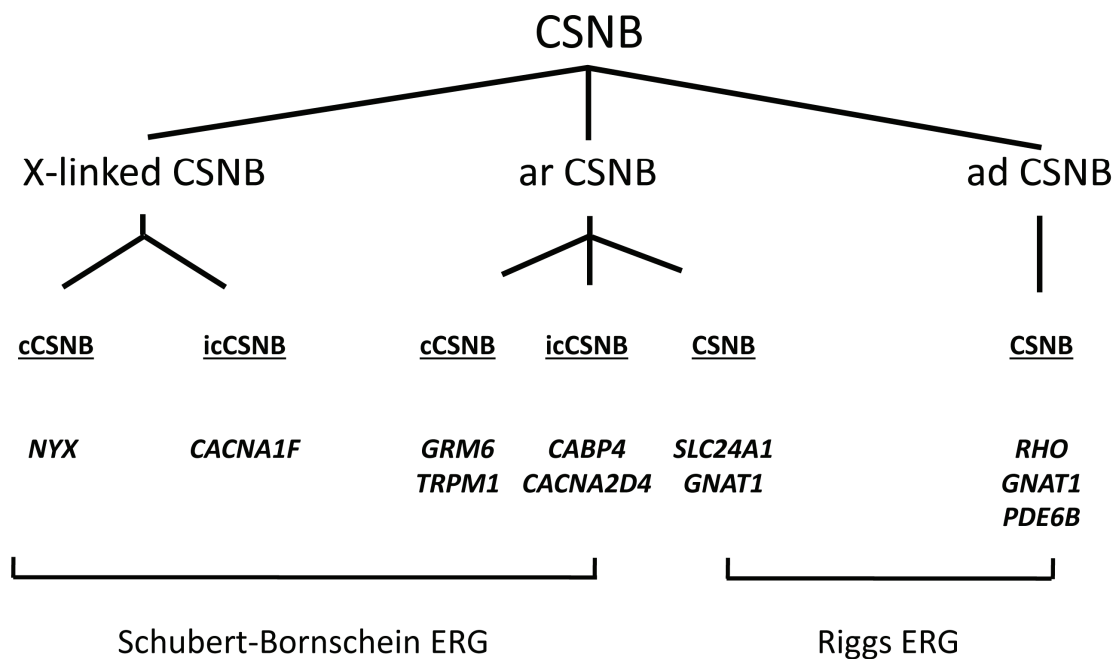


Figure 13: Genes underlying CSNB (modified from Audo, I et al., (51)). Different forms of CSNB are classified according to their mode of inheritance, phenotype, and mutated genes. Abbreviations are as follow: cCSNB: complete CSNB; icCSNB: incomplete CSNB; ar: autosomal recessive; ad: autosomal dominant. Genes are indicated in italics.

b) Signaling cascade between rod photoreceptor and ON-bipolar cell

My project concerned cCSNB, therefore I will focus only on gene defects implicated in cCSNB. Genes involved in cCSNB are expressed at the upper part of the INL of the retina (58-60) and encode proteins localized at the dendritic tips of ON-bipolar cells (9, 53, 61-63). All proteins are implicated in signaling from photoreceptors to bipolar cells. Synaptic transmission between rod photoreceptor and ON-bipolar cell is mediated by the neurotransmitter glutamate, which is released by photoreceptors. *GRM6* encodes a G protein-coupled receptor (GPCR): the metabotropic glutamate receptor GRM6 (also called mGluR6)

(64-67). During darkness, upon glutamate stimulation, GRM6 activates its trimeric G protein, by exchanging its guanosine diphosphate (GDP) with guanosine triphosphate (GTP), and producing activated G α -GTP and free G $\beta\gamma$ (68). Subsequently, activated G α -GTP inhibits TRPM1 cation channel opening. Excitation of photoreceptors by light leads to reduced glutamate release at the synaptic cleft, which is sensed by ON-bipolar cells. This leads to a reduction in G α activation, and to TRPM1 opening, resulting in ON-bipolar cell depolarization and to the formation of the b-wave in scotopic ERG (67, 69). *NYX*, coding for nyctalopin, is necessary for the dendritic tip localization of TRPM1 (62) (Figure 14). During my thesis, *LRIT3*, coding for leucine-rich-repeat, immunoglobulin-like, and transmembrane-domain 3, a new protein which underlies cCSNB when mutated and presenting specific intracellular motifs, was identified. *NYX* and *LRIT3* are suggested to be both important for the correct localization of TRPM1 to the dendritic tips of ON-bipolar cells (62, 70-72).

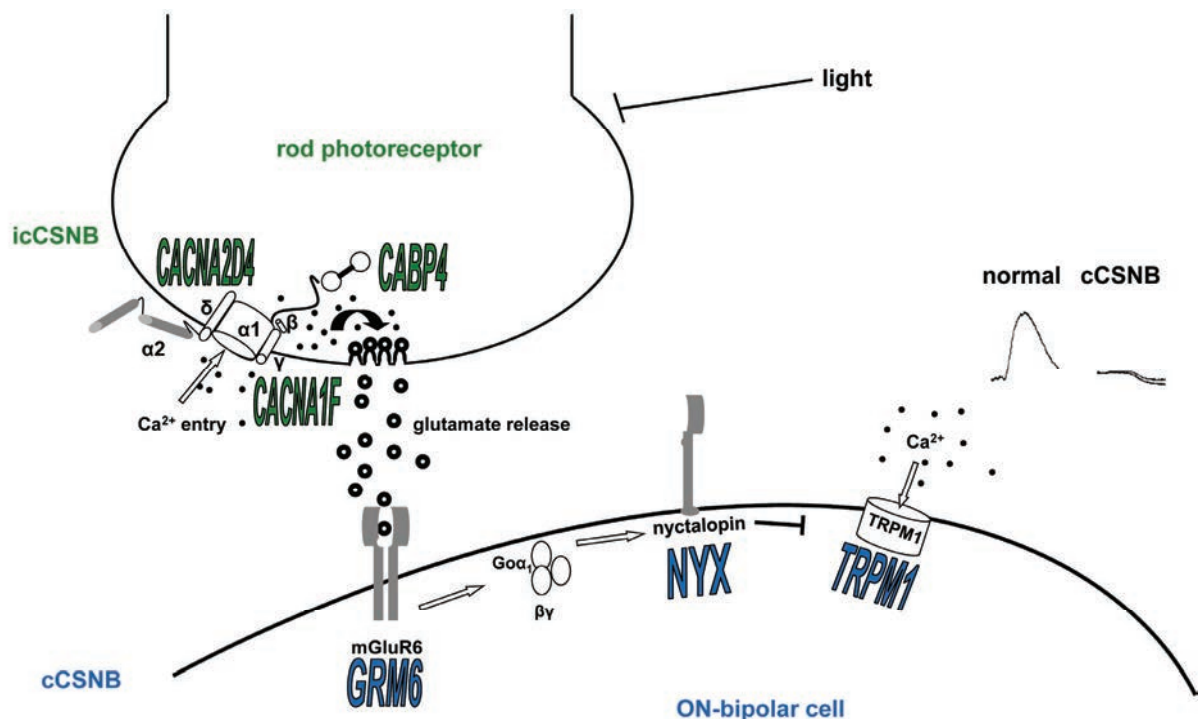


Figure 14: Schematic drawing of proteins involved in signal transmission from rod photoreceptor to ON-bipolar cell (modified from Audo, I et al., (51)). In darkness, Ca²⁺ ions enter the rod photoreceptor, which results in glutamate release from the photoreceptor in the synaptic space. Activated GRM6 activates G α , which then closes the TRPM1 channel. Nyctalopin is essential to the localization of TRPM1 at the dendritic tips of ON-bipolar cells. Upon light stimulation, photoreceptors are hyperpolarized, glutamate release is reduced, leading to less G α activated by GRM6, and consequent opening of TRPM1 visualized by the electroretinogram with the scotopic b-wave, severely reduced in cCSNB patients. Genes underlying incomplete CSNB (icCSNB) are in green, and complete CSNB (cCSNB) in blue.

After their activation by their GPCR, such as GRM6, G proteins spontaneously deactivate at a slow rate. They require assistance of regulator of G protein signaling (RGS) proteins to inactivate them by increasing the rate of GTP hydrolysis of the G protein (73). RGS7, RGS11 and guanine nucleotide-binding protein subunit beta-5 (GNB5), which belong to the R7 family of the RGS proteins since they are similarly organized (74), have been implicated in the complex that regulates *G α* deactivation in ON-bipolar cell cascade. GNB5 was the first described and GNB5 knock-out mice harbor a no b-wave phenotype on scotopic ERG (75). RGS7 and RGS11 were described to co-localize with GNB5 at the dendritic tips of ON-bipolar cells (76, 77), but neither RGS7 nor RGS11 knock-out mice harbored the expected no b-wave phenotype (78). However, double knock-out mice exhibited this phenotype, proving the redundancy of RGS7 and RGS11 but also their role in *G α* deactivation (79). Both RGS7 and RGS11 were acting as a complex with GNB5 for *G α* deactivation (80). The specificity of RGS proteins depends on the formation of macromolecular complexes with other proteins that dictate their compartmentalization. Two homologous membrane anchoring subunits have been shown to form complexes with R7 RGS proteins: regulator of G protein signaling 9 binding protein (RGS9BP) and regulator of G-protein signaling 7 binding protein (RGS7BP). RGS9BP was found to form complexes with RGS11 but not with RGS7 (81) and RGS9BP KO mouse showed complete loss of RGS11 at dendritic tips of ON-bipolar cells (82). RGS7BP was shown to be a universal partner for all members of the R7 RGS family (83) and to increase the activity of RGS7-GNB5 complex by targeting it at the plasma membrane (84).

3. Animals models for cCSNB

Animal models have been shown to be an excellent tool for identifying and elucidating the pathogenic mechanism(s) of gene defects underlying cCSNB. Clinically, the phenotypes of these models can be assessed as in patients by registration of full-field ERG, and OCT. Retinal structure can also be investigated post mortem. This aspect is valuable for a better assessment of histological changes since access to human retinas remains extremely difficult. In addition, animal models are crucial to develop pharmaceutical or genetic treatments. Various animal models have been design or are naturally occurring for cCSNB with dysfunction in molecules important for the signaling from the photoreceptors to the adjacent bipolar cells. At the time we started the study, one horse model for *TRPM1* (85), two zebrafish models for *nyx* (86) and *grm6* (87), and six mouse models for *Nyx* (88), *Grm6* (8, 89, 90) and *Trpm1* (69, 91) had already been published. The phenotype is stationary, and

characterized by dysfunction in scotopic conditions with absent b-waves on the ERG responses and no obvious morphological abnormalities.

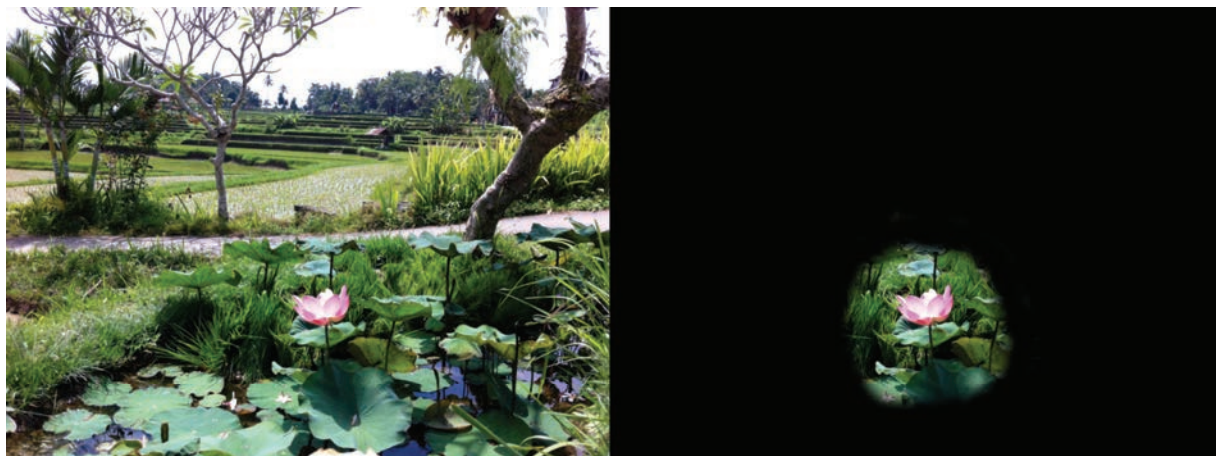
D. Rod-Cone Dystrophy or Retinitis Pigmentosa

1. Clinical manifestations

Rod-cone dystrophy (RCD), also known as retinitis pigmentosa, is a clinically and genetically heterogeneous group of progressive inherited retinal disorders, which often starts with dark adaptation problems and night blindness in adolescence and loss of mid-peripheral vision in young adulthood. As the disease advances, patients lose peripheral vision, develop tunnel vision, and finally lose central vision in most severe cases. RCD occurs in one of 4,000 births and affects more than 1 million individuals worldwide (92).

a) RCD course and associated clinical signs

Visual symptoms indicate the gradual loss of rods which is followed by the death of cones. Patients with RCD initially present a defective dark adaptation (night blindness), in relation with rod dysfunction and progressive degeneration and constitute the first manifestations of the disease that are often hardly noticeable by the affected individuals. The course of the disease leads more or less rapidly to constriction of the visual field (tunnel vision, Figure 15), which reflect in day light condition progressive cone dysfunction and degeneration. Central visual acuity is often preserved until later stages of the disease (92).



Normal Vision

Rod-Cone Dystrophy

Figure 15: Vision of an unaffected person and tunnel vision of a Rod-Cone Dystrophy patient.

RCD has to be distinguished from cone-rod dystrophy (CRD), resulting from primary cone photoreceptors involvement and later followed by the secondary loss in rod photoreceptors. The clinical signs associated with the course of CRD are decreased visual acuity, color vision defects, photoaversion and decreased sensitivity in the central visual field and in later stage progressive loss in peripheral vision and night blindness (93).

b) Diagnostics

RCD is mainly diagnosed by fundus examination, and functional testing of the retina. In early stages of the disease, the fundus may appear normal and functional tests are critical for a proper diagnosis. With disease progression, changes appear but are not specific to RCD, including arteriolar narrowing, retinal vessel attenuation, waxy pallor of the optic nerve head, posterior subcapsular cataracts, dust-like particles in the vitreous and white dots deep in the retina. The most classical modification observed in RCD, giving its name to the disease (retinitis pigmentosa), is pigment migration from the RPE within the outer retina, which form intraretinal clumps of melanin that appear like black spots on the retina (Figure 16). This pigment migration is related to photoreceptor cell death, is not specific of RCD and is typically absent in the early stages of the disease.

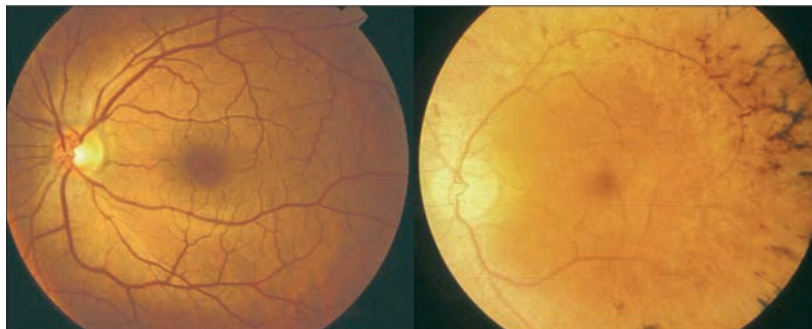


Figure 16: Fundi of a healthy individual (left) and a patient with rod-cone dystrophy (right) (adapted from Hartong, D et al., (92)). In the image of the diseased eye, optic-disc pallor, attenuated retinal arterioles, and peripheral intraretinal pigment deposits in a bone-spicule configuration are seen.

Fundus autofluorescence imaging using a scanning laser ophthalmoscope is a non-invasive technique that allows visualizing lipofuscin, which is the major fluorophore that accumulates in RPE cells and is derived from photoreceptors outer segments. RCD patients present decreased or absent fundus autofluorescence, usually in periphery. A parafoveal ring of hyperfluorescence (94), that is not visible on routine ophthalmoscopic examination, is present

in more than 60% of the patients and reflects preservation of retinal function within the ring (95). The diameter of this ring decreases with disease progression (96) (Figure 17).

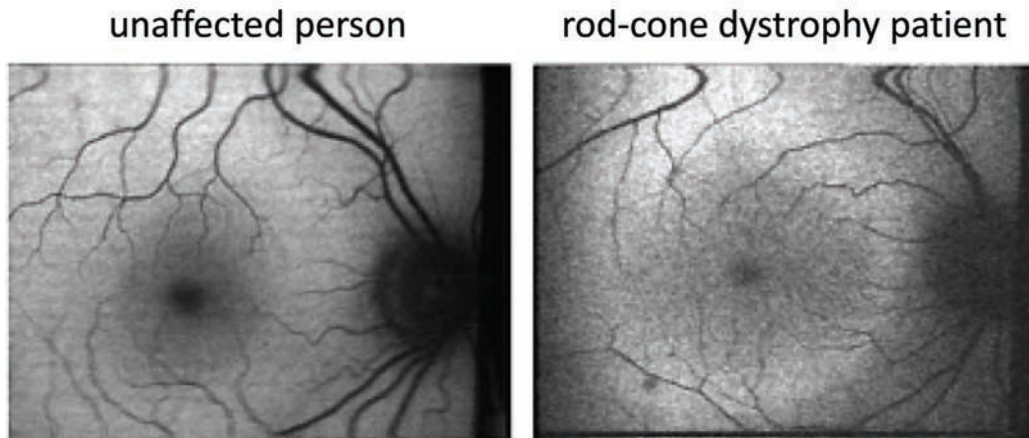


Figure 17: Fundus autofluorescence imaging of an unaffected person (left) and a patient with rod-cone dystrophy (right) (modified from Robson, A et al., (94)). The rod-cone dystrophy patient presents a decreased autofluorescence in the periphery and a parafoveal ring of hyperfluorescence.

SD-OCT can also be used to measure retinal thickness and thus follow the degeneration course. SD-OCT allows identification of each layer of the retina with RCD patients presenting a reduction in thickness of ONL and PR segment layers (Figure 18).

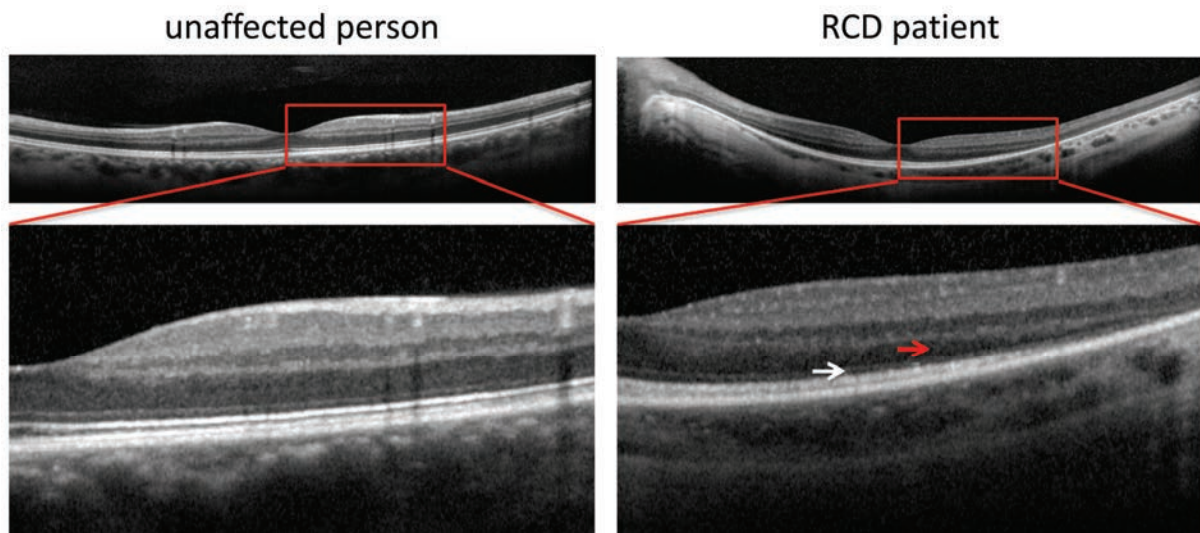


Figure 18: Spectral-Domain Optical Coherence Tomography of an unaffected person and a Rod-Cone Dystrophy patient (pictures are courtesy from Thomas Pugliese, Clinical Investigating Centre of Quinze Vingts Hospital, Paris). Spectral-Domain Optical Coherence Tomography (SD-OCT) of an unaffected person (left) and a Rod-Cone Dystrophy patient (right), first line: horizontal scans, second line: higher magnification of images from the first line. The unaffected person presents a normal SD-OCT, the RCD patient present a loss of outer segments of photoreceptors (depicted by the white arrow) and a decrease in peripheral photoreceptor nuclei thickness (depicted by the red arrow).

In addition to these purely descriptive aspects, functional criteria also participate to RCD diagnosis. Testing of the visual field is used to determine the presence of scotomas (area of decreased retinal sensitivity) corresponding to regions of photoreceptor dysfunction.

Full field ERG is the key examination for the diagnosis, in particular for the early stages of the disease, and will reflect primary photoreceptor dysfunction, i.e. a-wave reduced amplitude and delayed with a proportional reduction in the b-wave, with rod function being more affected than cone function (Figure 19).

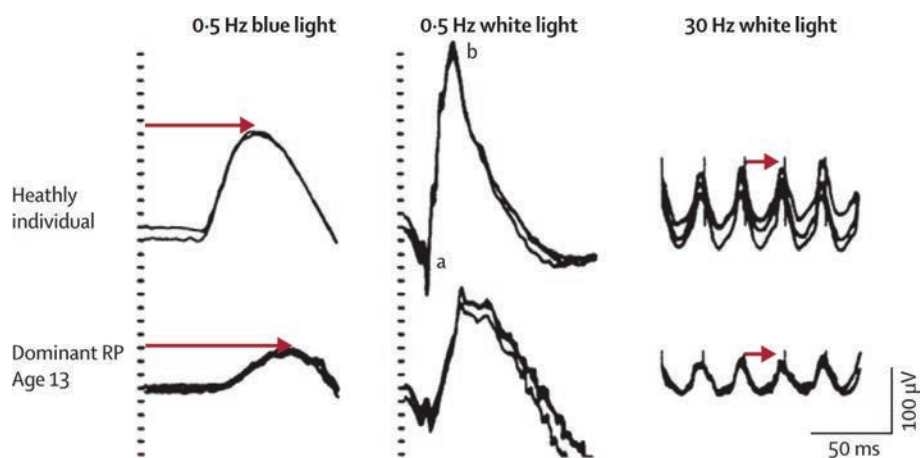


Figure 19: Full-field ERG responses from a healthy individual and from a patient with an early autosomal dominant retinitis Pigmentosa (RP) (adapted from Berson, E et al., (97)). a=a wave. b=b wave. Vertical dotted lines (left and centre columns) and vertical shock artifacts (right column) represent stimuli. Arrows indicate implicit time of the responses .

c) Genes associated with the disease

RCD is the most common inherited form of severe retinal degeneration, with a prevalence of about 1 in 4000 births and more than 1 million affected individuals over the world. The mode of inheritance can be X-linked (5–15%) autosomal dominant (30–40%) or autosomal recessive (50–60%). The remaining patients represent isolated cases of which the inheritance trait cannot be established (92).

In this work, we will focus on autosomal dominant RCD (adRCD). To date, mutations in 24 different genes are associated with adRCD (<http://www.sph.uth.tmc.edu/Retnet/>). Genes already characterized in adRCD mainly encode for proteins involved in various cellular

function including phototransduction, visual cycle, PR structure or gene expression, but also an important group of genes that encode for proteins implicated in splicing function. One of the major genes implicated in this disorder is Rhodopsin (*RHO*) coding for the light absorbing molecule that initiates the signal transmission cascade in rod photoreceptors. Interestingly, most of these genes are selectively expressed in rod photoreceptors although cones degenerate secondarily. Different hypothesis have been made to explain cone degeneration in these cases including the one developed by Professor Sahel's group implying that rods provide trophic support for cones. When rods degenerate this lack of trophic support would lead to cone cell death. At least two rod-derived viability factors have been identified that carry interesting therapeutic potentials (98, 99).

Of notes, despite comprehensive gene screening for mutations, 40% of RCD cases do not carry mutation in genes implicated in RCD suggesting additional gene defects to be discovered (Figure 20).

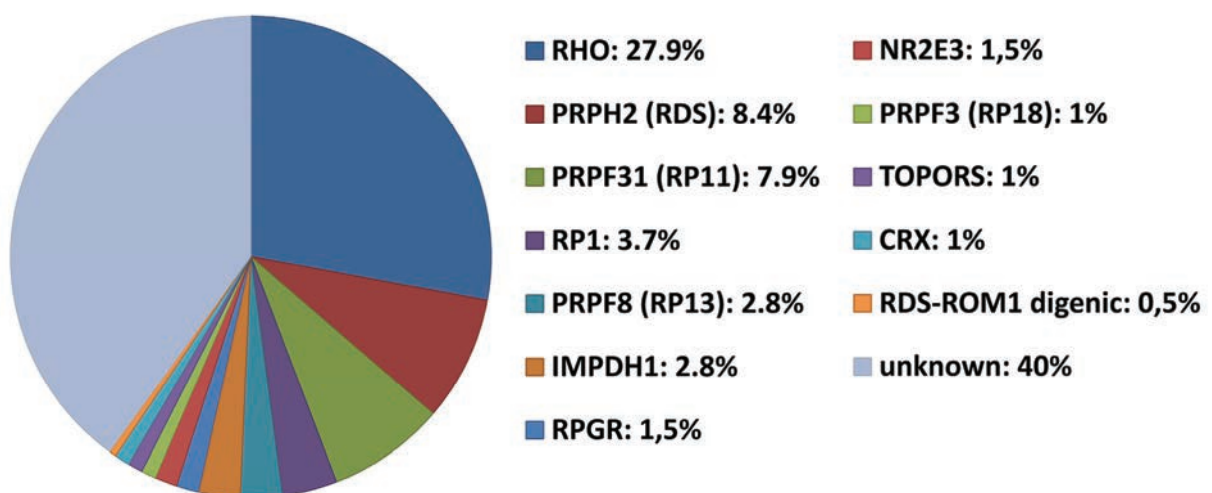


Figure 20: Genes and their relative contribution to autosomal dominant Rod-Cone Dystrophy (modified from Bowne, S et al., (100))

2. Rhodopsin

a) Function

Rhodopsin (RHO) is the most abundant protein in rod photoreceptors counting for nearly 30 % of the entire proteome and over 90% of outer segment proteins (101). RHO is the visual pigment found in rod photoreceptors and is a member of class A of the G- protein-coupled receptor superfamily, which represents a large group of cell surface signaling receptors that

transduce extracellular signals into intracellular pathways through the activation of heterotrimeric G proteins (102).

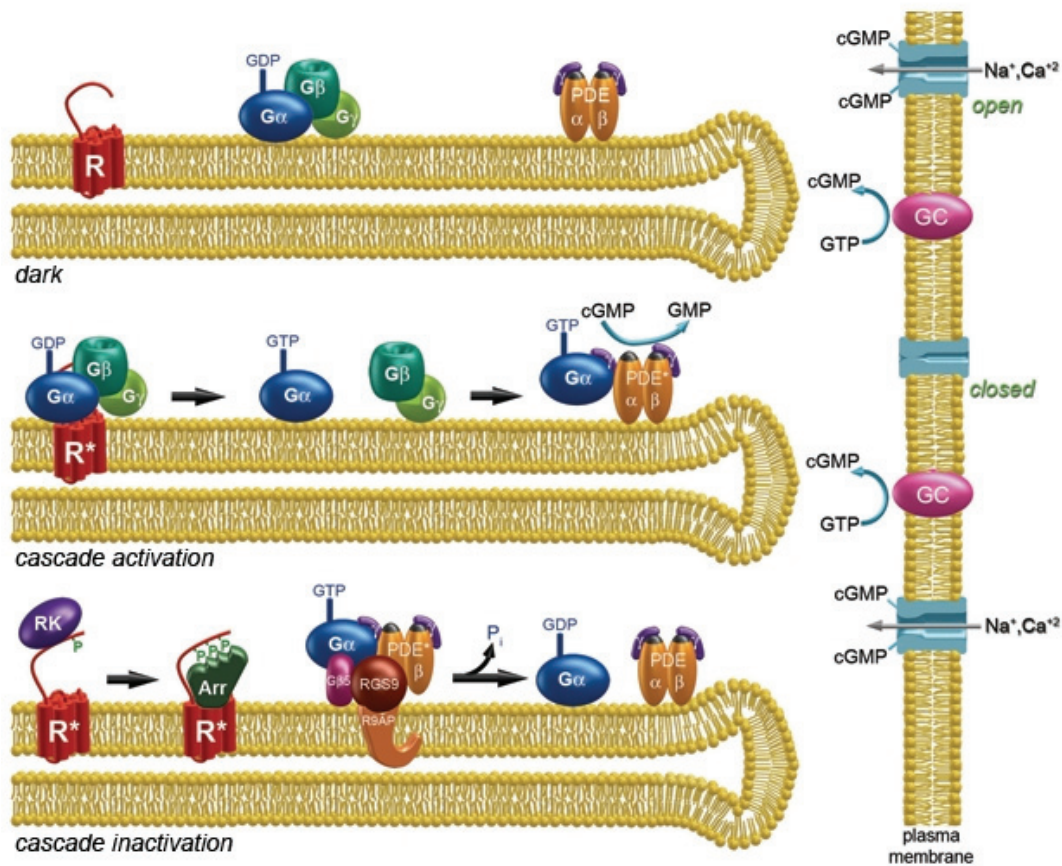


Figure 21: Phototransduction cascade (adapted from Arshavsky, V; (103)) In the dark, opsin is bound to 11-*cis*-retinal to form inactive Rhodopsin (R) in the disc membranes, cGMP level is high, and the cation channel calmodulin is open. Light induce photoisomerization of 11-*cis*-retinal to all-*trans*-retinal, forming activated Rhodopsin (R*), which binds and activates the heterotrimeric G protein, transducin. The GTP-bound transducin α subunit ($G\alpha$) activates cGMP phosphodiesterase (PDE), which hydrolyzes cGMP to GMP, reducing the cGMP concentration and the binding of cGMP to the cGMP-gated channel. With increasing intensity of light, calmodulin channel closes. In the dark, Rhodopsin kinase (RK) phosphorylate R*, resulting in arrestin binding (Arr) to R* and quenching R* activity. $G\alpha$ is inactivated when the terminal phosphate of its bound GTP is hydrolyzed. Although $G\alpha$ has intrinsic GTPase activity, this capacity is only enabled when the activated $G\alpha$ is bound to PDE and when, in addition, the GTPase accelerator protein RGS9-GNB5 also binds. The resulting complex rapidly hydrolyzes the GTP to GDP, resulting in inactivation of $G\alpha$. The inactive $G\alpha$ -GDP dissociates from the PDE, so that the PDE and $G\alpha$ are inactivated simultaneously.

RHO is responsible for converting photons into chemical signals and is formed from the 348 amino acid long rod opsin protein and the chromophore 11-*cis*-retinal. When a photon of light strikes rhodopsin, the isomerisation of the 11-*cis*-retinal to 11-*all*-retinal initiates the phototransduction cascade in the rod photoreceptor by the isomerisation of the rhodopsin into metarhodopsin I and then metarhodopsin II, which activates the G protein transducin (G_T). Transducin α subunit bound to GTP, activate the cGMP phosphodiesterase which hydrolyses cGMP. cGMP can then no longer activate cation channels, and this leads to the

hyperpolarization of rod photoreceptor (a-wave of the ERG). Metarhodopsin II is also rapidly deactivated after transducin by rhodopsin kinase and arrestin. RHO is then regenerated (104) (Figure 21).

b) Rhodopsin mutations

Rhodopsin was the first gene identified to underlie RCD when mutated (105). More than 100 different *RHO* mutations have been reported to date, which account for 30–40% of adRCD cases in United States (92) and 16% in France (106). The c.68G>A, p.Pro23His mutation (P23H exchange) is the most prevalent cause of RCD, and is found only in the United States, presumably because of a founder effect (105). In Europe, the most frequent mutation is c.1040C>T, p.Pro347Leu (P347L exchange) (107).

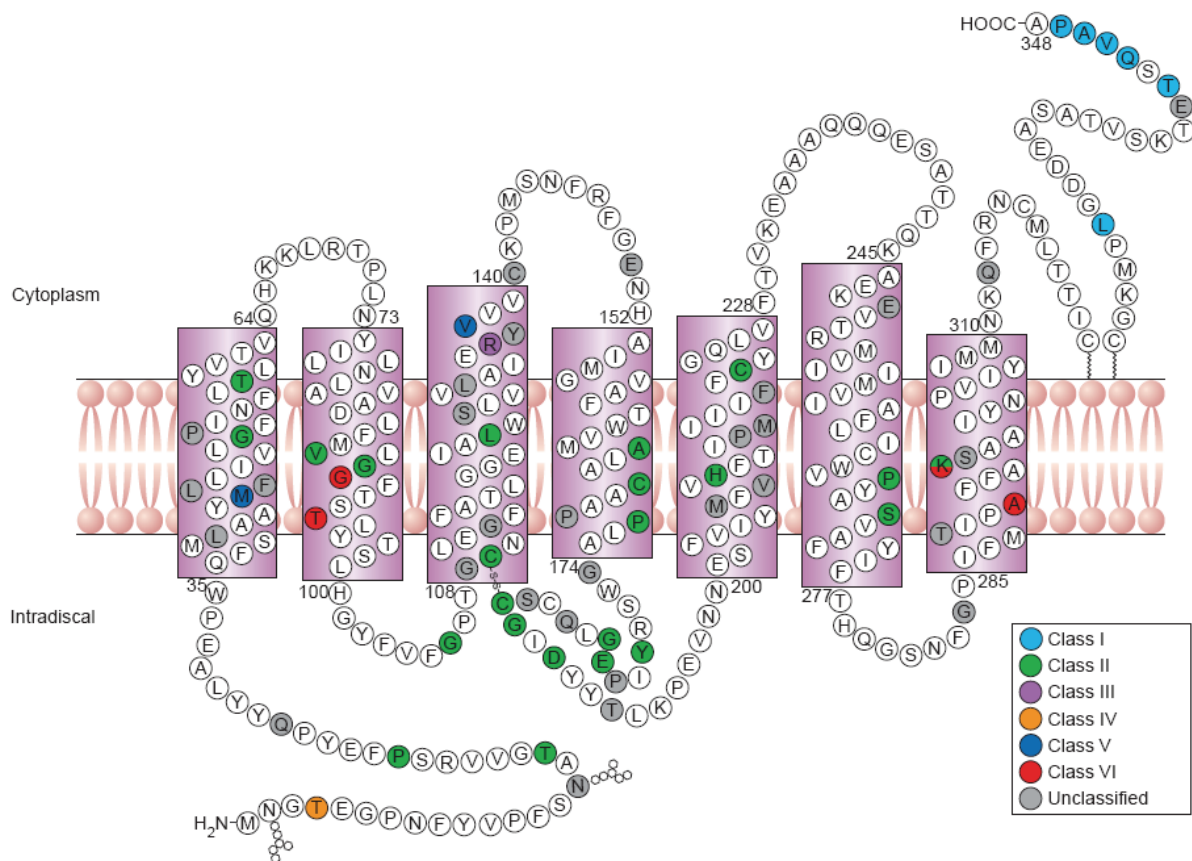


Figure 22: RHO mutants (adapted from Mendes, H et al.,(104)). Secondary structure of RHO showing the location of point mutations. Transmembrane helices are shown in boxed sections. Mutated residues are highlighted in colors corresponding to the different classifications.

Six classes of RHO mutants have been proposed based on their cellular and biochemical characteristics (104). Class I mutants fold normally but are not trafficked to the outer segment correctly. Class II mutants are misfolded, retained in the ER and cannot easily reconstitute with 11-*cis*-retinal. Class III mutants affect endocytosis. Class IV mutants do not necessarily

affect folding but affect Rhodopsin stability and post-translational modifications. Class V mutants show increased activation rate for transducin. Class VI mutants show constitutive activation of opsin in the absence of the chromophore in the dark. Finally, some mutants were not classified because of any observed biochemical defect or lack of studies (Figure 22).

c) Dominant negative effect of P23H exchange

One of the best studied *RHO* mutations is the c.68G>A mutation leading to P23H exchange. P23 is located in the N-terminus of RHO, within the intradiscal space. The c.68G>A, p.Pro23His mutation belongs to the class II and exhibits characteristics of both types of dominant mutation: toxic gain-of-function, and dominant negative effect (104). Many gain-of-function mechanisms were described for the P23H exchange. Indeed, *in vitro* expression of the P23H mutant RHO showed that the misfolded protein is retained in the endoplasmic reticulum (ER), unlike wild-type RHO, which is glycosylated and transported to the plasma membrane (107-109). The accumulation of misfolded proteins causes ER stress and induces the unfolded protein response (UPR), allowing reduction of misfolded proteins accumulation (104). The misfolded RHO can also be degraded through the ubiquitin-proteasome system (UPS), or aggregated into cytosolic ubiquitinated protein inclusions when misfolded RHO is not degraded (110, 111), with protein inclusions directly impairing the function of the UPS and also increasing aggregation (112). The dominant negative effect is due to the inclusions. Ubiquitinated aggregates disrupt the processing of wild-type RHO synthesized in the same cell. When expressed together, as in adRCD patients, wild-type and P23H RHO are both aggregated in the cytosolic inclusions (111), resulting in an enhanced proteasome mediated degradation of wild-type RHO (113).

d) Animal models with *RHO* mutations

There is a high degree of sequence homology in *RHO* among different species including human. Many animal models have also been created to study *RHO* by identifying and elucidating the pathogenic mechanism of gene defects underlying RCD and to develop therapeutic approaches. Two kinds of animal models related to *RHO* have been described: those allowing investigation of physiopathological mechanism of *RHO* mutations and those aiming to investigate the effects of RHO quantity.

(1) Animal models with RHO mutations

There are many *RHO* mutated animal models available for adRCD. One of them is a naturally occurring dog model (114), and all others are transgenic animals created in different species: mouse (115-122), rat (123, 124), pig (125, 126) but also rabbit (127), zebrafish (128), *xenopus laevis* (129) and fly (130). Several classes of mutations were studied with animals presenting exchanges in different aminoacids as Q344 (117, 124, 128) and P347 (119, 125, 127) for class I, P23 (115, 116, 120, 123, 126, 129, 130), D190 (121) and K296 (118) for class II, and T4 (114) for class IV. All these models accurately reproduce RCD clinical signs observed in humans.

(2) Animal models to study RHO quantity effect

To better understand the functional and structural role of *RHO* in the normal retina, knock-out animals with *Rho* disruption have been created (131, 132). Retinas of knock-out animals initially develop normally, except that rod photoreceptor outer segments failed to form. Several months later, photoreceptor cells degenerate completely (131, 132). Retinas from mice with one allele of *Rho* develop normally, and rod photoreceptors elaborate outer segments of normal size. Photoreceptors of these mice also degenerate but with a slower time course, suggesting that RHO is essential for the development and maintenance of rod photoreceptors (131, 132). Furthermore, *Rho* overexpression in animal models created with several wild-type *Rho* transgene also leads to photoreceptors degeneration (115). RHO amount is also to take into consideration and is also important for rod photoreceptor homeostasis (115).

3. Current therapeutic approaches for RCD

There is currently no approved therapy able to stop photoreceptors degeneration or to restore vision. Several preventive approaches to slow down the disease evolution were adopted as vitamin A supplementation, solar protection and retinotoxic drugs as well as tobacco eviction. A psychological and social support for families is encouraged.

However, different approaches to cure RCD are tested and can be divided into two groups, depending on the stage of RCD and photoreceptor degeneration.

a) **By preventing photoreceptor degeneration**

Several approaches aiming to stop or slow down the disease course were attempted or are under investigation with genetic targeted approaches and genetically independent strategies.

(1) Through genetic targeted approaches

Before the degeneration of photoreceptors, gene therapy could avoid the degeneration by restoring the function of the mutated gene and/or correcting the underlying biochemical defect.

The eye represents a unique target organ for gene therapy for several reasons. Thanks to the blood-ocular barrier, the eye is one of the few immunologically privileged sites in the body, so vectors used for gene therapy are unlikely to cause a systemic immune response. Given the defined volume of the eye, small amounts of viral vectors can be used, reducing the risk of toxicity and increasing the likelihood of being able to manufacture quantities of vector sufficient to treat the retina. The eye allows localized treatment thanks to its transparency and the effects of these localized ocular treatments can also be easily observed and monitored for efficacy and safety, by using the non-treated eye as a control. Finally, in the case of retinal gene therapy, most of the retinal cells are post-mitotic, meaning that in principle gene transfer is permanent (133).

For these approaches, vectors for correct delivery are necessary to target the appropriate cells.

(a) Viral vectors for retinal gene therapy

Due to the inefficient transfer of naked DNA or RNA alone, success of gene therapy by gene augmentation or genome editing is highly depending on vectorisation of the therapeutic gene. The vector allows specifically targeting the cell of interest and expression of the gene in this cell. Synthetic vectors and viral vectors are the two types of vectors that have been mainly studied. Synthetic vectors as liposomes or polymers allow DNA to enter the cell through the plasma membrane by being endocytosed. Their main advantages are the facility of production in high quantities, the high transport capacity, and the low risk of virulence. However, they present tendency to aggregate, low efficiency for *in vivo* intracellular delivery and even lower

nuclear addressing rate. Viral vectors have emerged as highly efficient gene therapy delivery vehicles. Retrovirus, lentivirus, adenovirus and Adeno-Associated Virus (AAV) are the main studied viruses for gene delivery. Their ability to cross the extracellular and intracellular barriers allows gene delivery in the nucleus of the cell of interest. However, they present an immunogenic effect and a possible risk of insertion into the genome. Once AAVs are modified, they do not insert into the genome and present lower immunogenic potential than retroviruses, lentiviruses and adenoviruses, explaining their large use for gene delivery (134-136).

AAVs belong to the Parvoviridae family. These non-human pathogens possess a linear, single-stranded DNA genome that can replicate in the presence of different helper viruses such as adenoviruses, herpes viruses or papilloma viruses. AAVs were originally isolated as contaminants from laboratory stocks of adenoviruses. The AAV genome of 4,7 kb consists of two open reading frames, rep, required for viral genome replication; and cap, encoding AAV structural proteins; rep and cap DNA sequences being enclosed within two symmetric T-shaped palindromic terminal sequences called inverted terminal repeats (ITRs). More than 100 different natural serotypes of AAV have been isolated, and among them 10 have been more extensively characterized and classified. They differ on the composition of their capsids, and consequently, for their affinity for cell surface receptors, determining their tropism. Moreover, natural AAVs may integrate into human chromosome 19 or persist in an episomal form (137, 138) (Figure 23).

Recombinant AAVs (rAAV) vector were generated by deleting the rep and cap sequences from the genome and by inserting between the ITRs a promoter followed by the therapeutic gene of interest. rAAV are then produced by cotransfection of the rAAV vector plasmid and a helper plasmid coding AAV rep and cap in the presence of a helper virus infection. The nomenclature of this rAAV indicates then for the first number the origin of the ITR of the recombinant genome and for the second one to the capsid (136) (Figure 23).

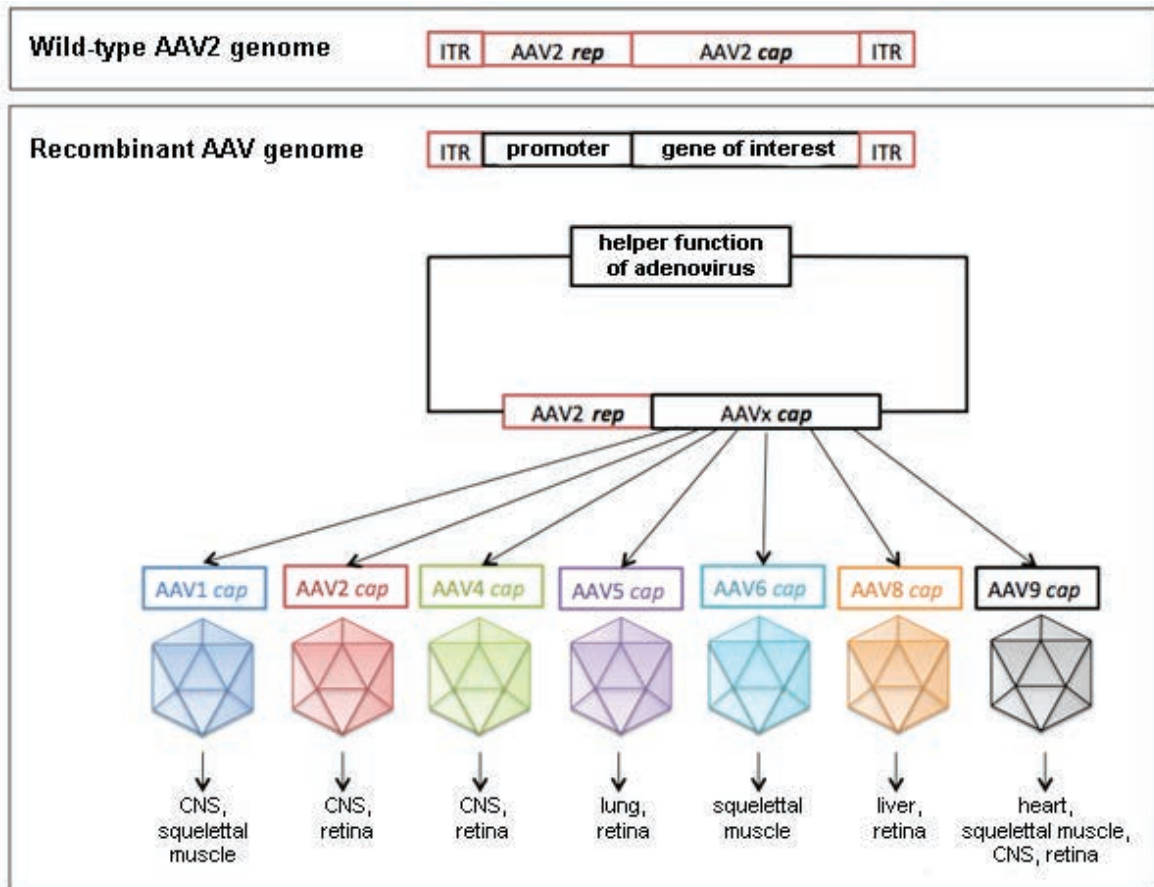


Figure 23: Production of recombinant AAV from wild-type AAV (modified from Khabou, H et al., (136)) . ITR: Inverted Terminal Repeat, rep: replication, cap: capsid, CNS: Central Nervous System.

rAAVs lacking their viral coding sequences are also rendered replication-defective and unlikely to trigger host immune responses. They are capable of transducing non-dividing target cells. Since DNA is stabilized in an episomal form, there is in theory little concern for random and disease-causing integration into the host's genome, known as insertional mutagenesis. The virus has a tropism for long-lived cell types, including those in the central nervous system, and long-term expression can be achieved even in the absence of integration. The primary disadvantage with this class of vector is a limiting 4,7 kb gene packaging capacity (138). Nevertheless, rAAVs are one of the most employed viral vector in gene therapy since it allows to specifically infect a given cell type, does not produce insertional mutagenesis, express persistently and at a high level the transgene when combined to a specific promoter and present low immunogenicity.

rAAVs have been the vectors of choice for retinal gene delivery. The first rAAV that allowed gene expression in the retina was the rAAV2/2 serotype and showed infection of a large cell

population of the retina, including ganglion cells, Müller cells, photoreceptors and RPE cells, without any sign of inflammatory response or toxicity, after subretinal injection in adult mice (139). Gene expression was then restricted to rod photoreceptors, by using the rod-specific promoter *Rho* (140). In addition, different combinations of natural AAV variant capsids of rAAV2 as rAAV2/2 and rAAV2/5 (141), rAAV2/7, rAAV2/8 and rAAV2/9 (142) were described to target photoreceptors and RPE when injected subretinally in mice. However, when injected intravitreally, the majority of AAV serotypes do not infect the retina with the exception of AAV2/2. This is presumably caused by the presence of physical barriers, such as the inner limiting membrane (143). To overcome this issue, Dalkara and coworkers developed an *in vivo* directed evolution approach to iteratively enrich for AAV variants capable of reaching the outer retina from the vitreous. Briefly, they injected intravitreally three libraries of AAV mutated on their capsid protein and expressing RHO–green fluorescent protein (RHO-GFP). One week later, eyes were enucleated and retinas were dissociated followed by FACS isolation of photoreceptors. Subsequently, viral cap genes from the isolated cells were PCR-amplified from genomic extractions with polymerases prone to errors to introduce variability. Repackaging was performed, followed by several rounds as described above to select an AAV2/2 variant (7m8) that was able to infect mouse photoreceptors and RPE following intravitreal injection (144).

(b) Gene augmentation

Gene augmentation is efficient for recessive diseases, which lead to a loss of function. The principle is to introduce a wild-type version of the mutated gene into the cells and then restore the expression of the normal gene. The gene defect underlying the disease has also to be identified. The most famous and extensively studied therapy by gene augmentation for retinal dystrophy is *RPE65* gene replacement for Leber Congenital Amaurosis (LCA), a severe form of RCD. Several genes have been described to be mutated in LCA, including *RPE65* which is the retinoid isomerase that recycles the 11-*cis*-retinal during pigment regeneration (145). The proof-of-principle of *RPE65* gene replacement therapy in Briard dogs, a natural occurring model with mutation in *RPE65* (146), demonstrated dramatic improvements in the light sensitivity of rod and cone photoreceptors (147), with expression of *RPE65* being stable for more than four years (148). Phase I clinical trials in humans showed a sustained improvement in subjective and objective measurements of vision, without any major side effects reported (149-153).

Regarding *Rho*, gene augmentation would not counteract the dominant negative effect and overexpression of *Rho* was initially thought to be toxic (154). However, Frederick and coworkers showed that in mouse harboring a dominant negative mutated *Rho*, increased expression of normal *Rho* reduces the rate of retinal degeneration (155). Mice of a transgenic line expressing a triple mutant *Rho* (V20G, P23H, and P27L) were crossed with *Rho* knock-out (*Rho*^{-/-}), heterozygous (*Rho*^{+/-}) and wild-type (*Rho*^{+/+}) mice. In transgenic mice with no wild-type RHO, ONL was reduced by 80% by postnatal day 30. In mice with one copy of wild-type *Rho*, there was only a 50% reduction at the same time point, and in mice with two copies of wild-type *Rho*, there was no retinal degeneration at day 30, although by postnatal day 90 photoreceptor loss was complete on all genetic backgrounds (155). These results suggested that degeneration could be decreased or slowed by increasing the ratio wild-type/mutant *Rho* and were converted into a gene therapy application by gene augmentation (156). In P23H *Rho* transgenic mice, wild-type *Rho* delivery by subretinal injection of an AAV2.5 at postnatal 15 slowed retinal degeneration. Analysis of ERG at 6 months showed that a-wave amplitudes were increased by 100% and b-wave amplitudes by 79%. These results were correlated with improvement of retinal structure: thickness of ONL was increased by 80% compared with control eyes. In contrast, treated wild-type mice demonstrated a decrease in the ERG responses and ONL thickness, confirming the damaging effect of *Rho* overexpression in normal photoreceptors (156). These findings suggested that wild-type *Rho* could be delivered to rescue retinal degeneration in mice carrying a *Rho* mutation and that increased production of normal RHO could suppress the effect of the mutated protein. However, the toxicity of *Rho* excess in wt mice suggested that a precise understanding of the dose response is required before applying this approach to patients with *RHO* mutations.

(c) Gene silencing

For dominant mutations, mutated allele inactivation or silencing, at the DNA or RNA level, would be more relevant than gene augmentation. The endogenous wild-type allele or a resistant exogenous wild-type gene fulfills then the function of the gene.

At the DNA level, zinc finger artificial transcription factors (ZF-ATFs) can be used. Zinc fingers (ZFs) are DNA-binding domains present in many transcription factors and able to recognize three to four base pairs. By combining six to seven ZF modules, a specific DNA

sequence can be targeted. ZFs linked to transcriptional regulators are ZF-ATFs and can be combined to repressor domains. Indeed, the Zinc Finger DNA binding domain allows binding to a target promoter, and the transcription factor and repressor can then modify its activity, and thus repress the expression of a specific gene. This strategy was effective at suppressing both wild-type and mutant *Rho* expression in a P347S transgenic mouse model of adRCD. An exogenous *RHO* with modified codon refractory to ZF-ATF repression thanks to the genetic code degeneracy was also brought for a two-step repression–replacement strategy and finally led to improvements in retinal morphology and function (157). Nevertheless, photoreceptors are sensitive to changes in Rhodopsin levels, as mentioned above, and once the mutated *Rho* silenced, overabundance of RHO can lead to retinal degeneration (154). The amount of exogenous *RHO* has therefore to be carefully adjusted for applications in patients.

At the RNA level, three approaches have been proposed to silence the mutated gene: RNA interference, ribozymes and spliceosome-mediated RNA *trans*-splicing. They all target the RNA, and also need to be functional during the whole cell life to be efficient for a therapeutic rescue. RNA interference (RNAi) is a well-conserved gene-defense mechanism based on the repression of gene expression by a short antisense RNA to induce degradation of a targeted endogenous mRNA or inhibit its translation by post-transcriptional gene silencing. Short interfering RNA (siRNA) is formed from long double-stranded RNA molecules and can be synthesized *in vitro* for targeted mRNA degradation/silencing (158). Two strategies can be performed: i/ the siRNA can be specific of the dominant mutated mRNA and the endogenous wild-type allele is then still expressed and fulfills the function of the gene, ii/ the siRNA can be non-specific of the allele and suppress all the expressed alleles of the gene. Then an exogenous wild-type allele, with silent variations in the sequence rendering the allele refractory to suppression is needed. Several studies in mouse and rat animal models were performed (159-162) and some of them showed improvements in structure and function of the retina. However, treatment efficacy was evaluated in comparing treated and untreated animals at a time point at which photoreceptor degeneration is almost complete and not by comparing to a wild-type animal. The rescue was also limited and may be not enough to restore useful vision. Another approach at the RNA level is by using ribozymes. Ribozymes or ribonucleic acid enzymes are RNA molecules that are able to catalyze a specific biochemical reaction, including the cleavage of a targeted mRNA. A specific mRNA can then be targeted for cleavage. This strategy was conducted *in vivo* in a rat model presenting the most frequent type of *Rho* mutation, the P23H rat, and showed a good long term preservation of the retinal

structure. However, structural rescue was not accompanied with functional rescue since ERG revealed only slight increased b-wave amplitudes at the end of the study. Recently, spliceosome-mediated RNA *trans*-splicing (SMaRT) technology has been proposed as another approach targeting RNA (163). *Trans*-splicing is a natural splicing mechanism that occurs between two different pre-mRNAs and results in a final mRNA consisting of the 5' part of the first pre-mRNA and the 3' part of the second pre-mRNA. In the SMaRT technology, engineered PTM (Pre mRNA *Trans*-splicing Molecule), which targets a mutated pre-mRNA, is introduced and allows *trans*-splicing based replacement of the mutated sequence by using the endogenous spliceosome machinery. Berger and coworkers designed a PTM targeting the first intron of *RHO* and aiming to replace exon 2 to 5, and also allowing repairing all the mutations being on these exons (163). *In vitro*, using two different cellular models, they showed from 22 to 40% of mRNA being *trans*-spliced and repaired. *In vivo*, injecting subretinally an AAV2.8 expressing the PTM in mouse harboring heterozygously a human P347L RHO, they obtained 22% of *trans*-splicing in transduced cells and 9% in the whole retina. This low rate in the whole retina due to the low rate of transduction was unfortunately not enough to stop or slow the degeneration quantified by SD-OCT but demonstrated the feasibility of *trans*-splicing *in vivo* (163).

(d) By genome editing for dominant mutations

(i) Genome editing strategy

Recently developed genomic editing technologies have generated potential powerful tools for gene therapy. Indeed, genome editing is a type of genetic engineering in which DNA is inserted, replaced or removed from a genome using artificially engineered nucleases that act like sequence specific molecular scissors. On the targeted sequence of the genome, the nucleases create specific double-stranded breaks (DSBs) that stimulate the cellular DNA repair mechanisms by natural processes of non homologous end joining (NHEJ) and homologous recombination (HR).

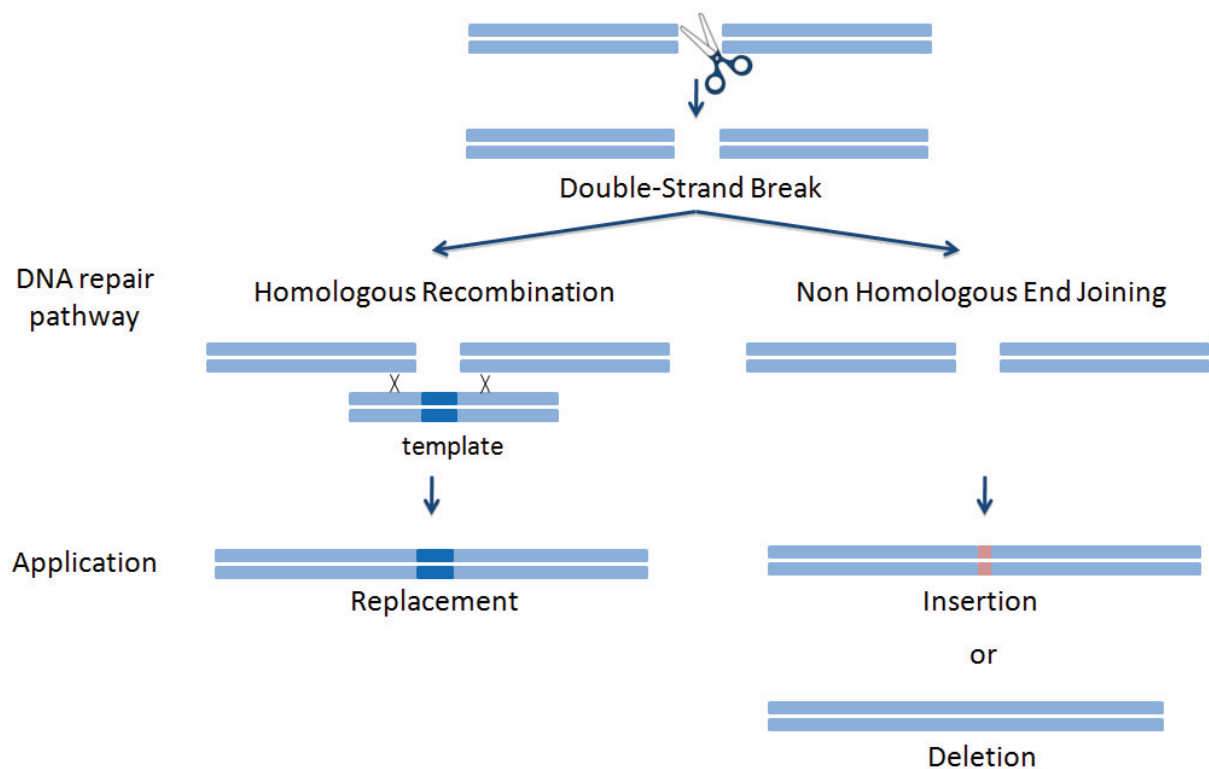


Figure 24: Endonuclease-induced gene targeting approaches.

NHEJ repair the DSB by directly rejoining the two DSB ends in a process that does not require any repair template. Although NHEJ-mediated DSB repair can be accurate, repeated repair of the same DSB by NHEJ machinery eventually results in the formation of small insertion or deletion mutations (indels). Indels introduced into the coding sequence of a gene can cause a frame shift in translation that leads to mRNA degradation by nonsense-mediated decay or results in the production of nonfunctional truncated proteins, both cases resulting in the suppression of the initial mutated protein (164). In comparison, HR is a type of genetic recombination that requires a repair template. This repair can be endogenous, with unbroken sister chromatid or the homologous chromosome. This template can also be exogenous, HR allowing then, with an appropriately designed repair template, to replace a mutated gene directly and restore mutated gene function without modification on the regulation of gene expression (165) (Figure 24).

Although HR and NHEJ have been well-defined in cycling mammalian cells (166), their characterization in mature neurons, which no longer divide, was not well known. To address the question in rod photoreceptors, Chan and coworkers (167) designed a mouse model that allowed them to detect NHEJ events by PCR-based methods and HR events by a highly

sensitive fluorescent assay where GFP expression in rod photoreceptors was possible only after homologous recombination. They induced DSB with a viral vector expressing a specific endonuclease and found that 100% of the transduced rod photoreceptors were edited. Correction was due in 85% of the cases to NHEJ and 15% of the cases to HR. Thus, they established that genome editing is possible in differentiated rod photoreceptors, and that the DSBs are repaired predominantly by NHEJ (167).

(ii) Endonucleases

Different endonucleases are available today and are in trials for different genome editing strategies. We will focus on three of them that I used in my PhD project: meganucleases, Transcription Activator-Like Effector Nuclease (TALEN) and Clustered Regularly Interspaced Short Palindromic Repeats (CRISPR)/ CRISPR Associated Protein 9 (CRISPR/Cas9).

(a) Meganuclease

Meganucleases (MNs), also called homing endonucleases, are naturally occurring gene-targeting enzymes that were initially discovered in yeast but are found in a large number of organisms including bacteria, phages, fungi, yeast, algae and some plants. There are five families or classes, of homing endonucleases. The most widespread and best known is the LAGLIDADG family which is composed of endonucleases that are homodimers as I-CreI (Figure 24) or internally symmetrical monomers as I-SceI.

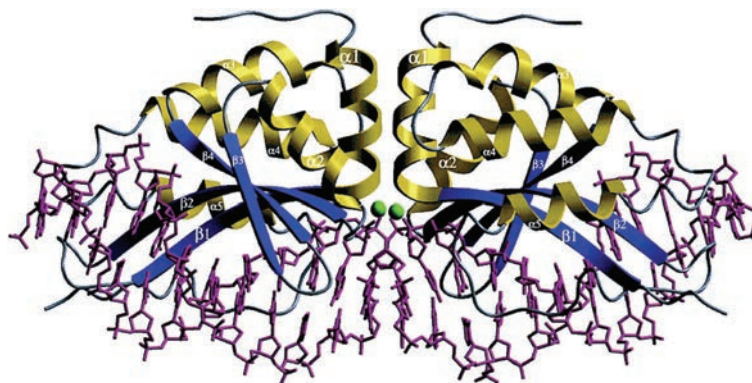


Figure 25: I-CreI Meganuclease in complex with a synthetic DNA (adapted from Jurica, M et al., (168))

The DNA binding site, which contains the catalytic domain, is composed of two parts on either side of the cutting point. The half-binding sites can be extremely similar and bind to a palindromic or semi-palindromic DNA sequence (I-CreI), or they can be non-palindromic (I-

SceI) (169). Meganucleases recognize DNA sequence of 14 to 40 base pairs, the DNA binding domain being also responsible for the cleavage of target sequence. Retargeting natural meganuclease requires challenging protein engineering since binding and catalytic sites are closely related and also catalytic efficiency can often be decreased when binding specificity is modified. However, numerous methods have been developed to test specificity and cutting efficiency as high-throughput assays in bacteria and yeast where meganuclease induce cleavage and eventually reconstitute a reporter gene on the extra-chromosomal target (170).

(b) TALEN

Transcription activator-like (TAL) effectors from the plant pathogenic bacteria *Xanthomonas* represent a class of naturally occurring DNA binding proteins that can be engineered to target novel DNA sequences. During infection, TAL effectors are deployed by the bacteria to modulate host gene expression, with each effector directly binding an effector-specific DNA target (171). The potential of these proteins for genome engineering was shown recently in 2009, when the TAL effector-DNA-binding code was discovered.

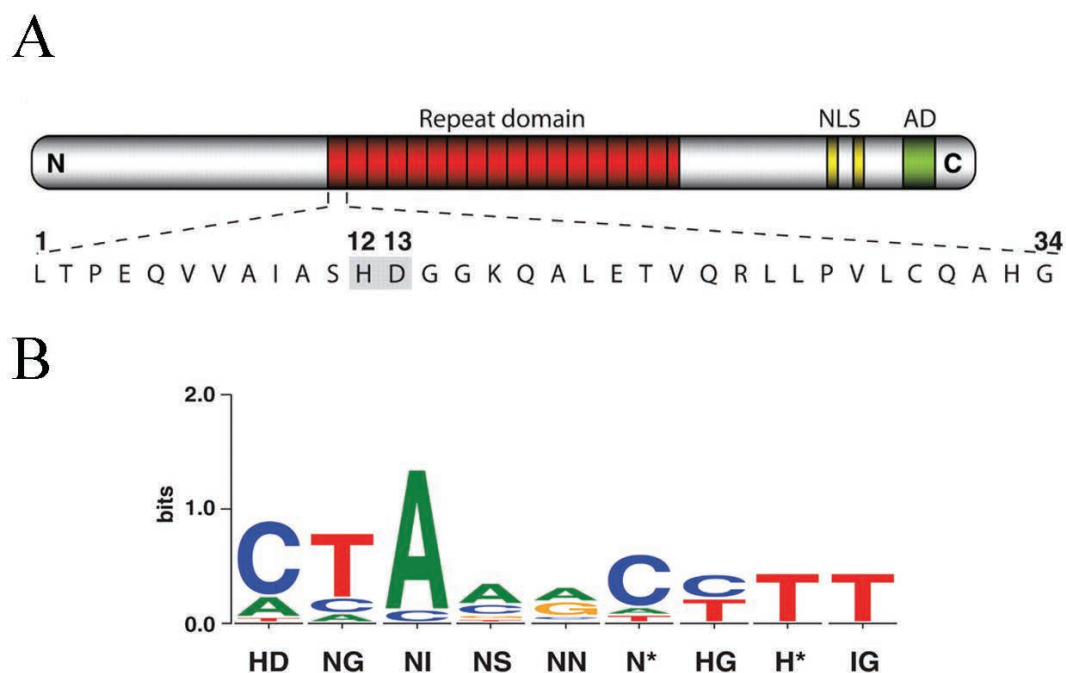


Figure 26: Schematic representation of a TAL (adapted from Boch, J et al., (172)). (A) TAL effector contains central domain repeats, nuclear localization signals, and an acidic transcriptional activation domain. Tandem amino acid repeats are shown with repeat variable diresidue (amino acids 12 and 13 important for the DNA recognition) shaded in gray. (B) Repeat variable diresidue sequence and corresponding nucleotides hits for the recognition. An asterisk indicates that amino acid 13 is missing in this repeat type.

TAL effectors are characterized by a central domain of variable number of tandem repeats, nuclear localization signals, and an acidic transcriptional activation domain. The tandem amino acid repeats of usually 34 residues in length determine the target(s) of each TAL effector. Repeat-to-repeat variation occurs primarily at residues 12 and 13 and was termed the repeat variable diresidue (RVD). The RVD sequence has been shown both computationally and experimentally to interact directly to the DNA target site sequence. Repeats with different RVDs preferentially associates with one of the four nucleotides in the target site, in a code-like fashion, with some degeneracy (172, 173) (Figure 26). Custom TAL effectors can be targeted to novel DNA sequences by assembling an array of repeats that corresponds to the intended target site (174). Designing custom TAL effectors for DNA targeting has proved to be a much simpler and less labor-intensive process than the mutagenesis to produce new meganucleases, and a variety of rapid construction methods for custom TAL effectors and TAL effector-based fusion proteins have recently been developed (175, 176) and adopted as tools for DNA targeting applications. Since 2010, site-specific DNA modification has been achieved using TAL effector-endonuclease fusion proteins (TAL effector nucleases or TALENs) (174), which create targeted DSB in DNA.

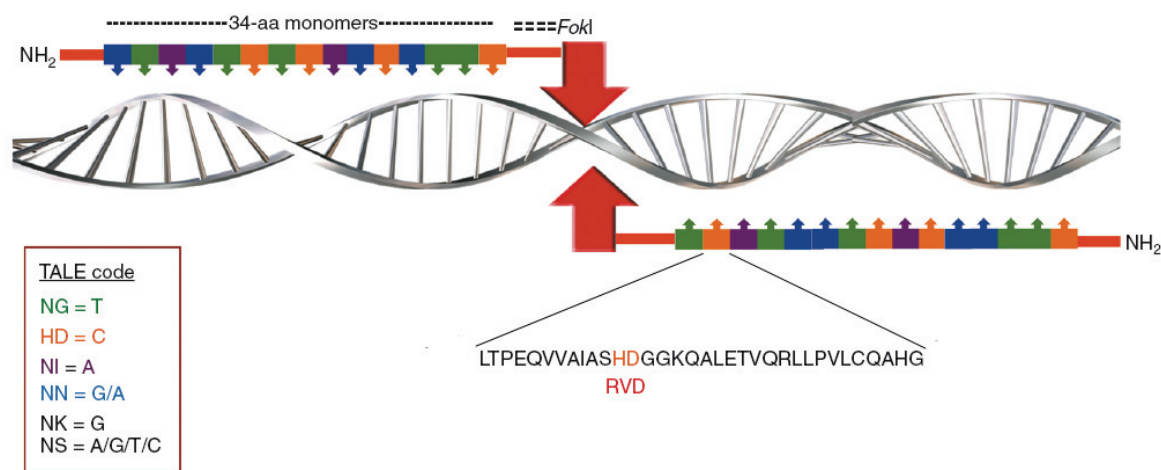


Figure 27: Schematic representation of a TALEN (adapted from Carlson, D et al., (177)) A TAL effector (TALE) polypeptide contains a series of typically 34-amino acid repeats, of which residues 12 and 13 [repeat variable diresidues (RVDs) shown in orange] are responsible for recognition of a specific base as shown in the box. FokI nuclease is fused to the C-terminal end of the protein. The number of tandem 34-amino acid repeats in the binding core defines the length of the recognition sequence. Two TALENs are shown to assemble on a genomic sequence in a tail-to-tail orientation to form a heterodimeric cleavage complex.

TALEN architecture combines the central repeat region and some portion of the flanking parts of the TAL effector with the catalytic domain of FokI endonuclease. For TALENs to function in genome editing, the FokI cleavage domain must dimerize to cleave both strands of the

DNA target. Therefore, two TALENs are used together to target the opposite DNA strands in a tail-to-tail orientation, with proper spacing between the two binding sites (176, 178) (Figure 27).

(c) **CRISPR/Cas9**

CRISPR systems are adaptable immune mechanisms used by many bacteria to protect themselves from foreign nucleic acids, such as viruses or plasmids (179, 180). Type II CRISPR systems initiate the immune mechanism by incorporating sequences from invading DNA between CRISPR repeat sequences encoded as arrays within the bacterial host genome. Transcripts from the CRISPR repeat arrays are processed into CRISPR RNAs (crRNAs), each harboring a variable sequence transcribed from the invading DNA, named as the “protospacer” sequence, and part of the CRISPR repeat. Each crRNA hybridizes with a second RNA, named transactivating CRISPR RNA (tracrRNA) and these two RNAs complex with the Cas9 nuclease. Essential for cleavage is the presence of a sequence motif immediately downstream of the target region, known as the protospacer-adjacent motif (PAM). The protospacer-encoded portion of the crRNA directs Cas9 to cleave complementary target-DNA sequences, when they are adjacent to the PAM (181-184) (Figure 28-a).

This CRISPR/Cas9 system has been adapted for inducing sequence-specific DSBs. For the cleavage of a targeted sequence of DNA, the RNA portion of the system has been simplified into a single guide transcript, consisting of a fusion of crRNA 3' end with a fixed tracrRNA 5' end, enabling binding and DNA recognition. Twenty nucleotides at the 5' end of the gRNA (corresponding to the protospacer portion of the crRNA) direct Cas9 to a specific target DNA. This target site must be followed immediately in 3' by a PAM sequence of NGG for the most used CRISPR/Cas9 system from *Streptococcus pyogenes*. Cas9 nuclease activity can also be directed to any DNA sequence of the form N₂₀-NGG simply by choosing the first 20 nucleotides of the gRNA to correspond to the target DNA sequence (181-184) (Figure 28-b).

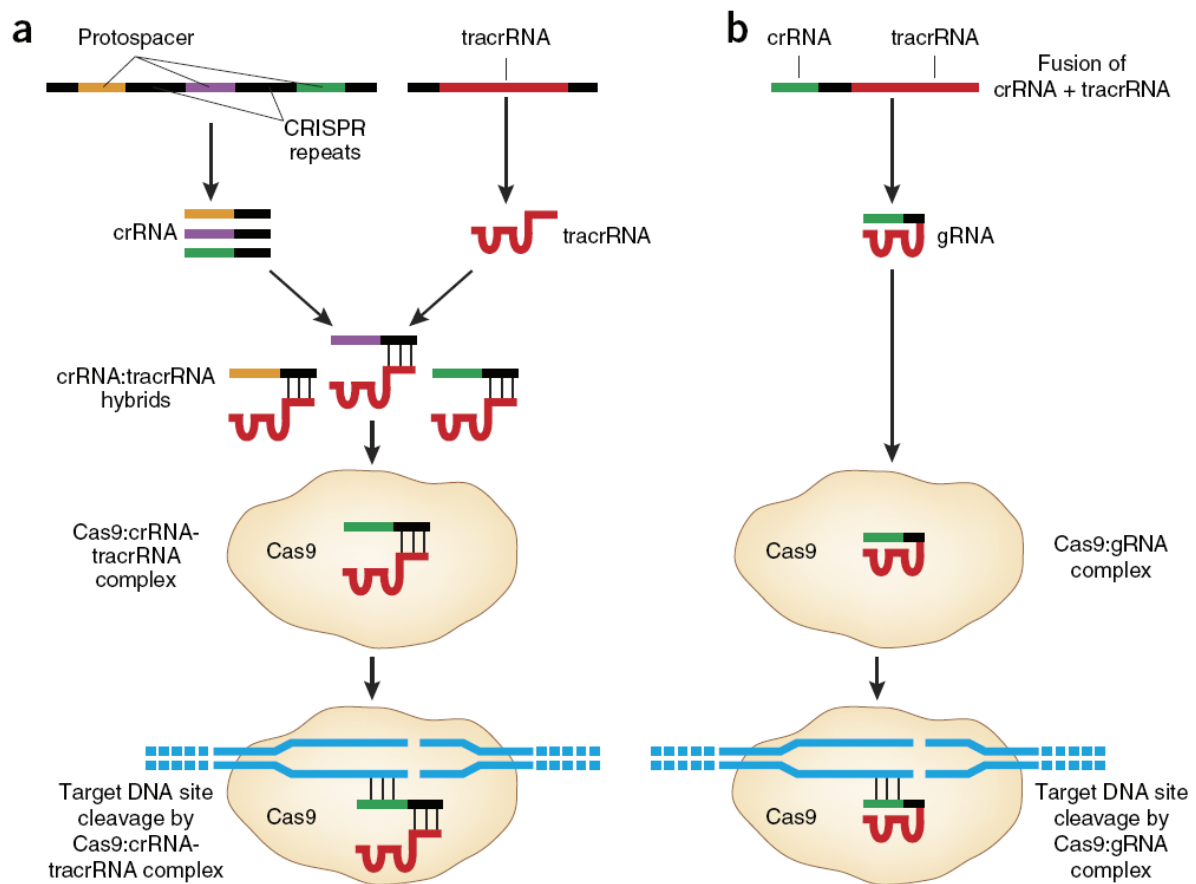


Figure 28: Naturally occurring and engineered CRISPR-Cas systems (adapted from Sander, J et al., (181)). (a) Naturally occurring CRISPR systems incorporate foreign DNA sequences into CRISPR arrays, which then produce crRNAs bearing “protospacer” regions that are complementary to the foreign DNA site. crRNAs hybridize to tracrRNAs (also encoded by the CRISPR system) and this pair of RNAs can associate with the Cas9 nuclease. crRNA-tracrRNA:Cas9 complexes recognize and cleave foreign DNAs bearing the protospacer sequences. (b) The most widely used engineered CRISPR-Cas system utilizes a fusion between a crRNA and part of the tracrRNA sequence. This single gRNA complexes with Cas9 to mediate cleavage of target DNA sites that are complementary to the 5' 20 nucleotides of the gRNA and that lie next to a PAM sequence.

(2) By preventing cell death through genetic-independent approaches

The second approach for stages with only few rod photoreceptors degenerated, aims to make the others photoreceptors survive to cell death by providing a protective environment, either by providing neurotrophic factors, or factors prevent cell death.

Neurotrophic factors play a large role in the development and maintenance of the central nervous system including the retina. The main interest on using neurotrophic factors is that it is mutation independent and thus, that the treatment can be applied on all patients at early-stages of RCD, regardless to the genetic diagnostic. Many neurotrophic factors that slow photoreceptor death in animal models have been identified: basic fibroblast-derived growth

factor (185, 186), brain-derived neurotrophic factor (187), glial-cell-line-derived neurotrophic factor (188-190) and ciliary neurotrophic factor (CNTF) (191-195). Among them, the use of encapsulated cells secreting CNTF into the vitreous has been extensively studied. A phase I safety trial (NCT00063765) as well as a phase II/III trial in advanced disease (NCT00447993) demonstrated the safety of CNTF delivery using encapsulated cell technology with a positive trend in visual acuity, however ERG responses were inconsistent (196). A phase II/III clinical trial (NCT00447980) is currently ongoing to investigate whether CNTF can improve photoreceptor function, in terms of visual acuity and visual field sensitivity, in RCD patients (197). Twelve months after the study started, first results showed no significant changes in visual acuity in CNTF-treated or sham-treated eyes. However, there was a decrease in visual field sensitivity in the high dose-treated eyes that was significantly greater than in the sham-treated eyes. There were no changes in visual field sensitivity in the low-dose eyes relative to sham eyes. A relative preservation of cones was observed but not accompanied by any detectable changes in visual function in a short-duration trial (198).

Rods also produce a neurotrophic factor, RdCVF that promotes cone survival. RdCVF injections in the P23H rat are able to rescue cones from degeneration with a better retinal function in the corresponding ERG at 9 months of age (199). Recently, two studies with AAV-delivered RdCVF showed encouraging results in *rd10* and *rd1* mouse models of RCD (200, 201). In *rd10* mice, RdCVF improved cone function and delayed cone loss slowed the rate of cone cell death and increased the amplitude of the photopic ERG (200). In *rd1* mice, RdCVF delivery by AAV protects cone density and improves length of cone outer segments (201). Together, these results suggest that RdCVF gene therapy has potential for slowing down retinal degenerative disease. However, neurotrophic factors are often pleiotropic and might have other effects on the retina that could question their long-term use.

A final common pathway of all types of RCD is photoreceptor cell death. Using factors that will avoid cell death in a mutation independent manner or by targeting one special toxic mechanism as in class II mutations of RHO is also possible. Several strategies of administration of anti-apoptotic factors (202), heat shock response activator (203) or enhancer (204) , anti-aggregating (205), or neuroprotective (206, 207) molecules and chaperones (208) have been attempted to slow the degeneration and demonstrated partial preservation of photoreceptor morphology and function. However, the effect was again to delay degeneration, enlarging the therapeutic window, but was not consistent since treatment

efficacy was evaluated in comparing treated and untreated animals less than one month after treatment, not allowing predictions on the long-term effect, or after a time point at which photoreceptor degeneration is almost complete. In addition, encouraging results were obtained with the antiepileptic drug valproic acid which was also shown to act as a chaperone molecule of RHO and is currently moving toward clinical trials (NCT01399515) (209). However, due to its side effects, applicability for therapy is questioned (210).

b) **By restoring vision after photoreceptor cell death**

For advanced stages with few or no functional photoreceptors, several more general therapeutic strategies are currently being developed.

(1) **By optogenetic**

Optogenetics refer to a neuromodulation technique which uses light-sensitive proteins as channelrhodopsin and archaebacterial halorhodopsin. These proteins are able to modulate membrane potential and lead to a depolarization or hyperpolarization, depending on the neurons in which they are expressed. In most retinal degenerations, rod photoreceptor degeneration precedes cone photoreceptor and inner retinal degeneration. Optogenetics, by introducing these light-sensitive proteins through gene transfer, can render cells photosensitive and create electric signals in the visual pathway that substitute for the usual input from photoreceptors (211). Optogenetics by using channelrhodopsin, which is a depolarizing channel activated by blue light, on ganglion cells of *rd1* mice restored the ability of the retina to encode light signals and transmit the light signals to the visual cortex (212). However, behavioral responses in the treated animals were lacking. Targeting ganglion cells did not enable to differentiate between ON and OFF pathways. Therefore, optogenetics was also conducted on ON-bipolar cells. By expressing channelrhodopsin or channelrhodopsin-2, under the control of the ON-bipolar cells specific *GRM6* promoter, behavioral responses were obtained on several treated mouse models of RCD (213-215). However, channelrhodopsins present a low light sensitivity and lack of physiological compatibility, since it implies elaborate technical equipment to boost light intensity and photo toxicity risk on the remaining retina. Different second generation microbial opsins were also developed as the ultrasensitive channelrhodopsin-2 calcium translocating channelrhodopsin CatCh (216) and red-actionable channelrhodopsin ReaChr (217), which are under investigation now. Another optogenetic strategy is to target "dormant" cones. Indeed, in some patients, although retinal function is severely affected, cone nuclei can survive late in the disease and could potentially be

"reactivated". Optogenetics by using archaeobacterial halorhodopsin, which is a hyperpolarizing chloride pump, on these remnant cones showed restored phototransduction cascade and light sensitivity, activated cortical circuits and mediated visually guided behaviors in different mouse models of RCD (218). On *ex vivo* human retina, halorhodopsin also reactivated remnant cones, demonstrating the potential of this strategy for clinical applications (218).

(2) With retinal implants

Electronic retinal implants can also be used to replace dead or degenerated photoreceptor cells. These devices capture images and convert them into an electronic signal, which is sent to bipolar cells or ganglion cells. These devices can be cortical (219), based on the stimulation of the visual cortex bypassing the eye, epiretinal (220), directly in contact with the inner retina, or subretinal (221), placed above the RPE. The Argus II retinal prosthesis was the first implanted in human clinical trial (NCT00407602), and has since received commercial use approval for its use as a retinal prosthesis device to treat adult patients with retinal degenerative disorders as late-stage RCD. This device is positioned on the surface of the retina and communicates with ganglion and bipolar cells in response to a light signal received from an external camera. Clinical trials showed a good safety profile with no detrimental effects (222) and improvements in object detection, object counting, object discrimination and direction of movement (223-225). Another type of retinal prosthesis is such which comprises subretinal implants that use the patient's own remnant cones to capture the image without the help of an external video camera. This implant comprises an electronic chip design provided by the Institute for Microelectronics at Stuttgart (IMS) in Germany and was also called alpha-IMS. Clinical trials on alpha-IMS device (NCT0102480) in late-stage RCD patients showed stable visual percepts, restoration of useful vision in daily life, and identification of objects and letter (221, 226). The alpha-IMS device also recently received commercial use approval.

(3) By stem cell therapy

Transplantation of stem cells and progenitors are another therapeutic strategy to restore vision in patients with advanced degenerative retinal disease. Transplanted cells promote then survival of surrounding cells, up regulate antiapoptotic genes and promote new synaptic connections. Photoreceptor precursor cells transplantation has been described to integrate the host retina, differentiate into rod photoreceptors, form synaptic connections and improve visual function (227). Embryonic stem cells (ESC) derived photoreceptor cell precursors

showed also ability to integrate, form outer segments and synaptic connections when implanted into different degeneration mouse models (228). Successful differentiation of neural retina from human induced pluripotent stem cells (hiPSCs) (229) and the generation of an optic cup from human ESC (230) *in-vitro* increased the feasibility of generating an expandable source of cells for human clinical trials. Nevertheless, for retinal dystrophies caused by photoreceptor-specific gene mutations, autologous adult derived cells do not initially appear to be the best source of new retinal neurons, as the genetic mutation will remain. Future treatment for retinal degeneration due to photoreceptor cell loss may also require a combination of gene and cell therapeutic strategies (231).

E. Objectives of the study

1. *GPR179* identification and functional characterization

Genotyping studies of our CNSB cohort revealed that in 13% of cases, mutations in the known genes underlying CSNB were not identified. This was a strong indication that mutations in other genes remain to be discovered, or mutations in unscreened regions, as regulatory elements and introns, might be involved. The objectives of my project were:

1. Identification of a novel gene defect underlying cCSNB
2. Study the expression of this novel gene and the immunolocalization of the respective protein
3. Analyze the physiopathological mechanisms of missense and splice-site mutations of this gene defect.
4. To further investigate the function of the gene, characterize phenotypically a knock-out mouse model for this gene defect.
5. Analyze the location of proteins of the ON-bipolar signaling cascade in the knock-out mouse model.

2. Genome editing approaches applied to Rhodopsin mutations

Currently, there is no treatment of RCD. However, different therapeutic strategies are under investigation. Among them, gene replacement strategy for recessive disorders is promising. Unfortunately, they cannot address dominant negative mutations. We wanted to bring the proof-of-concept of genome editing with endonucleases on *RHO* mutant acting as a dominant negative, on a project funded with European regional development fund (ERDF) of the European Union, and in collaboration with two companies, Collectis (Paris, France) and Iris Pharma (La Gaude, France). In order to test the endonucleases, we used the P23H rat, a frequently investigated model for translational research. The objectives of this project were:

1. Genotypic characterization of the P23H rat for endonuclease design.

2. Structural and functional phenotypic characterization of the P23H rat with non-invasive tools for better monitoring of the endonucleases treated animals.
3. *In vitro* and *ex vivo* testing of the meganucleases.
4. *In vitro*, *ex vivo* and *in vivo* testing of the TALEN.
5. *In vitro* testing of the CRISPR/Cas9 systems.

Material and Methods

A. Preamble

In this part, we will present only the methods that are displayed in the results and which are not described in the published articles of my thesis.

B. GPR179 KO first model characterization

1. Animal Care

All animal procedures were performed according to the Association for Research in Vision and Ophthalmology (ARVO) Statement for the Use of Animals in Ophthalmic and Visual Research. *Gpr179*^{tm1a(KOMP)Mbp} embryonic stem cells (ESC) from agouti C57BL6/N mice were obtained from the Knock-Out Mouse Project (KOMP, Davis, California, USA) Repository (www.komp.org). For the mutant allele, a cassette was inserted upstream of exon 2 of *Gpr179* (Figure 29). The cassette comprised a flippase recognition target (FRT) site followed by the complete lactose operon (*LacZ*) sequence with its termination codon, a cre recombinase recognition (LoxP) site, neomycin gene under the control of the human beta-actin promoter (*neo*), followed by a second FRT site and a second LoxP site. A last LoxP site is localized after exon 2. In this construction, *lacZ* contain a termination codon. Therefore, this construction we used for our mouse leads to a mutated *Gpr179* mRNA. This mRNA, when translated, leads to a mutated protein with amino-acids coded by exon 1 of *Gpr179* but also the entire *lac Z*, and also disruption of GPR179. Moreover, if mice harboring this construction are crossed with mice harboring flippase, *lac Z* and *neo* genes can be removed. Subsequently, if these mice are crossed with mice harboring cre recombinase expressed constitutively or tissue-specifically, *Gpr179* exon 2 can be removed, leading presumably to a premature termination codon and also disruption of the protein.



Figure 29: Construction of the cassette inserted for mutant allele creation. Exons are represented with grey squares. Abbreviations: FRT: flippase recognition target, SA: signal anchor, LacZ: lactose operon, pA: polyadenylation site, neo : neomycin

ESC were injected into blastocysts from non-agouti C57BL6/N females at the Mouse Clinical Institute (Illkirch, France) and chimeras were crossed with non-agouti C57BL6/N mice to obtain non-agouti C57BL6/N mice heterozygous for the *GPR179* mutation. The mice were then crossed twice with C57BL6/J to eliminate the homozygous *rd8* mutation, present in the

C57BL6/N strain. We subsequently rederived the mice (Charles River, Chatillon-sur-Chalaronne, France) in order to obtain a Specific Pathogen Free (SPF) sanitary status. Heterozygous knock-out mice for *Gpr179* were intercrossed (Centre d'Exploration et de Recherche Fonctionnelle Expérimentale CERFE, Evry, France) to produce wild-type (*Gpr179*^{+/+}), heterozygous (*Gpr179*^{+/-}) and mutant (*Gpr179*^{-/-}) offspring. ERG and SD-OCT were performed on 10 *Gpr179*^{+/+}, 12 *Gpr179*^{+/-} and 10 *Gpr179*^{-/-} at 3 months-of-age. Mice were housed in a temperature-controlled room with a 12-hour light/ dark cycle. Fresh water and rodent diet were available *ad libitum*.

2. Genotyping

a) Polymerase chain reaction (PCR) genotyping for *Gpr179*

DNA was extracted from mouse tails with 50 mM NaOH after incubation at 95°C for 30 min. Wild-type and mutant allele were amplified independently using a polymerase (HOT FIREPol, Solis Biodyne, Tartu, Estonia), the same forward primer (m*Gpr179*_Ef, 5' CTGCCCCACAGAATGTTCCCA3') and two specific reverse primers: m*Gpr179*_Er² (5'CACCGCCTCTTTACTCTGCCCA3') for the wild-type allele and m*Gpr179*_Kr (5' GGGCAAGAACATAAAGTGACCCTCC3') for the mutant one and the following program: 10 min at 95°C for denaturation, 30 cycles of 45 sec at 95°C, 1 min at 60°C, and 1 min at 72°C, and for final extension 10 min at 72°C. This gives rise to the following amplicons: PCR using m*Gpr179*_Ef and m*Gpr179*_Er² primers amplifies a product of 146 base pairs (bp) for wild-type allele and no product for mutant allele, PCR using m*Gpr179*_Ef and m*Gpr179*_Kr primers amplifies no product for wild-type allele and a 303 bp product for mutant allele. PCR products were separated by electrophoresis on 1% agarose gels, stained with ethidium bromide, and visualized using a documentation system (Gel Doc XR+ system, Bio-Rad, Hercules, California, USA) (Figure 30).

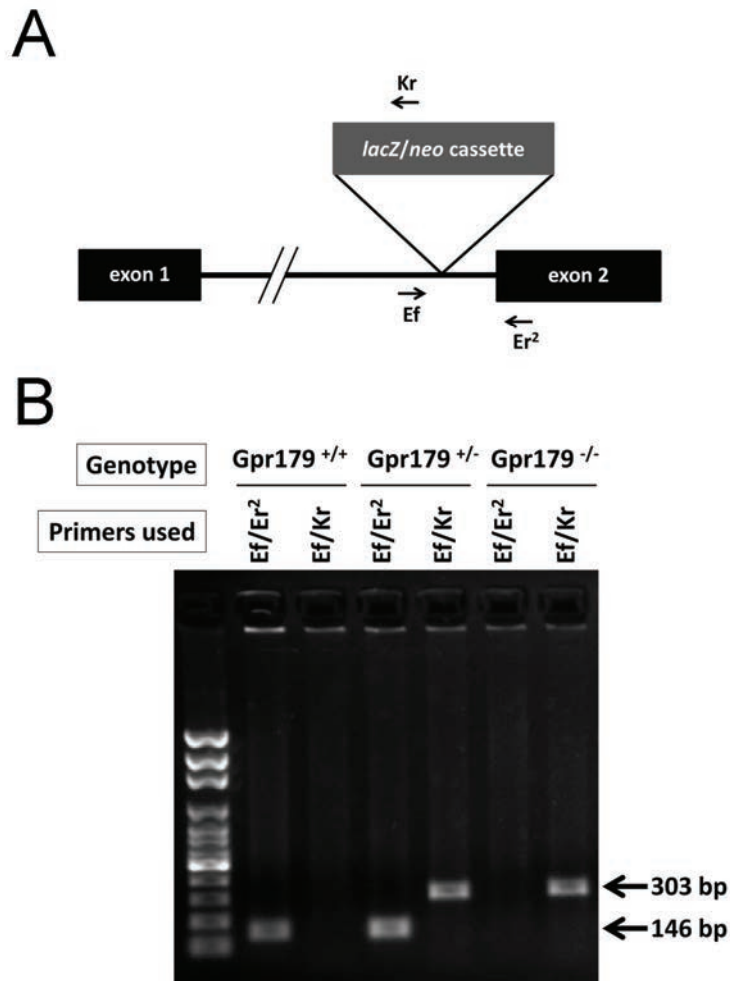


Figure 30: Genotyping of *Gpr179*^{+/+}, *Gpr179*^{+/-} and *Gpr179*^{-/-} mice. (A) Schematic drawing (not to scale) of the knock-out construction: *Gpr179*^{-/-} mice were created by insertion of a cassette comprising lactose operon and neomycin genes (*lacZ/neo* cassette) in intron 1. For genotyping, m*Gpr179*_Ef (Ef) and m*Gpr179*_Er² (Er²) primers were designed to amplify a 146 bp product on wild-type allele. Ef and m*Gpr179*_Kr (Er²) primers were designed to amplify a 303 bp product on knock-out allele. (B) After migration on 1% agarose gel, *Gpr179*^{+/+} exhibits a single fragment at the expected size of 146 bp, *Gpr179*^{-/-} exhibited a single fragment at the expected size of 303 bp and *Gpr179*^{+/-} exhibited both fragments.

b) Genotyping for common mutations found in laboratory mouse strains

The genotyping for the *CRB1*^{rd8}, *PDE6β*^{rd1}, and *GNAT2*^{cpfl3} mutations were carried out as previously described (71).

c) Genotyping for genes with mutations underlying cCSNB

DNA of founder mice were used to sequence the flanking intronic and exonic sequences of *Grm6*, *Gpr179*, *Nyx*, *Lrit3* and *Trpm1* as well as intron 2 of *Grm6* and intron 1 of *Gpr179* as previously described (71).

3. ERG

After overnight dark adaptation, mice were anesthetized with ketamine (80 mg/kg) and xylazine (8 mg/kg). Eye drops were used to dilate the pupils (0.5 % mydriaticum, 5 % neosynephrine). Body temperature was maintained at 37 °C through the use of a heating pad. Contact lens electrodes for mice (Mayo Corporation, Aichi, Japan) were placed on the corneal surface to record ERG. A needle electrode placed subcutaneously in the forehead served as reference and a needle electrode placed in the back served as ground. Recordings were made from both eyes simultaneously. Stimulus presentation and data acquisition were provided by the Espion E² system (Diagnosys LLC, Lowell, MA, USA). Eight levels of stimulus intensity ranging from 0.0003 cd.s/m² to 30 cd.s/m² were used for the dark-adapted ERG recording. Each scotopic ERG response represents the average of five responses from a set of five flashes of stimulation. To isolate cone responses 20-minute light adaptation at 20 cd/m² was performed to saturate rod photoreceptors. For the light-adapted ERG recording, a stimulus intensity of 3 cd.s/m² and six different frequencies ranging from 1 to 10 Hz were used. The light-adapted ERGs were recorded on the same rod pathway-suppressive white background as for the light adaptation. Each cone photopic ERG response represents the average of twenty responses to a set of twenty consecutive flashes.

4. SD-OCT

SD-OCT was performed, immediately after ERG on anesthetized animals, as previously described (71, 232). Briefly, pupils were dilated with eye drops (0.5% mydriaticum, 5% neosynephrine) and SD-OCT images were recorded for both eyes using a spectral domain ophthalmic imaging system (Bioptigen, Inc., Durham, NC, USA). We performed rectangular scans consisting of a 1.4 mm by 1.4 mm perimeter with 1000 A-scans per B-scan with a total B-scan amount of 100. Scans were obtained first while centered on the optic nerve, and then

with the nerve displaced either temporally/nasally or superiorly/inferiorly. SD-OCT scans were exported from InVivoVue as AVI files. These files were loaded into ImageJ (version 1.47; National Institutes of Health, Bethesda, MD) where they were registered using the Stackreg plug-in. If the optic nerve was placed temporally/nasally, three B scans at the level of the nerve were averaged and measurements were performed 500 μ m away from the optic disc, on each side. In the case where the optic nerve was placed superiorly/inferiorly, 3 B-scans placed 500 μ m away from the optic disc were averaged to perform the measurements. We measured the thickness of ONL, OPL, INL and a complex comprising IPL, GCL and NFL that we called IPL+GCL+NFL (Figure 9).

5. Immunohistochemistry

a) Preparation of retinal sections for immunohistochemistry

Mice were killed by CO₂ administration and cervical dislocation. Eyes were removed and prepared as follows. The anterior segment and lens were removed and the eyecup was fixed in ice cold 4% (w/v) paraformaldehyde in 0.12 M phosphate buffer, pH 7.2 for 20 min. The eyecup was washed three times in ice-cold PBS and cryoprotected with increasing concentrations of ice cold sucrose in 0.12 M phosphate buffer, pH 7.2 (10%, 20% for 1 h each and 30% overnight). Finally, the eyecup was embedded in 7.5% gelatin-10% sucrose and frozen in a dry ice-cooled isopentane bath. Sections were cut at a thickness of 20 μ m on a cryostat and mounted onto glass slides (Super-Frost, Thermo Fisher Scientific, Waltham, MA, USA). The slides were air dried and stored at -80°C.

b) Immunostaining of retinal cryosections

Primary antibodies used for immunostaining are listed in Table 1. TRPM1 antibody was a generous gift from Dr Kirill Martemyanov (The Scripps Institute, Jupiter FL, USA). Sections were blocked by incubation at room temperature for 60 min in 0.2% (w/v) gelatin, 0.25% (v/v) Triton X-100 in PBS. Subsequently, the sections were incubated with primary antibodies in blocking solution overnight at room temperature. After washing in 0.1% (v/v) Triton X-100 in PBS, the sections were incubated with secondary antibodies coupled to Alexa Fluor 488 or Cy3 (Jackson ImmunoResearch, West Grove, PA, USA) at a dilution of 1:1000 in the

washing solution for 1.5 h at room temperature. The slides were stained with DAPI and subsequently cover-slipped with mounting medium (Mowiol, Merck Millipore). None of the secondary antibodies used gave significant staining when used without primary antibodies (data not shown).

Table 1: Primary antibodies used in immunohistochemistry.

Antibody	Species	Dilution	Reference
GPR179	mouse	1:200	Ab-887-YOM (Primm, Milan, Italy)
LRIT3	rabbit	1:500	Neuille et al., 2015 (72)
TRPM1	sheep	1:500	Cao et al., 2011 (233)
GRM6	guinea pig	1:200	AP20134SU-N (Acris, Herford, Germany)
RGS11	goat	1:200	sc-9725 (Santa-Cruz, Dallas, Texas, USA)
GNB5	rabbit	1:300	ABIN1451282 (Antibodies Online, Aachen, Germany)
RGS7	rabbit	1:250	sc-28836 (Santa-Cruz)
Lectin PNA 488 conjugate	<i>Arachis hypogaea</i>	1:1000	L21409 (Life Technologies, Thermo Fisher Scientific, Waltham, Massachusetts, USA)
PKC α	mouse	1:1000	P5704 (Sigma-Aldrich, Saint Louis, Missouri, USA)
PKC α	rabbit	1:1000	SAB4502354 (Sigma-Aldrich)
G α	mouse	1:200	MAB3073 (Merck Millipore, Billerica, MA, USA)

c) Image acquisition

Fluorescent staining signals were captured with a confocal microscope (FV1000, Olympus, Hamburg, Germany) equipped with 405, 488, and 559 nm lasers. Confocal images were acquired with a 40x objective compatible with oil (lens NA: 1.3) imaging pixels of 310 nm and 77 nm in width and height for zoom 1 and 4, respectively, and using a 0.52 μ m step size. Each image corresponds to the projection of three optical sections. For figures, brightness and contrast were optimized (ImageJ, version 1.49; National Institutes of Health, Bethesda, MD, USA).

6. Statistical analyses

Statistical analyses were performed using SPSS Statistics (version 19.0, IBM, Armonk, NY, USA). *Post-hoc* comparisons were used to compare the genotypes two by two when the Kruskal-Wallis's test permitted to reject the hypothesis H₀. The number of animals used for the different phenotyping experiments and groups are described above (Animal Care). Results were considered as statistically significantly different if $p < 0.05$.

C. Endonucleases based therapy of Rhodopsin

1. Meganucleases

a) Meganucleases testing in HEK293 cells

(1) Meganucleases design and production

Our collaborator from a private company (Collectis, Paris, France) applied bioinformatics (234) to identify the best hits for meganuclease cut in human *RHO*. Meganucleases were selected after testing on extra-chromosomal substrate on yeast and CHO (Chinese Hamster Ovary) cells (235, 236). Briefly, a strain harbouring the expression vector encoding the meganucleases is crossed with a strain harbouring a reporter plasmid. In the reporter plasmid, a LacZ reporter gene is interrupted with an insert containing the targeted site sequence, flanked by two direct repeats. Upon crossing, if the meganuclease performs a DSB on the targeted site, restoration of a functional LacZ between the two flanking direct repeats occurs and gives a blue color to the strain. Four meganucleases targeting *RHO* and one positive control meganuclease targeting calpain small subunit 1 (*CAPNS1*) were delivered in five plasmids under the control of a CMV promoter (Table 2).

Table 2: Meganucleases and their target.

Meganuclease name	Target localization	Target sequence 5' to 3'
Rho 31	5'UTR	CTCCTCCCTTTTCCTGGATCCTGA
Rho 34	Exon 1	ACTTCCTCACGCTCTACGTCACCG
Rho 7	Exon 4	GTCAGCCACCACACAGAAGGCAGA
Rho 36	Intron 1	CAGATCCCCTAACAGAGAGGAA
CAPNS1	5'UTR	CAGGGCCGCGGTGCAGTGTCCGAC

(2) HEK 293 cells transfection with plasmids expressing meganucleases

Transient transfections of plasmids expressing meganuclease were performed in HEK 293 cells. In 10 cm diameter dish, 1.2×10^6 cells were seeded and cultured in 10 ml DMEM medium with 10% fetal bovine serum and 100 μ g/ml penicillin-streptomycin (all from Life

Technologies). The following day, cells were transfected with 3 µg plasmid using Lipofectamin 2000 (Life technologies). One dish was not transfected and constituted the negative control. One dish was transfected with plasmid expressing CAPNS1 and constituted the positive control. After 6 hours of incubation at 37°C and 5% CO₂, medium was changed. After 48 hours of incubation, cells were harvested and divided in two sets per condition: one was used for gDNA extraction, the other for protein extraction.

(3) gDNA extraction, PCR and deep sequencing

gDNA extraction was performed using a kit (DNAeasy Blood and Tissue kit, Qiagen, Hilden, Germany). Briefly, buffers in this kit allow direct cells lysis followed by selective binding of DNA to a membrane. Centrifugation removes contaminants and enzyme inhibitors. Purified DNA is then eluted in water. Primers were designed to amplify a fragment of 300 to 350 bp flanking each meganuclease-targeted site, in addition with specific adaptors required for deep sequencing (Table 3). Respective PCRs were performed using 50 ng of each treated or non treated gDNA with DNA polymerase (Herculase II, Agilent Technologies, Santa Clara, California, USA) and the primers mentioned above. The amplified products were purified using a gel extraction kit (Qiaquick Gel extraction kit, Qiagen) and sent to a company for deep sequencing (GATC biotech, Konstanz, Germany). Sequences were analyzed by our collaborators (Collectis) using an in-house-program by comparing each sequence to the normal template sequence (237).

Table 3: Primers for deep sequencing. Each primer comprises an adaptor sequence (lowercase) and a sequence specific for the targeted area (capital letters).

Primer name	Primer sequence 5' to 3'
MN_RHO31_For	ccatctcatccctgcgtgtctccgactcagagtaGGTAAGGGGCTGTGTGACGAGA
MN_RHO31_Rev	cctatcccctgtgtgccttggcagtgtagGCATCTGGGAGATTGGGGGTGTT
MN_RHO34_For	ccatctcatccctgcgtgtctccgactcagctacATGCGACGGGTGTGGTACGCAG
MN_RHO34_Rev	cctatcccctgtgtgccttggcagtgtagTGCATCCTGTGGGCCCCGAAGAC
MN_RHO36_For	ccatctcatccctgcgtgtctccgactcagtgccCAGGTGCCCTCCAGCCTCC
MN_RHO36_Rev	cctatcccctgtgtgccttggcagtgtagTGCAATGGCTGCTTCTAGCGTCT
MN_RHO7_For	ccatctcatccctgcgtgtctccgactcagcgagTCTTCACCGTCAAGGAGGTACGGG
MN_RHO7_Rev	cctatcccctgtgtgccttggcagtgtagTGGGACCGAAGTTGGAGCCCTG
MN_CAPNS1_For	ccatctcatccctgcgtgtctccgactcagacagCGAGTCAGGGCGGGATTAAG
MN_CAPNS1_Rev	cctatcccctgtgtgccttggcagtgtagCGAGACTTCACGGTTTCGCC

(4) Western-blot

HEK 293 cells were lysed using a buffer (RIPA lysis buffer, Santa Cruz Biotechnologies, Dallas, Texas, USA) supplemented with 1% (v/v) phenylmethylsulfonyl fluoride (Life technologies), 1% (v/v) sodium orthovanate (Sigma-Aldrich) and 1,5% (v/v) protease inhibitor cocktail (Sigma-Aldrich). Lysates were incubated for 10 min on ice. After centrifugation at 8,000 g at 4°C for 10 min, supernatants were recovered and Bradford quantification was performed. 40 µg of each protein extraction was boiled in Laemmli SDS protein sample buffer (60 mM Tris-Cl pH 6.8, 2% SDS, 10% glycerol, 5% β-mercaptoethanol, 0.01% bromophenol blue). Samples were separated on polyacrylamide gels (Nu-Page Novex Bis-Tris Min Gel 4-12%, Life Technologies) and transferred to a nitrocellulose membrane (iBlot Gel Transfer Stacks Nitrocellulose, Life Technologies) with a dry transfer device (iBlot Gel Transfer, Life technologies). Membranes were blocked for one hour at room temperature in 1X TBS (10mM Tris pH 8.0, 150 mM NaCl,) supplemented with 0.05% (v/v) Tween and 5% (w/v) dry skimmed milk powder (Régilait, Macon, France). Primary antibody incubation was carried out overnight at 4°C, with the following antibodies: polyclonal rabbit anti-I-CreI (Collectis, Romainville) for meganuclease recognition and mouse anti-tubulin (Abcam, Cambridge, Massachusetts, USA) for loading control at dilution of 1:20,000 and 1:100 respectively. Goat anti-rabbit-HRP coupled and goat anti-mouse-HRP coupled secondary antibodies were used both at 1:1000 dilution for detection (Jackson ImmunoResearch, West Grove, Pennsylvania, USA). In between and after antibody incubations, membranes were extensively washed in TBS-T (TBS containing 0.05% Tween-20). Western-blots were visualized using an enhanced chemiluminescence method (ECL Plus Western Blotting reactif, Amersham, GE Healthcare, Little Chalfont, United Kingdom).

b) Meganucleases testing on newborn rat retinal explants

(1) Meganuclease cloning into pCIG vector

Our industrial collaborator (Collectis) delivered the meganucleases in pCLS plasmids (Collectis), in which the meganucleases were flanked by AttB sequences. These sequences are used in Gateway technology (Life technologies), which is a recombination system between different acceptor and donor vectors comprising specific sequences and using specific recombinases. Subcloning of MN RHO 31 in pDONR221 vector (Life technologies) was

performed using a recombinase (LR clonase, Life technologies). Final cloning in pCIG vector (Addgene, Cambridge, Massachusetts, USA) was performed using another recombinase (BP clonase, Life technologies) and allowed expression of the meganuclease under the control of a CAG promoter and Green Fluorescent Protein (GFP) after an internal ribosome entry site (IRES).

(2) Retinal explants electroporation and culture

Sprague Dawley OFA pregnant rats were purchased from Charles River France (Saint Germain Nuelles, France). Retinal explants dissection and electroporation were performed in collaboration with Dr Olivier Goureau, Institut de la Vision. Newborn rats were sacrificed by decapitation and eyeballs were carefully removed and collected in a dish filled with D-PBS (Life technologies). Under a binocular dissection microscope, circumferential incision around the limbus was performed to remove the anterior part of the eye. Vitreous was carefully removed. Subsequently, retina was extracted from the sclera and RPE. Newborn rat retinas electroporation were conducted on eight half retinas per condition as previously described (238). Cloning of all the genes we wanted to express in the same cell was not possible. Therefore, we performed co-electroporation of several plasmids, assuming that if one plasmid expressing one of the genes was electroporated, the probability that the other plasmids expressing the others genes were co-electroporated was high (239). To validate the cutting efficiency of the meganuclease we used three conditions: i/ no meganuclease, ii/ RHO 31 meganuclease and iii/ Baat meganuclease (Table 4). In all conditions a plasmid expressing the cofactor Trex was included, which has been shown to increase NHEJ when DSB occurs (240). In addition pCIG_IRES_GFP was used in the negative and positive control to document GFP transfection efficiency. The positive control represented a plasmid overexpressing a Baat meganuclease, which has been proven to efficiently target mouse and rat *Baat* (Personal communication, Collectis) (Table 4).

Table 4: Plasmids used for each electroporation conditions.

Condition	Plasmids
Negative control	“empty” pCIG_IRES_GFP + plasmid expressing Trex cofactor
RHO 31 meganuclease	pCIG_MNRHO31_IRES_GFP + plasmid expressing Trex cofactor
Positive control	“empty” pCIG_IRES_GFP + pCLS_MNBaat + plasmid expressing Trex cofactor

Central regions of retinas were dissected in CO₂-independent medium (Life technologies) and half of this region was submerged in 1 mg/ml for each plasmid. The outer layer of the retinas were facing the negative electrode and subjected to five electric pulses at 30 V with 50 ms duration and 950 ms intervals using an electroporator (CUY21 Single Cell BEX; Nepa Gene, Sonidel, Ichikawa-city, Japan) and bath platinum plate electrodes on Petri dishes (CUY520P5, Nepa Gene). Subsequently, explants were placed on polycarbonate filter discs (Dominique Dutscher, Brumath, France). Cultures were maintained up to 4 days in DMEM/F12 medium with 10 mM HEPES, pH 7.0 containing 5% fetal calf serum and 100 µg/ml penicillin-streptomycin (Life Technologies). After three days, 50% of the initial medium was changed to not induce acute pH modifications.

(3) Cell dissociation and FACS

Explants were detached from filters and dissociated with trypsin as previously described (238). Dissociated cells were resuspended in PBS 10% FBS and fluorescence-activated cell sorting (FACS) sorted for GFP positive cells by a platform (“Plateforme de cytométrie en flux”, Hopital Saint-Antoine, Paris, France)

(4) DNA extraction and Surveyor mutation detection kit assay

gDNA extraction was performed as previously described (see above Part C1a3). Primers were designed to amplify a fragment of 300 to 350 bp centered on the meganuclease-targeted site (Table 5). PCRs including each targeted site were performed using a DNA polymerase (Herculase II, Agilent Technologies) and 50 ng of gDNA from each treatment condition. Amplicons were purified using a kit (Nucleospin extract II, Qiagen).

Table 5: PCR primers for the loci targeted by the meganucleases.

Meganuclease	Primer name	Primer sequence 5' to 3'
RHO 31	ex1_rat_For	GTATTAGTGTGATATCTCCCG
RHO 31	ex1_rat_Rev	CCCAGTCCTTTCACACCCCCT
Baat	Baat_For	GTGGAGCTGGCCAGGAGATGC
Baat	Baat_Rev	GGTCTTCCAGCCTACACCCTGC

Cutting efficiency was controlled using a kit (Transgenomic Surveyor Mutation Detection Kit for Standard Gel Electrophoresis, Fisher Scientific, Thermo Fisher Scientific). Briefly, this kit uses a mismatch-specific DNA endonuclease (Cel-1 endonuclease) to scan for mutations and polymorphisms in heteroduplex DNA. Targeted site PCR is hybridized by heating and cooling the mixture to form hetero- and homoduplexes. Indeed, endonucleases used for genome editing are not totally efficient. Thus, targeted site PCR comprises non mutated strands and mutated strands with different mutations due to different indels occurring during NHEJ. Therefore, PCR products are inhomogeneous. During the cooling, single strand PCR products reanneal and when one strand is mutated and the other not (or not with the same mutation), a mismatch appears. Then, the annealed heteroduplex/homoduplex mixture is treated with Cel-1 endonuclease, which recognizes mismatches and induces DSBs. DNA fragments are analyzed by agarose gel electrophoresis. The formation of new cleavage products, due to the presence of one or more mismatches, is indicated by the presence of additional fragments. gDNA non treated with endonucleases we use for therapy constitutes the negative control. A mixture of one wild-type plasmid PCR and one mutated plasmid PCR constitute the positive control of the kit.

Concretely, 20 μ L of purified PCR product corresponding to 1 μ g of DNA was heated in 0.1 M KCl at a temperature of 95°C during 10 min, and cooled to 25°C to anneal single-strand DNA. These PCR products were then purified again using the same kit (Nucleospin extract II, Qiagen), and digested in a digestion buffer (10 mM TrisHCl pH 8.2, 1 mM MgSO₄, 30 mM KCl and 0.05% Triton) with 2 μ L Cel1 nuclease and 2 μ L enhancer (Transgenomic Surveyor Mutation Detection Kit for Standard Gel Electrophoresis) during 20 min at 42°C. Digested PCR were run immediately on an agarose gel for interpretation. Positive control of the kit was performed following manufacturer instructions.

2. TALEN

a) TALENs

Our industrial partner (Cellestis) delivered a TALEN targeting the c.68G>A, p.Pro23His mutation (P23H TALEN) on the mouse transgene (232) and a negative control targeting human *RAG* (170) (*RAG* TALEN) with no target in rat genome (Table 6).

Table 6: TALENs and their recognition site. TALEN right and left subunits recognition sites are represented with capital letters, cutting site is represented with lowercase.

TALEN	Target sequence 5' to 3'
P23H TALEN	TTTTTATGTGCCCTTCTccaacgtcacaGGCGTGGTGCGGAGTCA
RAG TALEN	TATATTTAAGCACTTATatgtgtgtaacaggtATAAGTAACCATAAACA

Both TALENs were delivered in two pCLS plasmids each, expressing each one TALEN subunit (left or right) under the control of the human elongation factor-1 alpha 1 promoter (pEF1 α 1) (Figure 31).

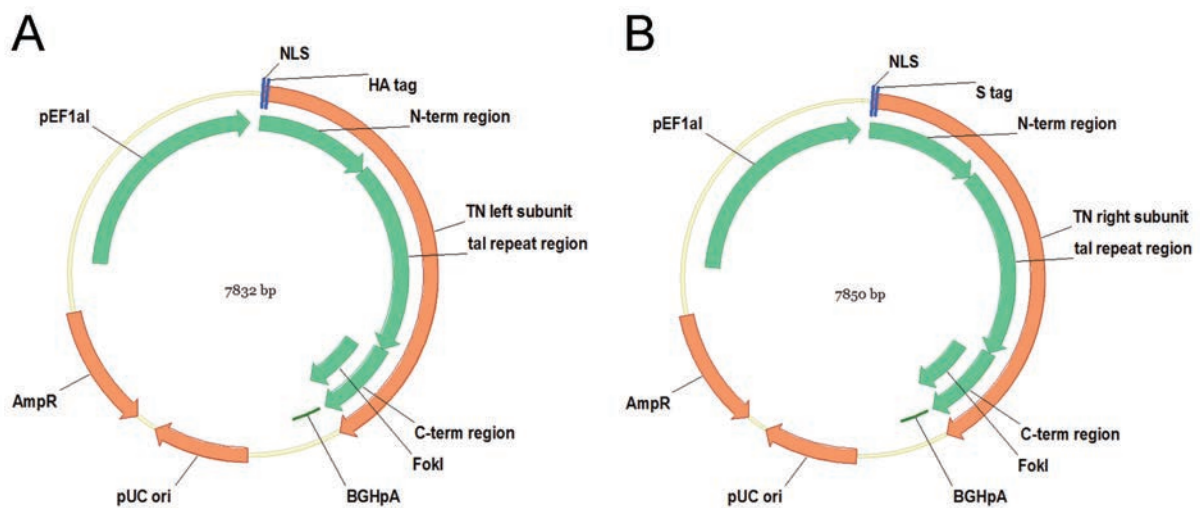


Figure 31: Schematic representation of plasmids coding for TALEN left (A) and right (B) subunits. Abbreviations: NLS: nuclear localization signal, HA-tag: human influenza hemagglutinin tag, S tag: pancreatic ribonuclease A tag, TN: TALEN, N-term: amino-terminus, C-term: carboxy-terminus, BGHpA: bovine growth hormone polyadenylation, pUC ori: pUC plasmide's origine of replication, AmpR: ampicillin resistance gene, pEF1 α 1: human elongation factor-1 alpha 1 promoter.

b) Animals

Transgenic homozygous P23H-1 rats were obtained from the laboratory of Matthew LaVail (241) and were crossed with wild-type albino Sprague-Dawley rats purchased from a company (Janvier, Le Genest-Saint-Isle, France) to produce hemizygous P23H-1 rats.

c) TALENs testing on P23H newborn rat retinal explants

Because of high repetitions in the sequence coding for TALEN subunits and the absence of available restriction enzyme site in the vector delivered by our industrial partner (Collectis), subcloning into the vector expressing GFP, to control efficient delivery, was not possible. We therefore co-electroporated the two plasmids expressing the TALEN subunits and the pCIG plasmid expressing GFP into 10 half retinal explants from P23H rat at P0 (Table 7), assuming that if one plasmid was electroporated (GFP), the probability that the other plasmids (TALEN) were co-electroporated was high (239). Retinal explant electroporation from hemizygous P23H-1 P0 rats was performed in collaboration with Dr Olivier Goureau, Institut de la Vision, as described before (see above Part C1b2).

Table 7: Plasmids used for each electroporation conditions.

Condition	Plasmids
No TN	“empty” pCIG_IRES_GFP
P23H TALEN	“empty” pCIG_IRES_GFP + pCLS expressing P23 TALEN right subunit + pCLS expressing P23 TALEN left subunit
RAG TALEN	“empty” pCIG_IRES_GFP + pCLS expressing RAG TALEN right subunit + pCLS expressing RAG TALEN left subunit

Cultures were maintained for 5 days and cell dissociation, FACS sorting and DNA extraction were performed as described above (see Parts C1a3, C1b3 and C1b4). For the PCR, primers were designed to specifically amplify a 670 bp fragment centered on the P23H TALEN-targeted site in the mouse mutated transgene of the P23H-1 rat (232) (Table 8). Primers were controlled for their specificity by performing a PCR on positive control wild-type mouse gDNA and negative control wild-type rat gDNA. As expected, we obtained a specific fragment of 670 bp using wild-type mouse gDNA and no fragment using wild-type rat gDNA on PCR product analysis in 1% agarose gel (data not shown).

Table 8: Primers for TALEN testing.

Primer name	Primer sequence 5' to 3'
ex1_mouse_For	ACCGATGTACCTTGGCCC
ex1_mouse_Rev	CCCTTTCGTGGCCCCTTGGC

PCR of the locus targeted by the P23H TALEN was performed using primers in Table 9 and as described above (see Part C1b4). Direct Sanger sequencing confirmed that the amplified fragment is, as expected, the mouse mutated transgene of P23H-1 rat and not the wild-type rat *Rho* (data not shown). Subsequently, the cutting efficiency using a kit (Transgenomic Surveyor Mutation Detection Kit for Standard Gel Electrophoresis, Fisher Scientific) was performed as described above (see Part C1b4).

d) TALENs encapsidation

rAAV cargo capacity is limited to 4,7 kb gene packaging capacity (138). Therefore, each TALEN subunit, with a size of 3.2 kb, was cloned into a separate viral vector AAV (serotype 2.1). Subsequently, encapsidation was performed into Y733F capsid mutant AAV2/8 (AAV8-Y733F) that express TALEN under the control of a ubiquitous promoter CMV (pCMV), and into 2YF capsid mutant AAV2/9 (AAV9-2YF) that express TALEN under the control of a rod photoreceptor specific promoter RHO (pRHO) in collaboration with Dr Deniz Dalkara's team, Institut de la Vision (143). Both viruses had previously been reported for their mouse rod photoreceptor tropism (242, 243). Control viruses expressing GFP were also produced. Viruses were tittered and were all at concentrations superior to 10^{14} viral genome (vg)/ml.

e) TALENs testing on P23H P21 rat retinal explants

(1) TALEN testing by P21 rat retinal explants infection

P21 P23H rats' retinas were dissected in D-PBS with calcium (Life technologies) and subsequently placed on polycarbonate filter discs (Dominique Dutscher) to culture in neurobasal medium (Life technologies) supplemented with 2 mM L-glutamine (Sigma-Aldrich), 1X B-27 supplement (Life technologies) and 10 μ g/ml gentamicine (Life technologies). The following day, retinal explants were infected with AAV8-Y733F-pCMV at 4.6×10^{14} vg/ml expressing TALEN subunit (5 μ l per AAV) by pipetting the virus between the explants and the polycarbonate filter discs (Table 9).

Table 9: Infection of P23H P21 retinal explants.

Condition	Virus
Not infected	No virus
GFP	2.3 10 ¹² vg AAV8-Y733F-pCMV-GFP
P23H TALEN	2.3 10 ¹² vg AAV8-Y733F-pCMV-P23HTALEN-right subunit +2.3 10 ¹² vg AAV8-Y733F-pCMV-P23HTALEN-left subunit
RAG TALEN	2.3 10 ¹² vg AAV8-Y733F-pCMV-RAGTALEN-right subunit +2.3 10 ¹² vg AAV8-Y733F-pCMV-RAGTALEN-left subunit

Three retinas were infected per condition. GFP fluorescence of retinal explants infected with AAV8-Y733F expressing GFP under the control of pCMV was monitored by epifluorescence microscopy. Best conditions for an efficient infection of retinal explants were determined to five days of incubation. Subsequently, after five days of incubation, two retinal explants per condition were used for gDNA extraction and one for immunohistochemistry. Cell dissociation, gDNA extraction, PCR and cutting efficiency evaluation using a kit (Transgenomic Surveyor Mutation Detection Kit for Standard Gel Electrophoresis, Fisher Scientific) were performed as described above (see Parts C1b3 and C1b4).

(2) Immunohistochemistry

Retinal explants were fixed at room temperature in 4% (w/v) paraformaldehyde in 0.12 M phosphate buffer, pH 7.2 for 20 min, washed three times in ice-cold PBS, cryoprotected overnight with 30% sucrose in 0.12 M phosphate buffer, pH 7.2, embedded in 7.5% gelatin-10% sucrose and frozen in a dry ice-cooled isopentane bath. Sections were cut at a thickness of 20 µm on a cryostat and mounted onto glass slides and stored at -80°C. Immunostaining was performed as previously described (see Part A5b) with chicken anti-GFP primary antibody (Abcam) and goat anti-chicken Alexa Fluor 488 secondary antibody (Life technologies).

f) TALENs testing *in vivo*

Two modes of delivery were chosen for TALENs administration: subretinally on P21 P23H rat with AAV8-Y733F injections, allowing TALEN to be directly in contact with targeted rod photoreceptors, and systematically on 1-day-old (P1) P23H rat with AAV9-2YF intracardiac injection, allowing the infection of a larger surface of the retina (Figure 32). GFP expressing viruses injections were performed to check the retinal delivery.

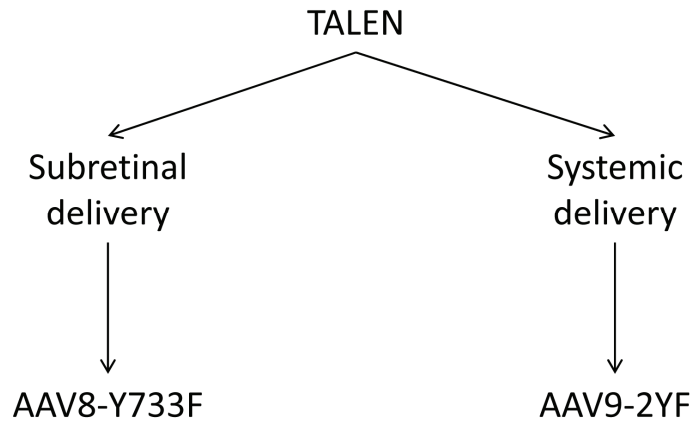


Figure 32: Delivery modes and used serotype for TALEN *in vivo* testing.

(1) by subretinal injections

(a) P21 subretinal injections

Subretinal injections were performed in collaboration with Dr Deniz Dalkara’s team. P23H P21 rats’ right eyes were injected subretinally with AAV8-Y733F-pCMV at 1×10^{14} vg/ml expressing TALEN subunit (1 μ l per AAV) under direct observation aided by a dissecting microscope (Table 10). The other eye remained uninjected.

Table 10: Subretinal injections of P23H P21 rats right eyes.

Condition	Virus
Not infected	Not injected
GFP	1×10^{11} vg AAV8-Y733F-pCMV-GFP
P23H TALEN	1×10^{11} vg AAV8-Y733F-pCMV-P23HTALEN-rightsubunit + 1×10^{11} vg AAV8-Y733F-pCMV-P23HTALEN-leftsubunit
RAG TALEN	1×10^{11} vg AAV8-Y733F-pCMV-RAGTALEN-rightsubunit + 1×10^{11} vg AAV8-Y733F-pCMV-RAGTALEN-leftsubunit

Four rats were injected for GFP condition. For the other conditions, twelve rat right eyes were injected.

(b) Fluorescence observation

Color and fluorescence fundus imaging of AAV8-Y733F-pCMV-GFP injected rat right eyes were performed 14 days after injection with a retinal imaging microscope (Micron II, Phoenix, Pleasanton, California, USA).

(c) Phenotype monitoring

Functional and structural retinal phenotype of P23H TALEN and *RAG* TALEN treated animals and 12 age-matched wild-type Sprague Dawley rats was documented by ERG recording and SD-OCT respectively at 1, 2, 3 and 6 months after injections as previously described (232).

(2) by systemic injections

(a) P1-old rat systemic injections

P23H P1 rats were injected intracardiacally with AAV9-2YF-pRHO at 3.4×10^{14} vg/ml expressing TALEN subunit (5 μ l per AAV) (Table 11). Fourteen rats were injected per conditions, except for GFP expressing virus injections which were conducted on 4 rats. Fourteen littermates were not injected and constituted the uninfected negative controls.

Table 11: Systemic injections of P23H P1 rats.

Condition	Virus
Not infected	Not injected
GFP	1.7×10^{12} vg AAV9-2YF-pRHO-GFP
P23H TALEN	1.7×10^{12} vg AAV9-2YF-pRHO-P23HTALEN-right subunit + 1.7×10^{12} vg AAV9-2YF-pRHO-P23HTALEN-left subunit
<i>RAG</i> TALEN	1.7×10^{12} vg AAV9-2YF-pRHO- <i>RAG</i> TALEN-right subunit + 1.7×10^{12} vg AAV9-2YF-pRHO- <i>RAG</i> TALEN-left subunit

(b) Fluorescence observation

Color and fluorescence fundus imaging of AAV9-2YF-pRHO-GFP injected rats' eyes were performed 14 days after injection.

(c) Phenotype monitoring

Functional and structural retinal phenotype of P23H TALEN, *RAG* TALEN treated animals and 14 age-matched untreated wild-type Sprague Dawley rats was documented by ERG recording and SD-OCT respectively at 1, 2, 3 and 6 months after injections as previously described (232).

g) TALENs testing *in vitro* on P23H rat embryonic fibroblasts

(1) P23H rat embryonic fibroblasts isolation

Rat embryonic fibroblasts (REF) isolation from P23H E15 rats (P23H REF) was performed in collaboration with Dr Olivier Goureau, Institut de la Vision (244). Uteri isolated from 15 days pregnant rat were washed with phosphate-buffered saline (PBS) without Mg^{2+} and Ca^{2+} . Head and visceral tissues were removed from isolated embryos. Remaining bodies were washed in fresh PBS, minced using a pair of scissors, transferred into a 0.1 mM trypsin/1 mM EDTA solution (Life technologies, 5 ml per embryo), incubated at 37°C for 30 min and pipetted up and down until tissue was dissociated. Cells were transferred into a new tube and 45 ml of REF medium was added (DMEM supplemented with 10% FBS, 1% non essential amino-acids, 1% penicillin-streptomycin (all from Life technologies) and 2 mM L-glutamine (Sigma)). Cells were collected by centrifugation ($200 \times g$ for 10 min at 20°C) and resuspended in 10 ml fresh REF medium and cultured on 10 cm dishes at 37°C with 5% CO₂. The following day, medium was changed. Cells were frozen at the second passage and were used at the fifth passage for the whole study.

(2) Fluorescent marker cloning into TALEN's subunits expressing plasmids

We cloned a construction comprising an IRES followed by GFP or iRFP coding sequences in pAAV2.1 vectors (see above Part 2d) expressing TALEN subunit under the control of pCMV with a new commercially available technique which is based on homologous recombination (InFusion cloning kit, Clontech, Takara Bio group, Shiga, Japan). Briefly, a PCR of IRES_GFP or IRES_iRFP was performed on plasmids comprising these constructions. A Hind III digestion was performed on pAAV2.1 vectors to linearize them and insertion of the PCR was performed using the kit instructions. For note, primers used for PCR of IRES_GFP or IRES_iRFP comprised a 5' tail homologous with sites framing Hind III digestion site on pAAV2.1 vectors, allowing insertion of the PCR on the Hind III site by homologous recognition. Thus, we obtained pAAV2.1 vectors expressing, under the control of pCMV, P23H or RAG TALEN right subunit followed by an IRES and iRFP (Figure 33 A) and pAAV2.1 vectors expressing, under the control of pCMV, P23H or RAG TALEN left subunit followed by an IRES and GFP (Figure 33 B).

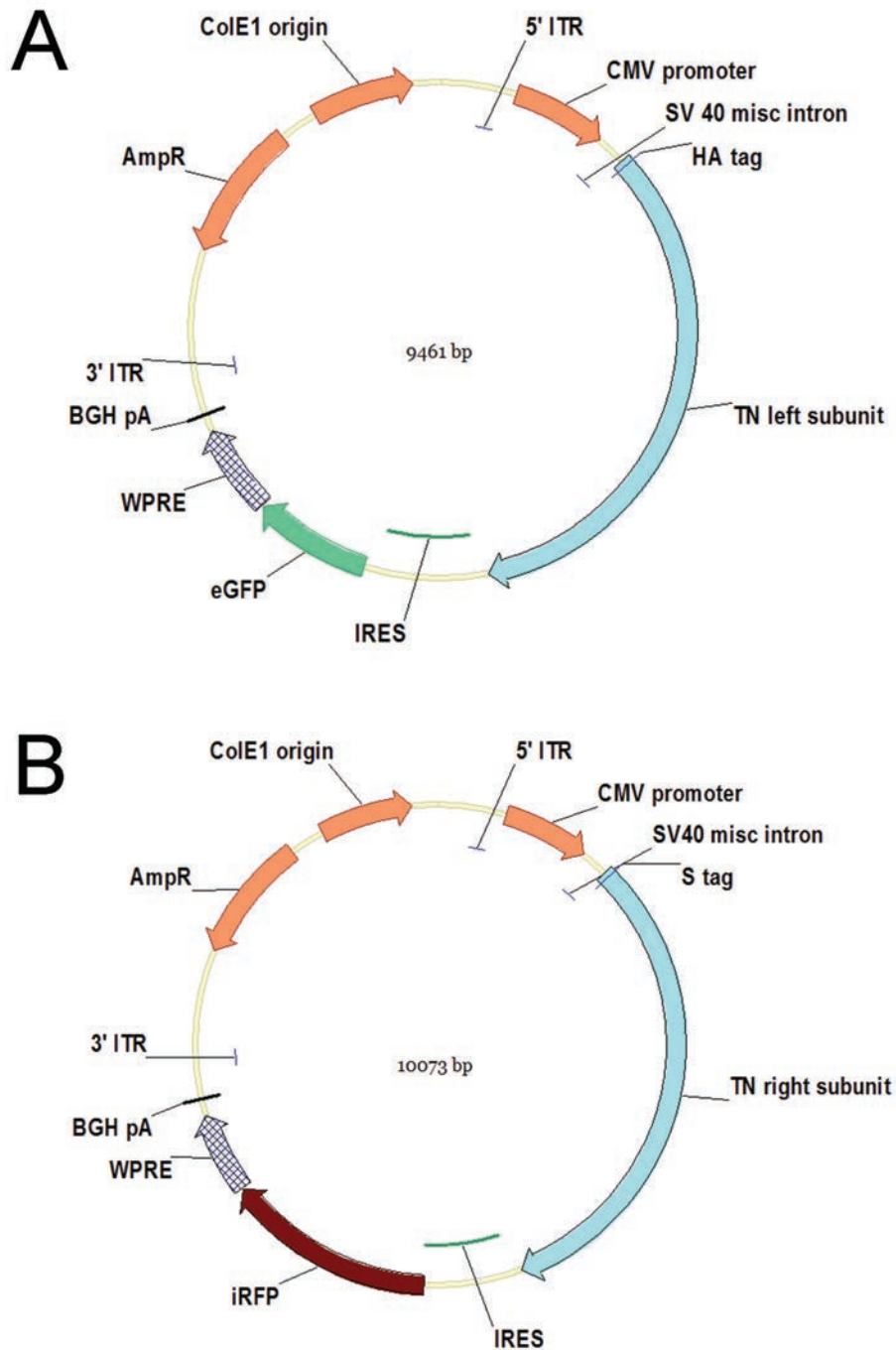


Figure 33: Schematic representation of the plasmids constructed for TALENs testing in P23H REF. (A) Plasmid expressing under a pCMV TALEN left subunit, an IRES and GFP. (B) Plasmid expressing under a pCMV TALEN right subunit, an IRES and iRFP.

(3) TALEN nucleofection into P23H REF

TALEN subunit-expressing plasmids (8 μ g of each) were nucleofected in $2 \cdot 10^6$ P23H REF per condition using a nucleofection device (Nucleofector 4D, Lonza, Basel, Switzerland), a mammal fibroblast nucleofection solution (V4XP-3012, Lonza) and the EH-100 program on

the device (Table 12). Cells were plated in 10 cm dishes in REF medium. The following day, medium was changed. After 3 days of incubation, cells were harvested and FACS sorted for GFP and iRFP positive cells. gDNA extraction, PCR and cutting efficiency evaluation using a kit (Transgenomic Surveyor Mutation Detection Kit for Standard Gel Electrophoresis, Fisher Scientific) were performed as described above (see Parts C1b3 and C1b4).

Table 12: Nucleofection conditions of P23H REF.

Condition	Plasmid
Not nucleofected	No plasmid
P23H TALEN	8 μ g pAAV2.1_pCMV_P23HTALEN-right subunit_IRES_iRFP +8 μ g pAAV2.1_pCMV_P23HTALEN-left subunit_IRES_GFP
RAG TALEN	8 μ g pAAV2.1_pCMV_RAGTALEN-right subunit_IRES_iRFP +8 μ g pAAV2.1_pCMV_RAGTALEN-left subunit_IRES_GFP

Results

A. GPR179 identification and functional characterization

This work led to one patent, two publications and two paper presentations and one poster presentation in national and international meetings. They are listed below.

Patent:

1. Zeitz, C., Audo, I., **Orhan, E.**, Bujakowska, K., and Sahel, J.A. (2013). Mutations of the gpr179 gene in congenital stationary night blindness (Europe: Google Patents).

Publications:

1. Audo, I., Bujakowska, K.*, **Orhan, E.***, Poloschek, C. M., Defoort-Dhellemmes, S., Drumare, I., Kohl, S., Luu, T. D., Lecompte, O., Zrenner, E., Lancelot, M. E., Antonio, A., Germain, A., Michiels, C., Audier, C., Letexier, M., Saraiva, J. P., Leroy, B. P., Munier, F. L., Mohand-Said, S., Lorenz, B., Friedburg, C., Preising, M., Kellner, U., Renner, A. B., Moskova-Doumanova, V., Berger, W., Wissinger, B., Hamel, C. P., Schorderet, D. F., De Baere, E., Sharon, D., Banin, E., Jacobson, S. G., Bonneau, D., Zanlonghi, X., Le Meur, G., Casteels, I., Koenekoop, R., Long, V. W., Meire, F., Prescott, K., de Ravel, T., Simmons, I., Nguyen, H., Dollfus, H., Poch, O., Leveillard, T., Nguyen-Bacharvet, K., Sahel, J. A., Bhattacharya, S. S., and Zeitz, C. (2012). Whole-exome sequencing identifies mutations in GPR179 leading to autosomal-recessive complete congenital stationary night blindness. *Am J Hum Genet* 90, 321-330. * These authors contributed equally to the work

2. **Orhan, E.**, Prezeau, L., El Shamieh, S., Bujakowska, K. M., Michiels, C., Zagar, Y., Vol, C., Bhattacharya, S. S., Sahel, J. A., Sennlaub, F., Audo, I., and Zeitz, C. (2013). Further insights into GPR179: expression, localization, and associated pathogenic mechanisms leading to complete congenital stationary night blindness. *Invest Ophthalmol Vis Sci* 54, 8041-8050.

Paper presentations:

1. Zeitz, C., Bujakowska, K., **Orhan, E.**, Sahel, J.-A., Bhattacharya, S.S., Audo, I., and CSNB study group. (2012). Mutations In A Novel Gene, GPR179 Lead To Autosomal Recessive Complete Congenital Stationary Night Blindness. Association for Research in Vision and Ophthalmology (CZ, Fort Lauderdale, USA).

2. **Orhan, E.**, and Zeitz, C. (2013). Elucidation of physiopathological mechanisms of GPR179. 2nd Annual meeting of the GDR-3545: RCPG-Physio-Med (EO, Illkirch, France).

Poster presentation:

1. **Orhan, E.**, Prezeau, L., Michiels, C., Vol, C., Sahel, J.A., Audo, I., and Zeitz, C. (2013). Elucidation of physiopathological mechanisms of GPR179. Association for Research in Vision and Ophthalmology (EO, Seattle, USA).

1. Whole exome sequencing identifies mutations in *GPR179* leading to autosomal recessive complete stationary night blindness

Genotyping studies of our CNSB cohort, comprising 160 patients, revealed that in 13% of cases, mutation(s) in the known genes underlying CSNB were not identified. This was a strong indication that mutations in other genes remain to be discovered, or mutations in unscreened regions, as regulatory elements and introns, might be involved.

Whole-exome sequencing in cCSNB patients lacking mutations in the known genes led to the identification of a homozygous missense mutation (c.1807C>T [p.His603Tyr]) in one consanguineous autosomal-recessive cCSNB family and a homozygous frameshift mutation in *GPR179* (c.278delC [p.Pro93Glnfs*57]) in a simplex male cCSNB patient. Additional screening with Sanger sequencing of 40 patients identified three other cCSNB patients harboring additional allelic mutations (c.376G>C [p.Asp126His] and c.1364G>A [p.Gly455Asp] missense mutations, c.598C>T [p.Arg200*] nonsense mutation, c.984delC [p.Ser329Leufs*4] and c.479_501del [Leu160Profs*38] frame shift mutations and c.17841G>A [r.spl?] splice-site mutation) in *GPR179*. *GPR179* codes for an orphan G protein-coupled receptor, which was functionally not characterized. Furthermore, indirect expression analysis on transcriptomic data of whole retina from wild-type and *rd1* mouse model with progressive rod photoreceptor degeneration suggest that *GPR179* is expressed in the inner nuclear layer.

Whole-Exome Sequencing Identifies Mutations in *GPR179* Leading to Autosomal-Recessive Complete Congenital Stationary Night Blindness

Isabelle Audo,^{1,2,3,4,5,39} Kinga Bujakowska,^{1,2,3,39} Elise Orhan,^{1,2,3} Charlotte M. Poloschek,⁶ Sabine Defoort-Dhellemmes,⁷ Isabelle Drumare,⁷ Susanne Kohl,⁸ Tien D. Luu,⁹ Odile Lecompte,⁹ Eberhart Zrenner,¹⁰ Marie-Elise Lancelot,^{1,2,3} Aline Antonio,^{1,2,3,4} Aurore Germain,^{1,2,3} Christelle Michiels,^{1,2,3} Claire Audier,^{1,2,3} Mélanie Letexier,¹¹ Jean-Paul Saraiva,¹¹ Bart P. Leroy,^{12,13} Francis L. Munier,¹⁴ Saddek Mohand-Saïd,^{1,2,3,4} Birgit Lorenz,¹⁵ Christoph Friedburg,¹⁵ Markus Preising,¹⁵ Ulrich Kellner,¹⁶ Agnes B. Renner,¹⁷ Veselina Moskova-Doumanova,^{1,2,3} Wolfgang Berger,^{18,19,20} Bernd Wissinger,⁸ Christian P. Hamel,²¹ Daniel F. Schorderet,²² Elfride De Baere,¹² Dror Sharon,²³ Eyal Banin,²³ Samuel G. Jacobson,²⁴ Dominique Bonneau,²⁵ Xavier Zanlonghi,²⁶ Guylene Le Meur,²⁷ Ingele Casteels,²⁸ Robert Koenekoop,²⁹ Vernon W. Long,³⁰ Françoise Meire,³¹ Katrina Prescott,³² Thomy de Ravel,³³ Ian Simmons,³⁰ Hoan Nguyen,⁹ Hélène Dollfus,^{34,35} Olivier Poch,⁹ Thierry Léveillard,^{1,2,3} Kim Nguyen-Ba-Charvet,^{1,2,3} José-Alain Sahel,^{1,2,3,4,5,36,37} Shomi S. Bhattacharya,^{1,2,3,5,38} and Christina Zeitz^{1,2,3,*}

Congenital stationary night blindness (CSNB) is a heterogeneous retinal disorder characterized by visual impairment under low light conditions. This disorder is due to a signal transmission defect from rod photoreceptors to adjacent bipolar cells in the retina. Two forms can be distinguished clinically, complete CSNB (cCSNB) or incomplete CSNB; the two forms are distinguished on the basis of the affected signaling pathway. Mutations in *NYX*, *GRM6*, and *TRPM1*, expressed in the outer plexiform layer (OPL) lead to disruption of the ON-bipolar cell response and have been seen in patients with cCSNB. Whole-exome sequencing in cCSNB patients lacking mutations in the known genes led to the identification of a homozygous missense mutation (c.1807C>T [p.His603Tyr]) in one consanguineous autosomal-recessive cCSNB family and a homozygous frameshift mutation in *GPR179* (c.278delC [p.Pro93Glnfs*57]) in a simplex male cCSNB patient. Additional screening with Sanger sequencing of 40 patients identified three other cCSNB patients harboring additional allelic mutations in *GPR179*. Although, immunohistological studies revealed *Gpr179* in the OPL in wild-type mouse retina, *Gpr179* did not colocalize with specific ON-bipolar markers. Interestingly, *Gpr179* was highly concentrated in horizontal cells and Müller cell endfeet. The involvement of these cells in cCSNB and the specific function of *GPR179* remain to be elucidated.

¹Institut National de la Santé et de la Recherche Médicale, U968, Paris 75012, France; ²Université Pierre et Marie Curie (UPMC Paris 06), UMR_S 968, Institut de la Vision, Paris 75012, France; ³Centre National de la Recherche Scientifique, UMR_7210, Paris 75012, France; ⁴Centre Hospitalier National d'Ophthalmologie des Quinze-Vingts, INSERM-DHOS CIC 503, Paris 75012, France; ⁵Institute of Ophthalmology, University College of London, London EC1V 9EL, UK; ⁶Department of Ophthalmology, University of Freiburg, Freiburg 79106, Germany; ⁷Laboratoire Neurosciences Fonctionnelles et Pathologies, CNRS FRE 2726, Hôpital Roger Salengro, Lille 59037 Cedex, France; ⁸Molecular Genetics Laboratory, Institute for Ophthalmic Research, Department for Ophthalmology, University of Tuebingen, Tuebingen 72076, Germany; ⁹Institut de Génétique et de Biologie Moléculaire et Cellulaire, Illkirch 67404 Cedex, France; ¹⁰Centre for Ophthalmology, Department for Ophthalmology, University Tuebingen, Tuebingen 72076, Germany; ¹¹IntegraGen, Genopole CAMPUS 1 bat G8 FR-91030, Evry 91000, France; ¹²Center for Medical Genetics, Ghent University, Ghent 9000, Belgium; ¹³Department of Ophthalmology, Ghent University, Ghent 9000, Belgium; ¹⁴Unit of Oculogenetics, Jules Gonin Eye Hospital, Lausanne 1004, Switzerland; ¹⁵Department of Ophthalmology, Justus-Liebig-University Giessen, Universitaetsklinikum Giessen and Marburg GmbH Giessen Campus, Giessen 35385, Germany; ¹⁶AugenZentrum Siegburg, Siegburg 53721, Germany; ¹⁷Department of Ophthalmology, University Medical Center Regensburg, 93053, Regensburg, Germany; ¹⁸Institute of Medical Molecular Genetics, University of Zurich, Zurich 8057, Switzerland; ¹⁹Neuroscience Center Zurich, University and ETH Zurich, Zurich 8057, Switzerland; ²⁰Center for Integrative Human Physiology, University of Zurich, Zurich 8057, Switzerland; ²¹National Centre for Genetic Sensory Diseases, Montpellier 34295 Cedex 05, France; ²²IRO-Institut de Recherche en Ophthalmologie and Faculté des Sciences du Vivant, Ecole Polytechnique Fédérale de Lausanne, University of Lausanne, Sion 1950, Switzerland; ²³Department of Ophthalmology, Hadassah-Hebrew University Medical Center, Jerusalem 91120, Israel; ²⁴University of Pennsylvania, Scheie Eye Institute, Philadelphia 19104, PA, USA; ²⁵UMR Institut National de la Santé et de la Recherche Médicale, U771-CNRS6214 et CHU, Angers 49000, France; ²⁶Service Exploration Fonctionnelle de la Vision et Centre basse vision de la Clinique Sourde, Nantes 44000, France; ²⁷CHU-Hotel Dieu, Service d'Ophthalmologie, Nantes 44093, France; ²⁸Department of Ophthalmology, University Hospitals, Leuven 3000, Belgium; ²⁹McGill Ocular Genetics Laboratory, McGill University, Montreal, QC H3H 1P3, Canada; ³⁰St James's University Hospital, Leeds LS9 7TF, UK; ³¹Hopital Des Enfants Reine Fabiola, Brussels 1020, Belgium; ³²Yorkshire Regional Genetics Service, Department of Clinical Genetics, Chapel Allerton Hospital, Leeds LS7 4SA, UK; ³³Centre for Human Genetics, Leuven University Hospitals, Leuven 3000, Belgium; ³⁴Centre de Référence pour les Affections Rares en Génétique Ophthalmologique, Hôpitaux Universitaires de Strasbourg, Strasbourg 67000, France; ³⁵Laboratoire de Physiopathologie des Syndromes Rares Hérités, équipe avenir INSERM, Faculté de Médecine, Université de Strasbourg, Strasbourg 67000, France; ³⁶Fondation Ophthalmologique Adolphe de Rothschild, Paris 75019, France; ³⁷Académie des Sciences-Institut de France, Paris 75006, France; ³⁸Department of Cellular Therapy and Regenerative Medicine, Andalusian Molecular Biology and Regenerative Medicine Centre (CABIMER), Isla Cartuja, Seville 41902, Spain

³⁹These authors contributed equally to this work

*Correspondence: christina.zeitz@inserm.fr

DOI 10.1016/j.ajhg.2011.12.007. ©2012 by The American Society of Human Genetics. All rights reserved.

Congenital stationary night blindness (CSNB) comprises a group of genetically and clinically heterogeneous retinal disorders. The associated genes encode proteins that are confined to the phototransduction cascade or are important in retinal signaling from photoreceptors to adjacent bipolar cells.¹ Most of the patients with mutations in these genes show a typical electrophysiological phenotype characterized by an electronegative waveform of the dark-adapted bright flash electroretinogram (ERG), in which the amplitude of the b-wave is smaller than that of the a-wave.² This so-called Schubert-Bornschein-type ERG response can be divided in two subtypes, incomplete CSNB ([icCSNB] CSNB2A [MIM 300071], CSNB2B [MIM 610427]) and complete CSNB ([cCSNB] CSNB1A [MIM 310500], CSNB1B [MIM 257270] and CSNB1C [MIM 613216]).³ icCSNB has been characterized by both a reduced rod b-wave and substantially reduced cone responses because of both ON- and OFF-bipolar cell dysfunction, whereas the complete type is associated with a drastically reduced rod b-wave response because of ON-bipolar cell dysfunction but largely normal cone b-wave amplitudes.⁴ icCSNB has been associated with mutations in *CACNA1F* [MIM 300110], *CABP4* [MIM 608965], and *CACNA2D4* [MIM 608171], whereas cCSNB has been associated with mutations in *NYX* [MIM 300278], *GRM6* [MIM 604096], and *TRPM1* [MIM 603576]. So far more than 280 mutations have been identified in these genes by us and others via direct sequencing of candidate genes (unpublished data) or microarray analysis.⁵ Prevalence studies determined that *CACNA1F*, *NYX*, and *TRPM1* mutations leading to incomplete and complete CSNB occur more frequently (unpublished data). Genotyping studies of our CSNB cohort, comprising 160 patients, reveal that in ~13% of cases mutations in known genes underlying CSNB were not identified. This is a strong indication that mutations in other genes remain to be discovered or that mutations in unscreened regions, that is regulatory elements and introns, might be involved. Mutations in many genes leading to CSNB have been identified through a candidate gene approach by comparing the human phenotype to similar phenotypes observed in knockout or naturally occurring animal models.^{6–13} The bottleneck of this approach is the size of a cohort and the identification of the “right” patient harboring the mutation in such a candidate gene. Novel techniques that use massively parallel sequencing of all human exons have recently been successful in identifying mutations in novel genes in other heterogeneous diseases such as Leber congenital amaurosis.^{14,15} To rapidly identify the missing mutations in our CSNB cohort after whole-exome enrichment (IntegraGen, Evry, France), we sequenced four exomes from a consanguineous autosomal-recessive cCSNB family (that included parents who were first cousins and two of three affected children) and from a sporadic male cCSNB patient of Portuguese origin (Figure S1A and S2, available online, shows the typical cCSNB ERG of patient CIC02756). One index patient from each family was previously excluded

by Sanger sequencing for mutations in *GRM6* and *TRPM1*. In addition, the sporadic male patient was also excluded for mutations in *NYX*. Research procedures were conducted in accordance with institutional guidelines and the Declaration of Helsinki. Prior to genetic testing, informed consent was obtained from all patients and their family members. Ophthalmic examination included best corrected visual acuity, slit lamp examination, funduscopy, perimetry, full-field (ERG) incorporating the International Society for Clinical Electrophysiology of Vision (ISCEV) standards,¹⁶ fundus autofluorescence (FAF), and optical coherence tomography (OCT) (the extent of investigation depended on the referring center). Exons of DNA samples were captured with in-solution enrichment methodology (SureSelect Human All Exon Kits Version 3, Agilent, Massy, France) with the company's biotinylated oligonucleotide probe library (Human All Exon v3 50 Mb, Agilent). Each genomic DNA was then sequenced on a sequencer as paired-end 75 bases (Illumina HISEQ, Illumina, San Diego, USA). Image analysis and base calling were performed with Real Time Analysis (RTA) Pipeline version 1.9 with default parameters (Illumina). The bioinformatic analysis of sequencing data was based on a pipeline (Consensus Assessment of Sequence and Variation [CASAVA] 1.8, Illumina). CASAVA performs alignment, calls the SNPs based on the allele calls and read depth, and detects variants (SNPs and indels). Genetic variation annotation was performed by an in-house pipeline (IntegraGen) and results were provided per sample or family in tabulated text files. After excluding variants observed in dbSNP 132, data were further filtered to keep only variants in coding and splice regions that were present in a homozygous state in the affected children and in a heterozygous state in the parents from the consanguineous family. This allowed us to reduce the number of variants from 5,901 indels to 1 and from 66,621 SNPs to 7. The observed deletion represented a repeat deletion in the penultimate exon of *VSIG10* and was therefore unlikely to be a disease-causing variant. However, three missense mutations predicted to be probably or possibly damaging were identified in three different genes (*KIAA0753*, *CRHR1* [MIM 122561], and *GPR179* [G protein-coupled receptor 179]) on chromosome 17. The p.Arg518Cys variant found in *KIAA0753* was considered unlikely to be disease causing because this arginine residue is not evolutionarily conserved. On the other hand, both the p.Arg259Gln substitution in *CRHR1* and the p.His603Tyr in *GPR179* affected highly evolutionary conserved amino acid residues (Figure 1 and Figure S1B). Interestingly, the other cCSNB patient (CIC02756), also studied by whole-exome sequencing, carried a homozygous 1 bp deletion, resulting in a frameshift and premature termination (p.Pro96Glnfs*57) in exon 1 of *GPR179*. These data strongly support the finding that mutations in *GPR179* lead to CSNB found in both families (Table 1). For the c.1807C>T (p.His603Tyr) mutation, both parents were found to be heterozygous because the nucleotide A was read 11 times and 7 times in the father and mother,

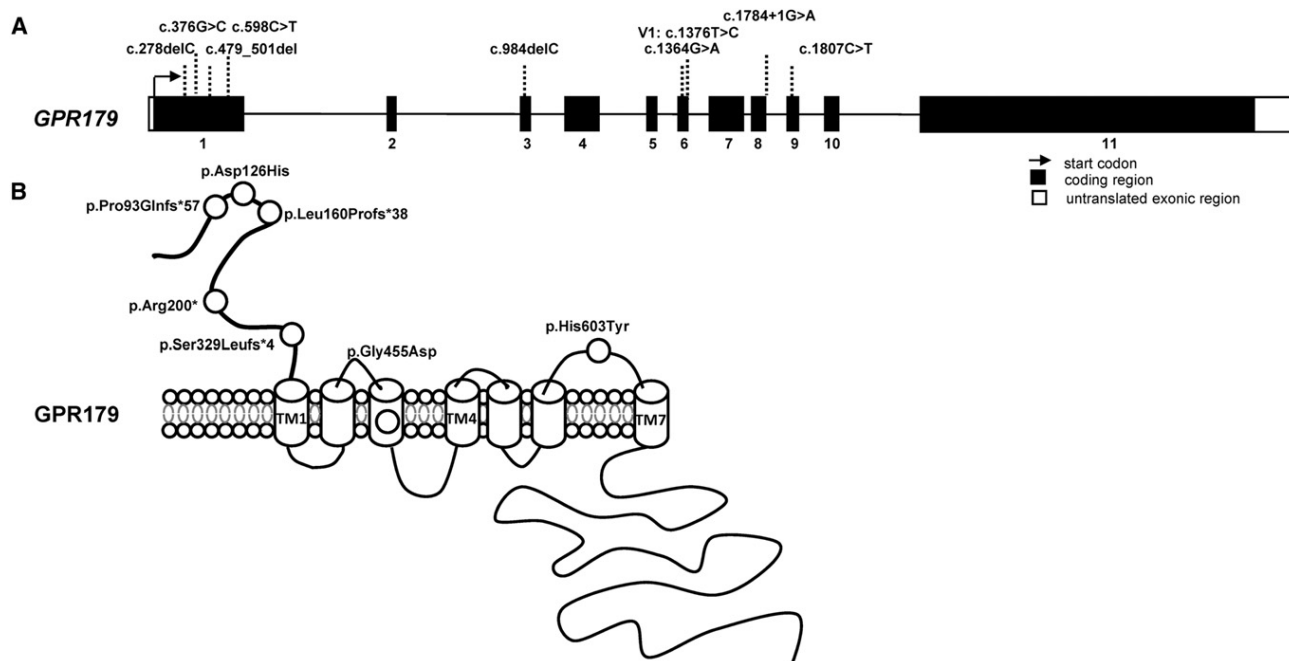


Figure 1. *GPR179* mutations in cCSNB.

(A) *GPR179* structure containing 11 coding exons (NM_001004334.2). Different mutations identified in cCSNB patients are depicted. (B) The specific domains for *GPR179* were estimated by a prediction program (UniProtKB/Swiss-Prot).

respectively, whereas the G was found 13 times and 11 times, respectively (reverse strand). The two affected children (patients CIC3308 and CIC4005) showed 26 times and 14 times the nucleotide A. The c.278delC deletion detected in the sporadic cCSNB patients was detected 22 times; 20 other reads of unknown type were also indicated. This might be due to the fact that at this position multiple Cs are present, and thus different reads might occur. Sanger sequencing confirmed the mutations in the index patients of each family. Both mutations cosegregated with the phenotype within the respective family (Figure S1A). In addition, next-generation sequencing data were used to analyze homozygous regions in the affected siblings (patients CIC03308 and CIC4005) of the consanguineous family. The analysis revealed seven major homozygous regions (>0.5 Mb), which were exclusively present on chromosome 17. *GPR179* was present in the second largest homozygous region (10.8 Mb), whereas *CRHR1* was present in a smaller region (1.3 Mb). In the other sporadic cCSNB patient, *GPR179* was not present in any major homozygous region; this can be explained by the fact that the parents were only distant cousins.

We screened 40 CSNB patients (cCSNB and unclassified CSNB) of various origins and from different clinical centers in Europe, the United States, Canada, and Israel by using Sanger sequencing for 27 fragments covering the 11 coding exons and flanking intronic regions of *GPR179* (NM_001004334.2). These were amplified by PCR in the presence of 1.5 mM MgCl₂ at an annealing temperature of 60°C. For one of the fragments a specific solution (solution S, 3×, fragment exon 11 m, Hot Fire Polymerase, Solis

BioDyne, Tartu, Estonia, and primers; Table S1) was used. The PCR products were sequenced with a sequencing mix (BigDyeTerm v1.1 CycleSeq kit, Applied Biosystems, Courtabœuf, France), analyzed on an automated 48-capillary sequencer (ABI 3730 Genetic analyzer, Applied Biosystems), and the results interpreted by applying SeqScape software (Applied Biosystems). We detected three additional cCSNB patients who carried compound heterozygous disease-causing mutations (Table 1). The mutation spectrum identified herein comprises missense, splice-site, and nonsense mutations and deletions. None of these changes were present in control chromosomes (≥366 chromosomes). For patients whose family members could be investigated, the mutations cosegregated with the cCSNB phenotype, and the genotypes were indicative of an autosomal-recessive mode of inheritance (Table 1 and Figure S1A). Missense mutations were predicted to be pathogenic by PolyPhen and SIFT programs and were also found to affect evolutionarily conserved amino acid residues (Figure S1B). On the basis of all of the above evidence, we conclude that mutations in *GPR179* lead to cCSNB. Interestingly, we found four cCSNB patients with no mutations in *GRM6*, *TRPM1*, *NYX*, or *GPR179*, indicating that mutations in additional genes probably remain to be identified to explain these cases of cCSNB. In addition, a few rare variants (Table S2) in *GPR179* were identified in patients screened by Sanger sequencing and were classified as variants of unknown pathogenicity because only one mutation was observed or they did not affect conserved amino acid residues. The frequencies of *GPR179* polymorphisms found in our patients are provided in Table S3.

Table 1. Patients with Pathogenic *CPRI79* Mutations

Patient Number	Relationship to Index Patient	Sex	Mutations Excluded in Following Genes	Ethnicity and Location	Exon	Nucleotide Exchange (RNA or Protein Effect)	Allele State	Control Alleles (Mutated or WT)	Phenotype Index
C1C02756 ^a	-	male	NYX, GRM6, TRPM1	Portuguese-French; Paris, France	1	c.278delC (p.Pro93Glnfs*57)	homozygous	0/366	cCSNB, high myopia, nystagmus, moderate decreased visual acuity
C1C02757	unaffected father	male	-		1	c.278delC (p.Pro93Glnfs*57)	heterozygous		
C1C02758	unaffected mother	female	-		1	c.278delC (p.Pro93Glnfs*57)	heterozygous		
C1C03631	-	female	GRM6, TRPM1	French; Lille, France	1, 3	c.376G>C (p.Asp126His), c.984delC (p.Ser329Leufs*4)	compound heterozygous	0/366 and 0/372	cCSNB, high myopia, strabismus, micronystagmus
7699	-	female	GRM6, TRPM1	Tübingen, Germany	1, 6	c.479_501del (Leu160Profs*38), c.1364G>A (p.Gly455Asp)	compound heterozygous	0/366 and 0/384	cCSNB, strabismus, minimal rotational nystagmus, normal visual field
7692	unaffected father	male	-		1	c.479_501del (p.Leu160Profs*38)	heterozygous		
7697	unaffected mother	female	-		6	c.1364G>A (p.Gly455Asp)	heterozygous		
Y1049	-	female	GRM6, TRPM1	Lille, France	1, IVS8	c.598C>T (p.Arg200*), c.1784+1G>A (rspl?)	compound heterozygous	0/378 0/378	cCSNB
Y1166	unaffected father	male	GRM6, TRPM1		IVS8	c.1784+1G>A (rspl)	heterozygous		
Y1167	unaffected mother	female	GRM6, TRPM1		1	c.598C>T (p.Arg200*)	heterozygous		
Y1048	affected sister	female	GRM6, TRPM1		1, IVS8	c.598C>T (p.Arg200*), c.1784+1G>A (rspl)	compound heterozygous		
26985 ^{b,c}	-	male	GRM6, TRPM1	Lebanon; Freiburg, Germany	9	c.1807C>T (p.His603Tyr)	homozygous	0/366	cCSNB, left exotropia, until age of 2 nystagmus
C1C03306	father	male	-		9	c.1807C>T (p.His603Tyr)	heterozygous		ERG b-wave were slightly reduced for high flash strength
C1C03307	unaffected mother	female	-		9	c.1807C>T (p.His603Tyr)	heterozygous		-
C1C03308	affected sister	female	-		9	c.1807C>T (p.His603Tyr)	homozygous		cCSNB
C1C04005	affected sister	female	-		9	c.1807C>T (p.His603Tyr)	homozygous		cCSNB, visual acuity reduced

CSNB mutations are annotated according to the recommendation of the Human Genome Variation Society, with nucleotide position +1 corresponding to the A of the translation-initiation codon ATG in the cDNA nomenclature RefSeq NM_001004334.2.

^a The parents of C1C02756 are far cousins (Figure S1A).

^b The diagnostic for GRM6 for this patient was performed in Zurich, Switzerland.

^c For this family consanguinity has been reported (Figure S1A).

To date no information is available on the functional characterization of *GPR179*. To predict the protein structure and the influence of the mutations identified herein, we created homology models. The human *GPR179* sequence (UniProtKB identifier Q6PRD1) was used as a probe for similarity searches in the UniProtKB database with the use of the BlastP program.^{17,18} In total, more than 100 metazoan sequences (excluding fragments) that were annotated or predicted as *GPR179*- or *GPR158*-like were highlighted and aligned with a customized version of the PipeAlign program.^{19–21} *GPR179* codes for a protein with 2,367 amino acids that can be divided into four main regions corresponding to a small signal peptide (positions 1–25), the N-terminal extracellular region (position 26–381), the seven transmembrane (7TM)-spanning region (position 382–628), and the intracellular C-terminal region (position 629–2367) (Figure 1B). Sequence analysis predicted that the N-terminal extracellular region contains a calcium-binding EGF-like domain (position 278–324), whereas the C-terminal intracellular region is characterized by the presence of a short motif centered on the sequence CPWE, which is repeated at least 22 times in the *GPR179*-related proteins. *GPR179* proteins are present in all vertebrates and are closely related to *GPR158* and *GPR158*-like proteins. It is noteworthy that the major differences between *GPR179* and the closely related *GPR158* proteins rely on the absence of the calcium-binding EGF-like domain at the N-terminal part and a reduced number of CPWE motifs (up to three) in all *GPR158* homologs. Interestingly, three other molecules, the regulator of G protein signaling 9 (RGS9 [MIM 604067]), the retinal rod rhodopsin-sensitive cGMP 3,5-cyclic phosphodiesterase subunit gamma (PDE6G [MIM 180073]) and the retinal cone rhodopsin-sensitive cGMP 3,5-cyclic phosphodiesterase subunit gamma (PDE6H [MIM 601190]) share the same protein motif CPWE. These molecules have been implicated in the inhibition of the G protein or amplification of the signal in the phototransduction cascade. Mutations in those genes lead to different retinal disorders, including bradyopsia [MIM 608415],²² rod-cone dystrophy [MIM 613582],²³ and cone dystrophy [MIM 610024].²⁴

Based on their seven transmembrane domain regions, both proteins (*GPR179* and *GPR158*) belong to the glutamate receptor or class C GPCR proteins. This class includes, among others, metabotropic glutamate receptors (GRMs), two γ -aminobutyric acid B receptor (GABABR), the calcium-sensing receptor (CASR), the sweet and umami taste receptors and various orphan receptors.²⁵ The different deletions and the early termination mutation in *GPR179* identified in our patients are located in exons 1 and 3 and are predicted to lead to nonsense-mediated mRNA decay, which might result in the absence of a protein product. Alternatively, if a protein is formed, only the first extracellular part would be present but would lack all transmembrane domains of *GPR179*, resulting in truncated protein (Figure 1B). The missense alterations

(p.Asp126His, p.Gly455Asp, and p.His603Tyr) affect evolutionarily conserved amino acid residues, which are predicted to be part of the first extracellular domain, within the third transmembrane domain, and in the last extracellular domain (Figure 1B). Multiple alignment analysis of more than 100 metazoan *GPR179*-related sequences shows strict conservation of the asparagine at position 126 (Asp126), the glycine at position 455 (Gly455), and the histidine at position 603 (His603) in vertebrate sequences. PolyPhen and SIFT programs annotated the three amino acid substitutions to be possibly pathogenic.²⁶ These programs use conservation among species and homologs to predict the pathogenic character of a mutation. In addition, an inductive logic programming prediction web server²⁷ predicted p.Gly455Asp and p.His603Tyr to be pathogenic. This program uses available 3D structures to predict the influence of a mutation. To date, no model of the 3D structure of the amino acid residues <300 is available, therefore the possible pathogenic effect of p.Asp126His could not be predicted with this program. To further gain insight into the deleterious effect of the missense mutations, we generated 3D models of the seven transmembrane (7TM)-spanning region of the human wild-type *GPR179* and of the two altered proteins (p.Gly455Asp and p.His603Tyr) by homology modeling with MODELER software (Figure 2).²⁰ Two known 7TM templates, the bovine taste receptor (PDB 1F88) and the squid rhodopsin (PDB 2ZIIY), were used to construct the homology models. For each 3D model construction, ten homology models were constructed, and the models with the best normalized discrete optimized potential energy (DOPE) score were selected.²⁸ The homology 3D models were visualized and analyzed by means of the SM2PH-db,²⁸ and figures were constructed with PyMOL software (version 0.99). Multilevel characterization of the mutants (physico-chemical changes and structural modifications induced by the substitution, as well as functional and structural features related to the mutated position) can be visualized and analyzed by the MSV3d web server. Structural analysis of the 3D homology models based on the squid RHO 3D model (2ZIIY) localized the His603 in the external loop bridging the sixth and seventh transmembranes, whereas the Gly455 is localized within the third transmembrane helix, which is part of a binding pocket (Figures 1B and 2). Our homology model predicts that the amino acid exchange p.Gly455Asp introduces a long negatively charged side chain that might point toward the cavity of the binding pocket. This suggests that the phenotypic consequences observed for this mutation might be related to some steric constraints hampering the normal functioning of the receptor. The steric constraints in respect to the p.His603Tyr mutation are less obvious. However, strong conservation across species and homologs are indicative of an important role for the histidine at position 603. Although, for the moment, the 3D structure of the amino acid residues <300 of *GPR179* is not available, we know from other receptors that the N

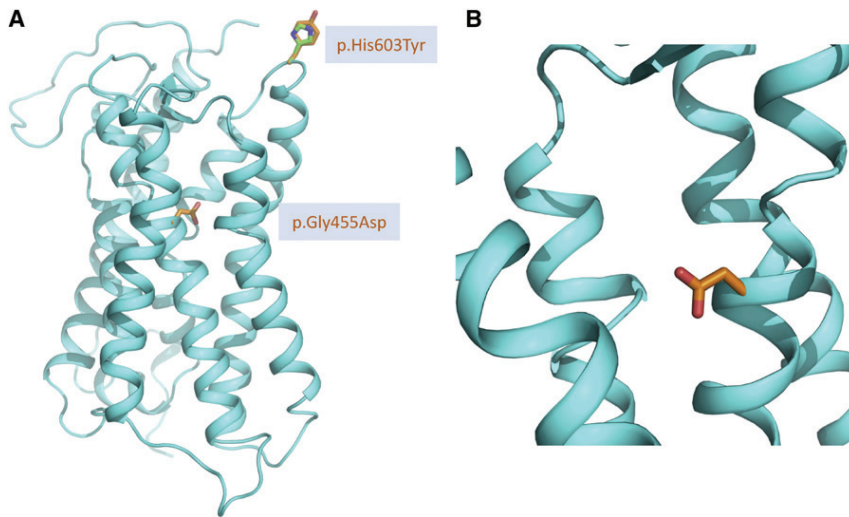


Figure 2. 3D Model of the Transmembrane Region of GPR179

(A) 3D homology model based on the 3D model of the wild-type squid rhodopsin (2Z1Y). Wild-type Gly455 and His603 residues are indicated in green and the mutated Asp455 and Tyr603 in orange. (B) Superimposition of 3D models of the wild-type residues and the Gly455Asp alteration (aspartate in orange).

terminus of such proteins is important for ligand binding, and thus the p.Asp126His mutation might be associated with loss of this binding. On the other hand, the amino acids that are mutated in our patients also might be important for structural properties of the protein in the endoplasmic reticulum. Thus a misfolded protein is likely to be excluded from the strictly regulated transport to the membrane. Similar findings were observed for mutations in *GRM6*, identified in cCSNB patients. Mutated metabotropic glutamate receptor 6 could not reach the membrane, leading to cCSNB.²⁹ Further functional analysis of the mutant variants is needed to determine whether these mutations lead to downregulation of the GPR179 transcript, trafficking problems, abolishment of ligand binding, or interactions with other proteins involved in signal transmission from photoreceptors to the adjacent bipolar cells.

As mentioned above, little is known about the structure and function of GPR179. However, an EST profile is available (Unigene database) and shows a restricted pattern of expression in the human eye, heart, and brain. Furthermore, transcriptomic data of whole retina from *rd1* mice revealed increased expression of *GPR179* compared to the expression in wild-type mice starting from postnatal day 12 (Figure 3). The *rd1* mouse, carrying *Pde6b* mutations, is a naturally occurring model with progressive rod photoreceptor degeneration, leading to a complete loss of all rods by postnatal day 36, and preserved inner retina.³⁰ This would suggest that *GPR179* is expressed in the inner nuclear layer of the retina. Interestingly, *Nyx*, another gene with mutations leading to cCSNB, shows a similar expression profile in the *rd1* mouse (Figure 3).

Real-time PCR experiments with two different primer sets (Table S4) confirmed the expression of *GPR179* in human retina (commercially available cDNA from Clontech, Saint-Germain-en-Laye, France), giving a signal of $\Delta C_T = 13.46$ ($C_{T\text{GPR179}} = 30.03$) in relation to beta-actin (*ACTB* [MIM 102630]) ($C_{T\text{ACTB}} = 16.57$) (primers Table S4). Sanger sequencing of the amplified RT-PCR products

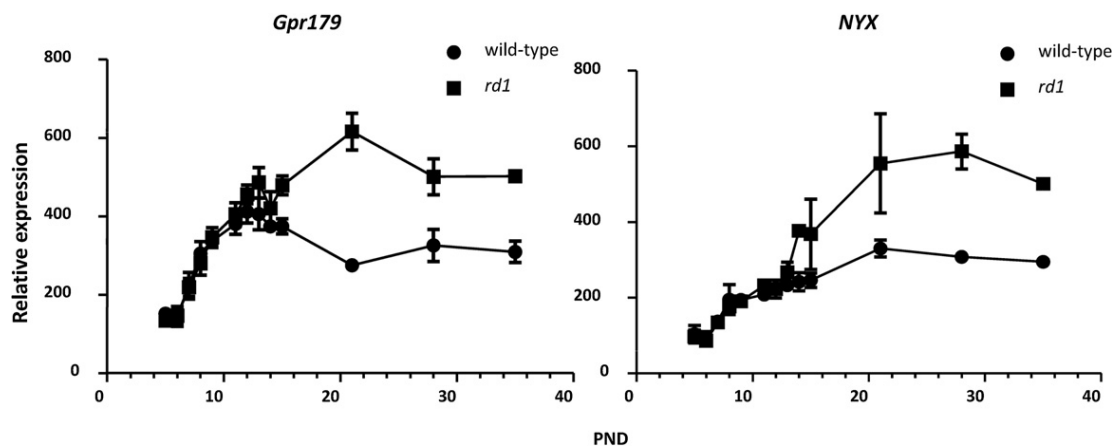


Figure 3. Indirect Expression Analysis of Gpr179 in rd1 and Wild-Type Mice

Expression of *Gpr179* (1459268_at) compared to the expression of *Nyx* (1446344_at, a known molecule expressed in the inner nuclear layer, also implicated in cCSNB) during rod degeneration in the *rd1* mouse. Neural retinas from *rd1* and wild-type mice on identical genetic backgrounds⁴⁷ were hybridized to the mouse genome 430 2.0 array (Affymetrix, High Wycombe, UK). The expression profiles are similar from postnatal day (PND) 5 to PND12. Thereafter, the expression of *Gpr179*, as well as *Nyx*, increases in the *rd1* retina. This phenomenon correlates temporally with the loss of rod photoreceptor cells and is likely due to the unaffected inner retinal cells in the *rd1* specimen at this age.

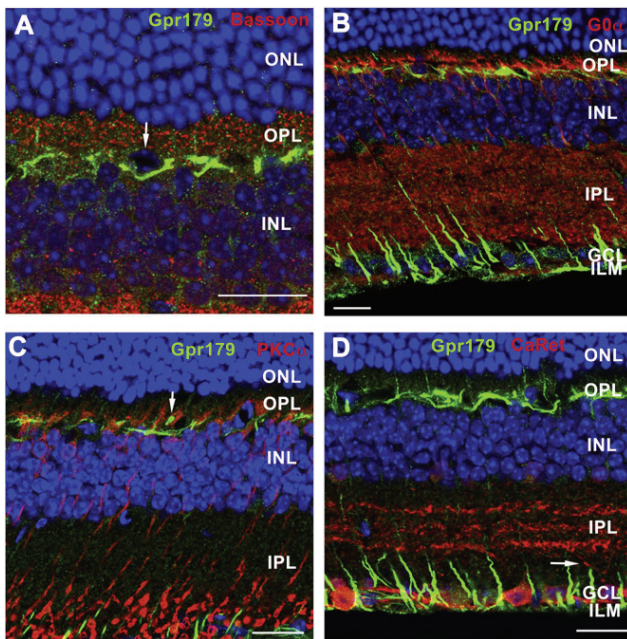


Figure 4. Gpr179 Immunohistochemistry on Retinal Sections of Wild-Type Mice

GPR179 signal (green) in the OPL and ILM double labeled with other retinal markers (red) were detected in wild-type mice by confocal microscopy. The scale bar represents 20 μ m. The following abbreviations are used: ONL, outer nuclear layer; OPL, outer plexiform layer; INL, inner nuclear layer; GCL, ganglion cell layer; and ILM, inner limiting membrane. Gpr179 did not colocalize with the presynaptic marker Bassoon (A), the ON-bipolar cell markers $Go\alpha$ (B) and $PKC\alpha$ (C), or with the ganglion cell labeled with calretinin (D). Some cells in the upper part of INL were surrounded by specific Gpr179 staining (arrow in A). The shape and the localization might indicate that these cells represent horizontal cells. Bipolar cell dendrites, stained with $PKC\alpha$ seem to surround Gpr179 (arrow in C). Calretinin antibody labeled specifically the ganglion cells, and their dendrites did not colocalize with Gpr179 (arrow in D). Instead, it seems that Gpr179 is highly concentrated in Müller cell endfeet (D); similar results have been previously shown for a potassium channel Kir4.1.³¹

from retinas confirmed the presence of the *GPR179* transcript. Using the same conditions, we could not detect the transcript in lymphocytes or HEK293 cells.

We investigated the localization of the Gpr179 protein in adult mouse retina by immunostaining coronal eye cryosections with a rabbit polyclonal antibody directed against GPR179 (Sigma-Aldrich, Saint-Quentin Fallavier, France). Bound primary antibody was detected with a secondary antibody (Alexa Fluor 488-conjugated, Invitrogen, Courtaboeuf, France), and the nuclei were counterstained (4',6-diamidino-2-phenylindole [DAPI], Euromedex, Souffelweyersheim, France). Immunofluorescence was analyzed with a confocal microscope (FV1000 fluorescent, Olympus, Hamburg, Germany). Gpr179 expression could be detected in the outer plexiform layer (OPL) and in the inner limiting membrane (ILM), in close proximity to the ganglion cells (Figure 4, green). Colocalization studies with a mouse anti-Bassoon (Enzo Lifesciences, Lyon, France), a specific marker for ribbon

synapse, excluded a close vicinity between Gpr179 and presynaptic terminals (Figure 4A). Furthermore, immunostaining with mouse antibodies against $Go\alpha$ (Millipore, Molsheim, France) and $PKC\alpha$ (Sigma-Aldrich), two specific ON-bipolar markers, demonstrated the absence of colocalization of Gpr179 with these proteins (Figures 4B and 4C). Instead, Gpr179 appears to be localized in a distinct compartment within bipolar cells or in other cells, such as horizontal cells (indicated by the arrow in Figure 4A). Interestingly, bipolar cell dendrites, stained with $PKC\alpha$, seem to surround Gpr179 (indicated by the arrow in Figure 4C). Alternatively, the Gpr179 OPL staining could also be localized within Müller cell processes present within this layer. In addition, a mouse antibody against calretinin (Millipore), a specific marker for ganglion cells and their dendrites, was used and did not show colocalization with Gpr179 immunostaining (Figure 4D, an example of a ganglion cell dendrite is marked with an arrow). Instead, Gpr179 was highly expressed in Müller cell endfeet at the level of the ILM; similar results had previously been shown for the potassium channel Kir4.1 macromolecular complex.^{31–33} Therefore, immunolocalization of Gpr179 suggests its localization in the OPL either in bipolar cells in a cellular compartment distinct from the synaptic membrane and cell body, and/or in horizontal cells, and/or in Müller cell processes as well as within the Müller cell endfeet.

The OPL localization of Gpr179 and the same associated ON-bipolar dysfunction phenotype as for *Grm6*, *Nyx*, or *Trpm1* alterations^{34–38} would suggest that *GPR179* is part of the same transduction pathway and could directly interact with any of these proteins. However, immunolocalization studies are not in keeping with this hypothesis. Instead, immunostaining suggests Müller cell localization and could place the Gpr179 functional role within these cells, possibly through the Kir4.1 macromolecular complex. This complex was shown to involve at least the potassium channel Kir4.1, the water channel aquaporin-4 (AQP4), and the dystrophin isoform Dp71. Interestingly, although Kir4.1 and Aqp4 knockout mice do not show Schubert-Bornschein ERG abnormalities,^{39,40} a subset of dystrophin mutations, responsible for Duchenne muscular dystrophy (DMD [MIM 310200]) are associated with such ERG abnormalities.^{41–44} Therefore, one hypothesis would be that Gpr179 is part of the Kir4.1 macromolecular complex. Gpr179 might directly interact with dystrophin isoforms, and its dysfunction would lead to cCSNB in a similar mechanism as in DMD. In order to reconcile the *Grm6*/*Nyx*/*Trpm1*-signaling pathway within bipolar cells and Gpr179 within Müller cells, one might hypothesize that Gpr179 could be involved in an as-yet unknown interaction between ON-bipolar cells and Müller cells that would be essential for ON-bipolar cell depolarization resulting in b-wave formation. On the other hand, our immunostaining studies could also suggest specific localization of Gpr179 within horizontal cells. Therefore, another hypothesis could be that ON-bipolar cells directly interact with horizontal cells. Lack of this interaction due

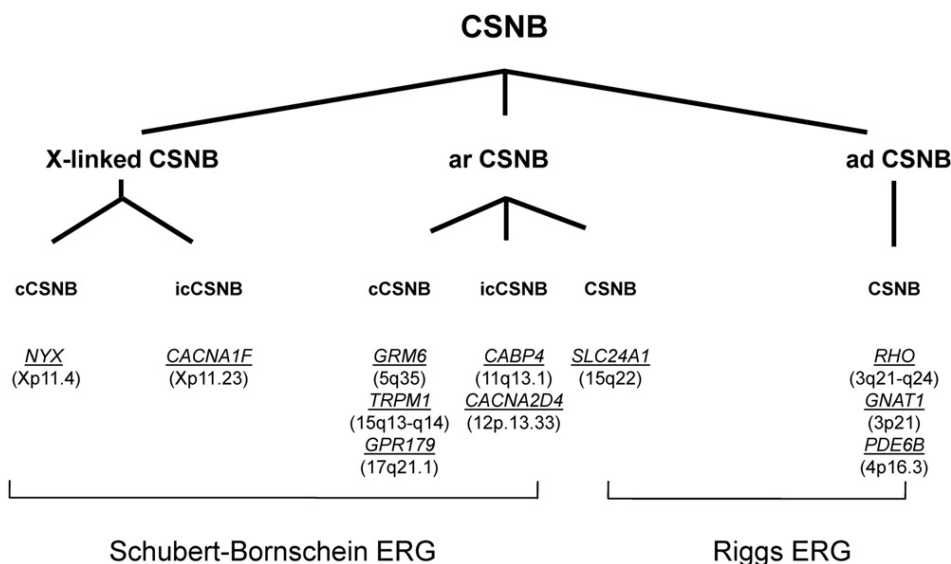


Figure 5. Genes Underlying CSNB

Different forms of CSNB in human are classified according to their electroretinographic feature, mode of inheritance, clinical phenotype, and mutated genes. Patients discussed herein show a complete Schubert-Bornschein type of ERG. The following abbreviations are used: cCSNB, complete CSNB; icCSNB, incomplete CSNB; ar, autosomal recessive; ad, autosomal dominant. Genes are indicated in italics and underlined. Chromosomal location is given between brackets. The phenotype of patients with mutations in icCSNB is more variable and can even lead to progressive cone or cone-rod dystrophy.¹

to Gpr179 dysfunction could lead to the reduced b-wave observed in patients with cCSNB.

Including the current study, mutations in four genes (*NYX*, *GRM6*, *TRPM1*, and *GPR179*) have been implicated in cCSNB (Figure 5).^{6,7,10–13,45,46} These genes code for nyctalopin, metabotropic glutamate receptor 6, transient receptor potential cation melastatin 1 channel, and G protein-coupled receptor 179, respectively. All but GPR179 localize postsynaptically to the photoreceptors in the retina in ON-bipolar cells.³⁵ Further functional studies will eventually clarify the exact role of this novel protein within the ON-bipolar cells pathway, which will also improve our understanding of the overall visual signal transduction through the retina.

Supplemental Data

Supplemental Data include two figures and four tables and can be found with this article online at <http://www.cell.com/AJHG/>.

Acknowledgments

The authors are grateful to the families described in this study; to Dominique Santiard-Baron and Christine Chaumeil for their help in DNA collection; to the clinical staff; and to Olivier Goreau, Serge Picaud, and Alvaro Rendon for antibodies used in the colocalization experiments. The project was supported by GIS-maladies rares (C.Z.), Retina France ([part of the 100-Exome Project] I.A., C.P.H., J.-A.S., H.D. and C.Z.), Foundation Voir et Entendre (C.Z.), Agence National de la Recherche (S.S.B), Foundation Fighting Blindness (FFB) grant CD-CL-0808-0466-CHNO (I.A. and the CIC503, recognized as an FFB center), FFB grant C-CMM-0907-0428-INSERM04, Ville de Paris and Région Ile de France, the French Association

against Myopathy (AFM) grant KBM-14390 (O.P.), and National Institutes of Health grant 1R01EY020902-01A1 (K.B.).

Received: October 20, 2011

Revised: November 18, 2011

Accepted: December 8, 2011

Published online: February 9, 2012

Web Resources

The URLs for data presented herein are as follows:

ESEfinder, <http://rulai.cshl.edu/cgi-bin/tools/ESE3/esefinder.cgi?process=home>

GenCards, <http://www.genecards.org/>

PolyPhen, <http://genetics.bwh.harvard.edu/pph/>

Sm2ph Central, <http://decryphon.igbmc.fr/sm2ph/cgi-bin/home>

National Center for Biotechnology Information, <http://ncbi.nlm.nih.gov/>

Online Mendelian Inheritance in Man (OMIM), <http://www.omim.org>

Pymol, <http://pymol.org/>

SIFT (Sorting Intolerant From Tolerant), <http://blocks.fhcrc.org/sift/SIFT.html>

UniProtKB/Swiss-Prot, <http://www.uniprot.org>

USCS Human Genome Browser, <http://genome.ucsc.edu/>

References

- Zeit, C. (2007). Molecular genetics and protein function involved in nocturnal vision. *Expert Rev. Ophthalmol.* 2, 467–485.
- Schubert, G., and Bornschein, H. (1952). Analysis of the human electroretinogram. *Ophthalmologica* 123, 396–413.

3. Miyake, Y., Yagasaki, K., Horiguchi, M., Kawase, Y., and Kanda, T. (1986). Congenital stationary night blindness with negative electroretinogram. A new classification. *Arch. Ophthalmol.* *104*, 1013–1020.
4. Audo, I., Robson, A.G., Holder, G.E., and Moore, A.T. (2008). The negative ERG: Clinical phenotypes and disease mechanisms of inner retinal dysfunction. *Surv. Ophthalmol.* *53*, 16–40.
5. Zeitz, C., Labs, S., Lorenz, B., Forster, U., Uksti, J., Kroes, H.Y., De Baere, E., Leroy, B.P., Cremers, F.P., Wittmer, M., et al. (2009). Genotyping microarray for CSNB-associated genes. *Invest. Ophthalmol. Vis. Sci.* *50*, 5919–5926.
6. Dryja, T.P., McGee, T.L., Berson, E.L., Fishman, G.A., Sandberg, M.A., Alexander, K.R., Derlacki, D.J., and Rajagopalan, A.S. (2005). Night blindness and abnormal cone electroretinogram ON responses in patients with mutations in the GRM6 gene encoding mGluR6. *Proc. Natl. Acad. Sci. USA* *102*, 4884–4889.
7. Zeitz, C., van Genderen, M., Neidhardt, J., Luhmann, U.F., Hoeben, F., Forster, U., Wycisk, K., Mátyás, G., Hoyng, C.B., Riemsdag, F., et al. (2005). Mutations in GRM6 cause autosomal recessive congenital stationary night blindness with a distinctive scotopic 15-Hz flicker electroretinogram. *Invest. Ophthalmol. Vis. Sci.* *46*, 4328–4335.
8. Zeitz, C., Kloeckener-Gruissem, B., Forster, U., Kohl, S., Magyar, I., Wissinger, B., Mátyás, G., Borruat, F.X., Schorderet, D.F., Zrenner, E., et al. (2006). Mutations in CABP4, the gene encoding the Ca²⁺-binding protein 4, cause autosomal recessive night blindness. *Am. J. Hum. Genet.* *79*, 657–667.
9. Wycisk, K.A., Zeitz, C., Feil, S., Wittmer, M., Forster, U., Neidhardt, J., Wissinger, B., Zrenner, E., Wilke, R., Kohl, S., and Berger, W. (2006). Mutation in the auxiliary calcium-channel subunit CACNA2D4 causes autosomal recessive cone dystrophy. *Am. J. Hum. Genet.* *79*, 973–977.
10. Audo, I., Kohl, S., Leroy, B.P., Munier, F.L., Guillonneau, X., Mohand-Said, S., Bujakowska, K., Nandrot, E.F., Lorenz, B., Preising, M., et al. (2009). TRPM1 is mutated in patients with autosomal-recessive complete congenital stationary night blindness. *Am. J. Hum. Genet.* *85*, 720–729.
11. Li, Z., Sergouniotis, P.I., Michaelides, M., Mackay, D.S., Wright, G.A., Devery, S., Moore, A.T., Holder, G.E., Robson, A.G., and Webster, A.R. (2009). Recessive mutations of the gene TRPM1 abrogate ON bipolar cell function and cause complete congenital stationary night blindness in humans. *Am. J. Hum. Genet.* *85*, 711–719.
12. van Genderen, M.M., Bijveld, M.M., Claassen, Y.B., Florijn, R.J., Pearring, J.N., Meire, F.M., McCall, M.A., Riemsdag, F.C., Gregg, R.G., Bergen, A.A., and Kamermans, M. (2009). Mutations in TRPM1 are a common cause of complete congenital stationary night blindness. *Am. J. Hum. Genet.* *85*, 730–736.
13. Nakamura, M., Sanuki, R., Yasuma, T.R., Onishi, A., Nishiguchi, K.M., Koike, C., Kadowaki, M., Kondo, M., Miyake, Y., and Furukawa, T. (2010). TRPM1 mutations are associated with the complete form of congenital stationary night blindness. *Mol. Vis.* *16*, 425–437.
14. Sergouniotis, P.I., Davidson, A.E., Mackay, D.S., Li, Z., Yang, X., Plagnol, V., Moore, A.T., and Webster, A.R. (2011). Recessive mutations in KCNJ13, encoding an inwardly rectifying potassium channel subunit, cause leber congenital amaurosis. *Am. J. Hum. Genet.* *89*, 183–190.
15. Bamshad, M.J., Ng, S.B., Bigam, A.W., Tabor, H.K., Emond, M.J., Nickerson, D.A., and Shendure, J. (2011). Exome sequencing as a tool for Mendelian disease gene discovery. *Nat. Rev. Genet.* *12*, 745–755.
16. Marmor, M.F., Fulton, A.B., Holder, G.E., Miyake, Y., Brigell, M., and Bach, M.; International Society for Clinical Electrophysiology of Vision. (2009). ISCEV Standard for full-field clinical electroretinography (2008 update). *Doc. Ophthalmol.* *118*, 69–77.
17. UniProt Consortium. (2010). The Universal Protein Resource (UniProt) in 2010. *Nucleic Acids Res.* *38* (Database issue), D142–D148.
18. Altschul, S.F., Madden, T.L., Schäffer, A.A., Zhang, J., Zhang, Z., Miller, W., and Lipman, D.J. (1997). Gapped BLAST and PSI-BLAST: A new generation of protein database search programs. *Nucleic Acids Res.* *25*, 3389–3402.
19. Plewniak, F., Bianchetti, L., Brelivet, Y., Carles, A., Chalmel, F., Lecompte, O., Mochel, T., Moulinier, L., Muller, A., Muller, J., et al. (2003). PipeAlign: A new toolkit for protein family analysis. *Nucleic Acids Res.* *31*, 3829–3832.
20. Eswar, N., Eramian, D., Webb, B., Shen, M.Y., and Sali, A. (2008). Protein structure modeling with MODELLER. *Methods Mol. Biol.* *426*, 145–159.
21. Eramian, D., Eswar, N., Shen, M.Y., and Sali, A. (2008). How well can the accuracy of comparative protein structure models be predicted? *Protein Sci.* *17*, 1881–1893.
22. Nishiguchi, K.M., Sandberg, M.A., Kooijman, A.C., Martemyanov, K.A., Pott, J.W., Hagstrom, S.A., Arshavsky, V.Y., Berson, E.L., and Dryja, T.P. (2004). Defects in RGS9 or its anchor protein R9AP in patients with slow photoreceptor deactivation. *Nature* *427*, 75–78.
23. Dvir, L., Srour, G., Abu-Ras, R., Miller, B., Shalev, S.A., and Ben-Yosef, T. (2010). Autosomal-recessive early-onset retinitis pigmentosa caused by a mutation in PDE6G, the gene encoding the gamma subunit of rod cGMP phosphodiesterase. *Am. J. Hum. Genet.* *87*, 258–264.
24. Piri, N., Gao, Y.Q., Danciger, M., Mendoza, E., Fishman, G.A., and Farber, D.B. (2005). A substitution of G to C in the cone cGMP-phosphodiesterase gamma subunit gene found in a distinctive form of cone dystrophy. *Ophthalmology* *112*, 159–166.
25. Lagerström, M.C., and Schiöth, H.B. (2008). Structural diversity of G protein-coupled receptors and significance for drug discovery. *Nat. Rev. Drug Discov.* *7*, 339–357.
26. Ng, P.C., and Henikoff, S. (2001). Predicting deleterious amino acid substitutions. *Genome Res.* *11*, 863–874.
27. Luu, T., Nguyen, N., Friedrich, A., Muller, J., Moulinier, L., and Poch, O. (2011). Extracting knowledge from a mutation database related to human monogenic disease using inductive logic programming. *International Conference on Bioscience, Biochemistry and Bioinformatics; Singapore. IACSIT* *5*, 83–100.
28. Friedrich, A., Garnier, N., Gagnière, N., Nguyen, H., Albou, L.P., Biancalana, V., Bettler, E., Deléage, G., Lecompte, O., Muller, J., et al. (2010). SM2PH-db: An interactive system for the integrated analysis of phenotypic consequences of missense mutations in proteins involved in human genetic diseases. *Hum. Mutat.* *31*, 127–135.
29. Zeitz, C., Forster, U., Neidhardt, J., Feil, S., Kälin, S., Leifert, D., Flor, P.J., and Berger, W. (2007). Night blindness-associated mutations in the ligand-binding, cysteine-rich, and intracellular domains of the metabotropic glutamate receptor 6 abolish protein trafficking. *Hum. Mutat.* *28*, 771–780.
30. Carter-Dawson, L.D., LaVail, M.M., and Sidman, R.L. (1978). Differential effect of the rd mutation on rods and cones in the mouse retina. *Invest. Ophthalmol. Vis. Sci.* *17*, 489–498.

31. Connors, N.C., and Kofuji, P. (2006). Potassium channel Kir4.1 macromolecular complex in retinal glial cells. *Glia* 53, 124–131.
32. Claudepierre, T., Rodius, F., Frasson, M., Fontaine, V., Picaud, S., Dreyfus, H., Mornet, D., and Rendon, A. (1999). Differential distribution of dystrophins in rat retina. *Invest. Ophthalmol. Vis. Sci.* 40, 1520–1529.
33. Dalloz, C., Sarig, R., Fort, P., Yaffe, D., Bordais, A., Pannicke, T., Grosche, J., Mornet, D., Reichenbach, A., Sahel, J., et al. (2003). Targeted inactivation of dystrophin gene product Dp71: Phenotypic impact in mouse retina. *Hum. Mol. Genet.* 12, 1543–1554.
34. Vardi, N., Duvoisin, R., Wu, G., and Sterling, P. (2000). Localization of mGluR6 to dendrites of ON bipolar cells in primate retina. *J. Comp. Neurol.* 423, 402–412.
35. Morgans, C.W., Ren, G., and Akileswaran, L. (2006). Localization of nyctalopin in the mammalian retina. *Eur. J. Neurosci.* 23, 1163–1171.
36. Gregg, R.G., Kamermans, M., Klooster, J., Lukasiewicz, P.D., Peachey, N.S., Vessey, K.A., and McCall, M.A. (2007). Nyctalopin expression in retinal bipolar cells restores visual function in a mouse model of complete X-linked congenital stationary night blindness. *J. Neurophysiol.* 98, 3023–3033.
37. Morgans, C.W., Zhang, J., Jeffrey, B.G., Nelson, S.M., Burke, N.S., Duvoisin, R.M., and Brown, R.L. (2009). TRPM1 is required for the depolarizing light response in retinal ON-bipolar cells. *Proc. Natl. Acad. Sci. USA* 106, 19174–19178.
38. Koike, C., Obara, T., Uriu, Y., Numata, T., Sanuki, R., Miyata, K., Koyasu, T., Ueno, S., Funabiki, K., Tani, A., et al. (2010). TRPM1 is a component of the retinal ON bipolar cell transduction channel in the mGluR6 cascade. *Proc. Natl. Acad. Sci. USA* 107, 332–337.
39. Kofuji, P., Ceelen, P., Zahs, K.R., Surbeck, L.W., Lester, H.A., and Newman, E.A. (2000). Genetic inactivation of an inwardly rectifying potassium channel (Kir4.1 subunit) in mice: Phenotypic impact in retina. *J. Neurosci.* 20, 5733–5740.
40. Li, J., Patil, R.V., and Verkman, A.S. (2002). Mildly abnormal retinal function in transgenic mice without Müller cell aquaporin-4 water channels. *Invest. Ophthalmol. Vis. Sci.* 43, 573–579.
41. Cibis, G.W., Fitzgerald, K.M., Harris, D.J., Rothberg, P.G., and Rupani, M. (1993). The effects of dystrophin gene mutations on the ERG in mice and humans. *Invest. Ophthalmol. Vis. Sci.* 34, 3646–3652.
42. De Becker, I., Riddell, D.C., Dooley, J.M., and Tremblay, F. (1994). Correlation between electroretinogram findings and molecular analysis in the Duchenne muscular dystrophy phenotype. *Br. J. Ophthalmol.* 78, 719–722.
43. Pillers, D.A., Bulman, D.E., Weleber, R.G., Sigesmund, D.A., Musarella, M.A., Powell, B.R., Murphey, W.H., Westall, C., Panton, C., Becker, L.E., et al. (1993). Dystrophin expression in the human retina is required for normal function as defined by electroretinography. *Nat. Genet.* 4, 82–86.
44. Pillers, D.A., Fitzgerald, K.M., Duncan, N.M., Rash, S.M., White, R.A., Dwinnell, S.J., Powell, B.R., Schnur, R.E., Ray, P.N., Cibis, G.W., and Weleber, R.G. (1999). Duchenne/Becker muscular dystrophy: Correlation of phenotype by electroretinography with sites of dystrophin mutations. *Hum. Genet.* 105, 2–9.
45. Bech-Hansen, N.T., Naylor, M.J., Maybaum, T.A., Sparkes, R.L., Koop, B., Birch, D.G., Bergen, A.A., Prinsen, C.F., Polomeno, R.C., Gal, A., et al. (2000). Mutations in NYX, encoding the leucine-rich proteoglycan nyctalopin, cause X-linked complete congenital stationary night blindness. *Nat. Genet.* 26, 319–323.
46. Pusch, C.M., Zeitz, C., Brandau, O., Pesch, K., Achatz, H., Feil, S., Scharfe, C., Maurer, J., Jacobi, F.K., Pinckers, A., et al. (2000). The complete form of X-linked congenital stationary night blindness is caused by mutations in a gene encoding a leucine-rich repeat protein. *Nat. Genet.* 26, 324–327.
47. Viczian, A., Sanyal, S., Toffenetti, J., Chader, G.J., and Farber, D.B. (1992). Photoreceptor-specific mRNAs in mice carrying different allelic combinations at the rd and rds loci. *Exp. Eye Res.* 54, 853–860.

2. Further insights into GPR179: expression, localization, and associated pathogenic mechanisms leading to complete congenital stationary night blindness

In this work, we wanted to know where *GPR179* was expressed and describe the protein localization. We performed RNA *in situ* hybridization on mouse retinas, which revealed *Gpr179* expression in the upper part of the INL, presumably in the somata of bipolar cells. Immunohistochemistry on human retinal sections revealed GPR179 localization at dendritic tips of bipolar cells in the OPL, which was in agreement with the results obtained in mouse (245, 246) and with localization of other proteins implicated in cCSNB. Furthermore, to better understand the pathophysiology of the previously identified missense mutations (245, 247), we performed *in vitro* studies using mammalian cells overexpressing wild-type and mutated GPR179 protein. Live-cell extracellular staining with subsequent intracellular immunolocalization and ELISA studies revealed that the missense mutations p.Tyr220Cys, p.Gly455Asp, and p.His603Tyr led to severely reduced cell surface localization, whereas p.Asp126His did not. We also investigated the pathophysiology of c.1784+1G>A splice site mutation. RT-qPCR studies on wild-type and c.1784+1G>A splice site-mutated mini-gene constructs transfected cells showed that *GPR179* splicing was altered. We concluded that for most of the missense mutations identified so far, mislocalization at the plasma membrane and for the p.Asp126His mutation that extracellular interaction dysfunction seem to be the underlying pathogenic mechanisms leading to this form of cCSNB. The splice site mutation leads to altered transcript, which may lead to a truncated protein or mRNA decay.

Further Insights Into GPR179: Expression, Localization, and Associated Pathogenic Mechanisms Leading to Complete Congenital Stationary Night Blindness

Elise Orhan,¹⁻³ Laurent Prézeau,⁴ Said El Shamieh,¹⁻³ Kinga M Bujakowska,¹⁻³ Christelle Michiels,¹⁻³ Yvrick Zagar,¹⁻³ Claire Vol,⁴ Shomi S. Bhattacharya,^{5,6} José-Alain Sahel,^{1-3,5,7-9} Florian Sennlaub,¹⁻³ Isabelle Audo,^{1-3,5,9} and Christina Zeitz¹⁻³

¹Institut National de la Santé et de la Recherche Médicale (INSERM), U968, Paris, France

²Centre National de la Recherche Scientifique (CNRS), UMR_7210, Paris, France

³Université Pierre et Marie Curie (UPMC Paris 06), Unité Mixte de Recherche (UMR)_S 968, Institut de la Vision, Paris, France

⁴Institut de Génomique Fonctionnelle CNRS UMR5203, INSERM U661, Université Montpellier 1 (UM1) & Université Montpellier 2 (UM2) Montpellier, France

⁵University College London (UCL)-Institute of Ophthalmology, London, United Kingdom

⁶Department of Cellular Therapy and Regenerative Medicine, Andalusian Molecular Biology and Regenerative Medicine Centre (CABIMER), Isla Cartuja, Seville, Spain

⁷Fondation Ophthalmologique Adolphe de Rothschild, Paris, France

⁸Académie des Sciences-Institut de France, Paris, France

⁹Centre Hospitalier National d'Ophtalmologie (CHNO) des Quinze-Vingts, INSERM-Direction de l'Hospitalisation et de l'Offre de Soins Centre d'Investigation Clinique (DHOS CIC) 503, Paris, France

Correspondence: Christina Zeitz, Department of Genetics, Institut de la Vision, 17, Rue Moreau, 75012 Paris, France; christina.zeitz@inserm.fr

Submitted: June 14, 2013

Accepted: November 2, 2013

Citation: Orhan E, Prézeau L, El Shamieh S, et al. Further insights into GPR179: expression, localization, and associated pathogenic mechanisms leading to complete congenital stationary night blindness. *Invest Ophthalmol Vis Sci.* 2013;54:8041-8050. DOI:10.1167/iovs.13-12610

PURPOSE. Mutations in *GPR179*, which encodes the G protein-coupled receptor 179, lead to autosomal recessive complete (c) congenital stationary night blindness (CSNB), which is characterized by an ON-bipolar retinal cell dysfunction. This study further defined the exact site of *Gpr179* expression and its protein localization in human retina and elucidated the pathogenic mechanism of the reported missense and splice site mutations.

METHODS. RNA in situ hybridization was performed with mouse retinal sections. A commercially available antibody was validated with GPR179-overexpressing COS-1 cells and applied to human retinal sections. Live-cell extracellular staining along with subsequent intracellular immunolocalization and ELISA studies were performed using mammalian cells overexpressing wild-type or missense mutated *GPR179*. Wild-type and splice site-mutated mini-gene constructs were transiently transfected, and RNA was extracted. RT-PCR-amplified products were cloned, and Sanger sequenced.

RESULTS. Mouse *Gpr179* transcript was expressed in the upper part of the inner nuclear layer, and the respective human protein localized at the dendritic tips of bipolar cells in human retina. The missense mutations p.Tyr220Cys, p.Gly455Asp, and p.His603Tyr led to severely reduced cell surface localization, whereas p.Asp126His did not. The mutated splice donor site altered *GPR179* splicing.

CONCLUSIONS. Our findings indicate that the site of expression and protein localization of human and mouse GPR179 is similar to that of other proteins implicated in cCSNB. For most of the mutations identified so far, loss of the GPR179 protein function seems to be the underlying pathogenic mechanism leading to this form of cCSNB.

Keywords: GPR179, expression and localization, cCSNB, pathogenicity, trafficking defect, mini-gene approach

Congenital stationary night blindness (CSNB) is a clinically and genetically heterogeneous disorder, which is characterized by impaired night vision and is often associated with other ocular problems such as decreased visual acuity, nystagmus, high myopia, and strabismus.¹ Clinically, this disorder can be classified according to two forms distinguished by particular full-field electroretinogram (ERG) abnormalities.² Patients with Riggs-type ERG responses reveal a reduced a- and b-wave, whereas patients with the Schubert-Bornschein-type of ERG are characterized by an electronegative scotopic ERG response in which the a-wave is larger than the b-wave.^{3,4} The

latter type can be further divided into the incomplete (ic) and complete (c) forms. In the former form, the patient shows reduced scotopic b-wave and severely reduced 30-Hz flicker and single-flash photopic ERG responses; in the latter form, the patient shows severely reduced scotopic b-wave and square-shaped a-wave photopic ERG responses with relatively preserved amplitude.⁵ Mutations in genes involved in the phototransduction cascade that cause autosomal dominant (ad) CSNB (*RHO*, *GNAT1*, *PDE6B*)⁶⁻¹⁰ and one gene that causes autosomal recessive (ar) CSNB (*SLC24A1*)¹¹ have been reported to lead to Riggs-type CSNB. However, most cases of CSNB

reported so far have a Schubert-Bornschein-type phenotype and are associated with mutations in the genes causing icCSNB (*CACNA1F*, *CABP4*, and *CACNA2D4*)^{12–15} and cCSNB (*NYX*, *GRM6*, *TRPM1*, *GPR179*, and *LRIT3*).^{16–25} Genes involved in cCSNB are expressed in the upper part of the inner nuclear layer (INL) of the retina^{26–28} and encode proteins localized at the dendritic tips of ON-bipolar cells.^{22,24,25,29–35} All proteins are implicated in signaling from photoreceptors to bipolar cells. *GRM6* encodes the metabotropic glutamate receptor mGluR6 (also called GRM6), which is important for glutamate-induced signaling from the photoreceptors. During darkness, glutamate binding leads to the activation of G α_o , the α subunit of the G protein of mGluR6³⁶ and, at the end of the cascade, to the closure of a non-selective ion channel, TRPM1.^{26,37,38} RGS7/G β 5 and RGS11/G β 5 complexes are GTPase accelerating proteins (GAP) in the same cascade and are important for the deactivation of G α_o .^{39,40} In daylight, the TRPM1 channel opens, resulting in depolarization of the ON-bipolar cells and formation of the ERG b-wave, which is absent in patients with cCSNB.⁴¹ Specific intracellular motifs present in LRIT3 and in vitro and in vivo studies of NYX and TRPM1 suggest that LRIT3 and NYX are important for the correct localization of TRPM1 at the dendritic tips of ON-bipolar cells.^{25,33} *GPR179*, which encodes the orphan G protein-coupled receptor 179, has only recently been identified as mutated in patients with cCSNB.^{23,24} Previous immunolabeling in mice showed that GPR179 is localized at the dendritic tips of bipolar cells^{24,35} and is essential for postsynaptic targeting of the G protein-deactivating RGS-G β 5 complex (mentioned above) to the dendritic tips of ON-bipolar cells.³⁵ Although we recently showed by RT-PCR experiments that *GPR179* is expressed in human retina,²³ the exact expression site and localization and the relevant pathogenic mechanism still need to be elucidated. In the current study, we aimed to define the exact expression site and protein localization of mouse and human GPR179 and to elucidate its underlying pathogenic mechanism(s) implicated in cCSNB.

MATERIALS AND METHODS

Preparation of Mouse and Human Retinas for RNA In Situ Hybridization and Protein Localization Studies

Six-week-old C57BL/6JrJ (Janvier, Genest Saint Isle, France) female mice were anesthetized with a mixture of 140 mg/kg xylazine (Bayer, Leverkusen, Germany)/14 mg/kg ketamine (Virbac, Carros, France) saline solution and were perfused transcardiacally with 4% paraformaldehyde (PFA) in 0.12 M phosphate buffer, pH 7.4. Eyes were collected and postfixed for 1 hour in 4% PFA before being dehydrated in 30% sucrose phosphate-buffered saline (PBS) solution. Thereafter, eyes were embedded in 7% gelatin/10% sucrose PBS and frozen in -40°C isopentane. Subsequently, 20- μm retinal sections were made with a cryostat (model HM560, Microm; Thermo Fisher, Walldorf, Germany). Animal handling was performed in accordance with the ARVO Statement for the Use of Animals in Ophthalmic and Vision Research and was approved by the local institutional review board. Human donor eyes without known history of retinal diseases were collected through the Minnesota Lions Eye bank after due consent in accordance with the Declaration of Helsinki. The posterior segment was dissected, postfixed, dehydrated, embedded, and sectioned as described above for the mouse retinas.

RNA In Situ Hybridization Studies

A cDNA fragment encompassing exon 7 to 9 of mouse *Gpr179* was cloned into a pBluescript II SK vector using a commercial

cloning service (GeneCust, Dudelange, Luxembourg). The plasmid was linearized using the restriction enzymes *SacI* and *KpnI*. Antisense and sense RNA in situ hybridization probes were synthesized using T7 and T3 RNA polymerase (Roche Diagnostics, Basel, Switzerland), respectively, and labeled with digoxigenin-UTP (Roche Diagnostics). Mouse retinal sections were postfixed in 4% PFA for 10 minutes, washed with PBS, and treated with proteinase K (10 $\mu\text{g}/\text{mL}$; Invitrogen, Carlsbad, Czech Republic) for 2 minutes. Following a wash with PBS, the sections were postfixed in 4% PFA, washed in PBS, and then acetylated in an acetylation buffer of 1.3% triethanolamine (Sigma-Aldrich, St. Quentin Fallavier, France), 0.25% acetic anhydride (Sigma-Aldrich), and 0.06% hydrochloric acid solution. The sections were washed in 1% Triton X-100 PBS solution and blocked for 2 hours in hybridization buffer containing 50% formamide, 5 \times SSC (saline sodium citrate [1 \times SSC is 0.15 M NaCl plus 0.015 M sodium citrate]), 1 \times blocking solution (Denhardt's solution; Sigma-Aldrich), 250 $\mu\text{g}/\text{mL}$ yeast tRNA (Roche Diagnostics), and 240 $\mu\text{g}/\text{mL}$ salmon sperm (Roche Diagnostics), pH 7.4. The sections were hybridized with digoxigenin-labeled probes overnight at 72 $^{\circ}\text{C}$, after which they were rinsed for 2 hours in 0.2 \times SSC at 72 $^{\circ}\text{C}$ and blocked for 1 hour at room temperature in 0.1 M Tris, 0.15 M NaCl (B1), 10% normal goat serum (NGS; Vectorshield, Burlingame, CA), pH 7.5. After blocking, slides were incubated overnight at room temperature with anti-digoxigenin antibody conjugated with alkaline phosphatase (1:5000 dilution; Roche Diagnostics) in B1 containing 1% NGS. After additional washes, the alkaline phosphatase activity was detected using nitro blue tetrazolium chloride (337.5 $\mu\text{g}/\text{mL}$; Roche Diagnostics) and 5-bromo-4-chloro-3-indolyl phosphate (175 $\mu\text{g}/\text{mL}$; Roche Diagnostics). Eight hours later, sections were mounted (Mowiol; Calbiochem/Merck, Carlstadt, NJ). Slides were scanned with a Nanozoomer 2.0 high throughput (HT) equipped with a 3-charge-coupled device time delay integration (TDI) camera (Hamamatsu Photonics, Hamamatsu, Japan).

Protein Immunolocalization in Human Retina

Retinal sections were incubated overnight with primary rabbit anti-GPR179 (product code, HPA017885-100UL; Sigma-Aldrich), mouse anti-G α_o (Merck-Millipore, Billerica, MA), mouse PKC α (Sigma-Aldrich), mouse calbindin (Swant, Marly, Switzerland), and mouse C-terminal-binding protein 2 (CtBP2; BD Transduction Laboratories, San Jose, CA) antibodies at dilutions of 1:400, 1:400, 1:200, 1:500, and 1:10,000. Prior to GPR179/G α_o antibody staining, retinal sections were postfixed for 5 minutes in methanol at -20°C . Thereafter, sections were washed 3 times for 5 min each in 1 \times PBS and then incubated with donkey anti-rabbit Alexa Fluor 488 (Jackson Immuno-Research Laboratories, Baltimore, MD) and donkey anti-mouse Cy3 (Jackson ImmunoResearch Laboratories) secondary antibodies and 4',6-diamidino-2-phenylindole (DAPI; Euromedex, Souffelweyersheim, France) at a dilution 1:1000 each for 1 hour at room temperature. Negative controls were performed with only the use of secondary antibodies. Sections were washed 3 times for 5 min in PBS and mounted with coverslips (Mowiol preparation; Calbiochem/Merck). Confocal fluorescence microscopy images were taken (model FV1000; Olympus, Hamburg, Germany).

Expression Constructs

The DNA coding sequence and *BamHI* and *NotI* linkers of the wild-type and mutated human *GPR179* genes were synthesized in an optimized way and cloned in an expression vector (pCDNA3; Invitrogen, Courtaboeuf, France) by a company (GeneCust). To validate the commercially available human anti-GPR179 antibody (product code HPA017885-100UL; Sigma-

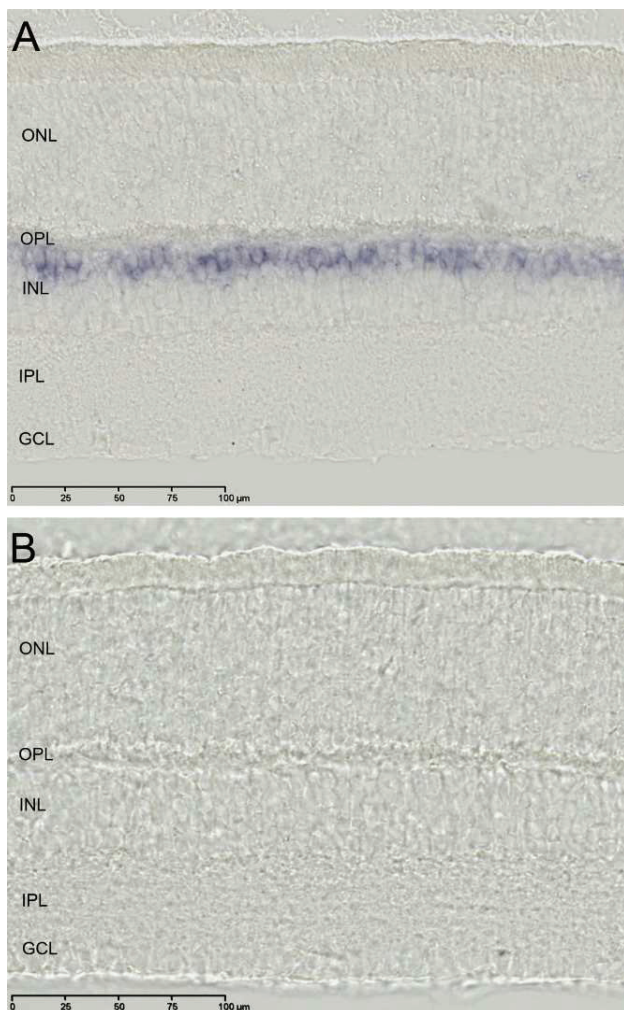


FIGURE 1. *GPR179* is expressed in the somata of the upper part of the INL in mouse retina. Hybridization was performed with antisense (A) and sense (B) *Gpr179* (exons 9–11) riboprobes (signal in purple). ONL, outer nuclear layer; OPL, outer plexiform layer; INL, inner nuclear layer; IPL, inner plexiform layer; GCL, ganglion cell layer.

Aldrich), we inserted in frame a flag-tag between the predicted signal sequence (after amino acid 26) and the main sequence. The sequences of the respective plasmids were verified by the company and in our laboratory by Sanger sequencing using standard conditions with an automated 48-capillary sequencer (BigDye Terminator version 1.1 cycle sequencing kit, model 3730 genetic analyzer; Applied Biosystems, Courtaboeuf, France) with specific primers designed against the wild-type and optimized synthetic *GPR179* sequence (see Supplementary Table S1) and vector oligonucleotides (T7, SP6, and BGH oligonucleotides).

Cell Culture, Transfection, and Immunofluorescence

Transient transfection studies were performed in COS-1 cells. In 24-well plates, 130,000 cells per well were seeded over coated coverslips and transfected after 6 hours with 10 μ g of human wild-type and mutated *GPR179* plasmids, applying the calcium phosphate method.⁴² To validate *in vitro* the human anti-*GPR179* antibody mentioned above, cells were permeabilized after 36 hours of transfection and stained for intracellular

GPR179 protein with the human anti-*GPR179* antibody and mouse anti flag-tag antibody (product code M2 F3165; Sigma-Aldrich) in the same experiment and visualized with anti-mouse Alexa Fluor 488 (Jackson Immunoresearch Laboratories) and donkey anti-rabbit Cy3 (Jackson Immunoresearch Laboratories) antibodies, respectively, at a dilution of 1:1000 each. To investigate the localization of wild-type and mutated *GPR179* proteins, extracellular live cell staining and subsequent intracellular staining were performed as previously described.⁴³ Stained cells were analyzed with confocal fluorescence microscopy (model FV1000; Olympus). Using standard protein extraction methods, we were not able to obtain a clear signal with this *GPR179* antibody by using Western blot analysis (data not shown).

Transfection of HEK293 Cells, ELISA for Quantification of Cell Surface Receptor Expression

HEK293 cells were cultured in modified Eagle medium supplemented with 10% fetal calf serum (FCS) and transfected by electroporation as previously described.⁴⁴ Ten million cells were transfected with 5 μ g of plasmid DNA encoding wild-type or mutated *GPR179* or wild-type *GPR158* used as a specificity control. Control cells were transfected with the empty vector. Briefly, cells were cultured at 30°C for 24 hours; fixed with 4% paraformaldehyde; and when needed, incubated for 3 minutes with 0.05% Triton X-100; and then blocked with blocking buffer (1% FCS in PBS). Rabbit polyclonal anti-*GPR179* antibody (product code HPA017885; Sigma-Aldrich) was applied for 30 minutes at 0.5 mg/L. After cells were washed with blocking buffer, the horseradish peroxidase-conjugated donkey anti-rabbit (product code NA934V, 1:1500 dilution; GE-Healthcare, Little Chalfont, UK) secondary antibody was applied for 30 minutes, and cells were washed with blocking buffer and then PBS. Chemiluminescence was detected using SuperSignal substrate (Pierce, Rockford, IL) and an Infinite F500 reader (Tecan, Männedorf, Switzerland). Data were collected using Tecan i-control software (Tecan).

Mini-Gene Approach

Patient genomic DNA containing the heterozygous c.1784+1G>A mutation was amplified between intron 6 and intron 9 with *GPR179* oligonucleotides used for the initial mutation screening (*GPR179_EX7F* and *GPR179_EX9R*)²³ with a DNA polymerase (HOT FIREPol; Solyis Biodine, Tartu, Estonia). The amplicon was subcloned in a vector (pCRII-TOPO vector; Invitrogen). Subsequent Sanger sequencing using standard M13 oligonucleotides was performed to verify the presence of the wild-type and splice site mutation in the obtained constructs. The inserts of the sequence-validated constructs were cloned into a vector (pBudCE4.1 vector; Invitrogen) using the *HindIII* and *XbaI* restriction sites. Transient transfection studies were performed in COS-1 cells in 6-well plates, and total RNA was extracted using a kit (RNeasy mini-kit; Qiagen, Hilden, Germany). Reverse transcription was performed using a reverse transcriptase (SuperscriptII; Invitrogen). To analyze the *in vitro* splicing products, PCR was performed using oligonucleotides present in exons 7 and 9 of *GPR179* (*RT_GPR179_EX7F* 5'-GTGCTGCAGCTGTTTCTGTC3' and *RT_GPR179_EX9R* 5'-AAGAGGAGGAGGGTCCAGTC3'). Five microliters of the RT-PCR products was investigated by electrophoresis on a 2% agarose gel; 1 μ L was cloned in a vector (pCRII-TOPO; Invitrogen), and 16 clones per condition were picked and Sanger sequenced using standard M13 oligonucleotides. To normalize *GPR179* RT-PCR values, a beta-actin PCR (using the primers ACTNBqPCR Ex4F CGCCAACACAGTGCTGTCTG and ACTNB_qPCR_Ex5R GGAGTACTTGCGCTCAGGAG) was performed on the obtained cDNA and was investigated as mentioned

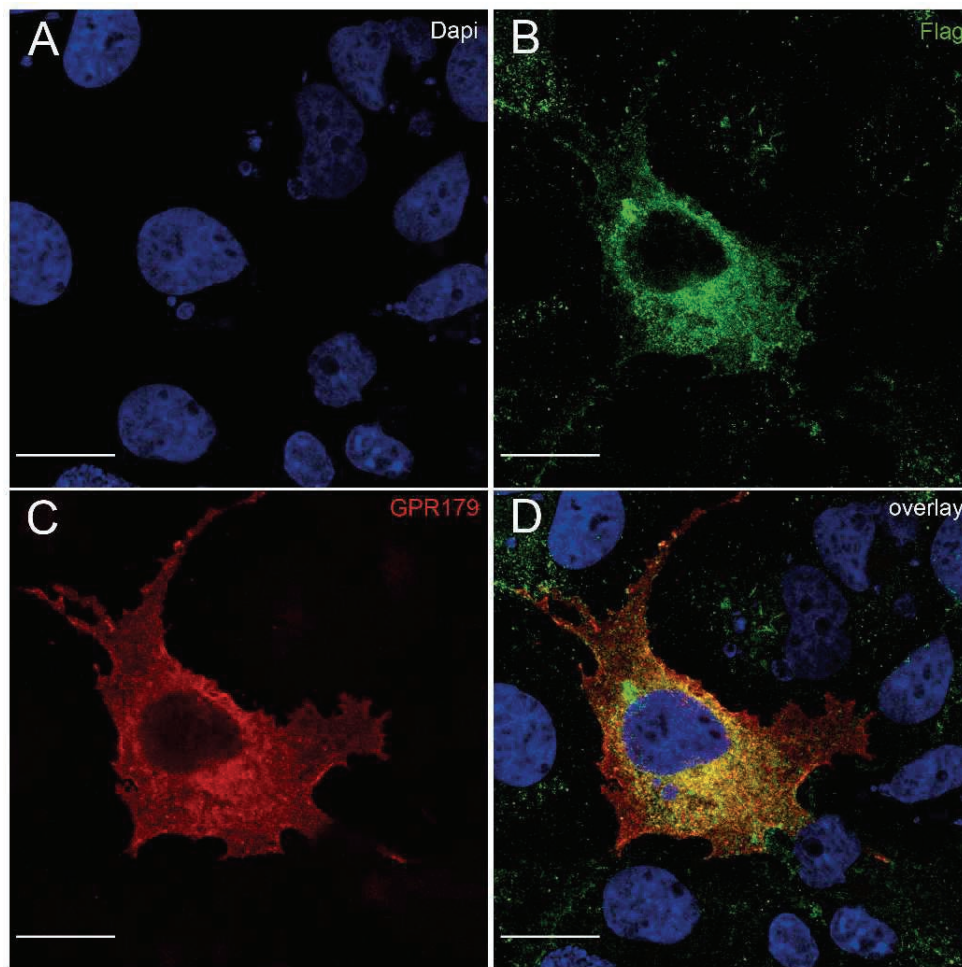


FIGURE 2. Commercial antibody raised against human GPR179 effectively detects human GPR179 in overexpressing COS-1 cells. Nuclei were stained with DAPI (blue) (A). The protein was detected by an anti-flag-tag antibody (green) (B) and an anti-GPR179 antibody (red) (C). (D) An overlay of the staining is shown. Scale bars: 20 μ m.

above for the GPR179 mini-gene RT-PCR. All PCR experiments were performed 5 times. Negative controls without DNA were included. Assessments of *GPR179* mRNA and ACTB (beta-actin) mRNA levels were performed using a semiquantitative analysis (ChemiDoc XRS and Quantity One version 4.4.0 software; Bio-Rad, Hercules, CA). Domain prediction was performed by applying the Uniprot algorithm (<http://www.uniprot.org>).

Statistical Analyses

Statistical analyses were performed using SPSS software (version 19.0; SPSS, Inc., Chicago, IL). An assessment of normality was performed prior to applying the required statistical tests. The threshold for statistical significance was set at a P value of ≤ 0.05 . To study the influence of the p.Asp126His, p.Tyr220Cys, p.Gly455Asp, and p.His603Tyr mutations on GPR179 chemiluminescence levels, mean comparisons between groups were analyzed by paired sample t -tests. The background noise was removed by subtracting its chemiluminescence value (plasmid pcDNA3) from the total chemiluminescence of other plasmids. Subsequently, all chemiluminescence values were proportionally transformed into percentages by fixing the permeabilized values to 100%. To study the influence of the c.1784+1G>A mutation on

GPR179 mRNA levels, mean comparisons between groups (wild-type and mutant) were analyzed by paired sample t -tests.

RESULTS

Expression and Immunolocalization of Mouse and Human GPR179 in the Retina

RNA in situ hybridization studies performed on mouse retina with a riboprobe against mouse *Gpr179* revealed expression in the somata of the upper part of the INL (Fig. 1A). No staining was observed using the respective sense riboprobe (Fig. 1B). To confirm that the antibody raised against the human GPR179 effectively detected it, we overexpressed a wild-type flag-tagged GPR179 plasmid in COS-1 cells and detected the protein with the anti-flag as well as with the anti-GPR179 antibody, indicating that this antibody indeed recognizes the human GPR179 protein in immunolocalization studies (Fig. 2). This antibody was then applied to a human retinal section, which revealed a clear staining in the outer plexiform layer (OPL) (Fig. 3A), more specifically in the dendritic tips of ON-bipolar cells contained for the specific markers of ON-bipolar cells: $G\alpha_o$ (Fig. 3B) and $PKC\alpha$ (Fig. 3C).^{45,46} Specific labeling of the presynaptic compartments of the ribbon synapses with CtBP2 excluded presynaptic localization of GPR179 (Fig. 3D).

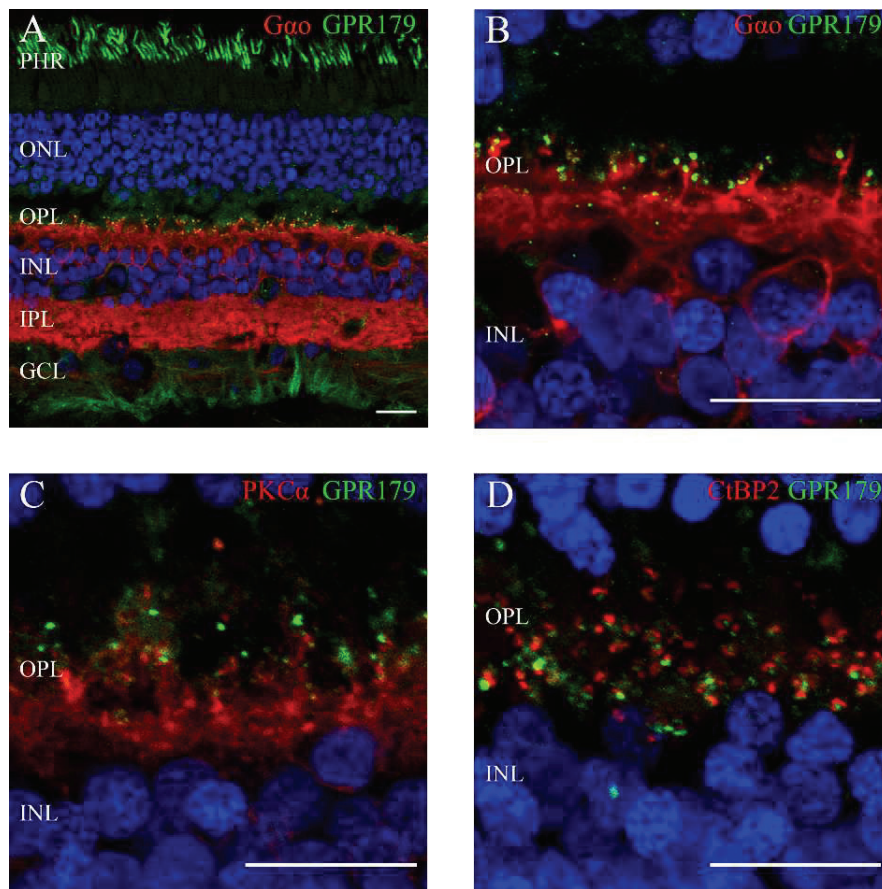


FIGURE 3. GPR179 is localized in the dendritic tips of ON-bipolar cells in whole human retina (A) and at $\times 4$ magnifications (B–D). Retinal sections were double-labeled with GPR179 (green) and markers of distinct synapse compartments (red): (A, B) with *Gαo* (ON-bipolar cells), (C) with PKC α (ON-bipolar cells), and (D) with CtBP2 (presynaptic compartment of ribbon synapse). Nuclei were stained with DAPI (blue). Scale bars: 20 μ m. PHR, photoreceptor layer.

Because of the specific expression of *Gpr179* in ON-bipolar cells (shown by our RNA in situ hybridization studies) and a background signal detected using only secondary antibody in the rod photoreceptors (negative controls in the Supplementary Data), we considered that the additional antibody staining found in the photoreceptor cell layer and Müller cells (Fig. 3A) represented non-specific staining. Similarly, in a study by Klooster et al.⁴⁷ published during the review process of our manuscript, a specific punctuate staining pattern in the OPL using the same GPR179 antibody and some unspecific labeling in other retina layers was detected, thus confirming our results.

Extra- and Intracellular Localization of Wild-Type and Mutated GPR179 Variants

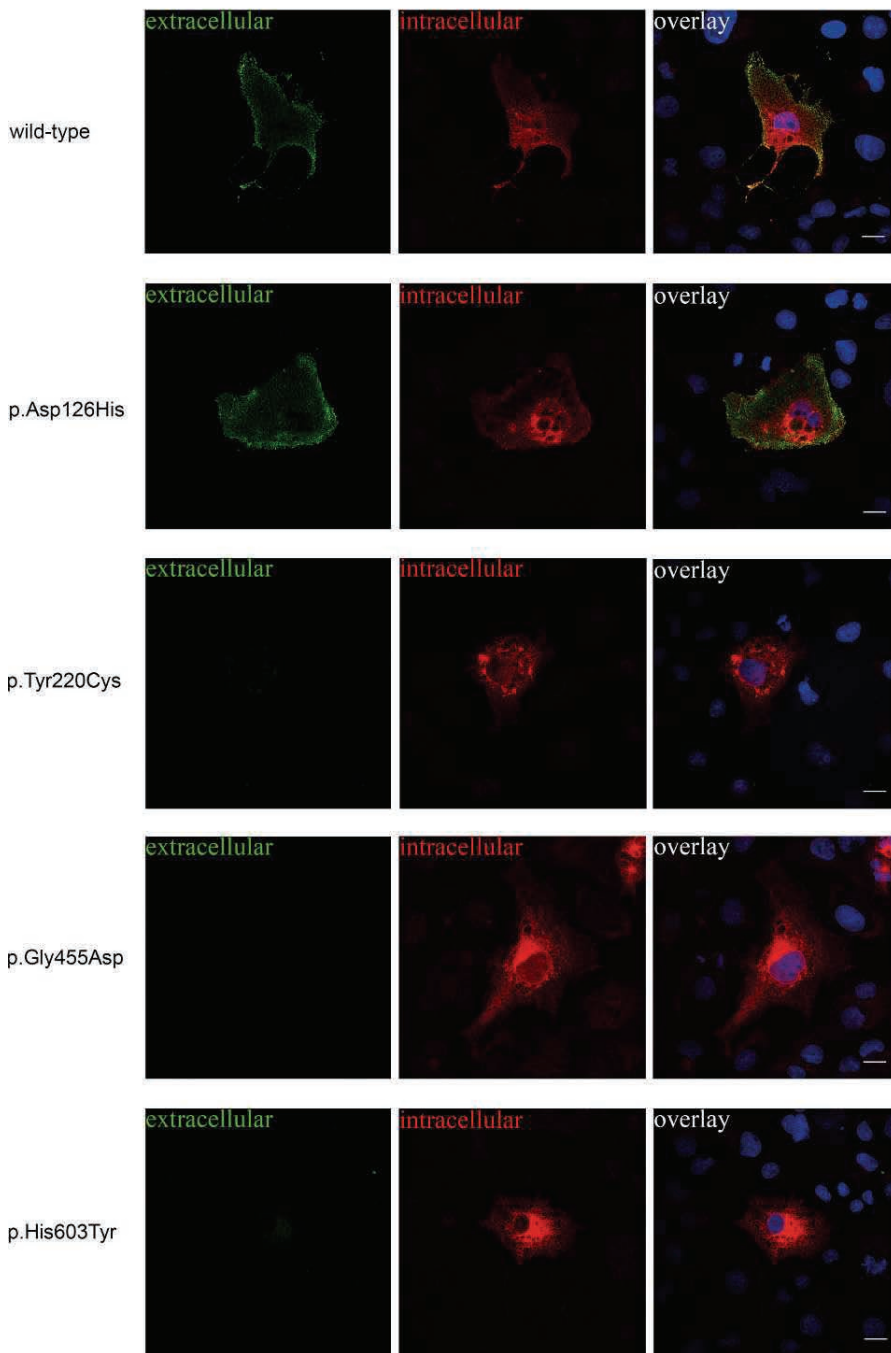
To further investigate the impact of missense mutations leading to cCSNB, the extra- and intracellular immunolocalization of GPR179 in COS-1 cells overexpressing the wild-type and four mutated variants (p.Asp126His, p.Tyr220Cys, p.Gly455Asp, and p.His603Tyr) were investigated. Using live-cell staining, we showed that the GPR179 protein localizes at the surface of the cell and in intracellular compartments, presumably in the endoplasmic reticulum and Golgi apparatus as expected for G protein-coupled receptors (Fig. 4A). This was also true for the p.Asp126His variant. However, the p.Tyr220Cys, p.Gly455Asp, and p.His603Tyr mutations abolished GPR179 surface staining, and these mutant proteins were seen only in intracellular

compartments (Fig. 4A). To validate this outcome with an independent method, we performed ELISA using the anti-GPR179 antibody to detect either the wild-type or the mutated GPR179 receptor transiently expressed in HEK293 cells. Again, while the p.Asp126His mutation was present at the cell surface at levels similar to those of the wild-type GPR179, levels of the other variants (p.Tyr220Cys, p.Gly455Asp, and p.His603Tyr) were severely reduced on the cell surface ($P = 0.002$ for p.Tyr220Cys and p.His603Tyr mutation and 0.0007 for the p.Gly455Asp mutation) (Fig. 4B).

Effect of Splice Site GPR179 Mutation

To investigate the effect of the *GPR179* splice site mutation c.1784+1G>A, we performed a mini-gene approach with wild-type (mini-wt) and mutant (mini-mut) exon 7 to exon 9 regions of *GPR179* amplified from the patient and wild-type genomic DNA, cloned in an expression vector, and tested their transcripts in COS-1 cells (Fig. 5A). RT-PCR analysis of the mini-wt transcript showed two bands: one of 286 base pairs (bp) and one of the expected size of 426 bp. In contrast, RT-PCR analysis of the mini-mut revealed one band of 286 bp but also another of 488 bp with the 426-bp band missing. Sequencing confirmed that the 426-bp band contained correctly spliced exons 7, 8, and 9 of *GPR179*. The band at 286 bp corresponds to a hitherto unknown alternatively spliced *GPR179* transcript lacking exon 8, whereas the 488-bp product contains exon 7 and 8 and part of intron 8 and

A



B

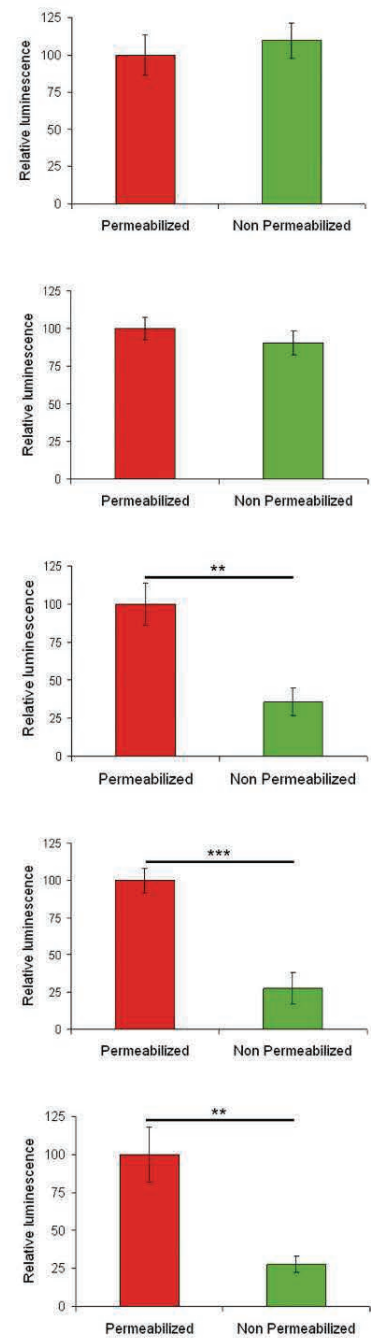


FIGURE 4. p.Tyr220Cys, p.Gly455Asp, and p.His603Tyr mutations affect cellular localization of GPR179. **(A)** Immunolocalization assay results are shown. Extracellular (green, column 1) and intracellular (red, column 2) staining were performed with COS-1 cells expressing wild-type GPR179 (row 1) and p.Asp126His (row 2), p.Tyr220Cys (row 3), p.Gly455Asp (row 4), and p.His603Tyr (row 5) mutated GPR179. An overlay of these stains and DAPI-stained nuclei are presented in column 3. Scale bar: 20 μ m. **(B)** ELISA results are shown. The wild-type GPR179 (row 1) and p.Asp126His (row 2), p.Tyr220Cys (row 3), p.Gly455Asp (row 4), and p.His603Tyr (row 5) mutated GPR179 receptors were transiently expressed in HEK293 cells. Their presence at the cell surface was detected by ELISA (green columns), the total expression being detected after permeabilization of the cell with Triton X-100 (red columns) ($n = 3$; $**P = 0.002$, $***P = 0.0007$, respectively).

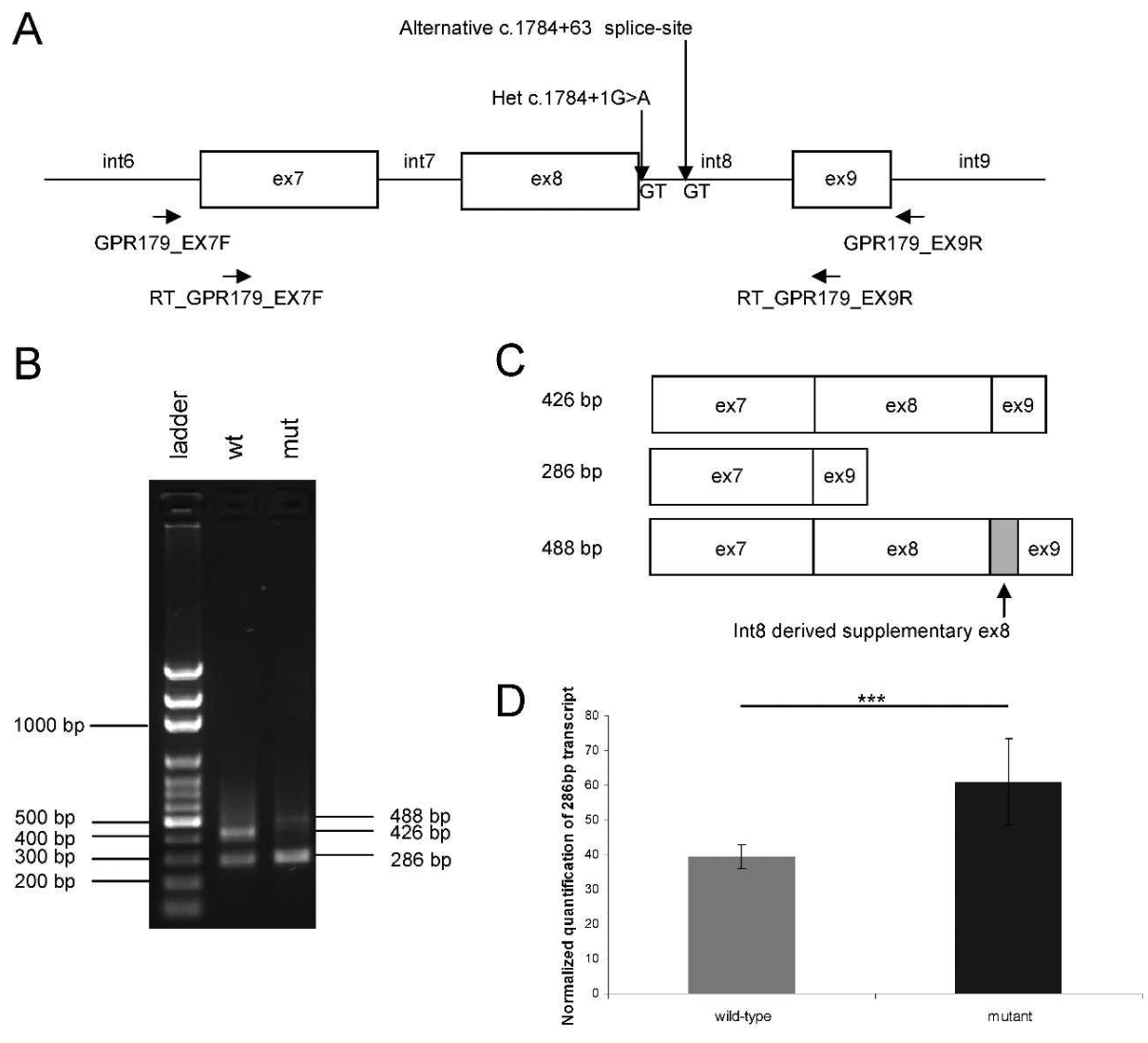


FIGURE 5. The *GPR179* carrying the c.1784+1G>A mutation interferes with splicing. (A) Schematic shows mini-genes used to analyze *GPR179* (NM_001004334.2) splicing. We compared splicing of *GPR179* control (mini-wt) and mutated (mini-mut) alleles with amplicons spanning genomic (g) regions of intron 6 to intron 9. The *horizontal arrows* show binding sites of GPR179_EX7F and GPR179_EX9R oligonucleotides used for patient gDNA PCR and the RT_GPR179_EX7F and RT_GPR179_EX9R primers used for RT-PCR analysis of mini-gene transcripts. The mutation c.1784+1G>A and the alternative c.1784+63 splice site are marked by *vertical arrows*. (B) Representative RT-PCR analyses of transfected COS-1 cells revealed two major transcripts (286 bp and 426 bp) for wild-type (wt) and mutated (mut) constructs (286 bp and 488 bp), respectively. (C) Schematic shows different splice transcripts identified by sequencing. The mini-wt 426-bp transcript includes complete exons 7, 8, and 9, whereas the mini-wt 286-bp isoform skips exon 8. The mini-mut 286-bp transcript is the same as the mini-wt 286-bp isoform, and the mini-mut 488-bp isoform includes exons 7 and 8 and a part of intron 8 and exon 9. (D) Semiquantitative RT-PCR showed a significant increase in skipped exon 8 PCR product in the mini-mut compared to those in mini-wt ($n = 5$; $***P = 0.005$).

exon 9. This supplementary part of intron 8 is presumably due to a cryptic splice donor site localized at c.1784+63 (Figs. 5B, 5C). The difference of a 286-bp transcript between cells transfected with mini-wt and mini-mut has been observed in 5 independent PCR experiments. Five independent actin PCRs were performed with the obtained cDNA to normalize the *GPR179* mini-gene values. The 286-bp product was 1.5-fold more highly expressed in mini-mut than in mini-wt cells ($P = 0.005$) (Fig. 5D).

DISCUSSION

The present study reports the expression and localization pattern of *GPR179* in mouse and human retina, using RNA in

situ hybridization and immunohistochemistry. Furthermore, it describes the impact of the previously reported missense mutations (p.Tyr220Cys, p.Gly455Asp, and p.His603Tyr) by immunocytochemistry and ELISA and of a known splice site mutation (c.1784+1G>A), using a mini-gene approach.

In the current study, we observed *Gpr179* transcript expression in the somata of the upper part of the INL in mouse retina, which resembles the expression of other genes implicated in cCSNB such as *GRM6*, *NYX*, and *TRPM1* in rat,²⁷ chicken,⁴⁸ zebrafish,⁴⁹ mouse,^{26,32} or human.³⁴ Although mouse *GPR179* protein localization was confined to the dendritic tips of the bipolar cells,²⁴ the exact localization of *GPR179* protein in human retina has never been investigated. This question was addressed by using a commercially available

anti-human GPR179 antibody, which was tested for its specificity by immunolocalization in COS-1 cells overexpressing tagged human GPR179. In human retina, this antibody shows staining in the OPL and, more specifically, at the dendritic tips of bipolar cells, consistent with GPR179 location in mouse retina^{24,35} and other proteins implicated in cCSNB, such as GRM6,²⁹ NYX,⁵⁰ TRPM1,^{22,34} and LRIT3²⁵ and which was confirmed just very recently by an independent study.⁴⁷ The sites of expression and localization of GPR179 are in accordance with previous data for the function of GPR179 regulating G protein signaling by controlling localization and activity of the RGS7 complexes,³⁵ which are important for the termination of G protein-coupled receptor (GPCR) signaling pathway.⁵¹ The authors demonstrated that GPR179 colocalizes with RGS7 and RGS11 at the dendritic tips of the ON-bipolar cells in mouse retina and forms specific complexes with RGS7. This specific immunolocalization of RGS7 and RGS11 is absent in *Gpr179^{nob5/nob5}* mice, lacking functional GPR179.³⁵ The precise function of GPR179 needs to be further elucidated, particularly whether it has only a regulatory role or also an additional function as a coreceptor of GRM6 or is an independent receptor with its own ligand.

To elucidate pathogenic mechanisms associated with the *GPR179* gene defect, the previously reported missense mutations p.Asp126His, p.Tyr220Cys, p.Gly455Asp, and p.His603Tyr were studied in vitro.^{23,24} We demonstrated both by immunostaining and ELISA that the p.Tyr220Cys, p.Gly455Asp, and p.His603Tyr mutations were associated with cell surface mislocalization, whereas there were no differences between the non-mutated and the p.Asp126His variant. The Asp126 residue is localized in the predicted extracellular N-terminal region of the protein.²³ Although, the three-dimensional structure of the amino acid residues <300 of GPR179 is currently uncertain, we know from other receptors that the N-terminus of such proteins is important for ligand binding, and we could therefore hypothesize that the p.Asp126His mutation is also associated with the loss of GPR179 ligand binding²³ and not with a trafficking defect. However, to verify this hypothesis, the relevant ligand first needs to be identified. Although Tyr220 localizes in the extracellular N-terminal region of GPR179, the p.Tyr220Cys exchange is associated with a trafficking defect. This agrees with previous predictions that this mutation replaces a highly conserved Tyr with a new cysteine, which may have an impact on the structure of the protein.²⁴ The Gly455 residue is localized within the third transmembrane helix, predicted to be part of the GPR179 binding pocket. Because the p.Gly455Asp mutation introduces a long negatively charged side chain, we assumed this mutation could hamper the normal functioning of the receptor.²³ Here we demonstrate that GPR179 localization at the plasma membrane is severely reduced, which implies that the charge change induced by this mutation can disrupt the correct trafficking of the protein. The His603 residue is localized in the external loop, bridging the sixth and seventh transmembrane domain,²³ and is also associated with a trafficking problem. Similarly, missense mutations in *GRM6* associated with arcCSNB in three different domains also abolish proper trafficking.^{19,52} Finally, the effect of the c.1784+1G>A mutation on splicing of GPR179 was tested by using a mini-gene approach in COS-1 cells overexpressing exons 7, 8, and 9 of the wild-type and c.1784+1G>A-mutated *GPR179*. The wild-type mini-gene expression revealed two transcripts, one containing all exons and one lacking exon 8. The splice donor site mutant also showed a transcript lacking exon 8, expressed at a 1.5-fold higher level than in the wild-type construct and another transcript containing exons 7 and 8, one part of intron 8 with a cryptic donor site, and exon 9. The wild-type transcript with normal exons 7, 8, and 9 was missing. The as-

yet undescribed alternative splice product found with mini-wt and mini-mut lacking exon 8 leads to a shift in the open reading frame that may induce the synthesis of a truncated protein (p.Ala549Glyfs*31), which is predicted to delete GPR179 from the fifth transmembrane domain or may lead to nonsense-mediated mRNA decay. The cryptic donor site of the 488-bp product found only in the mutant form is predicted to lead to a nonsense mutation immediately after the last amino acid encoded by the exon 8 (p.F599*), which may delete GPR179 from the fourth and last extracellular domain and thus lead to a non-functional protein or to nonsense-mediated mRNA decay. The effect of the alternative splicing that leads to the transcript lacking exon 8 present in the wild-type and mutated variants needs to be further investigated to better understand whether the shorter GPR179 protein has a function through a possible dimerization with the full-length GPR179 as seen for other GPCRs.⁵³ If indeed nonsense-mediated mRNA decay occurs, eliminating both alternative transcripts, which then leads to loss of protein synthesis, the pathogenic mechanism of the c.1784+1G>A splice site mutation could also be explained by a loss of function.

Our results indicate that GPR179 is expressed in the INL and localized at the dendritic tips of ON-bipolar cells in the retina and that the cCSNB phenotype is the result of mislocalization of GPR179. This protein is important for the signaling cascade that occurs postsynaptically to the photoreceptors in ON-bipolar cells. The crystal structure of the protein is not available, so the exact role of each domain of GPR179 and the effect of the mutations are not known, but, based on homology models and on our new in vitro studies, we document for most of the missense and splice site mutations that the pathogenic mechanism is caused by a loss of function as it is also predicted for the frame shift and nonsense mutations previously identified in GPR179.^{23,24} Further studies are needed to better understand the exact role of GPR179 in ON-bipolar cell signal transduction cascade, including the identification of a putative ligand which may unravel other pathogenic mechanisms leading to cCSNB.

Acknowledgments

The authors thank Stéphane Fouquet and David Godefroy for imaging support using confocal microscopy and Nanozoomer, respectively (platforms from Institut de la Vision); Gilles Thuret and his laboratory for providing human retinas; Xavier Guillonnet and Kim Nguyen-Ba-Charvet for providing colocalization antibodies; Caroline Moreau-Fauvarque for technical help with RNA in situ hybridization; and Bob Gillan for proofreading and editing the manuscript.

Supported by Agence Nationale de la Recherche (ANR-12-BSVS1-0012-01_GPR179) (CZ), Fondation Voir et Entendre (CZ), Prix Dalloz for la recherche en ophtalmologie (CZ), Fondation Fighting Blindness (FFB) (CD-CL-0808-0466-CHNO) (IA), and the CIC503, recognized as an FFB center (FFB Grant C-CMM-0907-0428-INSERM04), Ville de Paris and Region Ile de France, Labex Lifesenses (reference ANR-10-LABX-65) supported by French state funds managed by the ANR within the Investissements d'Avenir programme (ANR-11-IDEX-0004-0), and the Regional Council of Ile-de-France (I09 - 1727/R) (EO).

Disclosure: **E. Orhan**, None; **L. Prézéau**, None; **S. El Shamieh**, None; **K.M. Bujakowska**, None; **C. Michiels**, None; **Y. Zagar**, None; **C. Vol**, None; **S.S. Bhattacharya**, None; **J.-A. Sahel**, None; **F. Sennlaub**, None; **I. Audo**, None; **C. Zeitz**, None

References

1. Zeitz C. Molecular genetics and protein function involved in nocturnal vision. *Expert Rev Ophthalmol*. 2007;2:467-485.

2. Traboulsi EI, Leroy BP, Zeitz C. Congenital stationary night blindness. In: Traboulsi EI, ed. *Genetic Diseases of the Eye*. New York: Oxford; 2012:476-483.
3. Riggs LA. Electroretinography in cases of night blindness. *Am J Ophthalmol*. 1954;38:70-78.
4. Schubert G, Bornschein H. Analysis of the human electroretinogram [in undetermined language]. *Ophthalmologica*. 1952; 123:396-413.
5. Miyake Y, Yagasaki K, Horiguchi M, Kawase Y, Kanda T. Congenital stationary night blindness with negative electroretinogram. A new classification. *Arch Ophthalmol*. 1986;104: 1013-1020.
6. Dryja TP, Berson EL, Rao VR, Oprian DD. Heterozygous missense mutation in the rhodopsin gene as a cause of congenital stationary night blindness. *Nat Genet*. 1993;4:280-283.
7. Gal A, Orth U, Baehr W, Schwinger E, Rosenberg T. Heterozygous missense mutation in the rod cGMP phosphodiesterase beta-subunit gene in autosomal dominant stationary night blindness. *Nat Genet*. 1994;7:551.
8. Rao VR, Cohen GB, Oprian DD. Rhodopsin mutation G90D and a molecular mechanism for congenital night blindness. *Nature*. 1994;367:639-642.
9. Dryja TP, Hahn LB, Reboul T, Arnaud B. Missense mutation in the gene encoding the alpha subunit of rod transducin in the Nougaret form of congenital stationary night blindness. *Nat Genet*. 1996;13:358-360.
10. al-Jandal N, Farrar GJ, Kiang AS, et al. A novel mutation within the rhodopsin gene (Thr-94-Ile) causing autosomal dominant congenital stationary night blindness. *Hum Mutat*. 1999;13: 75-81.
11. Riazuddin SA, Shahzadi A, Zeitz C, et al. A mutation in SLC24A1 implicated in autosomal-recessive congenital stationary night blindness. *Am J Hum Genet*. 2010;87:523-531.
12. Bech-Hansen NT, Naylor MJ, Maybaum TA, et al. Loss-of-function mutations in a calcium-channel alpha1-subunit gene in Xp11.23 cause incomplete X-linked congenital stationary night blindness. *Nat Genet*. 1998;19:264-267.
13. Strom TM, Nyakatura G, Apfelstedt-Sylla E, et al. An L-type calcium-channel gene mutated in incomplete X-linked congenital stationary night blindness. *Nat Genet*. 1998;19:260-263.
14. Zeitz C, Kloeckener-Gruissem B, Forster U, et al. Mutations in CABP4, the gene encoding the Ca²⁺-binding protein 4, cause autosomal recessive night blindness. *Am J Hum Genet*. 2006; 79:657-667.
15. Wycisk KA, Zeitz C, Feil S, et al. Mutation in the auxiliary calcium-channel subunit CACNA2D4 causes autosomal recessive cone dystrophy. *Am J Hum Genet*. 2006;79:973-977.
16. Bech-Hansen NT, Naylor MJ, Maybaum TA, et al. Mutations in NYX, encoding the leucine-rich proteoglycan nyctalopin, cause X-linked complete congenital stationary night blindness. *Nat Genet*. 2000;26:319-323.
17. Pusch CM, Zeitz C, Brandau O, et al. The complete form of X-linked congenital stationary night blindness is caused by mutations in a gene encoding a leucine-rich repeat protein. *Nat Genet*. 2000;26:324-327.
18. Dryja TP, McGee TL, Berson EL, et al. Night blindness and abnormal cone electroretinogram ON responses in patients with mutations in the GRM6 gene encoding mGluR6. *Proc Natl Acad Sci U S A*. 2005;102:4884-4889.
19. Zeitz C, van Genderen M, Neidhardt J, et al. Mutations in GRM6 cause autosomal recessive congenital stationary night blindness with a distinctive scotopic 15-Hz flicker electroretinogram. *Invest Ophthalmol Vis Sci*. 2005;46:4328-4335.
20. Li Z, Sergouniotis PI, Michaelides M, et al. Recessive mutations of the gene TRPM1 abrogate ON bipolar cell function and cause complete congenital stationary night blindness in humans. *Am J Hum Genet*. 2009;85:711-719.
21. Audo I, Kohl S, Leroy BP, et al. TRPM1 is mutated in patients with autosomal-recessive complete congenital stationary night blindness. *Am J Hum Genet*. 2009;85:720-729.
22. van Genderen MM, Bijveld MM, Claassen YB, et al. Mutations in TRPM1 are a common cause of complete congenital stationary night blindness. *Am J Hum Genet*. 2009;85:730-736.
23. Audo I, Bujakowska K, Orhan E, et al. Whole-exome sequencing identifies mutations in GPR179 leading to autosomal-recessive complete congenital stationary night blindness. *Am J Hum Genet*. 2012;90:321-330.
24. Peachey N, Ray T, Florijn R, et al. GPR179 is required for depolarizing bipolar cell function and is mutated in autosomal-recessive complete congenital stationary night blindness. *Am J Hum Genet*. 2012;90:331-339.
25. Zeitz C, Jacobson S, Hamel C, et al. Whole-exome sequencing identifies LRIT3 mutations as a cause of autosomal-recessive complete congenital stationary night blindness. *Am J Hum Genet*. 2013;92:67-75.
26. Morgans CW, Zhang J, Jeffrey BG, et al. TRPM1 is required for the depolarizing light response in retinal ON-bipolar cells. *Proc Natl Acad Sci U S A*. 2009;106:19174-19178.
27. Nakajima Y, Iwakabe H, Akazawa C, et al. Molecular characterization of a novel retinal metabotropic glutamate receptor mGluR6 with a high agonist selectivity for L-2-amino-4-phosphonobutyrate. *J Biol Chem*. 1993;268:11868-11873.
28. Gregg RG, Mukhopadhyay S, Candille SI, et al. Identification of the gene and the mutation responsible for the mouse nob phenotype. *Invest Ophthalmol Vis Sci*. 2003;44:378-384.
29. Vardi N, Duvoisin R, Wu G, Sterling P. Localization of mGluR6 to dendrites of ON bipolar cells in primate retina. *J Comp Neurol*. 2000;423:402-412.
30. Morgans CW, Ren G, Akileswaran L. Localization of nyctalopin in the mammalian retina. *Eur J Neurosci*. 2006;23:1163-1171.
31. Rao A, Dallman R, Henderson S, Chen CK. Gbeta5 is required for normal light responses and morphology of retinal ON-bipolar cells. *J Neurosci*. 2007;27:14199-14204.
32. Gilliam JC, Wensel TG. TRP channel gene expression in the mouse retina. *Vision Res*. 2011;51:2440-2452.
33. Pearring JN, Bojang P Jr, Shen Y, et al. A role for nyctalopin, a small leucine-rich repeat protein, in localizing the TRP melastatin 1 channel to retinal depolarizing bipolar cell dendrites. *J Neurosci*. 2011;31:10060-10066.
34. Klooster J, Blokker J, Ten Brink J, et al. Ultrastructural localization and expression of TRPM1 in the human retina. *Invest Ophthalmol Vis Sci*. 2011;52:8356-8362.
35. Orlandi C, Posokhova E, Masuho I, et al. GPR158/179 regulate G protein signaling by controlling localization and activity of the RGS7 complexes. *J Cell Biol*. 2012;197:711-719.
36. Nawy S. The metabotropic receptor mGluR6 may signal through G(o), but not phosphodiesterase, in retinal bipolar cells. *J Neurosci*. 1999;19:2938-2944.
37. Shen Y, Heimel JA, Kamermans M, Peachey NS, Gregg RG, Nawy S. A transient receptor potential-like channel mediates synaptic transmission in rod bipolar cells. *J Neurosci*. 2009;29: 6088-6093.
38. Koike C, Obara T, Uriu Y, et al. TRPM1 is a component of the retinal ON bipolar cell transduction channel in the mGluR6 cascade. *Proc Natl Acad Sci U S A*. 2010;107:332-337.
39. Morgans CW, Weiwei L, Wensel TG, et al. Gbeta5-RGS complexes co-localize with mGluR6 in retinal ON-bipolar cells. *Eur J Neurosci*. 2007;26:2899-2905.
40. Cao Y, Pahlberg J, Sarria I, Kamasawa N, Sampath AP, Martemyanov KA. Regulators of G protein signaling RGS7 and RGS11 determine the onset of the light response in ON

- bipolar neurons. *Proc Natl Acad Sci U S A*. 2012;109:7905-7910.
41. Kondo M, Sanuki R, Ueno S, et al. Identification of autoantibodies against TRPM1 in patients with paraneoplastic retinopathy associated with ON bipolar cell dysfunction. *PLoS One*. 2011;6:e19911.
 42. Bacchetti S, Graham FL. Transfer of the gene for thymidine kinase to thymidine kinase-deficient human cells by purified herpes simplex viral DNA. *Proc Natl Acad Sci U S A*. 1977;74:1590-1594.
 43. Zeitz C, Scherthan H, Freier S, et al. NYX (nyctalopin on chromosome X), the gene mutated in congenital stationary night blindness, encodes a cell surface protein. *Invest Ophthalmol Vis Sci*. 2003;44:4184-4191.
 44. Binet V, Duthey B, Lecaillon J, et al. Common structural requirements for heptahelical domain function in class A and class C G protein-coupled receptors. *J Biol Chem*. 2007;282:12154-12163.
 45. Vardi N, Matesic DE, Manning DR, Liebman PA, Sterling P. Identification of a G-protein in depolarizing rod bipolar cells. *Vis Neurosci*. 1993;10:473-478.
 46. Negishi K, Kato S, Teranishi T. Dopamine cells and rod bipolar cells contain protein kinase C-like immunoreactivity in some vertebrate retinas. *Neurosci Lett*. 1988;94:247-252.
 47. Klooster J, van Genderen MM, Yu M, et al. Ultrastructural localization of GPR179, and the impact of mutant forms on retinal function in CSNB1 patients and a mouse model. *Invest Ophthalmol Vis Sci*. 2013;54:6973-6981.
 48. Bech-Hansen NT, Cockfield J, Liu D, Logan CC. Isolation and characterization of the leucine-rich proteoglycan nyctalopin gene (cNyx) from chick. *Mamm Genome*. 2005;16:815-824.
 49. Bahadori R, Biehlmaier O, Zeitz C, et al. Nyctalopin is essential for synaptic transmission in the cone dominated zebrafish retina. *Eur J Neurosci*. 2006;24:1664-1674.
 50. Gregg R, Kamermans M, Klooster J, et al. Nyctalopin expression in retinal bipolar cells restores visual function in a mouse model of complete X-linked congenital stationary night blindness. *J Neurophysiol*. 2007;98:3023-3033.
 51. Slepak VZ. Structure, function, and localization of Gbeta5-RGS complexes. *Prog Mol Biol Transl Sci*. 2009;86:157-203.
 52. Zeitz C, Forster U, Neidhardt J, et al. Night blindness-associated mutations in the ligand-binding, cysteine-rich, and intracellular domains of the metabotropic glutamate receptor 6 abolish protein trafficking. *Hum Mutat*. 2007;28:771-780.
 53. Wise H. The roles played by highly truncated splice variants of G protein-coupled receptors. *J Mol Signal*. 2012;7:13.

3. Complementary ongoing results: *GPR179* KO first model characterization

Various animal models have been described for identifying and elucidating the pathogenic mechanism(s) of gene defects underlying cCSNB. Moreover, several other genes as *LRIT3* [MIM615004] (70), regulator of G protein signaling 11 (*RGS11*) [MIM603895] (248), regulator of G protein signaling 7 (*RGS7*) [MIM602517] (248) and guanine nucleotide-binding protein subunit beta-5 (*GNB5*) [MIM604447] (75) were described as coding proteins implicated in the same signaling cascade. When we first identified *GPR179* mutations in patients with cCSNB, GPR179 was a functionally unknown orphan receptor. To validate that *GPR179* mutations lead indeed to cCSNB and to better understand the physiopathology, we chose to study a mouse model for *GPR179*. We characterized this mouse model structurally by SD-OCT and functionally by ERG recordings. To better understand the role of GPR179 in the retina and localize it in this signaling cascade, localization of other proteins of the signaling cascade was investigated by immunohistochemistry.

a) Creation and genotyping of the *Gpr179* KO first mouse model

To further investigate the role of GPR179 *in vivo*, we studied a *Gpr179* knock-out mouse. The new model was constructed at the Institut Clinique de la Souris (ICS) (Strasbourg, France) with ES-clones generated by the trans-NIH “Knock-Out Mouse Project” (KOMP) and obtained from the KOMP Repository (www.komp.org). Prior to the study we genotyped the founder animals for the *Crb1^{rd8}*, *Pde6 β ^{rd1}*, and *Gnat2^{cpfl3}* mutations to exclude pathogenic variants common in laboratory mouse strains (249). We also sequenced flanking intronic and exonic regions of genes implicated in CSNB to ensure the absence of an additional defect in the model i.e *Grm6*, *Gpr179*, *Nyx*, *Lrit3* and *Trpm1* as well as intron 2 of *Grm6* as previously described (250). We did not find any mutation, except the homozygous *Crb1^{rd8}* mutation, which was already described in the C57Bl6/N strain (251) used for ES-clones. We backcrossed two generations of these animals with C57Bl6/J mice that were free of the *Crb1^{rd8}* mutation and obtained heterozygous knock-out mice for *Gpr179* free of any other mutation in the screened genes. Heterozygous knock-out mice for *Gpr179* were intercrossed to produce wild-type (*Gpr179^{+/+}*), heterozygous (*Gpr179^{+/-}*) and mutant (*Gpr179^{-/-}*) offspring.

b) Functional characterization by ERG recordings

ERG was performed on 10 *Gpr179*^{+/+}, 12 *Gpr179*^{+/-} and 10 *Gpr179*^{-/-} at 3 months-of-age.

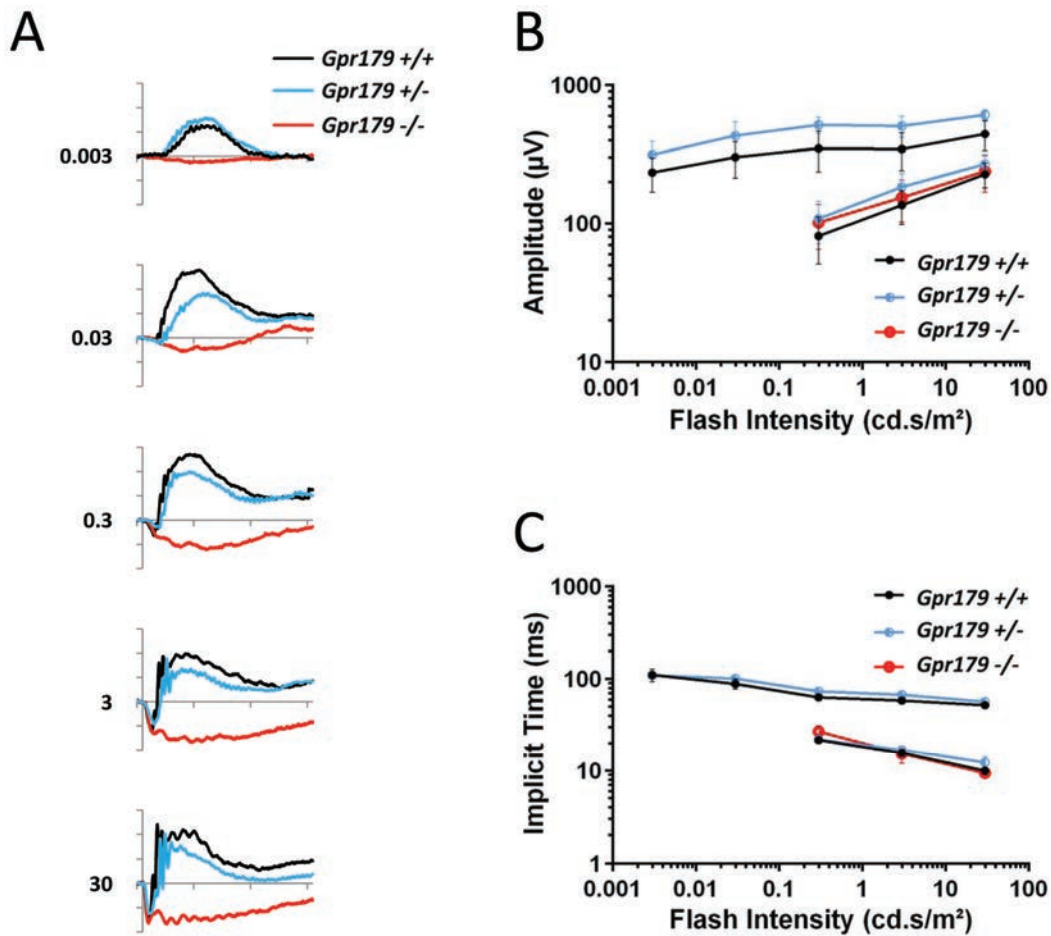


Figure 34: Scotopic ERG responses. Dark-adapted ERG series were obtained from 10 *Gpr179*^{+/+} (black line), 12 *Gpr179*^{+/-} (blue line) and 10 *GPR179*^{-/-} (red line) littermates. (A) Representative waveforms, as a function of stimulation intensity. The scale marks indicate 100 ms (time in abscissa) and 200 μV (amplitude in ordonnate). Values to the left of the waveforms indicate stimulation flash intensity in cd.s/m². Amplitude (B) and implicit time (C) of the major components of the dark-adapted ERG with increasing flash intensity. The b-wave component is absent in *Gpr179*^{-/-} mice and therefore this data is not plotted.

Under scotopic conditions, which allow testing of the rod-pathway function, *Gpr179*^{+/+} showed normal responses for both a- and b-wave. As expected, with increasing flash intensities, amplitudes of both a- and b-waves increased (Figure 34 A) and implicit times of both a- and b-waves decreased (Figure 34 B). ERG responses of *Gpr179*^{+/-} heterozygous mice were similar with *Gpr179*^{+/+} ERG responses (Figure 34 A-B). In contrast, *Gpr179*^{-/-} mice were lacking b-waves on their ERG responses, while a-waves were comparable in amplitude or implicit time to *Gpr179*^{+/+} and *Gpr179*^{+/-} (Figure 34 A-B), leading to an electronegative

ERG waveform in *Gpr179*^{-/-} where b-wave is absent and a-wave preserved. These results indicate a signal transmission defect between rod photoreceptors and ON-bipolar cells, whereas the phototransduction in rod photoreceptors is not affected.

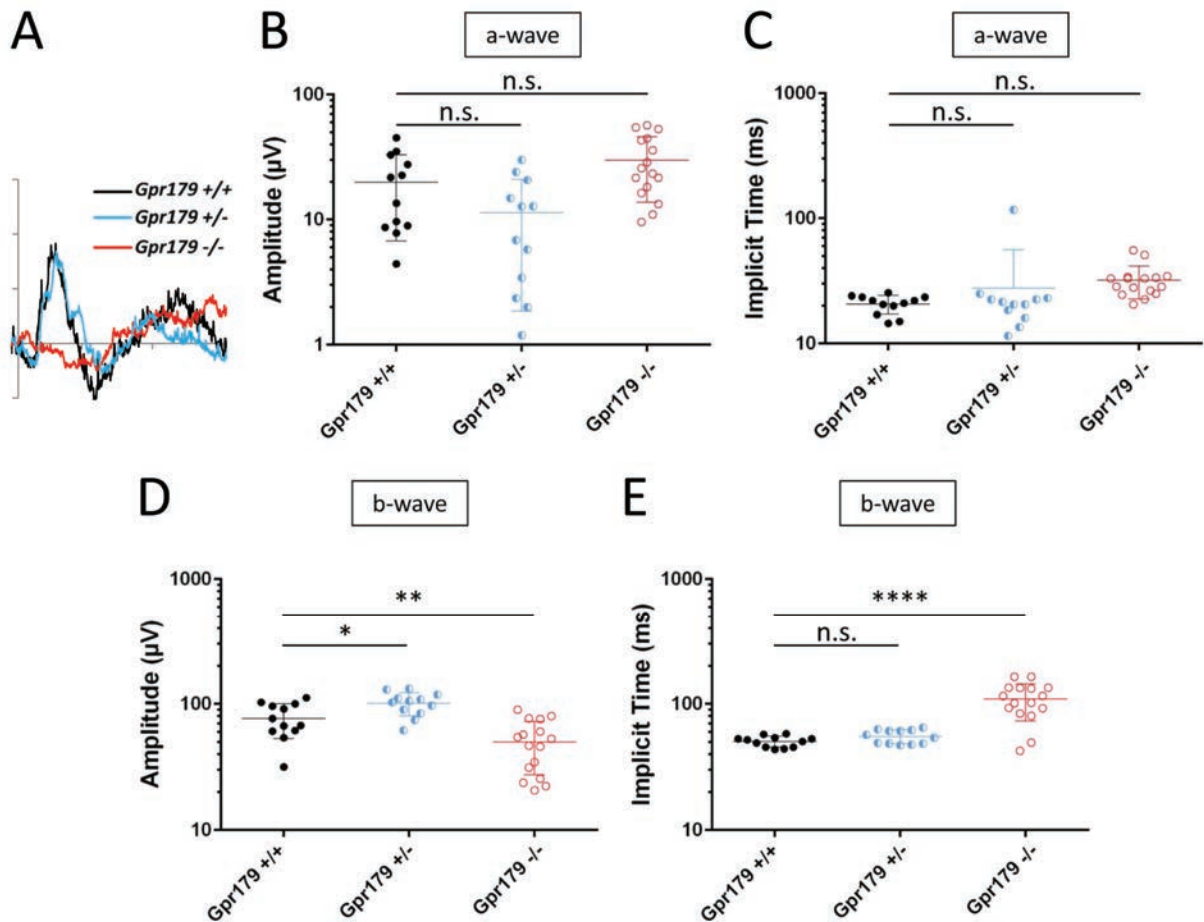


Figure 35: Photopic ERG responses. Light-adapted ERG recordings with a stimulus intensity of 3cd.s/m² were obtained from 10 *Gpr179*^{+/+} (black line), 12 *Gpr179*^{+/-} (blue line) and 10 *Gpr179*^{-/-} (red line) littermates. (A) Representative waveforms. The scale marks indicate 100 ms (time in abscissa) and 50 μV (amplitude in ordonnate). Amplitude (B) and implicit time (C) of the a-wave. Amplitude (D) and implicit time (E) of the b-wave. Abbreviations: n.s. = non significant, * : p<0.05, **: p<0.005, ****: p<0.0001.

Under photopic conditions, which allows testing cone function, *Gpr179*^{+/+} mice showed normal ERG responses for both a- and b-waves. Responses in *Gpr179*^{+/-} mice were not different from those of *Gpr179*^{+/+} (Figure 35 A-B and 35 D) except for b-wave amplitude where *Gpr179*^{+/+} showed smaller b-wave amplitude than *Gpr179*^{+/-} (Figure 35 C). In contrast, ERG responses for *Gpr179*^{-/-} were more variable and showed smaller b-wave amplitudes (Figure 35 C) and longer b-wave implicit times (Figure 35 D) than for *Gpr179*^{+/+}. These results are in keeping with cone-mediated pathway dysfunction in these mice.

c) Structural characterization by SD-OCT

SD-OCT was performed on 10 *Gpr179*^{+/+}, 12 *Gpr179*^{+/-} and 10 *Gpr179*^{-/-} at 3 months-of-age.

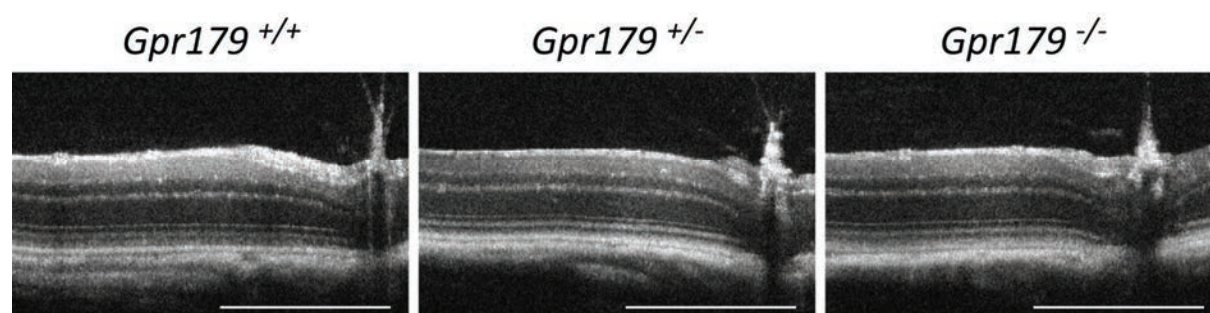


Figure 36: SD-OCT retinal morphology of 3-month-old *Gpr179*^{+/+}, *Gpr179*^{+/-} and *Gpr179*^{-/-} mice. Scale bar: 500µm

We compared retinal morphology for *Gpr179*^{+/+}, *Gpr179*^{+/-} and *Gpr179*^{-/-} mice and we did not notice any obvious modification (Figure 36). Measurements of different layer thicknesses are ongoing now.

d) Localization of the proteins of the cascade

To validate our *Gpr179* knock-out model, we performed immunohistochemistry to confirm that GPR179 protein was absent in *Gpr179*^{-/-} mouse. Immunohistochemistry on *Gpr179*^{+/+} mouse retinal sections revealed a clear staining in the OPL (Figure 37 A, 37 C and 37 E) which was absent in *Gpr179*^{-/-} (Figure 37 B, 37 D and 37 F). Some slight non-specific staining remained in the IPL and the GCL in both *Gpr179*^{+/+} and *Gpr179*^{-/-} mice (Figure 37 A-B). In *Gpr179*^{+/+} mouse retinal sections, the staining localized specifically at the dendritic tips of presumably all ON-bipolar cells (Figure 37 C and 37 E), co-stained for the specific marker of rod ON-bipolar cells PKC α (Figure 37 C), and for the cone pedicle specific marker PNA (Figure 37 E). This specific staining is absent in *Gpr179*^{-/-} mouse retinal sections, while PKC α and PNA staining is unaffected (Figure 37 B, 37 D and 37 F).

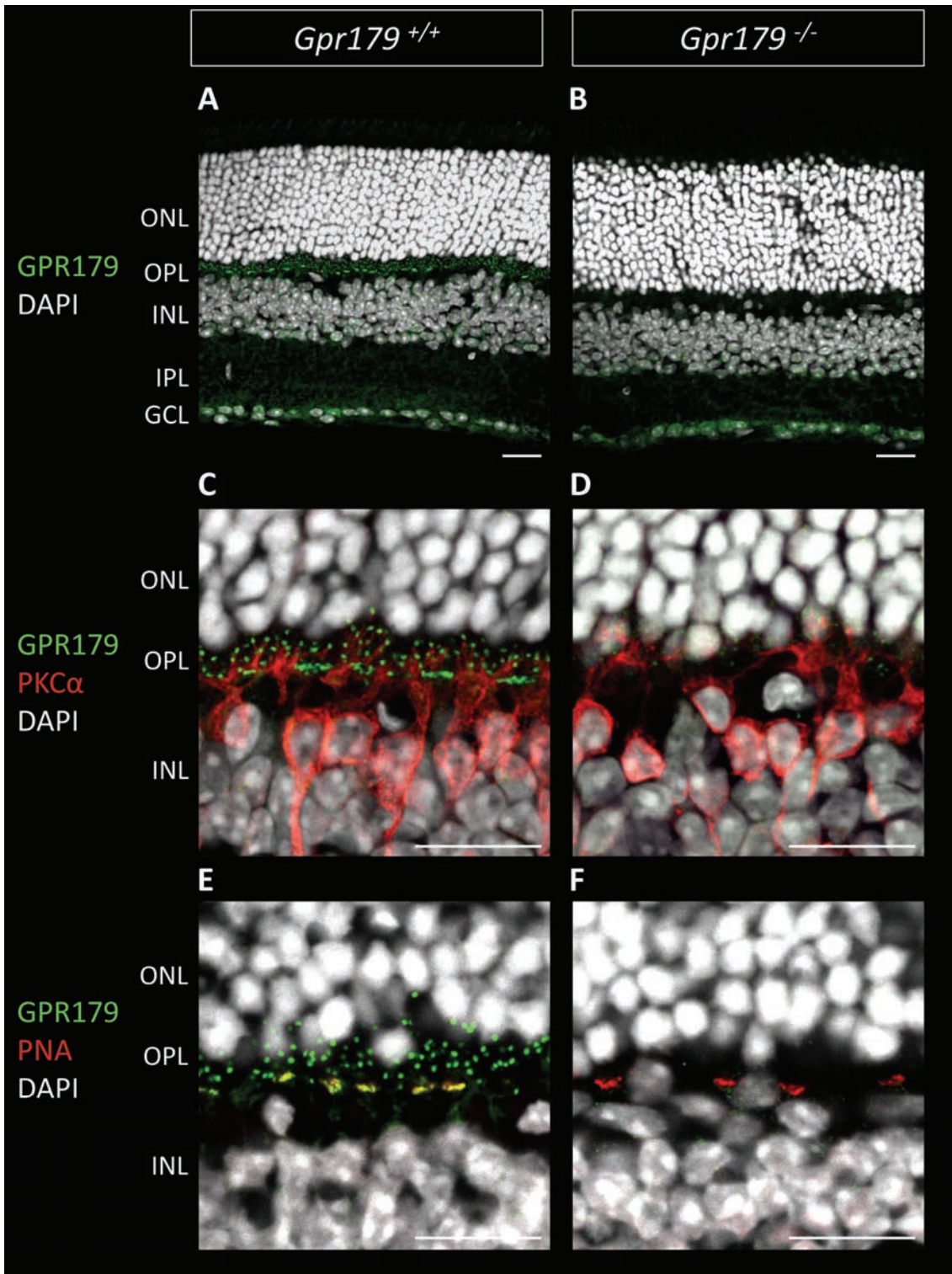


Figure 37: Validation of *Gpr179* knock-out model. Representative confocal images of *Gpr179*^{+/+} and *Gpr179*^{-/-} mouse retinal sections. *Gpr179*^{+/+} (A) and *Gpr179*^{-/-} (B) mouse retinal sections were stained with anti-GPR179 (green), and DAPI (white). (C) and (D) are 4X zoom focused on the outer plexiform layer (OPL) of (A) and (B), with additional staining of rod ON-bipolar cell specific marker PKC α (red). (E) and (F) are focused images on OPL of *Gpr179*^{+/+} (E) and *Gpr179*^{-/-} (F) mouse retinal sections stained with anti-GPR179 (green), anti-PNA which is a marker of cone pedicle (red) and DAPI (white). Scale bar: 20 μ m, ONL: outer nuclear layer; OPL: outer plexiform layer; INL: inner nuclear layer; IPL: inner plexiform layer; GCL: ganglion cell layer.

Once the model had been validated by immunohistochemistry, we studied the localization of various proteins involved in this ON-bipolar signal cascade. Immunohistochemistry on *Gpr179*^{-/-} mouse retinal sections revealed ON-bipolar cell dendritic tip staining for GRM6 (Figure 38 B), TRPM1 and LRIT3 (Figure 38 D) similar to findings in *Gpr179*^{+/+} mouse retinal sections (Figure 38 A and 38 C).

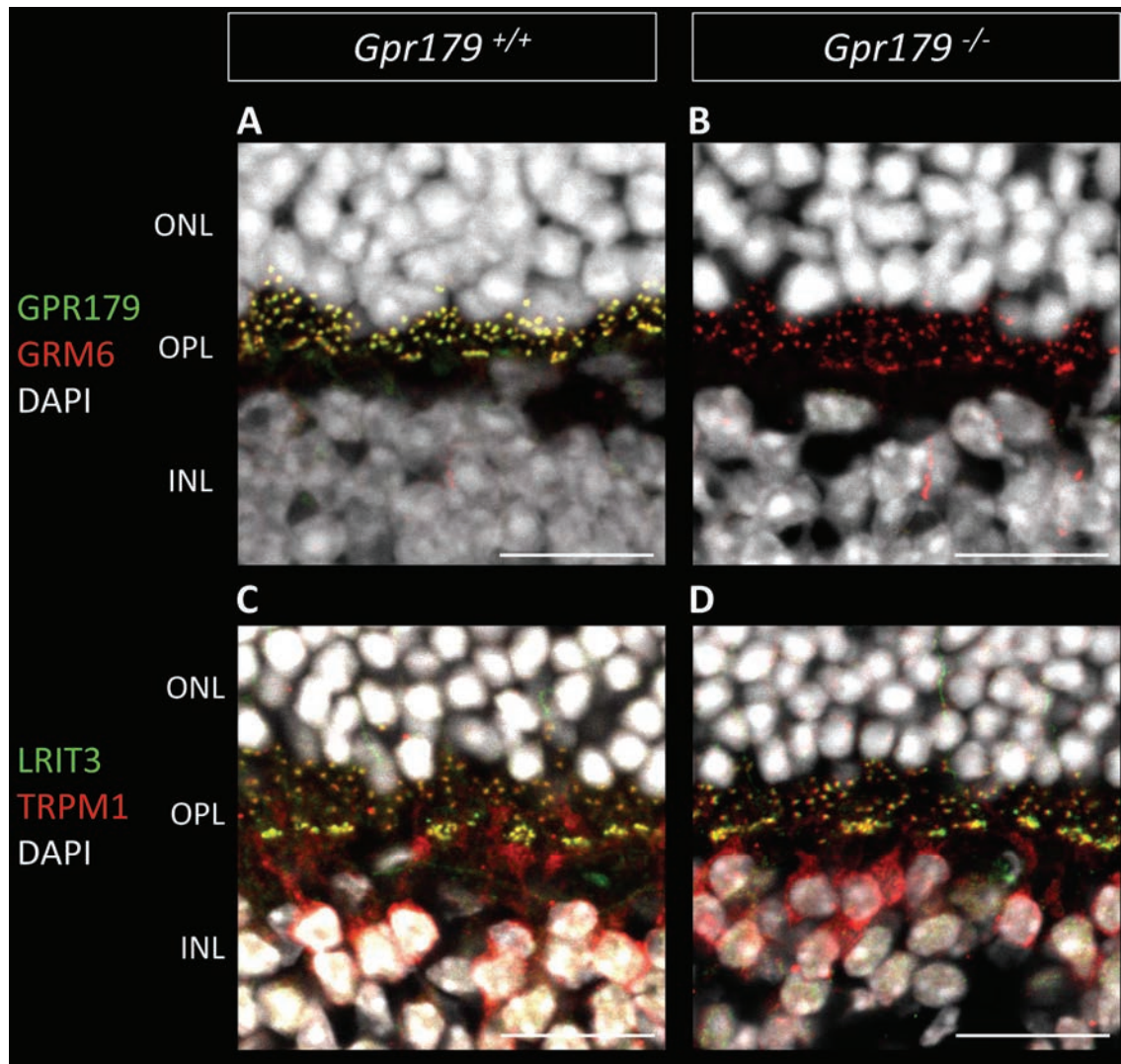


Figure 38: Localization of GRM6, TRPM1 and LRIT3 at the dendritic tips of ON-bipolar cells is independent of *Gpr179* expression. Representative confocal images of *Gpr179*^{+/+} and *Gpr179*^{-/-} mouse retinal sections. *Gpr179*^{+/+} (A) and *Gpr179*^{-/-} (B) mouse retinal sections were stained with anti-GPR179 (green), anti-GRM6 (red) and DAPI (white). *Gpr179*^{+/+} (C) and *Gpr179*^{-/-} (D) mouse retinal sections were stained with anti-LRIT3 (green), anti-TRPM1 (red) and DAPI (white). Scale bar: 20µm, ONL: outer nuclear layer; OPL: outer plexiform layer; INL: inner nuclear layer.

However, proteins of the G protein signaling (RGS) family showed a different profile (Figure 39). Immunohistochemistry on *Gpr179*^{+/+} mouse retinal sections against RGS7, RGS11 and GNB5 revealed the localization of these proteins at the dendritic tips of bipolar cells (Figure 39 A and 39 C), whereas on *Gpr179*^{-/-} mouse retinal sections, this staining was absent (Figure 39 B and 39 D).

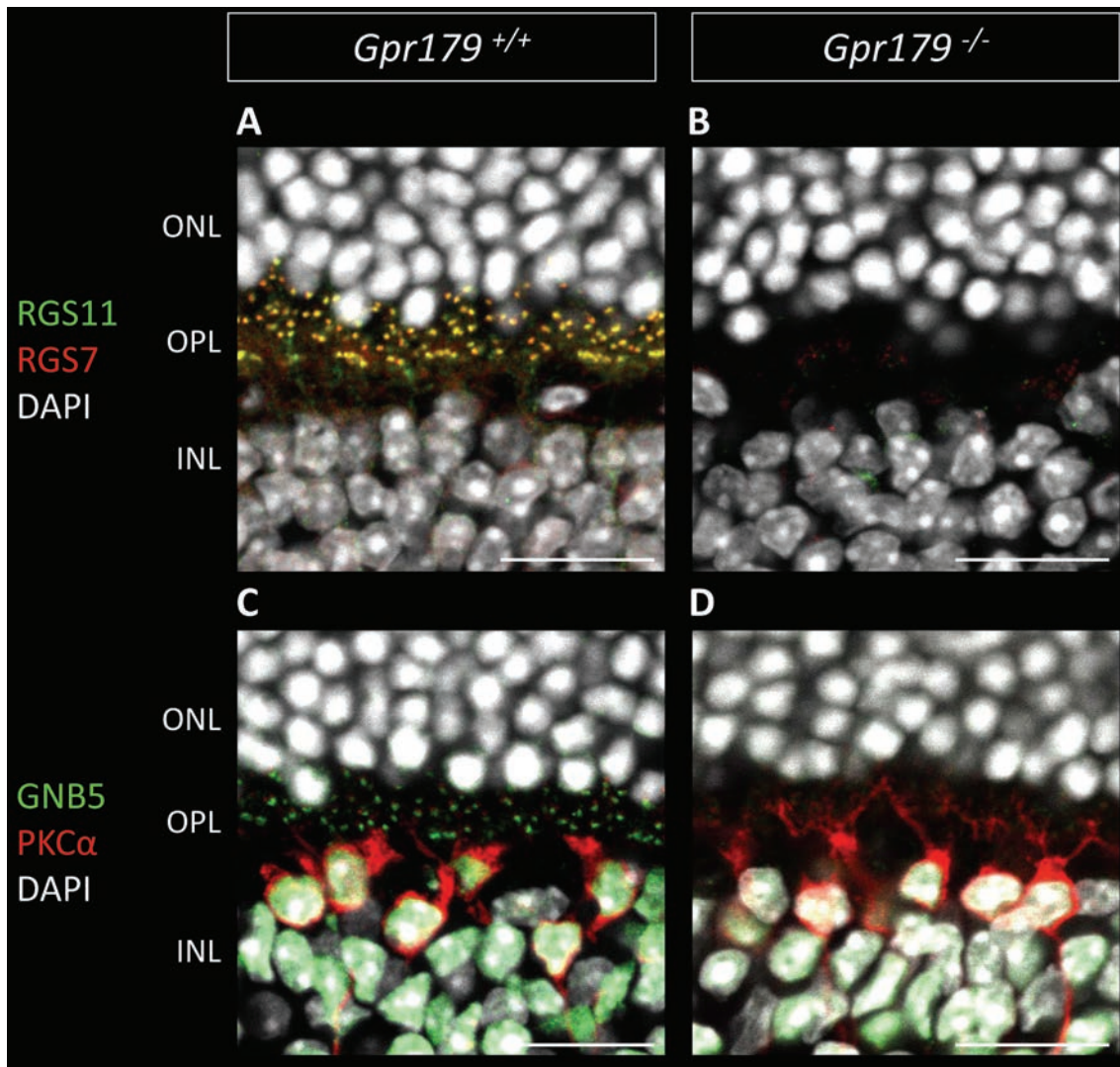


Figure 39: Localization of RGS11, RGS7 and GNB5 at the dendritic tips of ON-bipolar cells is dependent of *Gpr179* expression. Representative confocal images of *Gpr179*^{+/+} and *Gpr179*^{-/-} mouse retinal sections. *Gpr179*^{+/+} (A) and *Gpr179*^{-/-} (B) mouse retinal sections were stained with anti-RGS11 (green), anti-RGS7 (red) and DAPI (white). *Gpr179*^{+/+} (C) and *Gpr179*^{-/-} (D) mouse retinal sections were stained with anti-GNB5 (green), anti-PKC α (red) and DAPI (white). Scale bar: 20 μ m, ONL: outer nuclear layer; OPL: outer plexiform layer; INL: inner nuclear layer.

B. Genome editing approaches applied to Rhodopsin mutations

This work was supported by FEDER, Fondation Valentin Haüy and Retina France, led to three awards, one publication, two paper presentations and three poster presentations at national and international congresses. They are listed below.

Publication:

1. **Orhan, E.**, Dalkara, D., Neuille, M., Lechauve, C., Michiels, C., Picaud, S., Leveillard, T., Sahel, J. A., Naash, M. I., Lavail, M. M., Zeitz, C., and Audo, I. (2015). Genotypic and phenotypic characterization of P23H line 1 rat model. *PLoS One* *10*, e0127319.

Paper presentations:

1. **Orhan, E.**, and Audo, I. (2012). Preuve de concept de thérapie génique de Rhodopsine par Tale nucleases. Réunion Annuelle de la Société de Génétique Ophtalmologique Francophone (EO, Gand, Belgium).

2. **Orhan, E.**, Zeitz, C., and Audo, I. (2014). Genotypic and phenotypic characterization of P23H line 1 rat model. Société de Génétique Ophtalmique Francophone and Deutsche Ophtalmologische Gesellschaft joint meeting (EO, Giessen, Germany).

Poster presentations:

1. **Orhan, E.**, (2013). Proof of principal of “genome surgery” using Transcription Activator-Like Effector Nuclease applied to a model of retinitis pigmentosa, the P23H rat. 14th Annual Meeting of ED394 Physiologie, Physiopathologie and Thérapeutique graduate school of Pierre et Marie Curie University (EO, Paris, France).

2. **Orhan, E.**, (2014). Modeling of retinal disease: example of the P23H rat model. 15th Annual Meeting of ED394 Physiologie, Physiopathologie and Thérapeutique graduate school of Pierre et Marie Curie University (EO, Paris, France).

3. **Orhan, E.**, Dalkara, D., Lechauve, C., Picaud, S., Leveillard, T., Sahel, J.A., Naash, M., LaVail, M.M., Zeitz, C., and Audo, I. (2015). Genotypic and Phenotypic Characterization of the P23H Line 1 Rat Model. Association for Research in Vision and Ophtalmology EO, (Denver, USA).

Awards:

1. Best presentation award at the annual meeting of Société de Génétique Ophtalmologique Francophone (Gand, Belgium) in 2012 .

2. Poster award of the Graduate School (Paris, France) in 2013.

3. Poster award of the Graduate School (Paris, France) in 2014.

1. Genotypic and phenotypic characterization of P23H line 1 rat model

In order to test the endonucleases we wanted to apply for genome editing aiming to rescue the rod-cone dysfunction in RCD, we used the P23H rat, the most commonly used model to study adRCD. It has been created by incorporation of a mutated mouse Rhodopsin (*Rho*) transgene in the wild-type Sprague Dawley rat. Detailed genetic characterization of this animal has never been reported and was necessary for gene editing. Furthermore, we wanted to collect additional phenotypic information applying non-invasive tools for a therapeutic monitoring. Transgene sequence was analyzed by Sanger sequencing. Using quantitative PCR, transgene copy number was calculated and its expression measured in retinal tissue. ERG and SD-OCT were performed at 1-, 2-, 3- and 6-months of age. We showed that the line 1 P23H (P23H-1) rat carries the mutated mouse genomic *Rho* sequence from the promoter to the 3' UTR and identified the exact sequence. Transgene copy numbers were estimated at 9 and 18 copies in the hemizygous and homozygous rats respectively. In 1-month-old hemizygous P23H-1 rats, transgene expression represented 43% of all *Rho* expressed alleles. ERG showed a progressive rod-cone dysfunction peaking at 6 months-of-age. SD-OCT confirmed a progressive thinning of the photoreceptor cell layer leading to the disappearance of the outer retina by 6 months with additional morphological changes in the inner retina in hemizygous P23H-1 rats. These results provided precise genotypic information for the P23H-1 rat with additional phenotypic characterization that served as a basis for therapeutic interventions using endonucleases.

RESEARCH ARTICLE

Genotypic and Phenotypic Characterization of P23H Line 1 Rat Model

Elise Orhan^{1,2,3}, Deniz Dalkara^{1,2,3}, Marion Neuillé^{1,2,3}, Christophe Lechaue^{1,2,3}, Christelle Michiels^{1,2,3}, Serge Picaud^{1,2,3}, Thierry Léveillard^{1,2,3}, José-Alain Sahel^{1,2,3,4,5,6,7}, Muna I. Naash⁸, Matthew M. Lavail^{9,10}, Christina Zeitz^{1,2,3}, Isabelle Audo^{1,2,3,4,5*}

1 INSERM, U968, Paris, France, **2** CNRS, UMR_7210, Paris, France, **3** Sorbonne Universités, UPMC Univ Paris 06, UMR_S 968, Institut de la Vision, Paris, France, **4** Centre Hospitalier National d’Ophtalmologie des Quinze-Vingts, DHU ViewMaintain, INSERM-DHOS CIC 1423, Paris, France, **5** Institute of Ophthalmology, University College of London, London, United Kingdom, **6** Fondation Ophtalmologique Adolphe de Rothschild, Paris, France, **7** Academie des Sciences, Institut de France, Paris, France, **8** Department of Cell Biology, University of Oklahoma Health Sciences Center, Oklahoma City, Oklahoma, United States of America, **9** Department of Ophthalmology, University of California San Francisco, San Francisco, California, United States of America, **10** Department of Anatomy, University of California San Francisco, San Francisco, California United States of America

* isabelle.audo@inserm.fr



 OPEN ACCESS

Citation: Orhan E, Dalkara D, Neuillé M, Lechaue C, Michiels C, Picaud S, et al. (2015) Genotypic and Phenotypic Characterization of P23H Line 1 Rat Model. PLoS ONE 10(5): e0127319. doi:10.1371/journal.pone.0127319

Academic Editor: Knut Stieger, Justus-Liebig-University Giessen, GERMANY

Received: January 21, 2015

Accepted: April 13, 2015

Published: May 26, 2015

Copyright: © 2015 Orhan et al. This is an open access article distributed under the terms of the [Creative Commons Attribution License](https://creativecommons.org/licenses/by/4.0/), which permits unrestricted use, distribution, and reproduction in any medium, provided the original author and source are credited.

Data Availability Statement: All relevant data are within the paper.

Funding: This work was supported by Fondation Valentin Haüy (IA, EO), Retina France (IA, EO), e-rare RHORCOD (IA), Fondation de l’Oeil - Fondation de France (IA), Fondation Voir et Entendre (CZ), Fondation Fighting Blindness (FFB) (CD-CL-0808-0466-CHNO) (IA), and the FFB center grant (CD-CL-0808-0466-CHNO), Ville de Paris and Region Ile de France, Labex Lifesenses (reference ANR-10-LABX-65) supported by French state funds managed by the ANR within the Investissements d’Avenir programme (ANR-11-IDEX-0004-0), the Regional Council of Ile

Abstract

Rod-cone dystrophy, also known as retinitis pigmentosa (RP), is the most common inherited degenerative photoreceptor disease, for which no therapy is currently available. The P23H rat is one of the most commonly used autosomal dominant RP models. It has been created by incorporation of a mutated mouse rhodopsin (*Rho*) transgene in the wild-type (WT) Sprague Dawley rat. Detailed genetic characterization of this transgenic animal has however never been fully reported. Here we filled this knowledge gap on P23H Line 1 rat (P23H-1) and provide additional phenotypic information applying non-invasive and state-of-the-art *in vivo* techniques that are relevant for preclinical therapeutic evaluations. Transgene sequence was analyzed by Sanger sequencing. Using quantitative PCR, transgene copy number was calculated and its expression measured in retinal tissue. Full field electroretinography (ERG) and spectral domain optical coherence tomography (SD-OCT) were performed at 1-, 2-, 3- and 6-months of age. Sanger sequencing revealed that P23H-1 rat carries the mutated mouse genomic *Rho* sequence from the promoter to the 3' UTR. Transgene copy numbers were estimated at 9 and 18 copies in the hemizygous and homozygous rats respectively. In 1-month-old hemizygous P23H-1 rats, transgene expression represented 43% of all *Rho* expressed alleles. ERG showed a progressive rod-cone dysfunction peaking at 6 months-of-age. SD-OCT confirmed a progressive thinning of the photoreceptor cell layer leading to the disappearance of the outer retina by 6 months with additional morphological changes in the inner retinal cell layers in hemizygous P23H-1 rats. These results provide precise genotypic information of the P23H-1 rat with additional phenotypic characterization that will serve basis for therapeutic interventions, especially for those aiming at gene editing.

de France (I09 - 1727/R) (EO), the National Institute of Health grants EY10609 (MIN), EY001919 (MML) and EY006842 (MML) and the Foundation Fighting Blindness (MIN and MML). The funders had no role in study design, data collection and analysis, decision to publish, or preparation of the manuscript.

Competing Interests: The authors have declared that no competing interests exist.

Introduction

Rod-cone dystrophy, also known as retinitis pigmentosa (RP), is a clinically and genetically heterogeneous group of progressive inherited retinal disorders, which often start with night blindness and lead to visual field constriction, secondary macular involvement and in many cases results in loss of central vision and complete blindness [1]. RP occurs in 1 of 4,000 births and affects more than 1 million individuals worldwide [1]. The mode of inheritance can be autosomal dominant (ad), autosomal recessive (ar), or X-linked. Currently, there is no treatment for this disease but various therapeutic strategies are under investigation.

Mutations in the rhodopsin-encoding gene (*RHO*; MIM# 180380) were the first molecular defects identified in RP [2–5]. More than 100 different *RHO* mutations have been reported to date, which account for 30–40% of autosomal dominant RP (adRP) cases in United States [1] and 16% in France [6]. Furthermore, mutations in 25 other genes cause adRP (<http://www.sph.uth.tmc.edu/Retnet/>, last accessed date on December 16th, 2014) with mutations in *RHO* being the most prevalent [6, 7]. *RHO* encodes for the rod-specific protein rhodopsin, which belongs to the superfamily of 7 transmembrane G-protein—coupled receptors. Rhodopsin consists of an apoprotein (opsin) that is covalently bound to a small conjugated chromophore (11-*cis*-retinal), derived from vitamin A. Upon light absorption, the chromophore isomerizes into all-*trans*-retinal, with subsequent rhodopsin conformational changes leading to the activation of the phototransduction cascade [8].

The P23H exchange in *RHO* is the most prevalent cause of RP in the United States [3]. In this country, this mutation alone accounts for about 12% of adRP cases and about a third of those with a dominant *RHO* mutation [9]. Previous studies have suggested that the P23H mutant protein is misfolded, retained in the endoplasmic reticulum (ER) and unable to bind 11-*cis*-retinal [10–12]. The misfolded *RHO* can be degraded through the ubiquitin-proteasome system or aggregates in the cytoplasm [13, 14]. In order to better understand the disease and its pathogenic mechanisms, P23H transgenic albino rats were generated by incorporating a C57BL/6J mouse P23H mutated transgene into a Sprague-Dawley wild-type (WT) rat background. The transgene used was cloned from C57BL/6J mice. It was made from the entire wild type 15kb of the mouse rhodopsin genomic fragment (called lambda 11) as indicated in Al-Ubaidi *et al.* (1990) [15]. The 15 kb genomic fragment lacking the lambda arms with the P23H mutation was used to generate the rat models. It was initially generated to create a mouse model and therefore few variants were inserted in order to screen the mouse transgene in the presence of the wild-type mouse copy. Three lines of P23H transgenic albino rats were generated with this transgene: one represents a fast degeneration (Line 1), one a slower degeneration (Line 3) and one a very slow degeneration model (Line 2). All three lines suffer from a progressive rod degeneration initially associated with normal cone function [16] (UCSF School of Medicine, <http://www.ucsfeye.net/mlavailRDratmodels.shtml>). These phenotypes are consistent with the clinical findings in patients carrying the P23H *RHO* mutation. Photoreceptor loss correlates with full field electroretinogram (ERG) abnormalities in dark adapted (i.e., scotopic) conditions. Under these conditions, the a-wave amplitude, reflects rod photoreceptor hyperpolarization upon light stimulation, whereas the b-wave represents the subsequent bipolar cell depolarization upon signal transmission from the photoreceptors. Both a- and b- waves of the P23H rat are dramatically reduced over time. In light adapted (i.e., photopic) conditions, the b-wave is normal until the outer nuclear layer (ONL), containing photoreceptor nuclei, thins beyond 50% [17]. In addition to photoreceptor degeneration, there is a subsequent reduction in rod bipolar dendrites [18] and a substantial loss of retinal ganglion cells [19, 20]. By reproducing the clinical signs observed in patients, the P23H rat model is very valuable for testing therapeutic approaches for adRP. Nevertheless, the genotype of this popular animal model has not

been fully reported thus far. In this study, we focused on the P23H Line 1 (P23H-1) rat model frequently used due to its fast and sequential degeneration affecting first rod and then cone photoreceptors [17]. We established the exact sequence of the mutated transgene and report copy number and corresponding expression level. In addition, we sought to more precisely document the kinetics of retinal abnormalities applying two *in vivo* techniques, ERG and spectral-domain optical coherence tomography (SD-OCT), a high resolution imaging technique, allowing monitoring the thickness of retinal layers. Both of these *in vivo* assessment techniques are routinely applied to patients with retinal disease.

Material and Methods

Animals

Transgenic homozygous P23H-1 rats were obtained from the laboratory of Matthew LaVail (UCSF School of Medicine, <http://www.ucsfeye.net/mlavailRDratmodels.shtml>) and were crossed with WT albino Sprague-Dawley rats purchased from Janvier (Le Genest-Saint-Isle, France) to produce hemizygous P23H-1 rats. Animals were housed with a 12-hour dark/light cycle with food (standard diet R0425, Scientific Animal Food & Engineering, Augy, France) and water available *ad libitum*.

Light level was measured in the cage with a luxmeter (Illuminance Meter T10, Konica Minolta, Osaka, Japan) and varied between 20 and 180 lux depending on the position of the rat in the cage and the position of the cage in the rack. For more consistence, WT and hemizygous P23H-1 rats of a same group were housed on the same row.

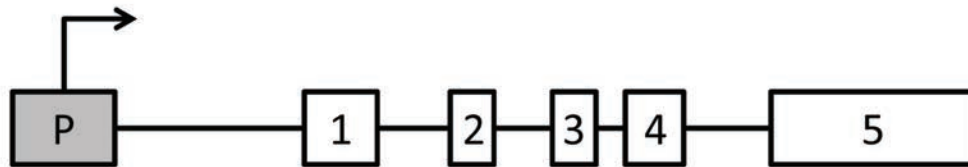
Ethic statements

All procedures were carried out according to the guidelines on the ethical use of animals from the European community council directive (86/609/EEC) and were approved by the French minister of agriculture (OGM agreement 5080).

Sanger sequencing of hemizygous P23H-1 rats

Genomic DNA (gDNA) was isolated from rat tails using a kit (DNeasy Blood & Tissue Kit, Qiagen, Venlo, The Netherlands). Nineteen couples of primers were designed to amplify the mouse *Rho* gene (NC_000072.6, gene structure depicted in Fig 1A) including the c.68C>A, p.Pro23His mutation (P23H mutated mouse *Rho* transgene) (Table 1). Amplicons were of 500-800-base-pair length covering the promoter region to the 3' untranslated region (UTR) of the gDNA of mouse *Rho* in the P23H-1 rat. The following PCR parameters were applied: 15 min at 95°C for denaturation, 35 cycles of 45 sec at 95°C, 1 min at 58°C, and 30 sec at 72°C, and for final extension 10 min at 72°C (HOT FIREPol, Solis Biodyne, Tartu, Estonia). WT rat gDNA was used as control. When it was not possible to design probes to specifically amplify the P23H mutated mouse transgene, adjacent mouse-specific flanking primers were used to amplify larger genomic regions encompassing the fragment of interest (amplicon 6, 9, 10 and 17). The following PCR parameters were then applied: 15 min at 95°C for denaturation, 35 cycles of 45 sec at 95°C, 1 min at 58°C, and 1 min at 72°C, and for final extension 10 min at 72°C (HOT FIREPol). The specificity of PCR products was checked for correct size by electrophoresis on 2% agarose gels, subsequently Sanger sequenced with a sequencing mix (BigDyeTerm v1.1 Cycle-Seq kit, Applied Biosystems, Courtaboeuf, France) and primers (Table 1), on an automated 48-capillary sequencer (ABI 3730 Genetic analyzer, Applied Biosystems, Life technologies, Carlsbad, California, USA). Sequences were compared to the reference sequence (NC_000072.6) using appropriate software (SeqScape, Applied Biosystems).

A



B

Codon	1	2	3	4	5	6	7	8	9	10
Nucleotide	ATG	AAC	GGC	ACA	GAG	GGC	CCC	AAT	TTT	TAT
Amino-acid	Met	Asn	Gly	Thr	Glu	Gly	Pro	Asn	Phe	Tyr
Codon	11	12	13	14	15	16	17	18	19	20
Nucleotide	GTG	CCC	TTC	TCC	AAC	GTC	ACA	GGC	GTG	GTG
Amino-acid	Val	Pro	Phe	Ser	Asn	Val	Thr	Gly	Val	Val
Codon	21	22	23	24	25	26	27	28	29	30
Nucleotide	CGG	<u>AGT</u>	<u>CAC</u>	TTC	GAG	CAG	CCG	CAG	TAC	TAC
Amino-acid	Arg	Ser	His	Phe	Glu	Gln	Pro	Gln	Tyr	Tyr
Codon	31	32	33	34	35	36	37	38	39	40
Nucleotide	CTG	GCG	GAA	<u>CCT</u>	TGG	CAG	TTC	TCC	ATG	CTG
Amino-acid	Leu	Ala	Glu	Pro	Trp	Gln	Phe	Ser	Met	Leu

Fig 1. P23H mutated mouse *Rho* transgene. (A) Schematic drawing of the sequence: the transgene comprises the gDNA of mouse *Rho* from the promoter to the 5'UTR, encompassing the exons and introns. (B) Exon 1 first 40 codon sequence: the c.68C>A missense mutation leading to the p.Pro23His exchange is framed, and the 2 variations surrounding the mutation are underlined.

doi:10.1371/journal.pone.0127319.g001

Transgene copy number quantification by quantitative PCR

Quantitative PCR (qPCR) to identify transgene copy number was adapted from Ballester and co-workers [21]. qPCR was conducted on 25ng of gDNA from 5 animals per genotype (WT, hemizygous P23H-1 and homozygous P23H-1 rats to check the validity of the method) with triplicate in a 20µl reaction using a kit (Taqman PCR Universal Master Mix no AmpErase UNG and the StepOnePlus Real-Time PCR system, both from Applied Biosystems). Probes (Applied Biosystems) were specific to the P23H mutated mouse transgene or the rat *Rho* gene (NC_005103.4). The final concentration of primers (Sigma-Aldrich, Saint-Louis, Missouri, USA) was 200 mM each and 250 nM for the probe (listed on Fig 2A). The qPCR was run using the following amplification parameters: 10 min at 95°C and 40 cycles of 15 sec at 95°C and 1 min at 60°C. Relative quantification of endogenous rat *Rho* and P23H mutated mouse *Rho* transgene was performed using the $2^{-\Delta\Delta Ct}$ method with the rat beta-actin gene for normalization.

RNA extraction, reverse transcription and transgene expression measurement by quantitative PCR

Total RNA was isolated from 1-month-old rat retinas using a kit (RNeasy Mini Kit, Qiagen), followed by a complementary treatment with RNase-free DNase (Qiagen) to ensure the

Table 1. P23H mutated mouse transgene Sanger sequencing primers.

Primer	Sequence 5' to 3'
P23H_TG_1F	TAAACTGCTAGTGGCCAACTCC
P23H_TG_1R	GGATGCTCCAGGATGACTGT
P23H_TG_2F	GGTACTGGCTTCTTGCATCCA
P23H_TG_2R	GGGAGGAGACACATTCTCTGT
P23H_TG_3F	CCCACATGCTCACCTGAATA
P23H_TG_3R	CATCTTGTCTGCCCCAGAGT
P23H_TG_4F	TCTGTCAAGTGAGCCATTGTC
P23H_TG_4R	GTAAGTGCAGGCTGCTCGAAGT
P23H_TG_5F	GAGCCGTCAAGTGGCTGAG
P23H_TG_5R	TGGGCCTTTAGATGAGACCA
P23H_TG_6F	GTGTAGCATGGGAGCCAAG
P23H_TG_6R	ACCTGGCGTAGCATAGTGGT
P23H_TG_7F	CGGCATCTCAAAGGATTCAT
P23H_TG_7R	GCATGGTACCCAGCTTCTA
P23H_TG_8F	GGTAGCACTGTTGGGCATCT
P23H_TG_8R	GAGAGCAGGCTAGGATGCAA
P23H_TG_9F	AAGAGCTTCTGTTTTGGCACA
P23H_TG_9R	TTGGAATGTCCAGGGTTCTC
P23H_TG_10F	CGAAAACCATCCTGGTGACT
P23H_TG_10R	GATGAGGAAAGAGGCCAGTG
P23H_TG_11F	AGGCTGAACCTTCCAAAAT
P23H_TG_11R	GCATGAATGGCTTTTACCTG
P23H_TG_12F	ACTCCCTTAACCACCGAAGG
P23H_TG_12R	CTAGCCCATGGCGTCTGTA
P23H_TG_13F	TGGTCCACTTCACCATTCTCT
P23H_TG_13R	TTGGTCCGCTGTATCTCACA
P23H_TG_14F	GGAGGCATTGCACTCAGACT
P23H_TG_14R	CACACAGCTTAAATGGGACAGA
P23H_TG_15F	AAACGCCACAGTCTCTCTGC
P23H_TG_15R	TCAAGCTGTCCCCATTGAGT
P23H_TG_16F	AGATGACGACGCCTCTGC
P23H_TG_16R	CTGGATTTGGGAGATCCAAC
P23H_TG_17F	CATACCTGCCCTGGTTTTCT
P23H_TG_17R	CCACTTGTTGCTGGTGTAG
P23H_TG_18F	AGATCCAGCCCTTCTCTTG
P23H_TG_18R	ACTGCCTCAAATTGGGTTTC
P23H_TG_19F	TACACTTGGTGGCAGTGGTG
P23H_TG_19R	CCTTTCTGGAAGGGTGTCTG

doi:10.1371/journal.pone.0127319.t001

absence of gDNA. RNA integrity was verified by agarose gel electrophoresis. One microgram of total RNA was reverse-transcribed with oligo-dT using a transcriptase (Superscript II Reverse Transcriptase, Invitrogen, Life technologies, Carlsbad, California, USA) following the manufacturer's instructions. qPCR was conducted on cDNA of 5 animals per genotype (WT and hemizygous P23H-1 rats) using a kit (StepOnePlus Real-Time PCR system, Applied Biosystems) and 2 couples of specific primers for each P23H mutated mouse *Rho* transgene and endogenous rat *Rho*, and one couple of primers for rat beta-actin (Sigma-Aldrich, listed on [Fig 3A](#)). The equivalent of 1.25 ng of cDNA was used per well as template for qPCR reactions with

A

Targets	Primers and probes	Sequences 5' to 3'
Endogenous rat beta-actin	rACTB qPCR F	GCCTTCCTTCCTGGGTAAGT
Endogenous rat beta-actin	rACTB qPCR R	TGCCACAGGATTCCATACCT
Endogenous rat beta-actin	rACTB qPCR probe	VIC-5'-GGTGACCAATGCTGGAGGCCA-3'-TAM
P23H mutated mouse <i>Rho</i> transgen	mRHOP23H qPCR promF	CAGTGCCTGGAGTTGTGCT
P23H mutated mouse <i>Rho</i> transgen	mRHOP23H qPCR promR	GTACTGCGGCTGCTCAAAGG
P23H mutated mouse <i>Rho</i> transgen	mRHOP23H qPCR probe	VIC-5'-AGCTGAGCTCGCCAGGCAGC-3'-TAM
Endogenous wild-type rat <i>Rho</i>	rRHOWT qPCR exon1F	GGATGCTCCAGGATGACTGT
Endogenous wild-type rat <i>Rho</i>	rRHOWT qPCR exon1F	GGTACTGGCTTCTTGCATCC
Endogenous wild-type rat <i>Rho</i>	rRHOWT qPCR probe	6FAM-5'-GGCCGATACGTGTGTGAAACATCCA-3'TAM

B

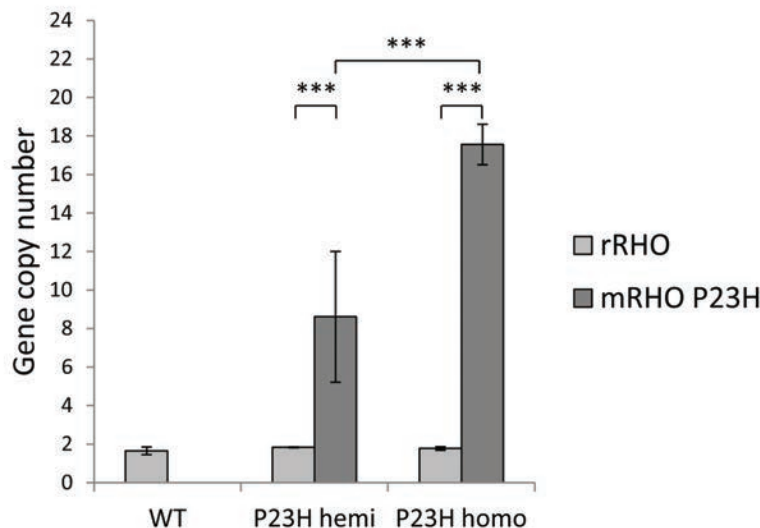


Fig 2. P23H mutated mouse *Rho* transgene copy number. (A) Target and sequence of primers and probes used for qPCR, FAM: 6-carboxyfluorescein and TAM: tetramethylrhodamine. (B) WT endogenous rat *Rho* (light grey) and P23H mutant mouse *Rho* (dark grey) copy numbers were evaluated by qPCR and $2^{-\Delta\Delta C_t}$ method for WT (WT), hemizygous P23H-1 (P23H hemi) and homozygous P23H-1 (P23H homo) rats. All experiments were conducted on the gDNA of 5 rats per group. Three asterisks (***) indicate a p value of <0.001, error bars represent standard errors.

doi:10.1371/journal.pone.0127319.g002

a SYBR green master mix (Power SYBR green PCR Master Mix, Applied Biosystems). Each condition was performed in triplicates; C_t values were obtained with a software (ABI 7500, v.2.0.6, Applied Biosystems). Comparative $\Delta\Delta C_t$ method with rat beta-actin as a housekeeping gene was used to determine the relative P23H mRNA from mouse *Rho* transgene versus endogenous rat *Rho*.

A

Targets	Primers	Sequences 5' to 3'
P23H mutated mouse <i>Rho</i> transgen	RTqPCR_mRHO_1F	CATCACTCCATGGCTACTTC
P23H mutated mouse <i>Rho</i> transgen	RTqPCR_mRHO_2R	AGACCACACCCATGATAGCG
P23H mutated mouse <i>Rho</i> transgen	RTqPCR_mRHO_3F	ACAGTCAAGGAGGCGGCT
P23H mutated mouse <i>Rho</i> transgen	RTqPCR_mRHO_4R	GCAAAGAAAGCTGGCAGAG
Endogenous wild-type rat <i>Rho</i>	RTqPCR_rRHO_1F	ACCTCACTGCATGGCTACTTT
Endogenous wild-type rat <i>Rho</i>	RTqPCR_rRHO_2R	AATGGCATGATTCTCCCA
Endogenous wild-type rat <i>Rho</i>	RTqPCR_rRHO_3F	GTCCACTTCACCATCCCC
Endogenous wild-type rat <i>Rho</i>	RTqPCR_rRHO_4R	CTGCCTTCTGAGTGGTAGCC
Endogenous rat beta-actin	RTqPCR_rACTB_F	CCTGGGTATGGAATCCTGTG
Endogenous rat beta-actin	RTqPCR_rACTB_R	CTTCTGCATCCTGTCAGCAA

B

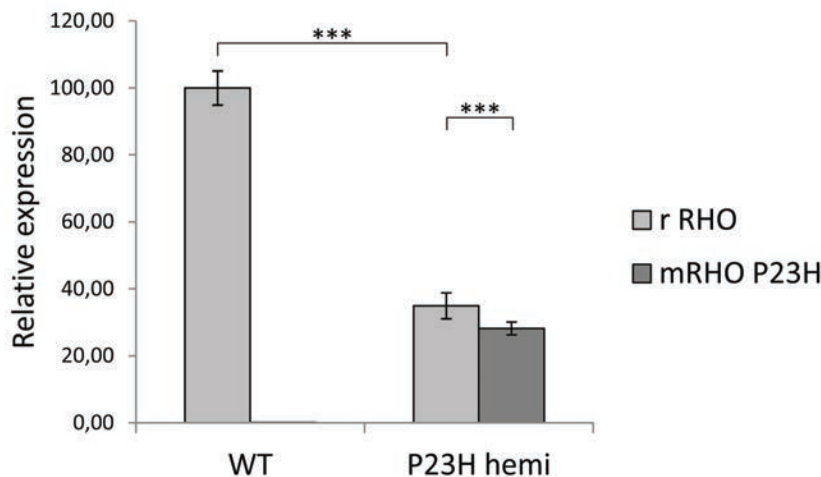


Fig 3. P23H mutated mouse *Rho* transgene expression. (A) Target and sequence of primers used for RT-qPCR. (B) WT endogenous rat *Rho* (light grey) and P23H mutant mouse *Rho* (dark grey) relative expressions were evaluated by qPCR and $2^{-\Delta\Delta Ct}$ method for 1-month-old WT (WT) and hemizygous P23H-1 (P23H hemi) rat retinas. In 1-month-old WT rats endogenous *Rho* expression was assessed at 100%. All experiments were conducted on the retinal cDNA of 5 rats per group. Three asterisks (***) indicate a p-value of <0.001, error bars represent standard errors.

doi:10.1371/journal.pone.0127319.g003

Full field electroretinogram (ERG)

ERG was performed at age 1, 2, 3, 6 and 7 months on 12 WT and 14 hemizygous P23H-1 rats. After overnight dark adaptation, rats were anesthetized with ketamine (100 mg/kg) and xylazine (10 mg/kg). Eye drops were used to dilate the pupils (0.5% tropicamide) and anesthetize the cornea (0.4% oxybuprocaine chlorhydrate). Body temperature was maintained at 37°C using a circulating hot water heating pad. Upper and lower lids were retracted to keep the eyes open and bulging. Custom-made gold contact lens electrodes were placed on the corneal surface to record the ERG (VisioSytem, SIEM Bio-medicale, Nimes, France). Needle electrodes

placed subcutaneously in cheeks served as reference and a needle electrode placed in the back served as ground. Recordings were made from both eyes simultaneously. The light stimulus was provided by a Ganzfeld stimulator (Visiosystem, SIEM Bio-medical). Responses were amplified and filtered (1 Hz-low and 300 Hz-high cut off filters) with a 1 channel DC-/AC-amplifier. Four levels of stimulus intensity ranging from 1.9 cd.s.m⁻² to 12 cd.s.m⁻² were used for the dark-adapted ERG recording. Each scotopic ERG response represents the average of 5 responses from a set of 5 flashes of stimulation. To isolate cone responses a 5-minute light adaptation at 20 cd.m⁻² was used to saturate rod photoreceptors. A 12 cd.s.m⁻² level of stimulus intensity was used for the light-adapted ERGs. The light-adapted ERGs were recorded on the same rod-suppressive white background as for the light adaptation. Each cone photopic ERG response represents the average of 10 responses. *The major components of the ERG were measured conventionally* [22]. All comparisons were done at 12 cd.s.m⁻² of intensity (scotopic and photopic responses).

Spectral domain optical coherence tomography (SD-OCT)

SD-OCT was performed at age 1, 2, 3 and 6 months on 9 WT and 9 hemizygous P23H-1 rats. Rats were anesthetized with ketamine (100 mg/kg) and xylazine (10 mg/kg). Eye drops were used to dilate the pupils (0.5% tropicamide) and eye dehydration was prevented by regular instillation of sodium chloride drops. SD-OCT images were recorded for both eyes using a spectral domain ophthalmic imaging system (Bioptigen, Inc., Durham, NC, USA). We performed rectangular scans consisting of a 2 mm by 2 mm perimeter with 1000 A-scans per B-scan with a total of 100 B-scans. Scans were obtained first while centering on the optic nerve, and then with the nerve displaced either temporally/nasally/dorsally or ventrally. SD-OCT scans were exported from InVivoVue as AVI files. These files were loaded into ImageJ (version 1.47; National Institutes of Health, Bethesda, MD, USA) where they were registered using the Stackreg plug-in. If the optic nerve was placed temporally/nasally, three B-scans at the level of the nerve were added, and measurements were performed 800 μm away from the optic disc, on each side. In the case where the optic nerve was placed dorsally/ventrally, 3 B-scans placed 800 μm away from the optic disc were added to perform the measurements. Thickness from the following layers were measured: ONL, outer plexiform layer (OPL), inner nuclear layer (INL), a complex comprising inner plexiform layer (IPL), ganglion cell layer (GCL) and nerve fiber layer (NFL) that we called IPL+GCL+NFL, and the whole inner retinal layers comprising OPL, INL and IPL + GCL + NFL

Statistical analyses

Statistical analyses were performed using the Mann-Whitney U test on statistical software (SPSS, version 19.0 Inc, Chicago, Illinois, USA). For transgene copy number quantification by qPCR, each gene copy number in the same group, and copy number of the same gene in each group, were compared. For transgene expression quantification by RT-qPCR, each gene relative expression in the same group, and relative expression of the same gene in each group were compared. For scotopic ERG, a- and b-wave amplitudes and implicit times of maximum intensity (cd.s.m⁻²) stimulus responses were compared between WT and hemizygous P23H-1. For photopic ERG, a-waves were not analyzed because of the low amplitudes and high variability in recordings. However, b-wave amplitude and implicit time were compared between WT and hemizygous P23H-1 rats. To compare rod and cone dysfunction, differences between WT and hemizygous P23H-1 b-wave amplitude at each time were performed and compared between scotopic and photopic conditions with Wilcoxon signed-rank test. For SD-OCT, in each group, comparison of thickness for each layer at each time point between the 4 positions of acquisitions

(temporal, nasal, dorsal, and ventral) revealed no statistical difference; therefore these values were combined. Then, all thickness values for each layer at a given time were compared between WT and hemizygous P23H-1 groups. Finally, Spearman rank correlation coefficients were calculated for P23H-1 rats on the means of scotopic a-wave amplitude for a stimulation of 12 cd.s.m⁻² and ONL thickness, scotopic a-wave and b-wave amplitudes for a stimulation of 12 cd.s.m⁻², and scotopic a-wave and b-wave implicit times for a stimulation of 12 cd.s.m⁻².

Results

P23H-1 rat genotyping

Transgene sequence. We first investigated the transgene sequence of the P23H-1 rat model thought to be a mouse P23H mutated allele inserted in a WT rat background. Sanger sequencing with mouse *Rho* specific primers revealed that this transgene contains the entire mouse opsin (*Rho*) genomic DNA (gDNA) from the promoter to the 3'UTR encompassing all exons and introns (Fig 1A). We confirmed the presence of the c.68C>A, p.Pro23His mutation. Two synonymous variations surrounding the P23H exchange (Fig 1B), were identified in addition to other variations in the promoter or 5'UTR (Table 2).

Quantification of P23H transgene copy number. P23H mutated mouse transgene copy number was determined in both hemizygous and homozygous P23H-1 rats. Rat beta-actin normalization allowed us to determine the endogenous rat *Rho* copy number to be 2 copies for both hemizygous and homozygous P23H-1 rats, validating our method (Fig 2B). The P23H transgene copy number was statistically different in the different groups. Eighteen copies were counted for homozygous P23H-1 rats and 9 for hemizygous P23H-1 animals. As expected, no P23H mutated mouse transgene copy was found in WT rats (Fig 2B).

Quantification of P23H transgene expression. Endogenous rat *Rho* (*rRHO*) expression in 1-month-old WT rats was set at 100%. As expected, there was no P23H transgene expression in this group (Fig 3B). However, in 1-month-old hemizygous P23H-1 rats, endogenous wild-type *Rho* expression was reduced to 66% of age-matched WT ($p < 0.001$). The mutated allele represented 43% of overall *Rho* expressed alleles, being also 20% lower than endogenous wild-type *Rho* ($p < 0.001$).

P23H-1 rat phenotyping

Full-field ERG recordings. ERG responses of WT and hemizygous P23H-1 rats were recorded at 1-, 2-, 3-, 6- and 7-months of age under scotopic and photopic conditions, allowing us to estimate respectively rod and cone photoreceptor function. Results are displayed for 12 cd.s.m⁻² stimulus intensity. Under scotopic conditions, amplitudes of both a- and b-waves were reduced as early as 1 month after birth in hemizygous P23H-1 rats compared to WT rats ($p < 0.001$ at each age). This decrease is accentuated with age leading to a flat a-wave at 6 months and an 88% reduction in b-wave amplitude at 7 months (137 μV for hemizygous P23H-1 rats and 1216 μV for WT rats, Fig 4A–4C). Moreover, b-wave implicit time is increased starting at 1 month of age ($p < 0.01$), with a maximum of 35% increase reached at 7 months ($p < 0.001$, Fig 4A and 4E). In contrast, there is no significant change in implicit time of a-wave (Fig 4A and 4D). Taken together, these results indicate rod photoreceptor dysfunction progressing with age.

In photopic conditions, a-wave amplitudes and implicit times are difficult to reliably measure due to their small amplitudes both in WT and mutant rats. Nevertheless, b-wave amplitudes and implicit times are well defined. As observed under scotopic conditions, b-wave amplitude is reduced from the first month of age in mutant compared to WT animals ($p < 0.001$ at each age), and this decrease progresses with age reaching 78% of diminution between hemizygous P23H-1 and WT rats at 7 months of age. Implicit time also increases

Table 2. P23H mutated mouse transgene variations.

Nomenclature	Type	Description
c.1-1448T>C	Upstream gene variant	rs31513717
c.1-1433A>G	Upstream gene variant	rs31513719
c.1-1290A>G	Upstream gene variant	rs31003645
c.1-1275A>G	Upstream gene variant	rs31513722
c.1-1201T>C	Upstream gene variant	rs31514804
c.1-1181A>G	Upstream gene variant	never described
c.1-1174dup	Upstream gene variant	never described
c.1-1139C>T	Upstream gene variant	rs31509484
c.1-1048A>G	Upstream gene variant	rs3666783
c.1-991G>A	Upstream gene variant	rs31509489
c.1-895T>A	Upstream gene variant	rs31509491
c.1-894del	Upstream gene variant	never described
c.1-700G>T	Upstream gene variant	rs30903457
c.1-546C>T	Upstream gene variant	never described
c.1-540dup	Upstream gene variant	never described
c.1-357A>G	Upstream gene variant	rs214120882
c.66C>T, p.Ser22Ser	Synonymous	never described
c.68C>A, p.Pro23His	Missense	Dryja, 1990, Nature
c.102A>T, p.Pro34Pro	synonymous	never described
c.1047+190G>A	3'UTR variant	rs31514859
c.1047+210T>C	3'UTR variant	rs31514861
c.1047+513T>C	3'UTR variant	rs21232304
c.1047+554A>G	3'UTR variant	rs237469398
c.1047+652T>G	3'UTR variant	rs250121950
c.1047+656A>G	3'UTR variant	rs115937375
c.1047+665_c.1047+675dup	3'UTR variant	rs262701018
c.1047+666A>G	3'UTR variant	rs250907798
c.1047+841C>T	3'UTR variant	rs239300315
c.1047+1249C>T	3'UTR variant	rs234137219
c.1047+1469C>T	3'UTR variant	rs31515781
c.1047+1531G>A	3'UTR variant	rs31515783
c.1047+1553A>G	3'UTR variant	rs216330615
c.1047+1591_c.1047+1592insT	3'UTR variant	rs217122073
c.1047+1629C>T	3'UTR variant	rs31516697
c.1047+2052G>A	3'UTR variant	rs107847221

doi:10.1371/journal.pone.0127319.t002

starting at 1 month with a maximum increase of 46% reached at 7 months of age (Fig 5A–5C). When comparing a- and b-wave amplitude, the Spearman rank correlation coefficient was $\rho = 0.87$ ($p < 0.0001$) on WT animals and $\rho = 0.83$ ($p < 0.0001$) on P23H-1 hemizygous rats while comparing the a- and b- wave implicit time $\rho = 0.47$ ($p = 0.00261$) for WT animals and $\rho = 0.627$ ($p < 0.0001$) for P23H-1 hemizygous rats.

Retinal layers assessment of the P23H-1 rats by SD-OCT. Representative SD-OCT images from 1-, 2-, 3- and 6-month hemizygous P23H-1 rats, compared to WT retinas, show a progressive thinning of the ONL (composed of rod and cone photoreceptor nuclei, described in Fig 6A and depicted by white arrows in Fig 6B). WT and hemizygous P23H-1 rat retinal layers (ONL, OPL, INL, IPL+GCL+NFL and inner retinal layers, described in Fig 6A) are all

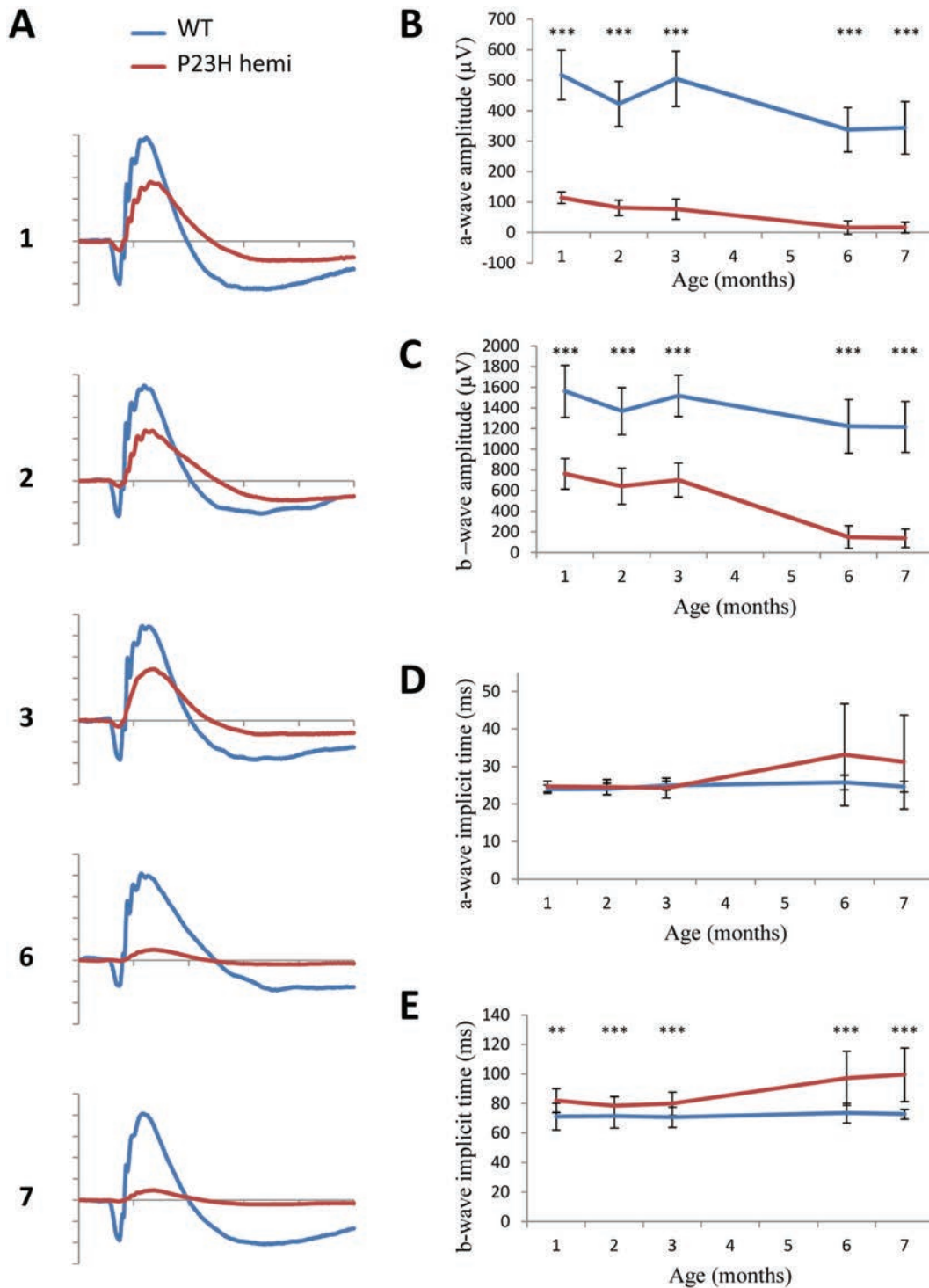


Fig 4. Scotopic ERG phenotype. Dark-adapted ERG series were obtained from representative WT ($n = 12$, blue line) and hemizygous P23H-1 ($n = 14$, red line) rats at 1,2,3,6 and 7 months of age and a 12 cd.s.m^{-2} stimulus intensity. (A) Representative waveforms, as a function of age. The scale marks indicate 50ms (time in abscissa) and $300\mu\text{V}$ (amplitude in ordinate) (B-C) Mean maximum amplitudes of a-wave (B) and b-wave (C) with increasing age. (D-E) Mean implicit times of a-wave (D) and b-wave (E) with increasing ages of rats. Asterisks indicate a significant test (** for $p < 0.005$ and *** for $p < 0.001$) between WT and hemizygous P23H-1 responses, error bars represent standard errors.

doi:10.1371/journal.pone.0127319.g004

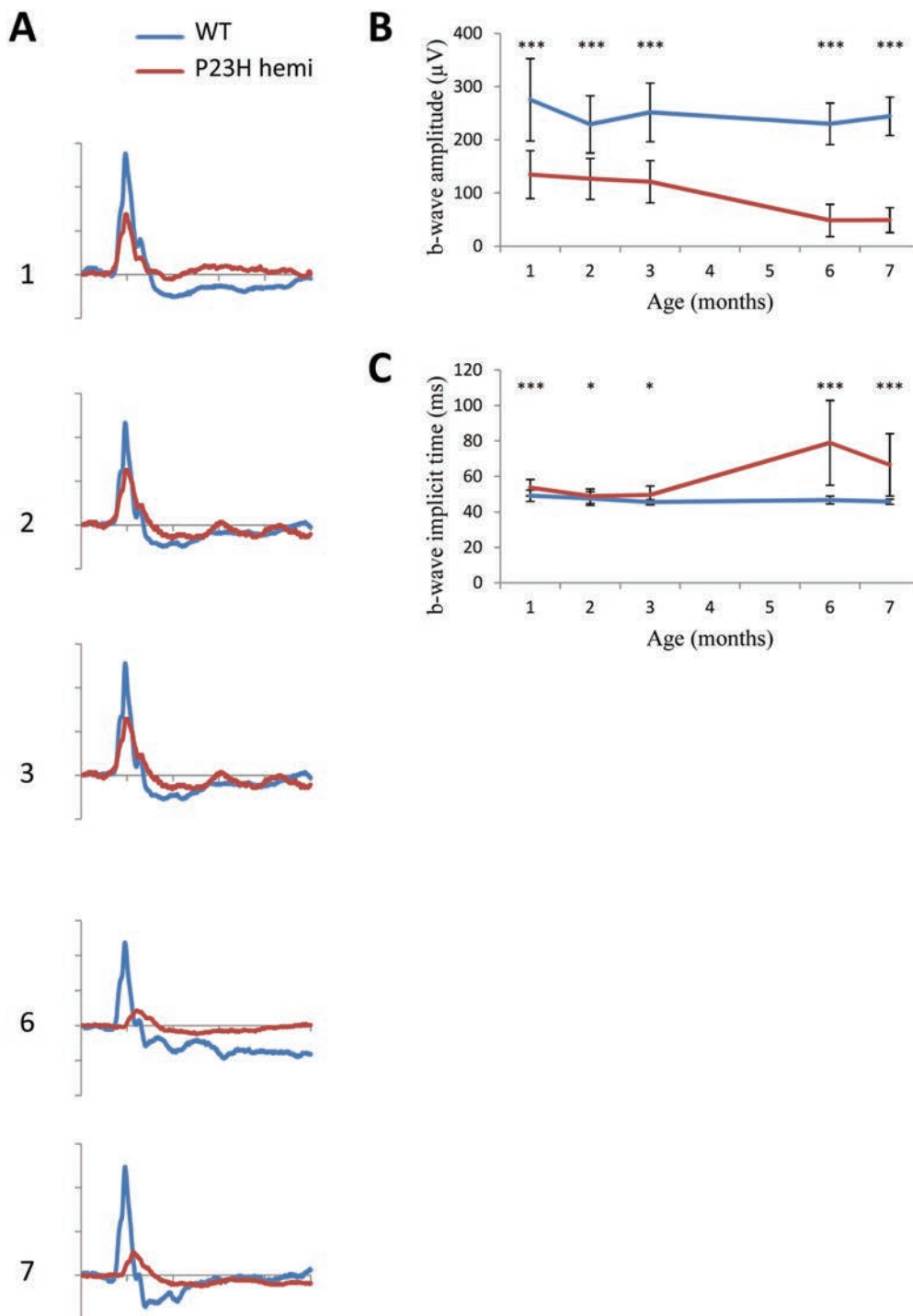


Fig 5. Photopic ERG phenotype. Light-adapted ERG series were obtained from representative WT ($n = 12$, blue line) and hemizygous P23H-1 ($n = 14$, red line) rats at 1,2,3,6 and 7 month of age and at 12 cd.s.m^{-2} stimulus intensity after a 5-minute light adaptation at 20 cd.m^{-2} . (A) Representative waveforms, as a function of age. The scale marks indicate 50ms (time in abscissa) and $100\mu\text{V}$ (amplitude in ordinate) (B-C) Mean maximum amplitudes (B) and implicit times (C) of b-wave in time. Because of the limit of sensitivity of the method, the a-wave component is not plotted. Asteriks indicate a significant test (** for $p < 0.005$ and *** for $p < 0.001$) between WT and hemizygous P23H-1 rats' responses, error bar represents standard errors.

doi:10.1371/journal.pone.0127319.g005

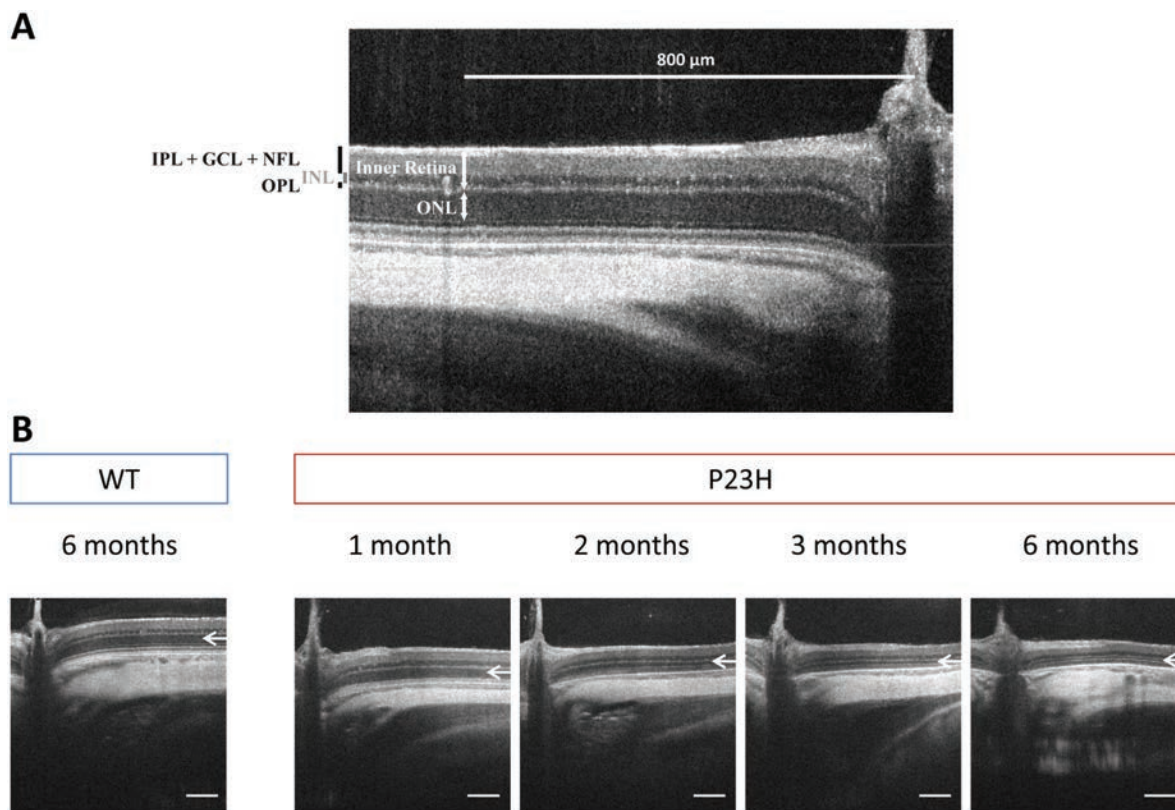


Fig 6. SD-OCT retinal thickness layers and retinal morphology (A) Outer nuclear layer (ONL), outer plexiform layer (OPL), inner nuclear layer (INL), a complex comprising inner plexiform layer (IPL), ganglion cell layer (GCL) and nerve fiber layer (NFL) called IPL+GCL+NFL, and inner retinal layer thickness are measured at 800 μm of the optic nerve on SD-OCT images (B) Representative SD-OCT section of a 6-month-old WT rat and 1-, 2-, 3-, and 6-month-old hemizygous P23H-1 rats. White arrows depict ONL. Scale bar: 200 μm .

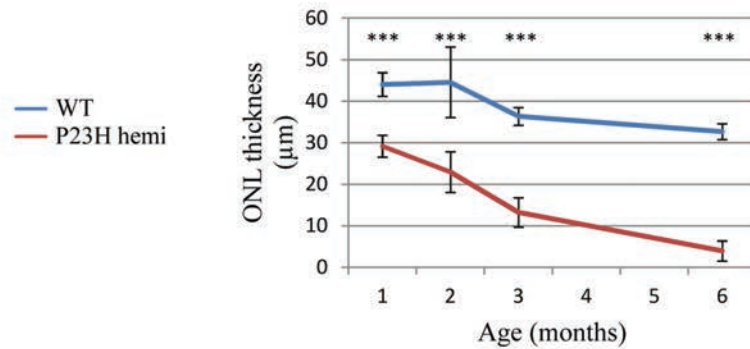
doi:10.1371/journal.pone.0127319.g006

thinned between 1 and 6 months of age (Fig 7 and Table 3). When studied separately, some changes appear between WT and hemizygous P23H-1 rat retinal layers. Hemizygous P23H-1 rat ONL thins with aging to finally reach 86% of decrease at 6-months-of-age when WT rat ONL is reduced by 27% ($p < 0.001$, Fig 7A and Table 3). One-month hemizygous P23H-1 rat inner retina is thinner than WT, and this difference is maintained but not modified with aging (Fig 7B and Table 3). If layers composing the inner retina are studied separately, changes appear in the OPL. Hemizygous P23H-1 rat OPL are decreased at 3-months ($p < 0.005$) and 6-months ($p < 0.001$) of age when compared to WT (Fig 7C and Table 3). Inner nuclear layer from 1-month hemizygous P23H-1 rat is thinner than WT ($p < 0.05$), but this difference disappears with aging (Fig 7D and Table 3). As observed for inner retina, 1-month hemizygous P23H-1 rat IPL + GCL + NFL is thinner than WT, and this difference remains constant with aging (Fig 7E and Table 3).

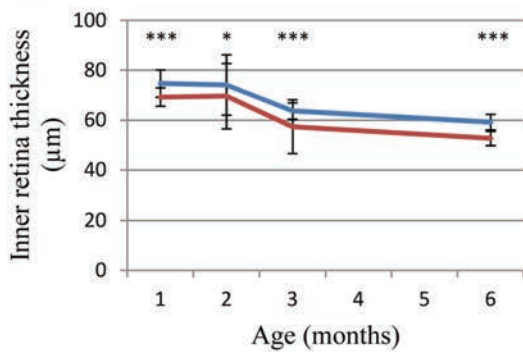
Discussion

The present study reports the exact sequence, copy number and retinal expression level of the P23H mutated transgene in the P23H-1 rat model, using Sanger sequencing, qPCR and RT-qPCR analysis. Furthermore it documents in greater detail the disease course in this rat model with functional and structural phenotypic assessment using *in vivo* evaluation by ERG and SD-OCT.

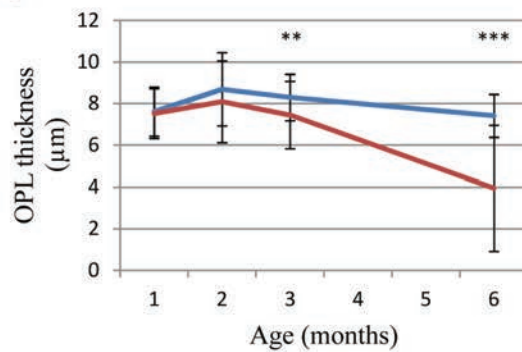
A



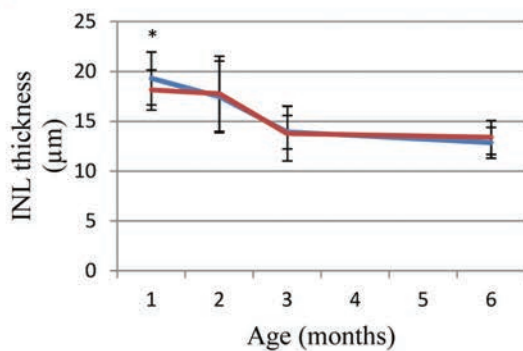
B



C



D



E

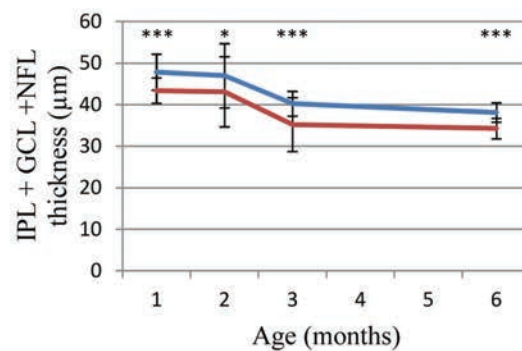


Fig 7. SD-OCT retinal thickness layer monitoring. Retinal layer thicknesses are measured at 800 µm of the optic nerve on SD-OCT images and compared to WT (blue line) and hemizygous P23H-1 (red line) at 1, 2, 3 and 6 months of age. (A) Outer nuclear layer (ONL), (B) inner retinal layer, (C) outer plexiform layer (OPL), (D) inner nuclear layer (INL), (E) a complex comprising inner plexiform layer (IPL), ganglion cell layer (GCL) and nerve fiber layer (NFL) called IPL+GCL+NFL. Asterisks indicate the following p values: * for p<0.05 and *** for p<0.001, error bars represent standard errors.

doi:10.1371/journal.pone.0127319.g007

P23H rat models were developed for translational research and study photoreceptor rescue strategies [23, 24]. By reproducing the degeneration observed in patients [19], these animal models are extremely helpful for therapeutic approaches for adRP, a yet incurable disease. P23H-1 rat model is the most commonly used model since it carries the most frequent

Table 3. Retinal layer thickness measured by SD-OCT in WT and hemizygous P23H-1 rats at 1, 2, 3 and 6 months of age.

	WT				P23H-1			
	1 month	2 months	3 months	6 months	1 month	2 months	3 months	6 months
ONL	44µm ±3µm	43 µm ±11 µm	36 µm ±2 µm	33 µm ±2 µm	29 µm ±3 µm	23µm ±5 µm	13 µm ±3 µm	3 µm ±2 µm
OPL	8µm ±1 µm	9 µm ±2 µm	7 µm ±3 µm	7 µm ±1 µm	8 µm ±1 µm	8 µm ±2 µm	8 µm ±1 µm	7 µm ±3 µm
INL	19 µm ±3 µm	17 µm ±4 µm	12 µm ±5 µm	13 µm ±2 µm	18 µm ±2 µm	18 µm ±4 µm	14 µm ±2 µm	13 µm ±3 µm
IPL+GCL+NFL	48 µm ±4 µm	47 µm ±4 µm	36 µm ±13 µm	38 µm ±2 µm	43 µm ±3 µm	43 µm ±6 µm	36 µm ±2 µm	34 µm ±2 µm
Inner retinal layers	75 µm ±5 µm	74 µm ±12µm	57 µm ±20 µm	60 µm ±3 µm	69 µm ±3 µm	70 µm ±13 µm	59 µm ±3 µm	53 µm ±3 µm

(mean ± standard deviation; ONL: outer nuclear layer, OPL: outer plexiform layer, INL: inner nuclear layer, IPL: inner plexiform layer, GCL: ganglion cell layer, NFL: nerve fiber layer)

doi:10.1371/journal.pone.0127319.t003

mutation in adRP in the US [1] and displays relatively fast degeneration over 6 months (<http://www.ucsfeye.net/mlavailRDratmodels.shtml>). This allows an easy documentation of the phenotype and fast monitoring of putative therapeutic rescue. Moreover, hemizygous animals were preferred to homozygous since it was supposed to more closely resemble the human autosomal dominant genetic conditions with one mutated allele and present a slower degeneration, more suitable for translational research. Several strategies of photoreceptor [25] and Muller glial cell [26] transplantation or administration of anti-apoptotic [27, 28], heat shock response activator [29] or enhancer [30], anti-aggregating [31], or neuroprotective [32, 33] molecules and chaperones [34] have been attempted to slow the degeneration and demonstrated partial preservation of photoreceptor morphology and function. However, treatment efficacy was evaluated in comparing treated and untreated animals less than 1 month after treatment, or after 6 months of age, a time point at which photoreceptor degeneration is almost complete. RNA-targeted therapy by gene silencing using ribozymes directed against the mouse transgene in P23H Line 3 rat model has also been attempted [23, 24, 35] and revealed some preservation of the ONL thickness. Functional characterization by ERG shows a slight increase in response amplitude in treated *versus* untreated eyes after 3 months of age [23, 35]. These approaches indicate that genetic-targeted therapies including selective mutated allele suppression or gene replacement at the DNA or RNA level could be tested. Despite multiple studies that attempt therapeutic intervention in the P23H model, the genotype of this animal model was not yet fully available. We first addressed this question by characterizing the exact sequence of the mutated transgene in P23H-1 rats. Our data confirmed that the transgene contains the entire mouse *Rho* genomic DNA sequence including the promoter, all 5 exons and 4 introns with the P23H mutation as well as most of the 3'UTR. Variations were also identified in the promoter, exon 1 and 3'UTR. These include [c.66C>T, p.Ser22Ser] and [c.102A>T, p.Pro34Pro] (Fig 1B). These variations are silent and most likely predicted to be benign but will need to be taken into account while investigating genome editing strategies. Furthermore, we investigated transgene copy numbers and identified that homozygous and hemizygous P23H-1 rats carry 18 and 9 copies of the P23H transgene, respectively. This is coherent with the Mendelian transmission of this transgene with half of the copies of the homozygous in the hemizygous P23H-1 rats supporting a tandem insertion at a unique locus. This result led us to investigate if all transgene copies were expressed. In 1-month-old hemizygous P23H-1 rat retinas, WT *Rho* expression was 66% reduced compared to the age-matched WT rats. This result was consistent with photoreceptor degeneration due to retinitis pigmentosa [31]. Interestingly, in 1-month-old hemizygous P23H-1 rats, the mutated allele represented 43% of overall *Rho* expressed alleles, despite the 9 copies of the transgene. This resembles

what is expected in patients with the P23H mutation, where both normal and mutated alleles are thought to be expressed at the same levels. This low expression of transgene in hemizygous P23H-1 rats could be due to WT and P23H *Rho* expression regulation at the mRNA levels, as described in a P23H mouse line with genomic mutated mouse opsin transgene [36]. Intrinsic silencing effect of multiple-copy tandem repeats on transgene expression could also be an explanation, since transcription inhibition can occur when more than 5 copies of the transgene are present [37, 38]. Insertion site of the transgene is also important since chromatin structure influences the expression level [39]. This result is favorable for intervention applying gene therapy, since low level of transcript is more likely to respond to gene silencing at the mRNA level than an overexpressed transgene. Altogether, our study provides important details on the P23H-1 rat's genotype by describing the exact transgene sequence with its P23H mutation and variations, its copy number and expression. These data can serve basis for mutated allele specific therapeutic interventions using this model. Nevertheless, we cannot exclude a drift of the inserted copy number in the various colonies of P23H rat available to the scientific community and would recommend testing such parameter before attempting therapeutic studies especially those aiming at genome editing.

Another purpose of this work was to better monitor natural history of the disease applying functional and high-resolution *in vivo* phenotyping techniques. Functional characterization of hemizygous P23H-1 rats revealed reduced rod and cone response amplitudes and delayed implicit time as seen in RP patients [1, 3, 40]. In both scotopic and photopic conditions, hemizygous P23H-1 rats already displayed decreased responses at 1-month, enhanced by aging especially after 3-months and flattening at 6-months of age. Scotopic responses were more affected than photopic responses, indicating that rod photoreceptor dysfunction was more severe than cone photoreceptor dysfunction. These results are concordant with previous observations [17] and confirmed the usefulness of this model to mimic human disease with rod-cone dystrophy [1, 3, 40, 41]. Our study also provides retinal thickness monitoring using high resolution imaging with SD-OCT in hemizygous P23H-1 rats. Indeed, this non invasive *in vivo* technique enables longitudinal studies and now achieves the resolution of histology, without its terminal nature. Moreover, this alleviates the fixation process on retinal sections, which is a potential source of variation in structure and thickness measurements [42]. Such structural studies applying SD-OCT may provide surrogate markers to monitor functional rescue in translational research. When observed with aging in our study, structural characterization of hemizygous P23H-1 rats revealed gradual ONL thinning reaching 86% at 6-months of age, consistent with histology [17]. Of note, 1- and 2-month-old P23H-1 rats showed slightly different ONL thickness compared to the histological data (respectively 20 μ m and 10 μ m) from the literature (<http://www.ucsfeye.net/mlavailRDratmodels.shtml>). Difference between SD-OCT and histology measurements were also described on the same animals, but good correlation in the decreasing values makes this technique interesting for monitoring [41]. Moreover, while the degeneration seems to be slowed herein, ONL thicknesses reached comparable values. Animal housing conditions such as light intensity and feeding were different between this and other studies, and may also explain an initially slower degeneration documented in the present study [43–46]. In a recent study, SD-OCT and retinal thickness measurements on histology were assessed in 4-months old pigmented hemizygous P23H rats [41]. These animals were obtained by crossing homozygous P23H-1 with Long Evans rats to more closely resemble the human disease providing that albino rodents are more sensitive to photic trauma [47]. The 4-months old pigmented hemizygous P23H-1 and WT rats showed less degeneration than the 3-months old albino hemizygous P23H-1 and WT albino rats in the present study and their pigmented status could account for this difference. However, the difference in genetic background brought by crossing may also induce variations in the course of the disease [48, 49]. Furthermore, patients

with a P23H mutation show regional distribution of retinal degeneration [50, 51]. In the P23H mouse, if dark reared, photoreceptor cell death was uniformly distributed across the retina, but when raised in cyclic light conditions, the density of apoptotic cells was greater, particularly in the inferior region of the retina [52], the region most severely affected in patients with the P23H mutation [50]. Photoreceptor degeneration was also accelerated by light exposure. Regional differences were not observed in our study on hemizygous P23H-1 nor on pigmented hemizygous P23H-1 rats [41] and one reason may be artificial light conditions in which they were raised. Interestingly, our study also demonstrates inner retinal abnormalities with no change in overall inner retinal thickness with age. Moreover, inner retinal abnormalities were described by OCT in regions where the ONL was thinned in patients with the P23H mutation [53]. Here we showed that hemizygous P23H-1 rats OPL thickness decreased dramatically with aging. This result is consistent with observations obtained on synaptic complexes by immunohistochemistry, where dendrites of bipolar cells were found less profuse in hemizygous albino and pigmented P23H-1 compared to WT, especially with aging [18, 41]. Synaptic connectivity of horizontal cells also changed after 3-months of age, with their dendrites being atrophied and condensed [41]. INL thickness composed of nuclei of bipolar, horizontal and amacrine cells, showed an initial decrease of 1 μ m in hemizygous P23H-1 compared to WT rats. With aging, no other difference appeared in the thickness of both hemizygous P23H-1 and WT rat INL. Immunohistochemistry on hemizygous albino P23H-1 rats showed that bipolar cell bodies were smaller at 40 days of age and confined to a single layer adjacent to the OPL and decrease in number between 5- and 9-months of age [18]. On pigmented hemizygous P23H-1 rats cell bodies were smaller after 2-months of age for horizontal cells and rod and cones bipolar cells, with a reduction in number particularly after 6-months of age [41]. These differences were not compared to the age-matched pigmented WT rats. We observed similar decreases by SD-OCT on albino WT and hemizygous P23H-1 rats, the role of the albino background on this degeneration remains also unclear. IPL+GCL+NFL thickness, comprising ganglion cells, their synapses with INL cells, and their axons forming the optic nerve, was 10% thinner in hemizygous P23H-1 than in WT rats. These results were consistent with immunohistochemistry on albino hemizygous P23H-1 rats, showing that ganglion cell population was initially smaller in hemizygous P23H-1 than in WT rats, and a difference in degeneration appeared after 6 months of age [19]. Immunohistochemistry on pigmented hemizygous P23H-1 rats showed horizontal and rod bipolar cells axons and varicosities were reduced after 2-months of age but these differences were not compared to the matched-aged pigmented WT rats [18, 41]. Finally, while correlating outer and inner retinal function (i.e., a- and b-wave parameter correlation), we find a close correlation that may imply the absence of additional inner retinal dysfunction to photoreceptor dysfunction suggesting that structural abnormalities do not result in functional alteration. However, the abnormalities observed in the inner retina need to be taken into account in the development of therapies aiming at restoring photoreceptor function, such as photoreceptor transplantation [54], subretinal implants [55], and optogenetic activation of dormant cone photoreceptor circuitry [56], as they all need functional inner retinal cells to be effective. A precise assessment would therefore be helpful to select candidates for appropriate treatments such as implants that could be placed either sub or epi-retinally and optogenetics that could be implemented on cones [56], bipolar [57] or ganglion cells [58] depending of these findings.

To conclude, this study clarifies the genotype of hemizygous P23H-1 rats, by identifying transgene sequence, numbering the gene copies and their expression. Functional and structural phenotypic and non-invasive *in vivo* evaluation by ERG and SD-OCT confirm previously reported functional and histological data in the literature and provide new endpoints for validation of preclinical therapeutic intervention. These results will serve as basis for the development of novel therapies, in particular those directly targeting the gene defect.

Acknowledgments

The authors are grateful to Manuel Simonutti, Julie Dégardin, Jennifer Da Silva, Samantha Beck and Caroline Carvalho for their valuable help in phenotyping (platform of Institut de la Vision) and to Isabelle Renault, Léa Biedermann and André Tiffocche for animal care (platform of Institut de la Vision). The authors thank Stéphane Fouquet for his support in developing a custom-made Image J macro to measure thickness of retinal layers.

This work was supported by Fondation Valentin Haüy (IA, EO), Retina France (IA, EO), e-rare RHORCOD (IA), Fondation de l'Œil—Fondation de France (IA), Fondation Voir et Entendre (CZ), Fondation Fighting Blindness (FFB) (CD-CL-0808-0466-CHNO) (IA), and the FFB center grant (CD-CL-0808-0466-CHNO), Ville de Paris and Region Ile de France, Labex Lifesenses (reference ANR-10-LABX-65) supported by French state funds managed by the ANR within the Investissements d'Avenir programme (ANR-11-IDEX-0004-0), the Regional Council of Ile de France (I09-1727/R) (EO), the National Institute of Health grants EY10609 (MIN), EY001919 (MML) and EY006842 (MML) and the Foundation Fighting Blindness (MIN and MML).

Author Contributions

Conceived and designed the experiments: EO IA CZ ML MIN CL. Performed the experiments: EO CM CL DD MN. Analyzed the data: EO CL DD IA CZ ML. Contributed reagents/materials/analysis tools: IA CZ ML MIN SP TL JS. Wrote the paper: EO IA ML MIN DD CZ CL.

References

1. Hartong DT, Berson EL, Dryja TP. Retinitis pigmentosa. *Lancet*. 2006; 368(9549):1795–809. PMID: [17113430](#).
2. Dryja TP, McGee TL, Hahn LB, Cowley GS, Olsson JE, Reichel E, et al. Mutations within the rhodopsin gene in patients with autosomal dominant retinitis pigmentosa. *N Engl J Med*. 1990; 323(19):1302–7. PMID: [2215617](#).
3. Dryja TP, McGee TL, Reichel E, Hahn LB, Cowley GS, Yandell DW, et al. A point mutation of the rhodopsin gene in one form of retinitis pigmentosa. *Nature*. 1990; 343(6256):364–6. PMID: [2137202](#).
4. Inglehearn CF, Bashir R, Lester DH, Jay M, Bird AC, Bhattacharya SS. A 3-bp deletion in the rhodopsin gene in a family with autosomal dominant retinitis pigmentosa. *Am J Hum Genet*. 1991; 48(1):26–30. PMID: [1985460](#).
5. Sung CH, Davenport CM, Hennessey JC, Maumenee IH, Jacobson SG, Heckenlively JR, et al. Rhodopsin mutations in autosomal dominant retinitis pigmentosa. *Proc Natl Acad Sci U S A*. 1991; 88(15):6481–5. PMID: [1862076](#).
6. Audo I, Manes G, Mohand-Said S, Friedrich A, Lancelot ME, Antonio A, et al. Spectrum of rhodopsin mutations in French autosomal dominant rod-cone dystrophy patients. *Invest Ophthalmol Vis Sci*. 2010; 51(7):3687–700. PMID: [20164459](#). doi: [10.1167/iovs.09-4766](#)
7. Sullivan LS, Bowne SJ, Birch DG, Hughbanks-Wheaton D, Heckenlively JR, Lewis RA, et al. Prevalence of disease-causing mutations in families with autosomal dominant retinitis pigmentosa: a screen of known genes in 200 families. *Invest Ophthalmol Vis Sci*. 2006; 47(7):3052–64. PMID: [16799052](#).
8. Stenkamp RE, Teller DC, Palczewski K. Rhodopsin: a structural primer for G-protein coupled receptors. *Arch Pharm (Weinheim)*. 2005; 338(5–6):209–16. PMID: [15952240](#).
9. Dryja TP, McEvoy JA, McGee TL, Berson EL. Novel rhodopsin mutations Gly114Val and Gln184Pro in dominant retinitis pigmentosa. *Invest Ophthalmol Vis Sci*. 2000; 41(10):3124–7. PMID: [10967073](#).
10. Sung CH, Schneider BG, Agarwal N, Papermaster DS, Nathans J. Functional heterogeneity of mutant rhodopsins responsible for autosomal dominant retinitis pigmentosa. *Proc Natl Acad Sci U S A*. 1991; 88(19):8840–4. PMID: [1924344](#).
11. Sung CH, Davenport CM, Nathans J. Rhodopsin mutations responsible for autosomal dominant retinitis pigmentosa. Clustering of functional classes along the polypeptide chain. *J Biol Chem*. 1993; 268(35):26645–9. PMID: [8253795](#).
12. Kaushal S, Khorana HG. Structure and function in rhodopsin. 7. Point mutations associated with autosomal dominant retinitis pigmentosa. *Biochemistry*. 1994; 33(20):6121–8. PMID: [8193125](#).

13. Illing ME, Rajan RS, Bence NF, Kopito RR. A rhodopsin mutant linked to autosomal dominant retinitis pigmentosa is prone to aggregate and interacts with the ubiquitin proteasome system. *J Biol Chem*. 2002; 277(37):34150–60. PMID: [12091393](#).
14. Saliba RS, Munro PM, Luthert PJ, Cheetham ME. The cellular fate of mutant rhodopsin: quality control, degradation and aggresome formation. *J Cell Sci*. 2002; 115(Pt 14):2907–18. PMID: [12082151](#).
15. al-Ubaidi MR, Pittler SJ, Champagne MS, Triantafyllos JT, McGinnis JF, Baehr W. Mouse opsin. Gene structure and molecular basis of multiple transcripts. *J Biol Chem*. 1990; 265(33):20563–9. PMID: [1978723](#).
16. Steinberg RH, Flannery JG, Naash M, Oh P, Matthes MT, Yasumura D, et al., editors. Transgenic rat models of inherited retinal degeneration caused by mutant opsin genes. *The Association for Research in Vision and Ophthalmology*; 1996. PMID: [8682606](#)
17. Machida S, Kondo M, Jamison JA, Khan NW, Kononen LT, Sugawara T, et al. P23H rhodopsin transgenic rat: correlation of retinal function with histopathology. *Invest Ophthalmol Vis Sci*. 2000; 41(10):3200–9. PMID: [10967084](#).
18. Cuenca N, Pinilla I, Sauve Y, Lu B, Wang S, Lund RD. Regressive and reactive changes in the connectivity patterns of rod and cone pathways of P23H transgenic rat retina. *Neuroscience*. 2004; 127(2):301–17. PMID: [15262321](#).
19. Garcia-Ayuso D, Salinas-Navarro M, Agudo M, Cuenca N, Pinilla I, Vidal-Sanz M, et al. Retinal ganglion cell numbers and delayed retinal ganglion cell death in the P23H rat retina. *Exp Eye Res*. 2010; 91(6):800–10. PMID: [20955700](#). doi: [10.1016/j.exer.2010.10.003](#)
20. Kolomiets B, Dubus E, Simonutti M, Rosolen S, Sahel JA, Picaud S. Late histological and functional changes in the P23H rat retina after photoreceptor loss. *Neurobiol Dis*. 38(1):47–58. PMID: [20060471](#). doi: [10.1016/j.nbd.2009.12.025](#)
21. Ballester M, Castello A, Ibanez E, Sanchez A, Folch JM. Real-time quantitative PCR-based system for determining transgene copy number in transgenic animals. *Biotechniques*. 2004; 37(4):610–3. PMID: [15517974](#).
22. Berson EL. Retinitis pigmentosa and allied retinal diseases: electrophysiologic findings. *Transactions Section on Ophthalmology American Academy of Ophthalmology and Otolaryngology*. 1976; 81(4 Pt 1):OP659–66. PMID: [960388](#).
23. Lewin AS, Drenser KA, Hauswirth WW, Nishikawa S, Yasumura D, Flannery JG, et al. Ribozyme rescue of photoreceptor cells in a transgenic rat model of autosomal dominant retinitis pigmentosa. *Nat Med*. 1998; 4(8):967–71. PMID: [9701253](#).
24. LaVail MM, Yasumura D, Matthes MT, Drenser KA, Flannery JG, Lewin AS, et al. Ribozyme rescue of photoreceptor cells in P23H transgenic rats: long-term survival and late-stage therapy. *Proc Natl Acad Sci U S A*. 2000; 97(21):11488–93. PMID: [11005848](#).
25. Yang Y, Mohand-Said S, Leveillard T, Fontaine V, Simonutti M, Sahel JA. Transplantation of photoreceptor and total neural retina preserves cone function in P23H rhodopsin transgenic rat. *PLoS One*. 2010; 5(10):e13469. PMID: [20976047](#). doi: [10.1371/journal.pone.0013469](#)
26. Jayaram H, Jones MF, Eastlake K, Cottrill PB, Becker S, Wiseman J, et al. Transplantation of photoreceptors derived from human Muller glia restore rod function in the P23H rat. *Stem cells translational medicine*. 2014; 3(3):323–33. doi: [10.5966/sctm.2013-0112](#) PMID: [24477073](#); PubMed Central PMCID: PMC3952927.
27. Fernandez-Sanchez L, Lax P, Pinilla I, Martin-Nieto J, Cuenca N. Tauroursodeoxycholic acid prevents retinal degeneration in transgenic P23H rats. *Invest Ophthalmol Vis Sci*. 2011; 52(8):4998–5008. PMID: [21508111](#). doi: [10.1167/iovs.11-7496](#)
28. Fernandez-Sanchez L, Lax P, Esquivia G, Martin-Nieto J, Pinilla I, Cuenca N. Safranal, a saffron constituent, attenuates retinal degeneration in P23H rats. *PLoS One*. 2012; 7(8):e43074. PMID: [22900092](#). doi: [10.1371/journal.pone.0043074](#)
29. Parfitt DA, Aguila M, McCulley CH, Bevilacqua D, Mendes HF, Athanasiou D, et al. The heat-shock response co-inducer arimoclochol protects against retinal degeneration in rhodopsin retinitis pigmentosa. *Cell death & disease*. 2014; 5:e1236. doi: [10.1038/cddis.2014.214](#) PMID: [24853414](#); PubMed Central PMCID: PMC4047904.
30. Aguila M, Bevilacqua D, McCulley C, Schwarz N, Athanasiou D, Kanuga N, et al. Hsp90 inhibition protects against inherited retinal degeneration. *Hum Mol Genet*. 2014. PMID: [24301679](#).
31. Vasireddy V, Chavali VR, Joseph VT, Kadam R, Lin JH, Jamison JA, et al. Rescue of photoreceptor degeneration by curcumin in transgenic rats with P23H rhodopsin mutation. *PLoS One*. 2011; 6(6):e21193. PMID: [21738619](#). doi: [10.1371/journal.pone.0021193](#)

32. Fernandez-Sanchez L, Lax P, Isiegas C, Ayuso E, Ruiz JM, de la Villa P, et al. Proinsulin slows retinal degeneration and vision loss in the P23H rat model of retinitis pigmentosa. *Hum Gene Ther*. 2012; 23(12):1290–300. PMID: [23017108](#). doi: [10.1089/hum.2012.067](#)
33. Lax P, Esquivá G, Altavilla C, Cuenca N. Neuroprotective effects of the cannabinoid agonist HU210 on retinal degeneration. *Exp Eye Res*. 2014; 120:175–85. PMID: [24495949](#). doi: [10.1016/j.exer.2014.01.019](#)
34. Gorbatyuk MS, Knox T, LaVail MM, Gorbatyuk OS, Noorwez SM, Hauswirth WW, et al. Restoration of visual function in P23H rhodopsin transgenic rats by gene delivery of BiP/Grp78. *Proc Natl Acad Sci U S A*. 2010; 107(13):5961–6. PMID: [20231467](#). doi: [10.1073/pnas.0911991107](#)
35. Gorbatyuk M, Justilien V, Liu J, Hauswirth WW, Lewin AS. Preservation of photoreceptor morphology and function in P23H rats using an allele independent ribozyme. *Exp Eye Res*. 2007; 84(1):44–52. PMID: [17083931](#).
36. Naash MI, Hollyfield JG, al-Ubaidi MR, Baehr W. Simulation of human autosomal dominant retinitis pigmentosa in transgenic mice expressing a mutated murine opsin gene. *Proc Natl Acad Sci U S A*. 1993; 90(12):5499–503. PMID: [8516292](#).
37. Garrick D, Fiering S, Martin DI, Whitelaw E. Repeat-induced gene silencing in mammals. *Nat Genet*. 1998; 18(1):56–9. doi: [10.1038/ng0198-56](#) PMID: [9425901](#).
38. Henikoff S. Conspiracy of silence among repeated transgenes. *BioEssays: news and reviews in molecular, cellular and developmental biology*. 1998; 20(7):532–5. doi: [10.1002/\(SICI\)1521-1878\(199807\)20:7<532::AID-BIES3>3.0.CO;2-M](#) PMID: [9723001](#).
39. Kouzarides T. Chromatin modifications and their function. *Cell*. 2007; 128(4):693–705. doi: [10.1016/j.cell.2007.02.005](#) PMID: [17320507](#).
40. Berson EL, Rosner B, Sandberg MA, Dryja TP. Ocular findings in patients with autosomal dominant retinitis pigmentosa and a rhodopsin gene defect (Pro-23-His). *Arch Ophthalmol*. 1991; 109(1):92–101. PMID: [1987956](#).
41. Cuenca N, Fernandez-Sanchez L, Sauve Y, Segura FJ, Martinez-Navarrete G, Tamarit JM, et al. Correlation between SD-OCT, immunocytochemistry and functional findings in an animal model of retinal degeneration. *Frontiers in neuroanatomy*. 2014; 8:151. doi: [10.3389/fnana.2014.00151](#) PMID: [25565976](#); PubMed Central PMCID: PMC4273614.
42. Berger A, Cavallero S, Dominguez E, Barbe P, Simonutti M, Sahel JA, et al. Spectral-domain optical coherence tomography of the rodent eye: highlighting layers of the outer retina using signal averaging and comparison with histology. *PLoS One*. 2014; 9(5):e96494. doi: [10.1371/journal.pone.0096494](#) PMID: [24788712](#); PubMed Central PMCID: PMC4008571.
43. Wang M, Lam TT, Tso MO, Naash MI. Expression of a mutant opsin gene increases the susceptibility of the retina to light damage. *Vis Neurosci*. 1997; 14(1):55–62. PMID: [9057268](#).
44. Aleman TS, Duncan JL, Bieber ML, de Castro E, Marks DA, Gardner LM, et al. Macular pigment and lutein supplementation in retinitis pigmentosa and Usher syndrome. *Invest Ophthalmol Vis Sci*. 2001; 42(8):1873–81. PMID: [11431456](#).
45. Moriguchi K, Yuri T, Yoshizawa K, Kiuchi K, Takada H, Inoue Y, et al. Dietary docosahexaenoic acid protects against N-methyl-N-nitrosourea-induced retinal degeneration in rats. *Exp Eye Res*. 2003; 77(2):167–73. PMID: [12873446](#).
46. Ishikawa F, Ohguro H, Ohguro I, Yamazaki H, Mamiya K, Metoki T, et al. Prolonged rhodopsin phosphorylation in light-induced retinal degeneration in rat models. *Invest Ophthalmol Vis Sci*. 2006; 47(12):5204–11. doi: [10.1167/iovs.05-1149](#) PMID: [17122104](#).
47. LaVail MM, Gorrin GM, Repaci MA. Strain differences in sensitivity to light-induced photoreceptor degeneration in albino mice. *Current eye research*. 1987; 6(6):825–34. PMID: [3608569](#).
48. Montagutelli X. Effect of the genetic background on the phenotype of mouse mutations. *Journal of the American Society of Nephrology: JASN*. 2000; 11 Suppl 16:S101–5. PMID: [11065339](#).
49. Jelcick AS, Yuan Y, Leehy BD, Cox LC, Silveira AC, Qiu F, et al. Genetic variations strongly influence phenotypic outcome in the mouse retina. *PLoS One*. 2011; 6(7):e21858. doi: [10.1371/journal.pone.0021858](#) PMID: [21779340](#); PubMed Central PMCID: PMC3136482.
50. Heckenlively JR, Rodriguez JA, Daiger SP. Autosomal dominant sectoral retinitis pigmentosa. Two families with transversion mutation in codon 23 of rhodopsin. *Arch Ophthalmol*. 1991; 109(1):84–91. PMID: [1987955](#).
51. Stone EM, Kimura AE, Nichols BE, Khadivi P, Fishman GA, Sheffield VC. Regional distribution of retinal degeneration in patients with the proline to histidine mutation in codon 23 of the rhodopsin gene. *Ophthalmology*. 1991; 98(12):1806–13. PMID: [1775314](#).

52. Naash ML, Peachey NS, Li ZY, Gryczan CC, Goto Y, Blanks J, et al. Light-induced acceleration of photoreceptor degeneration in transgenic mice expressing mutant rhodopsin. *Invest Ophthalmol Vis Sci*. 1996; 37(5):775–82. PMID: [8603862](#).
53. Aleman TS, Cideciyan AV, Sumaroka A, Windsor EA, Herrera W, White DA, et al. Retinal laminar architecture in human retinitis pigmentosa caused by Rhodopsin gene mutations. *Invest Ophthalmol Vis Sci*. 2008; 49(4):1580–90. PMID: [18385078](#). doi: [10.1167/iov.07-1110](#)
54. Mohand-Said S, Hicks D, Dreyfus H, Sahel JA. Selective transplantation of rods delays cone loss in a retinitis pigmentosa model. *Arch Ophthalmol*. 2000; 118(6):807–11. PMID: [10865319](#).
55. Zrenner E. Will retinal implants restore vision? *Science*. 2002; 295(5557):1022–5. doi: [10.1126/science.1067996](#) PMID: [11834821](#).
56. Busskamp V, Duebel J, Balya D, Fradot M, Viney TJ, Siebert S, et al. Genetic reactivation of cone photoreceptors restores visual responses in retinitis pigmentosa. *Science*. 2010; 329(5990):413–7. doi: [10.1126/science.1190897](#) PMID: [20576849](#).
57. Mace E, Caplette R, Marre O, Sengupta A, Chaffiol A, Barbe P, et al. Targeting Channelrhodopsin-2 to ON-bipolar Cells With Vitreally Administered AAV Restores ON and OFF Visual Responses in Blind Mice. *Mol Ther*. 2014. doi: [10.1038/mt.2014.154](#) PMID: [25095892](#).
58. Bi A, Cui J, Ma YP, Olshevskaya E, Pu M, Dizhoor AM, et al. Ectopic expression of a microbial-type rhodopsin restores visual responses in mice with photoreceptor degeneration. *Neuron*. 2006; 50(1):23–33. doi: [10.1016/j.neuron.2006.02.026](#) PMID: [16600853](#); PubMed Central PMCID: PMC1459045.

2. Complementary ongoing results: Genome editing approach for Rhodopsin mutants

Currently, there is no treatment for RCD and different therapeutic strategies are under investigation. We wanted to deliver the proof-of-concept of genome editing on *RHO* mutant acting as a dominant negative effect, which cannot be addressed by current gene replacement strategies.

a) Meganucleases

This project was part of a FEDER funded project in collaboration with a company (Collectis, Romainville, France). The initial rationale was to obtain several meganucleases allowing us to inactivate any of the dominant mutations we wanted to target through the human *RHO*. Bioinformatics were applied to identify the best fit for meganuclease cut in human *RHO*. Four meganucleases were selected after testing on extra-chromosomal substrate on yeast and CHO (Chinese Hamster Ovary) cells by a company (Collectis) (Figure 40).

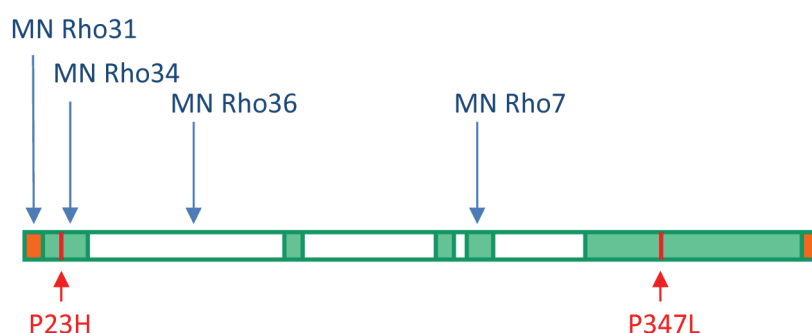


Figure 40: Meganucleases targets on human genomic *RHO*. Exons are in green, introns in white, 5'UTR and 3'UTR in orange. Meganucleases target are depicted with blue arrows, mutations leading to P23H and P347L exchange are depicted with red arrows.

(1) *In vitro* on HEK293 cells

HEK 293 (Human Embryonic Kidney 293) cells were transfected with plasmids encoding for meganucleases (targeting *RHO* or calpain small subunit 1 (*CAPNS1*) used as positive control), incubated for 48 hours, and subsequent protein and gDNA extracted. Western-blot using an anti-I-CreI antibody recognizing meganucleases was performed and confirmed strong expression of meganucleases (Figure 41).

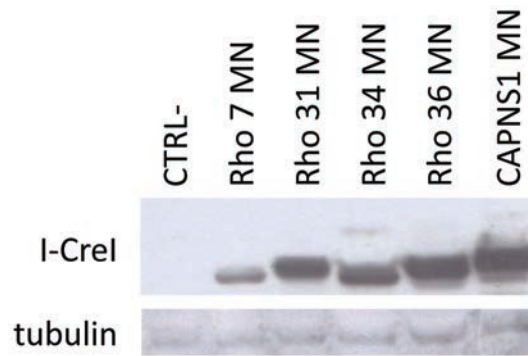


Figure 41: Western-blot evaluating the expression of meganucleases on transfected HEK 293 cells. HEK 293 cells were transfected with meganucleases, incubated for 48 hours and protein extracted. Western-blot was performed and membrane staining against I-CreI and tubulin to confirm expression of meganucleases. Abbreviations: CTRL -: not transfected; MN: meganuclease. All tested meganucleases show high protein expression.

Meganuclease cutting was tested by PCR-amplification of fragments of the targeted site of gDNA of meganucleases treated or untreated cells with subsequent deep sequencing and was considered as efficient if reaching at least 1% (252). Although positive control CAPNS1 meganuclease treatment was efficient with 8% of mutations, none of the tested RHO meganucleases was efficient to cut and induce NHEJ (Table 13).

Table 13: Percentage of mutation induced by various meganucleases evaluated by deep sequencing. Meganuclease-treated or untreated HEK 293 cells gDNA was amplified around meganuclease target site, percentage of mutations were numbered by analyzing sequences obtained by deep sequencing.

Target	Type	Mutations (%)
MN RHO7	Meganuclease treated	0.088
MN RHO7	Negative control	0.127
MN RHO 31	Meganuclease treated	0.31
MN RHO 31	Negative control	0.0
MN RHO 34	Meganuclease treated	0.028
MN RHO 34	Negative control	0.011
MN RHO 36	Meganuclease treated	0.058
MN RHO 36	Negative control	0.0
MN CAPNS1	Meganuclease treated	8.161
MN CAPNS1	Negative control	0.518

We hypothesized that this negative result can be due i/ to a difficult access of meganucleases to the endogeneous locus on cells that do not naturally express rhodopsin, ii/ to a low amount of transfected cells, where these cells would express strongly the meganucleases (refer to the western-blot evaluation), but more meganuclease expressing cells are necessary for efficiency and/or iii/ to the low efficiency of the selected meganucleases to induce DBS at the target site

if accessible. In order to avoid the difficult access of meganuclease to the endogenous loci, we decided to change the validation model.

(2) *Ex vivo* on rat retinal explant

We choose a model in which *RHO* is naturally expressed and therefore the endogenous *RHO* locus is more likely accessible to endonucleases by using newborn rat retinal explants. Meganuclease Rho 31 presented the highest mutation rate (Table 13), and its targeted sequence is conserved between human and rat. Therefore, we tested its cutting efficiency on rat retinal explants. A vector expressing Green Fluorescent Protein (GFP) was used to monitor meganuclease-encoding plasmid delivery. The meganuclease Rho 31-GFP plasmid was co-electroporated in newborn rat retinal explants with a cofactor that stabilizes DSB (Trex) and increases the NHEJ events when DSB occurs. A positive control condition was performed by co-electroporating three plasmids: one expressing Baat meganuclease, one expressing GFP, and one expressing Trex. Four days later, cells were dissociated and FACS sorted for GFP. Only 5% of the cells were GFP positive. Evaluation of NHEJ was performed on gDNA of GFP positive cells.

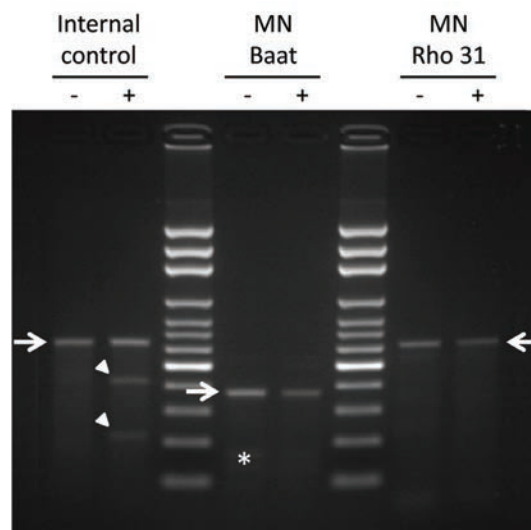


Figure 42: Evaluation of NHEJ with Surveyor mutation detection kit induced by meganuclease on newborn rat retina. Newborn rat retinas were electroporated with plasmids co-expressing Baat or Rho 31 meganucleases (MN Baat and MN Rho 31 respectively) and GFP and incubated for 4 days. Dissociated cells were FACS sorted when GFP positive and the mismatch detecting kit applied. Uncut fragments are depicted by arrows, cut fragments are depicted by arrow heads, non specific fragment is depicted by star. – untreated, + treated.

Evaluation of NHEJ revealed multiple bands for the internal control (Figure 42, arrow heads), but multiple bands for the Baat positive control, and the Rho 31 meganucleases could not be

visualized (Figure 42, arrows). A slight additional band of approximately 180 bp was visualized for the untreated Baat meganuclease condition but was considered as non specific since the cells were not treated with the meganuclease (Figure 42, star).

Although *Baat* is expressed at low levels in brain, thyroid and strongly in liver (<http://www.ncbi.nlm.nih.gov/UniGene/ESTProfileViewer.cgi?uglist=Mm.2859>), we were not sure if it is specifically expressed in the retina, which may explain the negative results for the Baat meganuclease. *Rho* is only weakly expressed in newborn rat retina, which may explain the negative results obtained for the Rho 31 meganuclease. To test meganuclease Rho 31, electroporation in older rat retinas is technically more challenging with poorer efficacy. When we exposed these negative results to our collaborators (Collectis), they proposed to switch to a new nuclease type, with a more flexible design: the TALENs.

b) TALENs

The major advantage of TALEN is the flexibility in design for any specific target to induce DSB. Again, for this part, we chose the P23H rat model described before. With the knowledge of the genetic characterization of this rat described herein (232), our collaborator (Collectis) designed a TALENs that specifically targets the P23H mutation on the mouse transgene of this model (P23H TALEN). DSB was validated on extra-chromosomal substrate in yeast and delivered to us in two plasmids coding for each subunit of the TALEN.

(1) *Ex vivo* on P23H rat retinal explants

In the absence of GFP in the vector delivered by our collaborators (Collectis) and no subcloning possibility in another vector, newborn P23H rat retinal explant electroporation was monitored by co-electroporation of a GFP expressing plasmid in addition to the two plasmids expressing the TALEN subunits. A TALEN targeting human *RAG* with no target in rat genome (*RAG* TALEN) served as a negative control. After FACS sorting, only 1% of the cells were GFP positive. The cutting efficiency evaluation test revealed no multiple bands for both the negative control *RAG* TALEN and the P23H TALEN (Figure 43, arrows), although we observed several bands for the positive control of the kit (Figure 43, arrowheads). A slight additional fragment of approximately 150 bp was visualized for PCR of untreated or treated

TALEN conditions, but was considered as non specific since the band is present for the untreated conditions (Figure 43, stars).

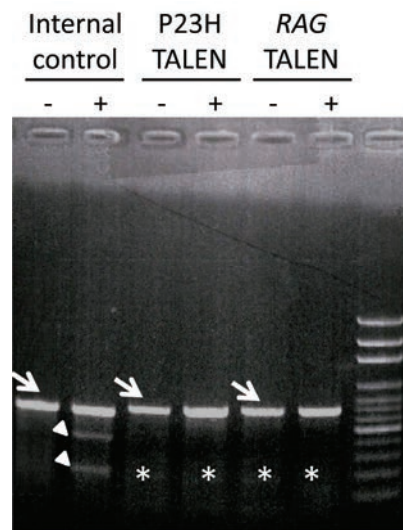


Figure 43: Evaluation of NHEJ with Surveyor mutation detection kit induced by TALEN on newborn rat retina. Newborn rat retinas were co-electroporated with the two plasmids expressing TALEN subunits and one plasmid expressing GFP and incubated for 5 days. Dissociated cells were FACS sorted when GFP positive and the mismatch detecting kit applied. Uncut fragments are depicted by arrows, cut fragments are depicted by arrow heads, non specific fragments are depicted by stars. –untreated, + treated.

This negative result can be due to i/ the inaccessibility of the endogenous *Rho* locus in retinal explants of newborn rats which express *Rho* weakly, ii/ an imperfect co-electroporation of GFP and both TALEN subunits and/or iii/ the low yield of DBS induced by the P23H TALEN. As mentioned before, electroporation in older rat retinal explants lead to lower electroporation efficacy. To improve the delivery, TALENs were encapsulated in AAV viruses and the efficient infection tested *ex vivo* on 21-day-old P23H rat retinal explants and *in vivo*.

(2) *Ex vivo* and *in vivo* infection with TALENs expressing AAV

Because of the FEDER grant deadline funding this project, we were eager to finalize the proof-of-concept of TALEN genome editing on *Rho* mutant. Therefore we decided to perform both *ex vivo* and *in vivo* experimentations in parallel.

(a) *Ex vivo* on 21-days-old P23H rat retinal explants

As described under methods, most efficient infection of retinal explants using AAV8-Y733F expressing GFP under the control of pCMV was obtained after 5 days of incubation yielding in the strongest fluorescence signal. Cutting efficiency evaluation test on P21 P23H rat retinal explants infected with 4.6×10^{14} vg/ml concentrated AAV8-Y733F expressing TALEN subunit (5 μ l per AAV) revealed no multiple bands for both negative control RAG TALEN and P23H TALEN (Figure 44, arrows) although we observed several bands for the positive control of the kit (Figure 44, arrowheads).

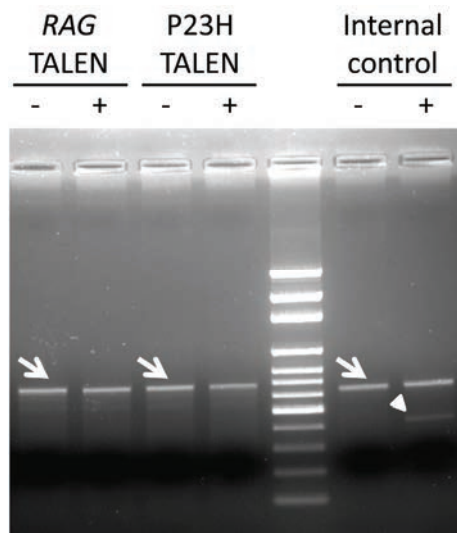


Figure 44: Evaluation of NHEJ with Surveyor mutation detection kit induced by TALEN on P21 P23H rat retina. P21 P23H rat retinal explants were infected with two AAV8-Y733F expressing each one TALEN subunit under the control of CMV promoter and incubated for 5 days. gDNA was extracted, PCR amplification was performed using probes flanking the TALEN targeted site and the mismatch detecting kit applied. Uncut fragments are depicted by arrows, cut fragments are depicted by arrow head. –untreated, + treated.

This result can be due to a low rate of rod photoreceptors infected by both viruses expressing TALEN subunits, or the lack of efficiency of TALENs. Albeit different approaches to establish the conditions to validate TALEN expression by immunohistochemistry in the absence of a positive control, we were not able to establish the conditions. Therefore, we evaluated the infection rate by anti-GFP immunohistochemistry on explants infected with AAV8-Y733F expressing GFP under the control of the CMV promoter (Figure 45).

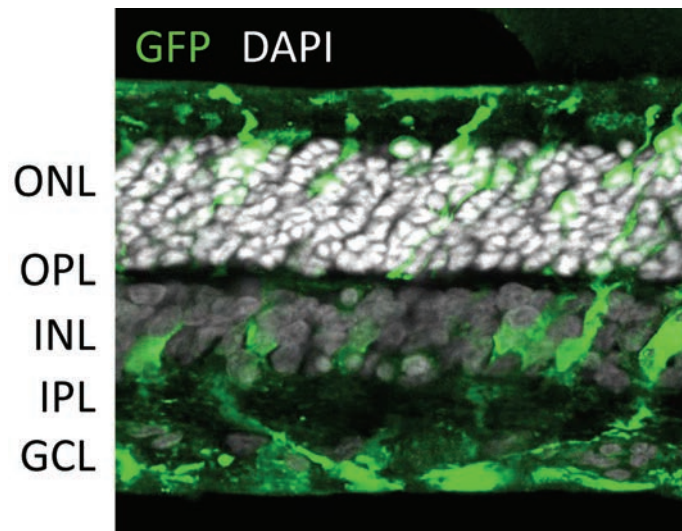


Figure 45: Visualization of GFP expression on infected P21 P23H rat retinal explants. P21 P23H rat retinas were infected with an AAV8-Y733F expressing GFP under the control of CMV promoter and incubated for 5 days. An anti-GFP immunohistochemistry revealed labeling in all retinal layers.

Although we observed anti-GFP labeling in all retinal layers, immunolocalisation in photoreceptors was seldom (Figure 45). Together, these results can be due to a low rate of rod photoreceptors infected by both viruses expressing the TALEN subunits, or the lack of efficiency of TALENs.

(b) *In vivo* delivery on P23H rats

As mentioned before, the following *in vivo* experiments were performed in parallel with the *ex vivo* infection of retinal explants of P23H rats.

(i) Subretinal injections at P21

Subretinal injections of 1 μ l of GFP expressing virus at 10^{14} vg/ml on 21 days old P23H rats' right eye showed strong GFP fluorescence localization on the retina 14 days after injections (Figure 46).

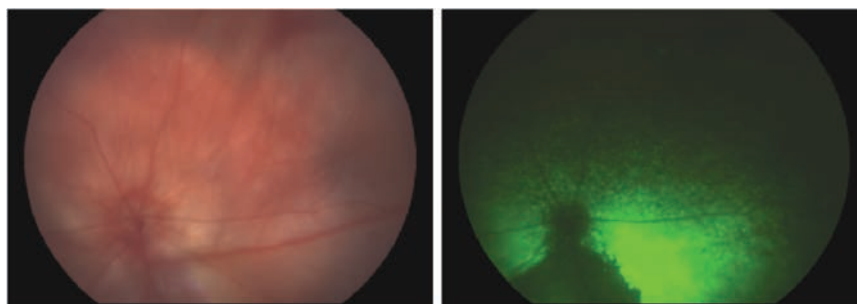


Figure 46: Color (right) and micron 3 (left) fundus imaging of GFP fluorescence for AAV8-Y733F infected animal 14 days after subretinal injection.

Subretinal injection in P21 P23H rat's right eyes of 1 μ l at 10¹⁴ vg/ml of each AAV8-Y733F virus coding for a P23H Rho TALEN subunit followed by ERG and SD-OCT monitoring revealed no functional (Figure 47) and structural (data not shown) rescue when compared to eyes injected with AAV8-Y733F viruses coding for RAG TALEN subunits or non injected eyes.

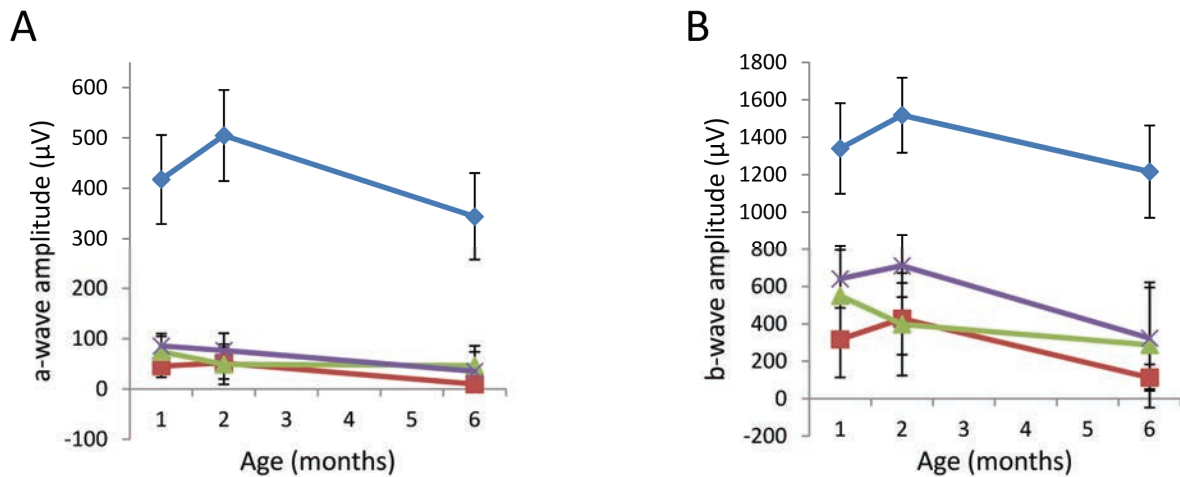


Figure 47: Scotopic ERG responses. Dark-adapted ERG recording was obtained at 1,2,3 and 6 months of ages and a 12 cd.s/m² stimulus intensity from wild-type rats (blue), untreated P23H rats (purple), P23H rats subretinally injected with AAV8-Y733F expressing TALEN against P23H *Rho* (green) and P23H rats subretinally injected with AAV8-Y733F expressing TALEN against RAG (red). (A) a-wave and (B) b-wave maximum amplitudes with increasing ages of rats are shown. Error bar represent standard error, n=12

Furthermore, damages at injection points were visualized by SD-OCT (data not shown). Thus, this negative result can be due to the damage caused by subretinal injection, a low rate of rod photoreceptors infected by both viruses respectively expressing one of the TALEN subunits, or the lack of efficiency of TALENs.

(ii) Systemic injections at P1

Subretinal injections of 10 μ L of GFP expressing virus at 8.5 10¹³ vg/ml on newborn P23H rats showed a diffuse GFP fluorescence of the retina 14 days after injections (Figure 48).

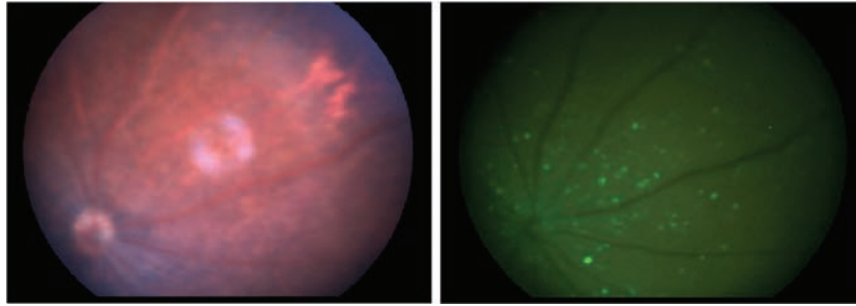


Figure 48: Color (right) and micron 3 (left) fundus imaging of GFP fluorescence for AAV9-2YF injected animal 14 days after systemic injection.

Systemic injection in newborn P23H rats eye of 5 μ L of each AAV9-2YF virus at 1.7×10^{14} coding for a P23H Rho TALEN subunit by followed ERG and SD-OCT monitoring revealed no functional (Figure 49) and structural (data not shown) rescue when compared to eyes of rats injected with injected with AAV9-2YF viruses coding for *RAG* TALEN subunits or non injected rats' eyes.

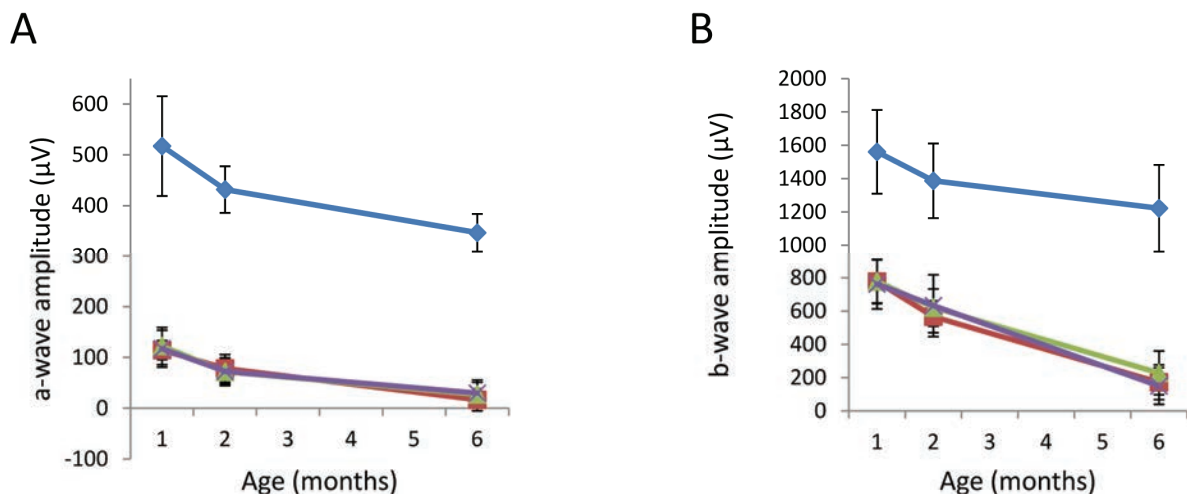


Figure 49: Scotopic ERG phenotype. Dark-adapted ERG series were obtained at 1,2,3 and 6 months of ages and a 12 cd.s/m² stimulus intensity from wild-type rats eyes (blue), untreated P23H rats eyes (purple), P23H rats injected with AAV9-2YF expressing TALEN directed against P23H *Rho* eyes (green) and P23H rats injected with AAV9-2YF expressing TALEN directed against *RAG* eyes (red). (A) a-wave and (B) b-wave maximum amplitudes with increasing ages of rats are shown. Error bar represent standard error, n=14

This result can be due to a low rate of rod photoreceptors infected by both viruses expressing TALENs subunits and/or the lack of efficiency of TALENs.

(3) *In vitro* on P23H rat embryonic fibroblasts

To ensure we did not miss the activity of TALENs because of the difficulty to deliver both TALEN subunits into the same cell, we performed an *ex vivo* assay on P23H rat embryonic fibroblasts. P23H rat embryonic fibroblasts (P23H REF) were isolated on E15 embryos. A construction comprising an IRES followed by GFP or iRFP into vectors expressing TALEN subunit (one distinct fluorescent marker per construct) were cloned. 18 % of nucleofected P23H REF with the two plasmids were GFP and iRFP positive after FACS sorting. Cutting efficiency evaluation test revealed no multiple bands for both negative control RAG TALEN and P23H TALEN (Figure 50, arrowheads) although we observed several bands for the positive control of the kit (Figure 50, arrows).

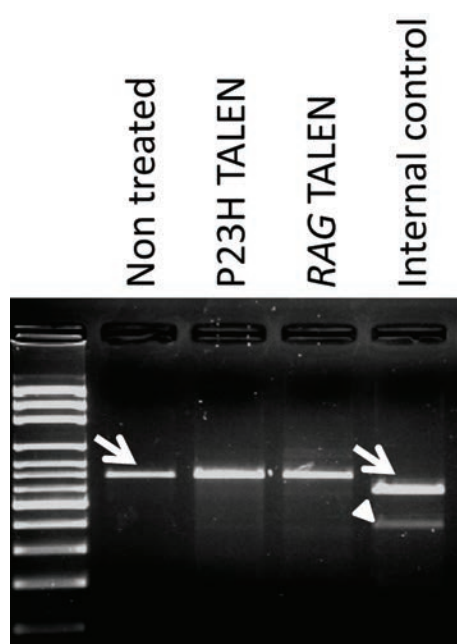


Figure 50: Evaluation of NHEJ with Surveyor mutation detection kit induced by TALEN on P23H REF. P23H REF were co-nucleofected with two plasmids expressing each one TALEN subunit and GFP or iRFP after an IRES (one fluorescent marker per subunit) and incubated for 3 days. Harvested cells were FACS sorted when GFP and iRFP positive and the mismatch detecting kit applied. Uncut fragments are depicted by arrows, cut fragments are depicted by arrow head.

Since we were sure that both TALEN subunits were expressed in these cells, we hypothesized that this negative result can be due to a difficult access of TALEN to the endogenous *Rho* locus gDNA target in this artificial system or to the lack of efficiency of TALENs.

C. Other projects

I also obtained results by contributing to different projects in my laboratory. My contributions and the communications are listed below. These results will not be discussed in the last part “Discussion and perspectives”.

RP1 mutations project: Sequencing

Publication:

1. Audo, I., Mohand-Said, S., Dhaenens, C. M., Germain, A., **Orhan, E.**, Antonio, A., Hamel, C., Sahel, J. A., Bhattacharya, S. S., and Zeitz, C. (2012). RP1 and autosomal dominant rod-cone dystrophy: novel mutations, a review of published variants, and genotype-phenotype correlation. *Hum Mutat* 33, 73-80.

LRIT3 identification and characterization project: Functional studies

Publications:

1. Zeitz, C., Jacobson, S. G., Hamel, C. P., Bujakowska, K., Neuille, M., **Orhan, E.**, Zanlonghi, X., Lancelot, M. E., Michiels, C., Schwartz, S. B., Bocquet, B., Antonio, A., Audier, C., Letexier, M., Saraiva, J. P., Luu, T. D., Sennlaub, F., Nguyen, H., Poch, O., Dollfus, H., Lecompte, O., Kohl, S., Sahel, J. A., Bhattacharya, S. S., and Audo, I. (2013). Whole-exome sequencing identifies LRIT3 mutations as a cause of autosomal-recessive complete congenital stationary night blindness. *Am J Hum Genet* 92, 67-75.

2. Neuille, M., El Shamieh, S., **Orhan, E.**, Michiels, C., Antonio, A., Lancelot, M. E., Condroyer, C., Bujakowska, K., Poch, O., Sahel, J. A., Audo, I., and Zeitz, C. (2014). Lrit3 Deficient Mouse (nob6): A Novel Model of Complete Congenital Stationary Night Blindness (cCSNB). *PLoS One* 9, e90342.

3. Neuille, M., Morgans, C. W., Cao, Y., **Orhan, E.**, Michiels, C., Sahel, J. A., Audo, I., Duvoisin, R. M., Martemyanov, K. A., and Zeitz, C. (2015). LRIT3 is essential to localize TRPM1 to the dendritic tips of depolarizing bipolar cells and may play a role in cone synapse formation. *The European journal of neuroscience*, 56.

Paper presentation:

1. Neuillé, M., El Shamieh, S., **Orhan, E.**, Michiels, C., Bujakowska, K.M., Poch, O., Sahel, J.A., Audo, I., and Zeitz, C. (2014). A novel mouse model for complete Congenital Stationary Night Blindness (cCSNB). Association for Research in Vision and Ophthalmology (MN, Orlando, USA).

Poster presentation:

1. Zeitz, C., Jacobson, S., Hamel, C., Bujakowska, K., Neuillé, M., **Orhan, E.***, Zanlonghi, X., Sahel, J., Bhattacharya, S., and Audo, I. (2013). Whole exome sequencing identifies mutations in LRIT3 as a cause for autosomal recessive complete congenital stationary night blindness. Association for Research in Vision and Ophthalmology (* Due to the pregnancy of CZ, EO presented the poster, Seattle, USA).

ITM2B identification and characterization project: Functional studies

Publication:

1. Audo, I., Bujakowska, K., **Orhan, E.**, El Shamieh, S., Sennlaub, F., Guillonneau, X., Antonio, A., Michiels, C., Lancelot, M. E., Letexier, M., Saraiva, J. P., Nguyen, H., Luu, T. D., Leveillard, T., Poch, O., Dollfus, H., Paques, M., Goureau, O., Mohand-Said, S., Bhattacharya, S. S., Sahel, J. A., and Zeitz, C. (2014). The familial dementia gene revisited: a missense mutation revealed by whole-exome sequencing identifies ITM2B as a candidate gene underlying a novel autosomal dominant retinal dystrophy in a large family. *Hum Mol Genet* 23, 491-501.

Poster presentation:

1. Audo, I., Bujakowska, K., **Orhan, E.**, Sennlaub, F., Guillonneau, X., Leveillard, T., Mohand-Said, S., Bhattacharya, S., Sahel, J., and Zeitz, C. (2013). The familial dementia gene revisited: ITM2B missense mutation causes a new dominant retinal dystrophy. Association for Research in Vision and Ophthalmology (IA, Seattle, USA).

KIZ identification and characterization project: Functional studies

Publication :

1. El Shamieh, S., Neuille, M., Terray, A., **Orhan, E.**, Condroyer, C., Demontant, V., Michiels, C., Antonio, A., Boyard, F., Lancelot, M. E., Letexier, M., Saraiva, J. P., Leveillard, T., Mohand-Said, S., Goureau, O., Sahel, J. A., Zeitz, C., and Audo, I. (2014). Whole-exome sequencing identifies KIZ as a ciliary gene associated with autosomal-recessive rod-cone dystrophy. *Am J Hum Genet* 94, 625-633.

Paper presentations:

1. El Shamieh, S., Neuille, M., Terray, A., **Orhan, E.**, Condroyer, C., Demontant, V., Michiels, C., Antonio, A., Boyard, F., Leveillard, T., Mohand-Said, S., Goureau, O., Sahel, J. A., Zeitz, C., and Audo, I. (2014). Whole exome sequencing identifies a new ciliary gene underlying autosomal recessive rod-cone dystrophy. Young Researchers in Life Sciences (SES, Paris, France).

2. Zeitz, C., El Shamieh, S., Neuille, M., Terray, A., **Orhan, E.**, Leveillard, T., Mohand-Said, S., Goureau, O., Sahel, J.A., and Audo, I. (2014). Comprehensive genetic analysis in inherited retinal diseases applying next-generation sequencing. International Society for Eye Research (CZ, San Francisco, USA).

GRM6 gene therapy project: *In vivo* and functional studies

Paper presentation:

1. Miranda de Sousa Dias, M., Neuille, M., **Orhan, E.**, Dalkara, D., Audo, I., and Zeitz, C. (2014). Gene replacement therapy for CSNB as a proof-of-concept for other inner retinal disorders. Société de Génétique Ophtalmique Francophone and Deutsche Ophtalmologische Gesellschaft joint meeting (MMdSD, Giessen, Germany).

Discussion and Perspectives

A. Motivation

Genetic studies of human population provide a gateway to better understand the intact physiology of a system. New gene defects identification enables, by deciphering the causal relationship between the mutation and the disease, to gain unpredicted insight into a cellular pathway. Moreover, knowledge of genetic defects has a high clinical impact since it provides an opportunity to design therapeutic strategies to address this defect.

On these two aspects, this thesis gives several insights on the retinal physiology. On one hand, *GPR179* identification, localization and physiopathological studies and mouse model characterization provide a better understanding of the first visual synapse between photoreceptors and ON-bipolar cells. On the other hand, genome editing strategies applied to *RHO* mutations helped to a better understanding of the P23H-1 rat adRCD rat model and revealed how challenging the setting of genome editing strategies was.

B. Accuracy and limitations of our animal models and new insights into retinal physiology

Either for physiological and physiopathological mechanism studies or proof-of-concept of therapeutic approach, an animal model that allows transferability of information is needed. The accuracy with which the animal model predicts the course or outcome of the human phenomenon constitutes the principal criterion of relevance. The other considerations we took into account were i/availability, ii/housing and maintenance requirements, iii/cost, iv/opportunity to perform invasive or manipulative research but also v/number of people who are already using this model, allowing better knowledge of the animal model (253). In our two studies, murine models were chosen. Mouse and rat's eyes are similar to human eyes, with some exceptions: the size is smaller, and the composition of the retina differs at the level of photoreceptors. Mice and rats do not have a macula, and present also a higher rod/cone photoreceptor ratio than humans. They also express distinct cone opsin making their visible light spectrum different from humans (19, 254). Finally, they also have a later development of their retina compared to humans, with rod photoreceptors being totally mature around ten days after birth (255). This last difference had to be particularly taken into account, especially for newborn rat's retinal explant electroporation. However, even with these differences between murine and human eyes, mice and rats present very similar eye compared to humans in terms of structure and function, making them good models for translational research.

1. *Gpr179*^{-/-} mouse model

The *Gpr179*^{-/-} model presented the first four advantages listed above. At the time we started the study, one horse (85), two zebrafish (86, 87) and six mouse models (8, 69, 88-91) were already published for cCSNB, making mouse the main specie studied for this disease. Since ES clones for a *GPR179* knock-out were available, the gene defect in humans had to be confirmed in a different model and GPR179 function had to be further elucidated, we developed a mouse model, allowing comparisons of our model and the different models for the other genes of the same signaling cascade. These studies have been initiated when we were not aware that another group characterized a naturally occurring *Gpr179* mouse model,

which was used for a candidate gene approach for cCSNB patient screening and led with our study to a back-to-back publication in the American Journal of Human Genetics (245, 247). *Gpr179*^{-/-} turned out to be an excellent model since the initial functional characterization revealed the same abnormalities as observed in patients (247). Indeed, *Gpr179*^{-/-} mice and cCSNB patients with *GPR179* mutations present a Schubert-Bornschein type ERG with a normal a-wave and severely reduced b-wave under scotopic conditions. In photopic conditions, both photopic single flash responses present an a-wave with normal amplitude and a reduced b/a ratio. Our results were also consistent with the other *Gpr179* mutant mouse line harboring a *Gpr179* transposon mutation, and a morpholino knockdown of *Gpr179* in zebrafish (245). ERG in scotopic conditions of both mouse models presents a no b-wave phenotype with normal a-wave (245). In photopic conditions, we obtained a reduced b-wave amplitude for the photopic single flash responses as described for the other *Gpr179* mouse model. The immunohistochemistry results we obtained were also consistent with results obtained on the other *Gpr179* mouse model (245, 246, 256-258). On one hand, GRM6 (245, 258), TRPM1 (246, 258) and for the first time LRIT3 shown by us are not mislocalized when GPR179 is lacking. On the other hand, GPR179 disruption leads to the absence at the dendritic tips of ON-bipolar cells of RGS7 (246), RGS11 (246) and for the first time GNB5 shown by us. Proteomic screening identified GPR179 as a binding partner of RGS proteins (246). Together these findings suggest that GPR179 has a role to target and/or maintain either RGS7-GNB5 or RGS11-GNB5 complexes at the dendritic tips of ON-bipolar cells. It is also known that GPR179 forms macromolecular complexes with GRM6 and TRPM1 (256), suggesting a role in the compartmentalization of the principal elements of the cascade by bringing RGS proteins into close proximity to key elements of the cascade they regulate. Our studies showed that the localization of various proteins involved in ON-bipolar signal transmission including LRIT3 is maintained, whereas proteins of the RGS family, which are known to regulate GRM6 (82), are no longer localized at the dendritic tips of ON-bipolar cells (Figure 51). Thus, the availability of our mouse model will be useful to further characterize the signaling cascade from the photoreceptor to bipolar cells. Future studies, for instance using optomotor response measurements under scotopic and photopic conditions, histology and proteomics needs to be performed to refine the phenotypic and functional characterization and confirm these findings. Furthermore, electrophysiological experiments need to be conducted to better understand the role of GPR179 in sensitivity of GRM6 signaling cascade (258). Finally, GPR179 is an orphan seven transmembrane GPCR, and additional studies are needed to deorphanize the receptor by the identification of a putative ligand or to prove that GPR179

serves only as a regulator in the RGS complex. Determining the hierarchical relationship and determinants for complex formation at the dendritic tip of ON-bipolar cells, will likely yield important insights into the organization of the postsynaptic compartment of the cascade.

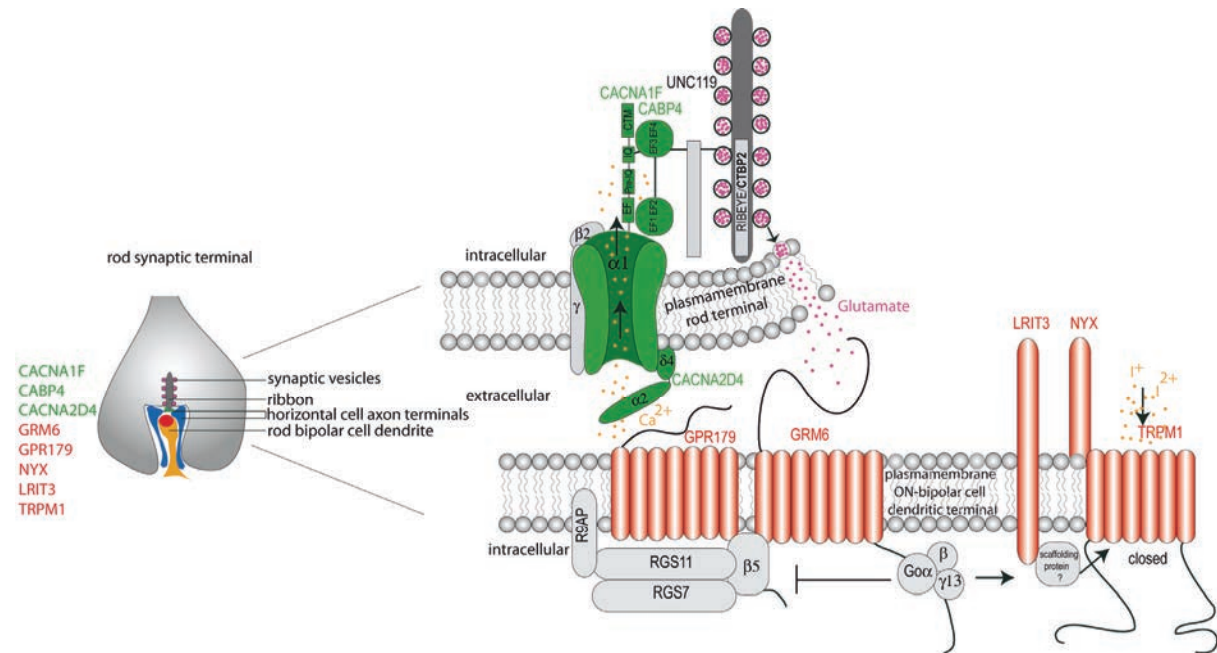


Figure 51: Schematic drawing of major molecules important for the first visual synapse between photoreceptors and ON-bipolar cells (modified from Zeitz, C. et al., (30))

2. P23H-1 rat model

The P23H-1 rat model was chosen because it presents the five advantages mentioned above. The P23H-1 rat harbors progressive rod degeneration initially associated with normal cone function, this phenotype is consistent with the clinical findings in patients carrying the p.P23H RHO exchange. Moreover, the P23H-1 rat presents a late degeneration (232, 241) allowing successful rescue of the phenotype. However, when we started our study, little information was available on the rat genotype. As a primary step for genome editing, we sequenced the transgene, allowing the design of endonucleases, and started the experiments to bring a fast proof-of-concept of genome editing. Subsequently, we showed that nine copies of the transgene were present in the hemizygous P23H-1 rat (232). The low expression rate of the transgene supposed a tandem insertion of these copies with only one or few transgene(s) expressed or insertion in regions suppressed by epigenetic phenomenon such as chromatin compaction (232). Nevertheless, these nine copies of transgene hemizygous P23H-1 rat

constitute the major drawback of this model. We did not know if the endonuclease we were testing would be able to inactivate all the transgene copies that were actually expressed, to rescue the phenotype. With the low transgenic expression, P23H-1 rat would qualify to test therapy targeting mRNA. A better model for genome editing would have been the recent P23H knock-in mouse which has a wild-type mouse allele, and a P23H mutated transgene (120). Nevertheless, we performed the cutting efficiency evaluation assay directly on the transgenic DNA. The limit of sensitivity of this test was recently described at 10% (259). So if the endonuclease had induced DSB and NHEJ in a rate superior to 10%, we should have visualized it and may be able to discriminate between a low activity rate superior to 10% with little chance for rescue of the phenotype from the total absence of activity or low activity rate inferior to 10%. Deep sequencing was a more sensitive assay. However, we did not use it anymore because we assumed that an edited photoreceptor rate inferior to 10% would be unlikely to show a therapeutic effect. Depending on the high or low activity rate of the endonuclease and the effective inactivation of the expressed copies of transgene, we could therefore visualize respectively phenotypic rescue and genome editing at a gDNA level, or only the genome editing at a gDNA level.

C. Accuracy and limitations of our genome-editing models

For our genome-editing experiments, we performed experiments on several models, each of which with advantages and drawbacks but overall complementing each others.

1. HEK 293 cells

HEK293 cells are a cell line derived from human embryonic kidney. They are very easy to grow, provide an abundant material, and are easy to transfect. However they do not allow the evaluation of functional rescue in case of successful genome editing since they do not express *RHO*. Thus, we choose HEK293 cells only to validate the efficacy of meganuclease at the genomic level on human *RHO*. The major drawback of this model is indeed the absence of *RHO* expression that may suggest that at the *RHO* locus, chromatin may be compacted and therefore the gDNA not accessible to meganuclease targeting. Indeed, at the time we were performing our experiments, chromatin status had been shown to modulate the efficacy of weak endonucleases such as meganucleases (260, 261). Therefore, we decided to change the model.

2. REFs

REFs were isolated from E15 (embryonic 15-day-old) embryos. They are easy to grow and provide abundant material. The major advantage of this model was the perspectives. If we had been able to treat efficiently REFs with TALEN, then we could have selected edited fibroblastes, reprogram them into induced pluripotent stem cells and retina-like structure to validate phenotypic rescue. Physiological characterization could have been done and eventually cellular therapy could be considered. The other advantage is the possibility to perform FACS sorting or enrichment with magnetic beads of cells expressing endonucleases after nucleofection. The major drawback of this model may have been, similarly to HEK293 cells, the absence of locus accessibility, since fibroblastes don't naturally express *Rho*.

3. Newborn rat retinal explants

We performed newborn (postnatal 1 or P1) rat retinal explant electroporation to test meganucleases and TALENs. We choose this model since it allows endonuclease delivery directly to photoreceptors, where *Rho* is expressed. We were assuming that the chromatin state should be favorable to an access of endonucleases since *RHO* expression in rat retina starts at detectable levels at P2 and increases rapidly (262) to reach a plateau after P10. Electroporation in older rat retinas than P1 leads to poor delivery efficacy, explaining why we performed electroporation at P1. The other major reason of electroporation at P1 was that it was enabling genome editing before the cells were engaged into apoptotic mechanisms.

We electroporated a plasmid that co-expressed meganuclease and GFP (see Results Part B.2.b.2) or three plasmids, which express each one a subunit of TALEN or GFP (see Results Part B.2.c.1). The FACS sorting allowed ensuring that the endonucleases were expressed. Nevertheless, the major limit of this model was that we did not know if it was expressed in rod photoreceptors, which we wanted to target or in other retinal cell types since electroporation was performed on whole retinal explants. Low rate of cells (<5%) were GFP positive when FACS sorted, and cell type testing by as example immunocytochemistry with specific cell markers was not performed. Furthermore, for TALEN electroporation, we could not technically check if both plasmids encoding each subunit were co-transfected in the same cells.

4. P21 rat retinal explants

We performed P21 rat retinal explant infection with two AAV8-Y733F expressing TALEN subunits under the control of pCMV. There were two major improvements and advantages in this model compared to P1 retinal explant electroporation: i/ at P21, photoreceptors were mature and were expressing *RHO* at a high rate, so the chromatin state was favorable to access the TALEN target, ii/ we were expecting a higher rate of infection with AAV compared to the yield of electroporation. This model was also relevant to validate efficacy at the genomic level before testing functional rescue. The major drawback lies on the fact that we needed three viruses in this strategy: two for each subunit of the TALEN and one to monitor infection. In the absence of an effective immunohistochemistry using antibodies raised against two tags comprised in each one of the TALEN subunit, it was difficult to control the amount of cells indeed expressing both TALEN subunits that would be actively

genome edited. Therefore, we evaluated the infection rate by anti-GFP immunohistochemistry on explants infected with the virus expressing GFP and although we observed anti-GFP labeling in all retinal layers, we showed that immunolocalisation in photoreceptors was seldom. A better infection by testing different doses and/or serotypes would thus be beneficial for testing in this model.

5. P23H-1 rat model

Two modes of delivery were chosen for administration of two distinct AAV expressing each TALEN subunit.

a) Subretinal injections at P21

Subretinal injections at P21 were performed using two AAV8-Y733F expressing each a TALEN subunit under the control of pCMV. This AAV serotype had been reported to successfully deliver a gene to rod photoreceptors in the mouse (242). The major advantages were that we were providing TALEN subunit expressing AAVs under the control of a strong and ubiquitous promoter directly in contact with the photoreceptors at a stage when the retina is mature and *RHO* locus likely to be accessible for genome editing. If the treatment was efficient, we should also be able to document phenotypic rescue by functional and structural characterization of the rats. The drawbacks were that i/ we were not able to monitor if the infected cells were actually infected with both TALEN-subunit-expressing AAVs and ii/ we were not sure if the TALEN delivery time was early enough to salvage rod photoreceptors from apoptosis. Furthermore, by performing SD-OCT to monitor the expected rescue, we observed that our injections at P21 were damaging the retina. More precise subretinal injection performed by a surgeon without damaging the retina would also be beneficial.

b) Systemic injections at P1

Systemic injections at P1 were performed using two AAV9-2YF expressing the TALEN subunits under the control of pRHO, specific of rod photoreceptor expression. This AAV serotype had been reported to efficiently infect photoreceptors when injected systemically in the mouse (243). The major advantages were that i/ the treatment was performed at an early stage, enabling genome editing before the cells were engaged into apoptotic mechanisms, ii/ the retina was not damaged by the injection, iii/ by using a rod photoreceptor specific

promoter, we were limiting possible off-target effects on other cells in the body. Similarly as above for subretinal injections, the major drawback was that we were not able to monitor whether infected cells were actually expressing both TALEN subunits. Moreover, our injections were performed intracardiacally at P1 since it was the best time point recognized for injections in mouse (243). We subsequently tested different time points for optimization of this AAV infection, and as it was revealed later in mouse (200), we had better infection efficacy at P4. P1 injections resulted in low infection rate and we hypothesized that TALEN subunits were probably not efficiently enough delivered in the same cells to visualize a rescue.

Although none of the used models was perfect they were all complementary with their advantages and limits, allowing several approaches testing for endonucleases effect visualization at gDNA or organism level. Further work is needed to reach a proof-of concept for TALEN efficiency. We still think that demonstrating DSB on P21 P23H retinal explants would be a prerequisite to move to *in vivo* testing: therefore, we would need to determine better conditions for rod photoreceptor efficient delivery of both TALEN subunits. Viral vectors appear so far to be the best delivery mode. Different titers could be tested to optimize infections; other serotypes could also be tested to improve delivery. In particular, in the perspective of *in vivo* testing, new 7m8 serotype allowing intravitreal injection may be of interest to achieve higher intraocular titers than intracardiac injection without damaging the retina unlike subretinal injection (144, 263). We also need to find a way to better monitor cells that are effectively expressing both TALEN subunits after infection with cloning in new delivery vectors. An optimal test to assess DSB would be by deep sequencing being more sensitive than other more indirect methods. Once the proof-of-concept through retinal explants would be achieved, optimal kinetic determination for injection with a preference for an early injection time point before significant photoreceptor cell death is needed. Treatment point for which chromatin containing the mutant transgene(s) is likely accessible to TALENs would be an important criteria. If possible from *ex vivo* experiments, intravitreal injections to achieve a high virus titer into the eye and limit photoreceptor damage would be the method of choice. Subsequently, *in vivo* treatment efficacy would be monitored functionally by ERG, and structurally by SD-OCT as we performed in the current project for *in vivo* testing. Additional immunohistochemistry could also be planned to document the cellular phenotype of

rescued rod photoreceptors. Again for this part, as for the *ex vivo* testing, the limiting factor would be to monitor *in vivo* the efficacy of photoreceptor expression of both TALEN subunits.

D. The future of genome editing strategies to prevent dominant negative mutations induced diseases

Over the last decade, as DNA-sequencing technology became faster and cheaper, our understanding of the human genome has increased accordingly. Genome editing strategies are potentially applicable to therapy with the development of different endonucleases. We, and others, opened the field by designing and testing them on endogenous locus. New tools allowing gene editing identification as deep sequencing was valuable for detection and understanding of genome editing mechanisms, and advances on new endonucleases identification. Many success were published for animal model creation, however the number of therapeutic success is still low, presumably because the efficiency of these endonucleases to perform DNA cut is still low (264).

Of the current generation of endonucleases, the most rapidly developing is the CRISPR/Cas 9 system, which major advantage is its easy design at low costs for targeting nearly any desired sequence in the genome, with the only requirement to be next to a NGG PAM sequence. For these reasons, we also decided to test the CRISPR/Cas 9 system for our genome editing project. Unfortunately, it was not possible to target specifically the c.68G>A, p.Pro23His mutation because of the absence of an NGG next to it. We therefore designed 7 gRNA specifically targeting exon 1 of the mutated mouse transgene of P23H-1 rat and cloned them into a vector expressing gRNA, Cas 9 protein and CD4, which allows bead-based enrichment of CRISPR/Cas9 expressing cells. Our plan is now to validate the efficiency of genomic cut through the *in vitro* assay of embryonic fibroblasts we developed. If we succeed to generate NHEJ on P23H REF, we will select edited fibroblasts, reprogram them into induced pluripotent stem cells and retina-like structure to validate phenotypic rescue. Then, we will set the conditions to efficiently infect rod photoreceptors presumably by acting on the serotype of the virus and delivery, injection time and dose of the virus. This will allow *in vivo* testing of the selected CRISPR/Cas9 for phenotypic rescue on P23H rats.

Our work outlines challenges inherent to genome editing and the hurdles to achieve proof-of-concept before it can be considered as therapy. A better understanding of variations on gDNA accessibility due to epigenetic mechanisms would be beneficial to design therapy aiming to

edit the genome. A better understanding of DSB repair mechanisms on the treated cell line would also be useful to develop strategies aiming more at HR than NHEJ and targeting different mutations in the same gene. Off-target activity of the endonucleases is also a major issue for therapeutic applications. Future studies and new design of endonucleases need to address this concern. As examples, chimeric endonucleases fusing catalytically inactive Cas9 to Fok1 nuclease, will take advantage of the easy targeting of CRISPR/Cas9 system combined to the dimerization necessity of Fok1. Therefore, two adjacent chimeric Cas9-Fok1 will be needed for target recognition and cleavage, requiring double of the length of a conventional CRISPR/Cas 9 system target and thus, being beneficial to decrease the off-target events incidence (265, 266). Alternatively, the development of nickase, with Cas9 enzymes inducing single strand break and used by pair to break the two strand of DNA on two close loci (267), are strategies that can be envisaged. Finally, new vectors allowing more efficient and precise delivery of the endonucleases at the expected time would be beneficial for therapeutic genome editing.

Science never solves a problem without creating ten more...

George Bernard Shaw

... and that is exactly what's challenging in Science.

Elise Orhan

Bibliography

1. Wright, A. F., Chakarova, C. F., Abd El-Aziz, M. M., and Bhattacharya, S. S. (2010) Photoreceptor degeneration: genetic and mechanistic dissection of a complex trait. *Nature reviews. Genetics* **11**, 273-284
2. Fliegau, M., Benzing, T., and Omran, H. (2007) When cilia go bad: cilia defects and ciliopathies. *Nature reviews. Molecular cell biology* **8**, 880-893
3. Panda-Jonas, S., Jonas, J. B., Jakobczyk, M., and Schneider, U. (1994) Retinal photoreceptor count, retinal surface area, and optic disc size in normal human eyes. *Ophthalmology* **101**, 519-523
4. Osterberg, G. (1935) Topography of the layer of rods and cones in the human retina. *Acta Ophthalmol (Copenh)* **13**, 1-103
5. Carter-Dawson, L. D., and LaVail, M. M. (1979) Rods and cones in the mouse retina. I. Structural analysis using light and electron microscopy. *The Journal of comparative neurology* **188**, 245-262
6. Nathans, J. (1994) In the eye of the beholder: visual pigments and inherited variation in human vision. *Cell* **78**, 357-360
7. Nomura, A., Shigemoto, R., Nakamura, Y., Okamoto, N., Mizuno, N., and Nakanishi, S. (1994) Developmentally regulated postsynaptic localization of a metabotropic glutamate receptor in rat rod bipolar cells. *Cell* **77**, 361-369
8. Masu, M., Iwakabe, H., Tagawa, Y., Miyoshi, T., Yamashita, M., Fukuda, Y., Sasaki, H., Hiroi, K., Nakamura, Y., Shigemoto, R., and et al. (1995) Specific deficit of the ON response in visual transmission by targeted disruption of the mGluR6 gene. *Cell* **80**, 757-765
9. Vardi, N., Duvoisin, R., Wu, G., and Sterling, P. (2000) Localization of mGluR6 to dendrites of ON bipolar cells in primate retina. *The Journal of comparative neurology* **423**, 402-412
10. Brandstatter, J. H., Koulen, P., and Wassle, H. (1998) Diversity of glutamate receptors in the mammalian retina. *Vision Res* **38**, 1385-1397
11. Morigiwa, K., and Vardi, N. (1999) Differential expression of ionotropic glutamate receptor subunits in the outer retina. *The Journal of comparative neurology* **405**, 173-184
12. Qin, P., and Pourcho, R. G. (1999) AMPA-selective glutamate receptor subunits GluR2 and GluR4 in the cat retina: an immunocytochemical study. *Vis Neurosci* **16**, 1105-1114
13. Haverkamp, S., and Wassle, H. (2000) Immunocytochemical analysis of the mouse retina. *The Journal of comparative neurology* **424**, 1-23
14. Haverkamp, S., Grunert, U., and Wassle, H. (2001) The synaptic architecture of AMPA receptors at the cone pedicle of the primate retina. *J Neurosci* **21**, 2488-2500
15. Ghosh, K. K., Bujan, S., Haverkamp, S., Feigenspan, A., and Wassle, H. (2004) Types of bipolar cells in the mouse retina. *The Journal of comparative neurology* **469**, 70-82
16. Euler, T., Haverkamp, S., Schubert, T., and Baden, T. (2014) Retinal bipolar cells: elementary building blocks of vision. *Nature reviews. Neuroscience* **15**, 507-519
17. Boycott, B., and Wassle, H. (1999) Parallel processing in the mammalian retina: the Proctor Lecture. *Invest Ophthalmol Vis Sci* **40**, 1313-1327
18. Masland, R. H. (2001) The fundamental plan of the retina. *Nature neuroscience* **4**, 877-886
19. Wassle, H. (2004) Parallel processing in the mammalian retina. *Nature reviews. Neuroscience* **5**, 747-757
20. Hood, D. C., and Birch, D. G. (1996) Abnormalities of the retinal cone system in retinitis pigmentosa. *Vision Res* **36**, 1699-1709
21. Robson, J. G., and Frishman, L. J. (1995) Response linearity and kinetics of the cat retina: the bipolar cell component of the dark-adapted electroretinogram. *Vis Neurosci* **12**, 837-850
22. Shiells, R. A., and Falk, G. (1999) Contribution of rod, on-bipolar, and horizontal cell light responses to the ERG of dogfish retina. *Vis Neurosci* **16**, 503-511

23. Bush, R. A., and Sieving, P. A. (1994) A proximal retinal component in the primate photopic ERG a-wave. *Invest Ophthalmol Vis Sci* **35**, 635-645
24. Bush, R. A., and Sieving, P. A. (1996) Inner retinal contributions to the primate photopic fast flicker electroretinogram. *J Opt Soc Am A Opt Image Sci Vis* **13**, 557-565
25. Stockton, R. A., and Slaughter, M. M. (1989) B-wave of the electroretinogram. A reflection of ON bipolar cell activity. *The Journal of general physiology* **93**, 101-122
26. Sieving, P. A., Murayama, K., and Naarendorp, F. (1994) Push-pull model of the primate photopic electroretinogram: a role for hyperpolarizing neurons in shaping the b-wave. *Vis Neurosci* **11**, 519-532
27. Ueno, S., Kondo, M., Niwa, Y., Terasaki, H., and Miyake, Y. (2004) Luminance dependence of neural components that underlies the primate photopic electroretinogram. *Invest Ophthalmol Vis Sci* **45**, 1033-1040
28. Yaqoob, Z., Wu, J., and Yang, C. (2005) Spectral domain optical coherence tomography: a better OCT imaging strategy. *Biotechniques* **39**, S6-13
29. Zeitz, C. (2007) Molecular genetics and protein function involved in nocturnal vision. *Exp Rev of Ophthalmol* **2**, 467-485
30. Zeitz, C., Robson, A. G., and Audo, I. (2015) Congenital stationary night blindness: An analysis and update of genotype–phenotype correlations and pathogenic mechanisms. *Progress in Retinal and Eye Research* **45**, 58-110
31. Riggs, L. A. (1954) Electroretinography in cases of night blindness. *Am J Ophthalmol* **38**, 70-78
32. Manes, G., Cheguru, P., Majumder, A., Bocquet, B., Senechal, A., Artemyev, N. O., Hamel, C. P., and Brabet, P. (2014) A truncated form of rod photoreceptor PDE6 beta-subunit causes autosomal dominant congenital stationary night blindness by interfering with the inhibitory activity of the gamma-subunit. *PLoS One* **9**, e95768
33. Schubert, G., and Bornschein, H. (1952) [Analysis of the human electroretinogram]. *Ophthalmologica. Journal internationale d'ophtalmologie. International journal of ophthalmology. Zeitschrift für Augenheilkunde* **123**, 396-413
34. Miyake, Y., Yagasaki, K., Horiguchi, M., Kawase, Y., and Kanda, T. (1986) Congenital stationary night blindness with negative electroretinogram. A new classification. *Arch Ophthalmol* **104**, 1013-1020
35. Miyake, Y., Yagasaki, K., Horiguchi, M., and Kawase, Y. (1987) On- and off-responses in photopic electroretinogram in complete and incomplete types of congenital stationary night blindness. *Japanese journal of ophthalmology* **31**, 81-87
36. Audo, I., Robson, A. G., Holder, G. E., and Moore, A. T. (2008) The negative ERG: clinical phenotypes and disease mechanisms of inner retinal dysfunction. *Survey of ophthalmology* **53**, 16-40
37. Dryja, T. P., Berson, E. L., Rao, V. R., and Oprian, D. D. (1993) Heterozygous missense mutation in the rhodopsin gene as a cause of congenital stationary night blindness. *Nat Genet* **4**, 280-283
38. Rao, V. R., Cohen, G. B., and Oprian, D. D. (1994) Rhodopsin mutation G90D and a molecular mechanism for congenital night blindness. *Nature* **367**, 639-642
39. Sieving, P. A., Richards, J. E., Naarendorp, F., Bingham, E. L., Scott, K., and Alpern, M. (1995) Dark-light: model for nightblindness from the human rhodopsin Gly-90-->Asp mutation. *Proc Natl Acad Sci U S A* **92**, 880-884
40. al-Jandal, N., Farrar, G. J., Kiang, A. S., Humphries, M. M., Bannon, N., Findlay, J. B., Humphries, P., and Kenna, P. F. (1999) A novel mutation within the rhodopsin gene (Thr-94-Ile) causing autosomal dominant congenital stationary night blindness. *Hum Mutat* **13**, 75-81
41. Zeitz, C., Gross, A. K., Leifert, D., Kloeckener-Gruissem, B., McAlear, S. D., Lemke, J., Neidhardt, J., and Berger, W. (2008) Identification and functional characterization of a novel rhodopsin mutation associated with autosomal dominant CSNB. *Invest Ophthalmol Vis Sci* **49**, 4105-4114
42. Dryja, T. P., Hahn, L. B., Reboul, T., and Arnaud, B. (1996) Missense mutation in the gene encoding the alpha subunit of rod transducin in the Nougaret form of congenital stationary night blindness. *Nat Genet* **13**, 358-360

43. Szabo, V., Kreienkamp, H. J., Rosenberg, T., and Gal, A. (2007) p.Gln200Glu, a putative constitutively active mutant of rod alpha-transducin (GNAT1) in autosomal dominant congenital stationary night blindness. *Hum Mutat* **28**, 741-742
44. Naeem, M. A., Chavali, V. R., Ali, S., Iqbal, M., Riazuddin, S., Khan, S. N., Husnain, T., Sieving, P. A., Ayyagari, R., Riazuddin, S., Hejtmancik, J. F., and Riazuddin, S. A. (2012) GNAT1 associated with autosomal recessive congenital stationary night blindness. *Invest Ophthalmol Vis Sci* **53**, 1353-1361
45. Gal, A., Xu, S., Piczenik, Y., Eiberg, H., Duvigneau, C., Schwinger, E., and Rosenberg, T. (1994) Gene for autosomal dominant congenital stationary night blindness maps to the same region as the gene for the beta-subunit of the rod photoreceptor cGMP phosphodiesterase (PDEB) in chromosome 4p16.3. *Hum Mol Genet* **3**, 323-325
46. Riazuddin, S. A., Shahzadi, A., Zeitz, C., Ahmed, Z. M., Ayyagari, R., Chavali, V. R., Ponferrada, V. G., Audo, I., Michiels, C., Lancelot, M. E., Nasir, I. A., Zafar, A. U., Khan, S. N., Husnain, T., Jiao, X., MacDonald, I. M., Riazuddin, S., Sieving, P. A., Katsanis, N., and Hejtmancik, J. F. (2010) A mutation in SLC24A1 implicated in autosomal-recessive congenital stationary night blindness. *Am J Hum Genet* **87**, 523-531
47. Bech-Hansen, N. T., Naylor, M. J., Maybaum, T. A., Sparkes, R. L., Koop, B., Birch, D. G., Bergen, A. A., Prinsen, C. F., Polomeno, R. C., Gal, A., Drack, A. V., Musarella, M. A., Jacobson, S. G., Young, R. S., and Weleber, R. G. (2000) Mutations in NYX, encoding the leucine-rich proteoglycan nyctalopin, cause X-linked complete congenital stationary night blindness. *Nat Genet* **26**, 319-323
48. Pusch, C. M., Zeitz, C., Brandau, O., Pesch, K., Achatz, H., Feil, S., Scharfe, C., Maurer, J., Jacobi, F. K., Pinckers, A., Andreasson, S., Hardcastle, A., Wissinger, B., Berger, W., and Meindl, A. (2000) The complete form of X-linked congenital stationary night blindness is caused by mutations in a gene encoding a leucine-rich repeat protein. *Nat Genet* **26**, 324-327
49. Dryja, T. P., McGee, T. L., Berson, E. L., Fishman, G. A., Sandberg, M. A., Alexander, K. R., Derlacki, D. J., and Rajagopalan, A. S. (2005) Night blindness and abnormal cone electroretinogram ON responses in patients with mutations in the GRM6 gene encoding mGluR6. *Proc Natl Acad Sci U S A* **102**, 4884-4889
50. Zeitz, C., van Genderen, M., Neidhardt, J., Luhmann, U. F., Hoeben, F., Forster, U., Wycisk, K., Matyas, G., Hoyng, C. B., Riemsdag, F., Meire, F., Cremers, F. P., and Berger, W. (2005) Mutations in GRM6 cause autosomal recessive congenital stationary night blindness with a distinctive scotopic 15-Hz flicker electroretinogram. *Invest Ophthalmol Vis Sci* **46**, 4328-4335
51. Audo, I., Kohl, S., Leroy, B. P., Munier, F. L., Guillonneau, X., Mohand-Said, S., Bujakowska, K., Nandrot, E. F., Lorenz, B., Preising, M., Kellner, U., Renner, A. B., Bernd, A., Antonio, A., Moskova-Doumanova, V., Lancelot, M. E., Poloschek, C. M., Drumare, I., Defoort-Dhellemmes, S., Wissinger, B., Leveillard, T., Hamel, C. P., Schorderet, D. F., De Baere, E., Berger, W., Jacobson, S. G., Zrenner, E., Sahel, J. A., Bhattacharya, S. S., and Zeitz, C. (2009) TRPM1 is mutated in patients with autosomal-recessive complete congenital stationary night blindness. *Am J Hum Genet* **85**, 720-729
52. Li, Z., Sergouniotis, P. I., Michaelides, M., Mackay, D. S., Wright, G. A., Devery, S., Moore, A. T., Holder, G. E., Robson, A. G., and Webster, A. R. (2009) Recessive mutations of the gene TRPM1 abrogate ON bipolar cell function and cause complete congenital stationary night blindness in humans. *Am J Hum Genet* **85**, 711-719
53. van Genderen, M. M., Bijveld, M. M., Claassen, Y. B., Florijn, R. J., Pearing, J. N., Meire, F. M., McCall, M. A., Riemsdag, F. C., Gregg, R. G., Bergen, A. A., and Kamermans, M. (2009) Mutations in TRPM1 are a common cause of complete congenital stationary night blindness. *Am J Hum Genet* **85**, 730-736
54. Strom, T. M., Nyakatura, G., Apfelstedt-Sylla, E., Hellebrand, H., Lorenz, B., Weber, B. H., Wutz, K., Gutwillinger, N., Ruther, K., Drescher, B., Sauer, C., Zrenner, E., Meitinger, T., Rosenthal, A., and Meindl, A. (1998) An L-type calcium-channel gene mutated in incomplete X-linked congenital stationary night blindness. *Nat Genet* **19**, 260-263
55. Bech-Hansen, N. T., Naylor, M. J., Maybaum, T. A., Pearce, W. G., Koop, B., Fishman, G. A., Mets, M., Musarella, M. A., and Boycott, K. M. (1998) Loss-of-function mutations in a

- calcium-channel $\alpha 1$ -subunit gene in Xp11.23 cause incomplete X-linked congenital stationary night blindness. *Nat Genet* **19**, 264-267
56. Zeitz, C., Kloeckener-Gruissem, B., Forster, U., Kohl, S., Magyar, I., Wissinger, B., Matyas, G., Borruat, F. X., Schorderet, D. F., Zrenner, E., Munier, F. L., and Berger, W. (2006) Mutations in CABP4, the gene encoding the Ca²⁺-binding protein 4, cause autosomal recessive night blindness. *Am J Hum Genet* **79**, 657-667
 57. Wycisk, K. A., Zeitz, C., Feil, S., Wittmer, M., Forster, U., Neidhardt, J., Wissinger, B., Zrenner, E., Wilke, R., Kohl, S., and Berger, W. (2006) Mutation in the auxiliary calcium-channel subunit CACNA2D4 causes autosomal recessive cone dystrophy. *Am J Hum Genet* **79**, 973-977
 58. Morgans, C. W., Zhang, J., Jeffrey, B. G., Nelson, S. M., Burke, N. S., Duvoisin, R. M., and Brown, R. L. (2009) TRPM1 is required for the depolarizing light response in retinal ON-bipolar cells. *Proc Natl Acad Sci U S A* **106**, 19174-19178
 59. Nakajima, Y., Iwakabe, H., Akazawa, C., Nawa, H., Shigemoto, R., Mizuno, N., and Nakanishi, S. (1993) Molecular characterization of a novel retinal metabotropic glutamate receptor mGluR6 with a high agonist selectivity for L-2-amino-4-phosphonobutyrate. *J Biol Chem* **268**, 11868-11873
 60. Gregg, R. G., Mukhopadhyay, S., Candille, S. I., Ball, S. L., Pardue, M. T., McCall, M. A., and Peachey, N. S. (2003) Identification of the gene and the mutation responsible for the mouse nob phenotype. *Invest Ophthalmol Vis Sci* **44**, 378-384
 61. Morgans, C. W., Ren, G., and Akileswaran, L. (2006) Localization of nyctalopin in the mammalian retina. *The European journal of neuroscience* **23**, 1163-1171
 62. Pearing, J. N., Bojang, P., Jr., Shen, Y., Koike, C., Furukawa, T., Nawy, S., and Gregg, R. G. (2011) A role for nyctalopin, a small leucine-rich repeat protein, in localizing the TRP melastatin 1 channel to retinal depolarizing bipolar cell dendrites. *J Neurosci* **31**, 10060-10066
 63. Klooster, J., Blokker, J., Ten Brink, J. B., Unmehopa, U., Fluiter, K., Bergen, A. A., and Kamermans, M. (2011) Ultrastructural localization and expression of TRPM1 in the human retina. *Invest Ophthalmol Vis Sci* **52**, 8356-8362
 64. Vardi, N., Dhingra, A., Zhang, L., Lyubarsky, A., Wang, T. L., and Morigiwa, K. (2002) Neurochemical organization of the first visual synapse. *The Keio journal of medicine* **51**, 154-164
 65. Okawa, H., and Sampath, A. P. (2007) Optimization of single-photon response transmission at the rod-to-rod bipolar synapse. *Physiology* **22**, 279-286
 66. Morgans, C. W., Brown, R. L., and Duvoisin, R. M. (2010) TRPM1: the endpoint of the mGluR6 signal transduction cascade in retinal ON-bipolar cells. *BioEssays : news and reviews in molecular, cellular and developmental biology* **32**, 609-614
 67. Koike, C., Obara, T., Uriu, Y., Numata, T., Sanuki, R., Miyata, K., Koyasu, T., Ueno, S., Funabiki, K., Tani, A., Ueda, H., Kondo, M., Mori, Y., Tachibana, M., and Furukawa, T. (2010) TRPM1 is a component of the retinal ON bipolar cell transduction channel in the mGluR6 cascade. *Proc Natl Acad Sci U S A* **107**, 332-337
 68. Nawy, S. (1999) The metabotropic receptor mGluR6 may signal through G(o), but not phosphodiesterase, in retinal bipolar cells. *J Neurosci* **19**, 2938-2944
 69. Shen, Y., Heimel, J. A., Kamermans, M., Peachey, N. S., Gregg, R. G., and Nawy, S. (2009) A transient receptor potential-like channel mediates synaptic transmission in rod bipolar cells. *J Neurosci* **29**, 6088-6093
 70. Zeitz, C., Jacobson, S. G., Hamel, C. P., Bujakowska, K., Neuille, M., Orhan, E., Zanlonghi, X., Lancelot, M. E., Michiels, C., Schwartz, S. B., Bocquet, B., Antonio, A., Audier, C., Letexier, M., Saraiva, J. P., Luu, T. D., Sennlaub, F., Nguyen, H., Poch, O., Dollfus, H., Lecompte, O., Kohl, S., Sahel, J. A., Bhattacharya, S. S., and Audo, I. (2013) Whole-exome sequencing identifies LRIT3 mutations as a cause of autosomal-recessive complete congenital stationary night blindness. *Am J Hum Genet* **92**, 67-75
 71. Neuille, M., El Shamieh, S., Orhan, E., Michiels, C., Antonio, A., Lancelot, M. E., Condroyer, C., Bujakowska, K., Poch, O., Sahel, J. A., Audo, I., and Zeitz, C. (2014) Lrit3 Deficient Mouse (nob6): A Novel Model of Complete Congenital Stationary Night Blindness (cCSNB). *PLoS One* **9**, e90342

72. Neuille, M., Morgans, C. W., Cao, Y., Orhan, E., Michiels, C., Sahel, J. A., Audo, I., Duvoisin, R. M., Martemyanov, K. A., and Zeitz, C. (2015) LRIT3 is essential to localize TRPM1 to the dendritic tips of depolarizing bipolar cells and may play a role in cone synapse formation. *The European journal of neuroscience* **56**
73. Ross, E. M., and Wilkie, T. M. (2000) GTPase-activating proteins for heterotrimeric G proteins: regulators of G protein signaling (RGS) and RGS-like proteins. *Annual review of biochemistry* **69**, 795-827
74. Hollinger, S., and Hepler, J. R. (2002) Cellular regulation of RGS proteins: modulators and integrators of G protein signaling. *Pharmacological reviews* **54**, 527-559
75. Rao, A., Dallman, R., Henderson, S., and Chen, C. K. (2007) Gbeta5 is required for normal light responses and morphology of retinal ON-bipolar cells. *J Neurosci* **27**, 14199-14204
76. Song, J. H., Song, H., Wensel, T. G., Sokolov, M., and Martemyanov, K. A. (2007) Localization and differential interaction of R7 RGS proteins with their membrane anchors R7BP and R9AP in neurons of vertebrate retina. *Molecular and cellular neurosciences* **35**, 311-319
77. Morgans, C. W., Weiwei, L., Wensel, T. G., Brown, R. L., Perez-Leon, J. A., Bearnot, B., and Duvoisin, R. M. (2007) Gbeta5-RGS complexes co-localize with mGluR6 in retinal ON-bipolar cells. *The European journal of neuroscience* **26**, 2899-2905
78. Chen, F. S., Shim, H., Morhardt, D., Dallman, R., Krahn, E., McWhinney, L., Rao, A., Gold, S. J., and Chen, C. K. (2010) Functional redundancy of R7 RGS proteins in ON-bipolar cell dendrites. *Invest Ophthalmol Vis Sci* **51**, 686-693
79. Cao, Y., Pahlberg, J., Sarria, I., Kamasawa, N., Sampath, A. P., and Martemyanov, K. A. (2012) Regulators of G protein signaling RGS7 and RGS11 determine the onset of the light response in ON bipolar neurons. *Proc Natl Acad Sci U S A* **109**, 7905-7910
80. Zhang, J., Jeffrey, B. G., Morgans, C. W., Burke, N. S., Haley, T. L., Duvoisin, R. M., and Brown, R. L. (2010) RGS7 and -11 complexes accelerate the ON-bipolar cell light response. *Invest Ophthalmol Vis Sci* **51**, 1121-1129
81. Jayaraman, M., Zhou, H., Jia, L., Cain, M. D., and Blumer, K. J. (2009) R9AP and R7BP: traffic cops for the RGS7 family in phototransduction and neuronal GPCR signaling. *Trends in pharmacological sciences* **30**, 17-24
82. Cao, Y., Masuho, I., Okawa, H., Xie, K., Asami, J., Kammermeier, P. J., Maddox, D. M., Furukawa, T., Inoue, T., Sampath, A. P., and Martemyanov, K. A. (2009) Retina-specific GTPase accelerator RGS11/G beta 5S/R9AP is a constitutive heterotrimer selectively targeted to mGluR6 in ON-bipolar neurons. *J Neurosci* **29**, 9301-9313
83. Martemyanov, K. A., Yoo, P. J., Skiba, N. P., and Arshavsky, V. Y. (2005) R7BP, a novel neuronal protein interacting with RGS proteins of the R7 family. *J Biol Chem* **280**, 5133-5136
84. Drenan, R. M., Doupnik, C. A., Jayaraman, M., Buchwalter, A. L., Kaltenbronn, K. M., Huettner, J. E., Linder, M. E., and Blumer, K. J. (2006) R7BP augments the function of RGS7*Gbeta5 complexes by a plasma membrane-targeting mechanism. *J Biol Chem* **281**, 28222-28231
85. Bellone, R. R., Brooks, S. A., Sandmeyer, L., Murphy, B. A., Forsyth, G., Archer, S., Bailey, E., and Grahn, B. (2008) Differential gene expression of TRPM1, the potential cause of congenital stationary night blindness and coat spotting patterns (LP) in the Appaloosa horse (*Equus caballus*). *Genetics* **179**, 1861-1870
86. Bahadori, R., Biehlmaier, O., Zeitz, C., Labhart, T., Makhankov, Y. V., Forster, U., Gesemann, M., Berger, W., and Neuhauss, S. C. (2006) Nyctalopin is essential for synaptic transmission in the cone dominated zebrafish retina. *The European journal of neuroscience* **24**, 1664-1674
87. Huang, Y. Y., Haug, M. F., Gesemann, M., and Neuhauss, S. C. (2012) Novel expression patterns of metabotropic glutamate receptor 6 in the zebrafish nervous system. *PLoS One* **7**, e35256
88. Pardue, M. T., McCall, M. A., LaVail, M. M., Gregg, R. G., and Peachey, N. S. (1998) A naturally occurring mouse model of X-linked congenital stationary night blindness. *Invest Ophthalmol Vis Sci* **39**, 2443-2449

89. Maddox, D. M., Vessey, K. A., Yarbrough, G. L., Invergo, B. M., Cantrell, D. R., Inayat, S., Balannik, V., Hicks, W. L., Hawes, N. L., Byers, S., Smith, R. S., Hurd, R., Howell, D., Gregg, R. G., Chang, B., Naggert, J. K., Troy, J. B., Pinto, L. H., Nishina, P. M., and McCall, M. A. (2008) Allelic variance between GRM6 mutants, Grm6nob3 and Grm6nob4 results in differences in retinal ganglion cell visual responses. *The Journal of physiology* **586**, 4409-4424
90. Pinto, L. H., Vitaterna, M. H., Shimomura, K., Siepka, S. M., Balannik, V., McDearmon, E. L., Omura, C., Lumayag, S., Invergo, B. M., Glawe, B., Cantrell, D. R., Inayat, S., Olvera, M. A., Vessey, K. A., McCall, M. A., Maddox, D., Morgans, C. W., Young, B., Pletcher, M. T., Mullins, R. F., Troy, J. B., and Takahashi, J. S. (2007) Generation, identification and functional characterization of the nob4 mutation of Grm6 in the mouse. *Vis Neurosci* **24**, 111-123
91. Peachey, N. S., Pearing, J. N., Bojang, P., Jr., Hirschtritt, M. E., Sturgill-Short, G., Ray, T. A., Furukawa, T., Koike, C., Goldberg, A. F., Shen, Y., McCall, M. A., Nawy, S., Nishina, P. M., and Gregg, R. G. (2012) Depolarizing bipolar cell dysfunction due to a Trpm1 point mutation. *J Neurophysiol* **108**, 2442-2451
92. Hartong, D. T., Berson, E. L., and Dryja, T. P. (2006) Retinitis pigmentosa. *Lancet* **368**, 1795-1809
93. Hamel, C. P. (2007) Cone rod dystrophies. *Orphanet J Rare Dis* **2**, 7
94. Robson, A. G., Saihan, Z., Jenkins, S. A., Fitzke, F. W., Bird, A. C., Webster, A. R., and Holder, G. E. (2006) Functional characterisation and serial imaging of abnormal fundus autofluorescence in patients with retinitis pigmentosa and normal visual acuity. *The British journal of ophthalmology* **90**, 472-479
95. Murakami, T., Akimoto, M., Ooto, S., Suzuki, T., Ikeda, H., Kawagoe, N., Takahashi, M., and Yoshimura, N. (2008) Association between abnormal autofluorescence and photoreceptor disorganization in retinitis pigmentosa. *Am J Ophthalmol* **145**, 687-694
96. Robson, A. G., Tufail, A., Fitzke, F., Bird, A. C., Moore, A. T., Holder, G. E., and Webster, A. R. (2011) Serial imaging and structure-function correlates of high-density rings of fundus autofluorescence in retinitis pigmentosa. *Retina* **31**, 1670-1679
97. Berson, E. L. (1976) Retinitis pigmentosa and allied retinal diseases: electrophysiologic findings. *Transactions. Section on Ophthalmology. American Academy of Ophthalmology and Otolaryngology* **81**, OP659-666
98. Sahel, J. A. (2005) Saving cone cells in hereditary rod diseases: a possible role for rod-derived cone viability factor (RdCVF) therapy. *Retina* **25**, S38-S39
99. Leveillard, T., Fridlich, R., Clerin, E., Ait-Ali, N., Millet-Puel, G., Jaillard, C., Yang, Y., Zack, D., van-Dorselaer, A., and Sahel, J. A. (2014) Therapeutic strategy for handling inherited retinal degenerations in a gene-independent manner using rod-derived cone viability factors. *Comptes rendus biologiques* **337**, 207-213
100. Bowne, S. J., Sullivan, L. S., Gire, A. I., Birch, D. G., Hughbanks-Wheaton, D., Heckenlively, J. R., and Daiger, S. P. (2008) Mutations in the TOPORS gene cause 1% of autosomal dominant retinitis pigmentosa. *Mol Vis* **14**, 922-927
101. Hargrave, P. A. (2001) Rhodopsin structure, function, and topography the Friedenwald lecture. *Invest Ophthalmol Vis Sci* **42**, 3-9
102. Fredriksson, R., Lagerstrom, M. C., Lundin, L. G., and Schioth, H. B. (2003) The G-protein-coupled receptors in the human genome form five main families. Phylogenetic analysis, paralogon groups, and fingerprints. *Molecular pharmacology* **63**, 1256-1272
103. Arshavsky, V. <http://people.duke.edu/~arsha001/research.html>.
104. Mendes, H. F., van der Spuy, J., Chapple, J. P., and Cheetham, M. E. (2005) Mechanisms of cell death in rhodopsin retinitis pigmentosa: implications for therapy. *Trends Mol Med* **11**, 177-185
105. Dryja, T. P., McGee, T. L., Hahn, L. B., Cowley, G. S., Olsson, J. E., Reichel, E., Sandberg, M. A., and Berson, E. L. (1990) Mutations within the rhodopsin gene in patients with autosomal dominant retinitis pigmentosa. *N Engl J Med* **323**, 1302-1307
106. Audo, I., Manes, G., Mohand-Said, S., Friedrich, A., Lancelot, M. E., Antonio, A., Moskova-Doumanova, V., Poch, O., Zanlonghi, X., Hamel, C. P., Sahel, J. A., Bhattacharya, S. S., and

- Zeitz, C. (2010) Spectrum of rhodopsin mutations in French autosomal dominant rod-cone dystrophy patients. *Invest Ophthalmol Vis Sci* **51**, 3687-3700
107. Sung, C. H., Davenport, C. M., and Nathans, J. (1993) Rhodopsin mutations responsible for autosomal dominant retinitis pigmentosa. Clustering of functional classes along the polypeptide chain. *J Biol Chem* **268**, 26645-26649
108. Sung, C. H., Schneider, B. G., Agarwal, N., Papermaster, D. S., and Nathans, J. (1991) Functional heterogeneity of mutant rhodopsins responsible for autosomal dominant retinitis pigmentosa. *Proc Natl Acad Sci U S A* **88**, 8840-8844
109. Kaushal, S., and Khorana, H. G. (1994) Structure and function in rhodopsin. 7. Point mutations associated with autosomal dominant retinitis pigmentosa. *Biochemistry* **33**, 6121-6128
110. Illing, M. E., Rajan, R. S., Bence, N. F., and Kopito, R. R. (2002) A rhodopsin mutant linked to autosomal dominant retinitis pigmentosa is prone to aggregate and interacts with the ubiquitin proteasome system. *J Biol Chem* **277**, 34150-34160
111. Saliba, R. S., Munro, P. M., Luthert, P. J., and Cheetham, M. E. (2002) The cellular fate of mutant rhodopsin: quality control, degradation and aggresome formation. *J Cell Sci* **115**, 2907-2918
112. Bence, N. F., Sampat, R. M., and Kopito, R. R. (2001) Impairment of the ubiquitin-proteasome system by protein aggregation. *Science* **292**, 1552-1555
113. Rajan, R. S., and Kopito, R. R. (2005) Suppression of wild-type rhodopsin maturation by mutants linked to autosomal dominant retinitis pigmentosa. *J Biol Chem* **280**, 1284-1291
114. Kijas, J. W., Cideciyan, A. V., Aleman, T. S., Pianta, M. J., Pearce-Kelling, S. E., Miller, B. J., Jacobson, S. G., Aguirre, G. D., and Acland, G. M. (2002) Naturally occurring rhodopsin mutation in the dog causes retinal dysfunction and degeneration mimicking human dominant retinitis pigmentosa. *Proc Natl Acad Sci U S A* **99**, 6328-6333
115. Olsson, J. E., Gordon, J. W., Pawlyk, B. S., Roof, D., Hayes, A., Molday, R. S., Mukai, S., Cowley, G. S., Berson, E. L., and Dryja, T. P. (1992) Transgenic mice with a rhodopsin mutation (Pro23His): a mouse model of autosomal dominant retinitis pigmentosa. *Neuron* **9**, 815-830
116. Naash, M. I., Hollyfield, J. G., al-Ubaidi, M. R., and Baehr, W. (1993) Simulation of human autosomal dominant retinitis pigmentosa in transgenic mice expressing a mutated murine opsin gene. *Proc Natl Acad Sci U S A* **90**, 5499-5503
117. Sung, C. H., Makino, C., Baylor, D., and Nathans, J. (1994) A rhodopsin gene mutation responsible for autosomal dominant retinitis pigmentosa results in a protein that is defective in localization to the photoreceptor outer segment. *J Neurosci* **14**, 5818-5833
118. Li, T., Franson, W. K., Gordon, J. W., Berson, E. L., and Dryja, T. P. (1995) Constitutive activation of phototransduction by K296E opsin is not a cause of photoreceptor degeneration. *Proc Natl Acad Sci U S A* **92**, 3551-3555
119. Li, T., Snyder, W. K., Olsson, J. E., and Dryja, T. P. (1996) Transgenic mice carrying the dominant rhodopsin mutation P347S: evidence for defective vectorial transport of rhodopsin to the outer segments. *Proc Natl Acad Sci U S A* **93**, 14176-14181
120. Sakami, S., Maeda, T., Bereta, G., Okano, K., Golczak, M., Sumaroka, A., Roman, A. J., Cideciyan, A. V., Jacobson, S. G., and Palczewski, K. (2011) Probing mechanisms of photoreceptor degeneration in a new mouse model of the common form of autosomal dominant retinitis pigmentosa due to P23H opsin mutations. *J Biol Chem* **286**, 10551-10567
121. Sancho-Pelluz, J., Tosi, J., Hsu, C. W., Lee, F., Wolpert, K., Tabacaru, M. R., Greenberg, J. P., Tsang, S. H., and Lin, C. S. (2012) Mice with a D190N mutation in the gene encoding rhodopsin: a model for human autosomal-dominant retinitis pigmentosa. *Molecular medicine* **18**, 549-555
122. Zhang, N., Kolesnikov, A. V., Jastrzebska, B., Mustafi, D., Sawada, O., Maeda, T., Genoud, C., Engel, A., Kefalov, V. J., and Palczewski, K. (2013) Autosomal recessive retinitis pigmentosa E150K opsin mice exhibit photoreceptor disorganization. *The Journal of clinical investigation* **123**, 121-137

123. Lewin, A. S., Drenser, K. A., Hauswirth, W. W., Nishikawa, S., Yasumura, D., Flannery, J. G., and LaVail, M. M. (1998) Ribozyme rescue of photoreceptor cells in a transgenic rat model of autosomal dominant retinitis pigmentosa. *Nat Med* **4**, 967-971
124. Green, E. S., Menz, M. D., LaVail, M. M., and Flannery, J. G. (2000) Characterization of rhodopsin mis-sorting and constitutive activation in a transgenic rat model of retinitis pigmentosa. *Invest Ophthalmol Vis Sci* **41**, 1546-1553
125. Petters, R. M., Alexander, C. A., Wells, K. D., Collins, E. B., Sommer, J. R., Blanton, M. R., Rojas, G., Hao, Y., Flowers, W. L., Banin, E., Cideciyan, A. V., Jacobson, S. G., and Wong, F. (1997) Genetically engineered large animal model for studying cone photoreceptor survival and degeneration in retinitis pigmentosa. *Nature biotechnology* **15**, 965-970
126. Ross, J. W., Fernandez de Castro, J. P., Zhao, J., Samuel, M., Walters, E., Rios, C., Bray-Ward, P., Jones, B. W., Marc, R. E., Wang, W., Zhou, L., Noel, J. M., McCall, M. A., DeMarco, P. J., Prather, R. S., and Kaplan, H. J. (2012) Generation of an inbred miniature pig model of retinitis pigmentosa. *Invest Ophthalmol Vis Sci* **53**, 501-507
127. Jones, B. W., Kondo, M., Terasaki, H., Watt, C. B., Rapp, K., Anderson, J., Lin, Y., Shaw, M. V., Yang, J. H., and Marc, R. E. (2011) Retinal remodeling in the Tg P347L rabbit, a large-eye model of retinal degeneration. *The Journal of comparative neurology* **519**, 2713-2733
128. Nakao, T., Tsujikawa, M., Notomi, S., Ikeda, Y., and Nishida, K. (2012) The role of mislocalized phototransduction in photoreceptor cell death of retinitis pigmentosa. *PLoS One* **7**, e32472
129. Tam, B. M., and Moritz, O. L. (2006) Characterization of rhodopsin P23H-induced retinal degeneration in a *Xenopus laevis* model of retinitis pigmentosa. *Invest Ophthalmol Vis Sci* **47**, 3234-3241
130. Galy, A., Roux, M. J., Sahel, J. A., Leveillard, T., and Giangrande, A. (2005) Rhodopsin maturation defects induce photoreceptor death by apoptosis: a fly model for RhodopsinPro23His human retinitis pigmentosa. *Hum Mol Genet* **14**, 2547-2557
131. Humphries, M. M., Rancourt, D., Farrar, G. J., Kenna, P., Hazel, M., Bush, R. A., Sieving, P. A., Sheils, D. M., McNally, N., Creighton, P., Erven, A., Boros, A., Gulya, K., Capecchi, M. R., and Humphries, P. (1997) Retinopathy induced in mice by targeted disruption of the rhodopsin gene. *Nat Genet* **15**, 216-219
132. Lem, J., Krasnoperova, N. V., Calvert, P. D., Kosaras, B., Cameron, D. A., Nicolo, M., Makino, C. L., and Sidman, R. L. (1999) Morphological, physiological, and biochemical changes in rhodopsin knockout mice. *Proc Natl Acad Sci U S A* **96**, 736-741
133. Allocca, M., Tessitore, A., Cotugno, G., and Auricchio, A. (2006) AAV-mediated gene transfer for retinal diseases. *Expert opinion on biological therapy* **6**, 1279-1294
134. Surace, E. M., and Auricchio, A. (2008) Versatility of AAV vectors for retinal gene transfer. *Vision Res* **48**, 353-359
135. Cox, D. B., Platt, R. J., and Zhang, F. (2015) Therapeutic genome editing: prospects and challenges. *Nat Med* **21**, 121-131
136. Khabou, H., and Dalkara, D. (2015) [Developments in gene delivery vectors for ocular gene therapy]. *Med Sci (Paris)* **31**, 529-537
137. Atchison, R. W., Casto, B. C., and Hammon, W. M. (1965) Adenovirus-Associated Defective Virus Particles. *Science* **149**, 754-756
138. Lusby, E., Fife, K. H., and Berns, K. I. (1980) Nucleotide sequence of the inverted terminal repetition in adeno-associated virus DNA. *Journal of virology* **34**, 402-409
139. Ali, R. R., Reichel, M. B., Thrasher, A. J., Levinsky, R. J., Kinnon, C., Kanuga, N., Hunt, D. M., and Bhattacharya, S. S. (1996) Gene transfer into the mouse retina mediated by an adeno-associated viral vector. *Hum Mol Genet* **5**, 591-594
140. Flannery, J. G., Zolotukhin, S., Vaquero, M. I., LaVail, M. M., Muzyczka, N., and Hauswirth, W. W. (1997) Efficient photoreceptor-targeted gene expression in vivo by recombinant adeno-associated virus. *Proc Natl Acad Sci U S A* **94**, 6916-6921
141. Auricchio, A., Kobinger, G., Anand, V., Hildinger, M., O'Connor, E., Maguire, A. M., Wilson, J. M., and Bennett, J. (2001) Exchange of surface proteins impacts on viral vector cellular specificity and transduction characteristics: the retina as a model. *Hum Mol Genet* **10**, 3075-3081

142. Allocca, M., Mussolino, C., Garcia-Hoyos, M., Sanges, D., Iodice, C., Petrillo, M., Vandenberghe, L. H., Wilson, J. M., Marigo, V., Surace, E. M., and Auricchio, A. (2007) Novel adeno-associated virus serotypes efficiently transduce murine photoreceptors. *Journal of virology* **81**, 11372-11380
143. Dalkara, D., Kolstad, K. D., Caporale, N., Visel, M., Klimczak, R. R., Schaffer, D. V., and Flannery, J. G. (2009) Inner limiting membrane barriers to AAV-mediated retinal transduction from the vitreous. *Mol Ther* **17**, 2096-2102
144. Dalkara, D., Byrne, L. C., Klimczak, R. R., Visel, M., Yin, L., Merigan, W. H., Flannery, J. G., and Schaffer, D. V. (2013) In vivo-directed evolution of a new adeno-associated virus for therapeutic outer retinal gene delivery from the vitreous. *Science translational medicine* **5**, 189ra176
145. den Hollander, A. I., Roepman, R., Koenekoop, R. K., and Cremers, F. P. (2008) Leber congenital amaurosis: genes, proteins and disease mechanisms. *Prog Retin Eye Res* **27**, 391-419
146. Veske, A., Nilsson, S. E., Narfstrom, K., and Gal, A. (1999) Retinal dystrophy of Swedish briard/briard-beagle dogs is due to a 4-bp deletion in RPE65. *Genomics* **57**, 57-61
147. Acland, G. M., Aguirre, G. D., Ray, J., Zhang, Q., Aleman, T. S., Cideciyan, A. V., Pearce-Kelling, S. E., Anand, V., Zeng, Y., Maguire, A. M., Jacobson, S. G., Hauswirth, W. W., and Bennett, J. (2001) Gene therapy restores vision in a canine model of childhood blindness. *Nat Genet* **28**, 92-95
148. Acland, G. M., Aguirre, G. D., Bennett, J., Aleman, T. S., Cideciyan, A. V., Bennicelli, J., Dejneka, N. S., Pearce-Kelling, S. E., Maguire, A. M., Palczewski, K., Hauswirth, W. W., and Jacobson, S. G. (2005) Long-term restoration of rod and cone vision by single dose rAAV-mediated gene transfer to the retina in a canine model of childhood blindness. *Mol Ther* **12**, 1072-1082
149. Bainbridge, J. W., Smith, A. J., Barker, S. S., Robbie, S., Henderson, R., Balaggan, K., Viswanathan, A., Holder, G. E., Stockman, A., Tyler, N., Petersen-Jones, S., Bhattacharya, S. S., Thrasher, A. J., Fitzke, F. W., Carter, B. J., Rubin, G. S., Moore, A. T., and Ali, R. R. (2008) Effect of gene therapy on visual function in Leber's congenital amaurosis. *N Engl J Med* **358**, 2231-2239
150. Hauswirth, W. W., Aleman, T. S., Kaushal, S., Cideciyan, A. V., Schwartz, S. B., Wang, L., Conlon, T. J., Boye, S. L., Flotte, T. R., Byrne, B. J., and Jacobson, S. G. (2008) Treatment of leber congenital amaurosis due to RPE65 mutations by ocular subretinal injection of adeno-associated virus gene vector: short-term results of a phase I trial. *Hum Gene Ther* **19**, 979-990
151. Maguire, A. M., Simonelli, F., Pierce, E. A., Pugh, E. N., Jr., Mingozzi, F., Bennicelli, J., Banfi, S., Marshall, K. A., Testa, F., Surace, E. M., Rossi, S., Lyubarsky, A., Arruda, V. R., Konkle, B., Stone, E., Sun, J., Jacobs, J., Dell'Osso, L., Hertle, R., Ma, J. X., Redmond, T. M., Zhu, X., Hauck, B., Zeleniaia, O., Shindler, K. S., Maguire, M. G., Wright, J. F., Volpe, N. J., McDonnell, J. W., Auricchio, A., High, K. A., and Bennett, J. (2008) Safety and efficacy of gene transfer for Leber's congenital amaurosis. *N Engl J Med* **358**, 2240-2248
152. Cideciyan, A. V., Hauswirth, W. W., Aleman, T. S., Kaushal, S., Schwartz, S. B., Boye, S. L., Windsor, E. A., Conlon, T. J., Sumaroka, A., Pang, J. J., Roman, A. J., Byrne, B. J., and Jacobson, S. G. (2009) Human RPE65 gene therapy for Leber congenital amaurosis: persistence of early visual improvements and safety at 1 year. *Hum Gene Ther* **20**, 999-1004
153. Simonelli, F., Maguire, A. M., Testa, F., Pierce, E. A., Mingozzi, F., Bennicelli, J. L., Rossi, S., Marshall, K., Banfi, S., Surace, E. M., Sun, J., Redmond, T. M., Zhu, X., Shindler, K. S., Ying, G. S., Ziviello, C., Acerra, C., Wright, J. F., McDonnell, J. W., High, K. A., Bennett, J., and Auricchio, A. (2010) Gene therapy for Leber's congenital amaurosis is safe and effective through 1.5 years after vector administration. *Mol Ther* **18**, 643-650
154. Wen, X. H., Shen, L., Brush, R. S., Michaud, N., Al-Ubaidi, M. R., Gurevich, V. V., Hamm, H. E., Lem, J., Dibenedetto, E., Anderson, R. E., and Makino, C. L. (2009) Overexpression of rhodopsin alters the structure and photoresponse of rod photoreceptors. *Biophysical journal* **96**, 939-950

155. Frederick, J. M., Krasnoperova, N. V., Hoffmann, K., Church-Kopish, J., Ruther, K., Howes, K., Lem, J., and Baehr, W. (2001) Mutant rhodopsin transgene expression on a null background. *Invest Ophthalmol Vis Sci* **42**, 826-833
156. Mao, H., James, T., Jr., Schwein, A., Shabashvili, A. E., Hauswirth, W. W., Gorbatyuk, M. S., and Lewin, A. S. (2011) AAV delivery of wild-type rhodopsin preserves retinal function in a mouse model of autosomal dominant retinitis pigmentosa. *Hum Gene Ther* **22**, 567-575
157. Mussolino, C., Sanges, D., Marrocco, E., Bonetti, C., Di Vicino, U., Marigo, V., Auricchio, A., Meroni, G., and Surace, E. M. (2011) Zinc-finger-based transcriptional repression of rhodopsin in a model of dominant retinitis pigmentosa. *EMBO molecular medicine* **3**, 118-128
158. McManus, M. T., and Sharp, P. A. (2002) Gene silencing in mammals by small interfering RNAs. *Nature reviews. Genetics* **3**, 737-747
159. Kiang, A. S., Palfi, A., Ader, M., Kenna, P. F., Millington-Ward, S., Clark, G., Kennan, A., O'Reilly, M., Tam, L. C., Aherne, A., McNally, N., Humphries, P., and Farrar, G. J. (2005) Toward a gene therapy for dominant disease: validation of an RNA interference-based mutation-independent approach. *Mol Ther* **12**, 555-561
160. O'Reilly, M., Palfi, A., Chadderton, N., Millington-Ward, S., Ader, M., Cronin, T., Tuohy, T., Auricchio, A., Hildinger, M., Tivnan, A., McNally, N., Humphries, M. M., Kiang, A. S., Humphries, P., Kenna, P. F., and Farrar, G. J. (2007) RNA interference-mediated suppression and replacement of human rhodopsin in vivo. *Am J Hum Genet* **81**, 127-135
161. Chadderton, N., Millington-Ward, S., Palfi, A., O'Reilly, M., Tuohy, G., Humphries, M. M., Li, T., Humphries, P., Kenna, P. F., and Farrar, G. J. (2009) Improved retinal function in a mouse model of dominant retinitis pigmentosa following AAV-delivered gene therapy. *Mol Ther* **17**, 593-599
162. Mao, H., Gorbatyuk, M. S., Rossmiller, B., Hauswirth, W. W., and Lewin, A. S. (2012) Long-term rescue of retinal structure and function by rhodopsin RNA replacement with a single adeno-associated viral vector in P23H RHO transgenic mice. *Hum Gene Ther* **23**, 356-366
163. Berger, A., Lorain, S., Josephine, C., Desrosiers, M., Peccate, C., Voit, T., Garcia, L., Sahel, J. A., and Bemelmans, A. P. (2015) Repair of rhodopsin mRNA by spliceosome-mediated RNA trans-splicing: a new approach for autosomal dominant retinitis pigmentosa. *Mol Ther* **23**, 918-930
164. Hentze, M. W., and Kulozik, A. E. (1999) A perfect message: RNA surveillance and nonsense-mediated decay. *Cell* **96**, 307-310
165. Silva, G., Poirot, L., Galetto, R., Smith, J., Montoya, G., Duchateau, P., and Paques, F. (2011) Meganucleases and other tools for targeted genome engineering: perspectives and challenges for gene therapy. *Current gene therapy* **11**, 11-27
166. Kass, E. M., and Jasin, M. (2010) Collaboration and competition between DNA double-strand break repair pathways. *FEBS Lett* **584**, 3703-3708
167. Chan, F., Hauswirth, W. W., Wensel, T. G., and Wilson, J. H. (2011) Efficient mutagenesis of the rhodopsin gene in rod photoreceptor neurons in mice. *Nucleic acids research* **39**, 5955-5966
168. Jurica, M. S., Monnat, R. J., Jr., and Stoddard, B. L. (1998) DNA recognition and cleavage by the LAGLIDADG homing endonuclease I-CreI. *Molecular cell* **2**, 469-476
169. Arnould, S., Delenda, C., Grizot, S., Desseaux, C., Paques, F., Silva, G. H., and Smith, J. (2011) The I-CreI meganuclease and its engineered derivatives: applications from cell modification to gene therapy. *Protein engineering, design & selection : PEDS* **24**, 27-31
170. Smith, J., Grizot, S., Arnould, S., Duclert, A., Epinat, J. C., Chames, P., Prieto, J., Redondo, P., Blanco, F. J., Bravo, J., Montoya, G., Paques, F., and Duchateau, P. (2006) A combinatorial approach to create artificial homing endonucleases cleaving chosen sequences. *Nucleic acids research* **34**, e149
171. Scholze, H., and Boch, J. (2011) TAL effectors are remote controls for gene activation. *Current opinion in microbiology* **14**, 47-53
172. Boch, J., Scholze, H., Schornack, S., Landgraf, A., Hahn, S., Kay, S., Lahaye, T., Nickstadt, A., and Bonas, U. (2009) Breaking the code of DNA binding specificity of TAL-type III effectors. *Science* **326**, 1509-1512

173. Moscou, M. J., and Bogdanove, A. J. (2009) A simple cipher governs DNA recognition by TAL effectors. *Science* **326**, 1501
174. Christian, M., Cermak, T., Doyle, E. L., Schmidt, C., Zhang, F., Hummel, A., Bogdanove, A. J., and Voytas, D. F. (2010) Targeting DNA double-strand breaks with TAL effector nucleases. *Genetics* **186**, 757-761
175. Cermak, T., Doyle, E. L., Christian, M., Wang, L., Zhang, Y., Schmidt, C., Baller, J. A., Somia, N. V., Bogdanove, A. J., and Voytas, D. F. (2011) Efficient design and assembly of custom TALEN and other TAL effector-based constructs for DNA targeting. *Nucleic acids research* **39**, e82
176. Li, T., Huang, S., Zhao, X., Wright, D. A., Carpenter, S., Spalding, M. H., Weeks, D. P., and Yang, B. (2011) Modularly assembled designer TAL effector nucleases for targeted gene knockout and gene replacement in eukaryotes. *Nucleic acids research* **39**, 6315-6325
177. Carlson, D. F., Fahrenkrug, S. C., and Hackett, P. B. (2012) Targeting DNA With Fingers and TALENs. *Molecular therapy. Nucleic acids* **1**, e3
178. Mahfouz, M. M., Li, L., Shamimuzzaman, M., Wibowo, A., Fang, X., and Zhu, J. K. (2011) De novo-engineered transcription activator-like effector (TALE) hybrid nuclease with novel DNA binding specificity creates double-strand breaks. *Proc Natl Acad Sci U S A* **108**, 2623-2628
179. Horvath, P., and Barrangou, R. (2010) CRISPR/Cas, the immune system of bacteria and archaea. *Science* **327**, 167-170
180. Wiedenheft, B., Sternberg, S. H., and Doudna, J. A. (2012) RNA-guided genetic silencing systems in bacteria and archaea. *Nature* **482**, 331-338
181. Sander, J. D., and Joung, J. K. (2014) CRISPR-Cas systems for editing, regulating and targeting genomes. *Nature biotechnology* **32**, 347-355
182. Carroll, D. (2014) Genome engineering with targetable nucleases. *Annual review of biochemistry* **83**, 409-439
183. Hsu, P. D., Lander, E. S., and Zhang, F. (2014) Development and applications of CRISPR-Cas9 for genome engineering. *Cell* **157**, 1262-1278
184. Pauwels, K., Podevin, N., Breyer, D., Carroll, D., and Herman, P. (2014) Engineering nucleases for gene targeting: safety and regulatory considerations. *New biotechnology* **31**, 18-27
185. Faktorovich, E. G., Steinberg, R. H., Yasumura, D., Matthes, M. T., and LaVail, M. M. (1990) Photoreceptor degeneration in inherited retinal dystrophy delayed by basic fibroblast growth factor. *Nature* **347**, 83-86
186. Uteza, Y., Rouillot, J. S., Kobetz, A., Marchant, D., Pecqueur, S., Arnaud, E., Prats, H., Honiger, J., Dufier, J. L., Abitbol, M., and Neuner-Jehle, M. (1999) Intravitreal transplantation of encapsulated fibroblasts secreting the human fibroblast growth factor 2 delays photoreceptor cell degeneration in Royal College of Surgeons rats. *Proc Natl Acad Sci U S A* **96**, 3126-3131
187. Okoye, G., Zimmer, J., Sung, J., Gehlbach, P., Deering, T., Nambu, H., Hackett, S., Melia, M., Esumi, N., Zack, D. J., and Campochiaro, P. A. (2003) Increased expression of brain-derived neurotrophic factor preserves retinal function and slows cell death from rhodopsin mutation or oxidative damage. *J Neurosci* **23**, 4164-4172
188. Frasson, M., Picaud, S., Leveillard, T., Simonutti, M., Mohand-Said, S., Dreyfus, H., Hicks, D., and Sabel, J. (1999) Glial cell line-derived neurotrophic factor induces histologic and functional protection of rod photoreceptors in the rd/rd mouse. *Invest Ophthalmol Vis Sci* **40**, 2724-2734
189. McGee Sanftner, L. H., Abel, H., Hauswirth, W. W., and Flannery, J. G. (2001) Glial cell line derived neurotrophic factor delays photoreceptor degeneration in a transgenic rat model of retinitis pigmentosa. *Mol Ther* **4**, 622-629
190. Dalkara, D., Kolstad, K. D., Guerin, K. I., Hoffmann, N. V., Visel, M., Klimczak, R. R., Schaffer, D. V., and Flannery, J. G. (2011) AAV mediated GDNF secretion from retinal glia slows down retinal degeneration in a rat model of retinitis pigmentosa. *Mol Ther* **19**, 1602-1608

191. LaVail, M. M., Yasumura, D., Matthes, M. T., Lau-Villacorta, C., Unoki, K., Sung, C. H., and Steinberg, R. H. (1998) Protection of mouse photoreceptors by survival factors in retinal degenerations. *Invest Ophthalmol Vis Sci* **39**, 592-602
192. Liang, F. Q., Aleman, T. S., Dejneka, N. S., Dudus, L., Fisher, K. J., Maguire, A. M., Jacobson, S. G., and Bennett, J. (2001) Long-term protection of retinal structure but not function using RAAV.CNTF in animal models of retinitis pigmentosa. *Mol Ther* **4**, 461-472
193. Liang, F. Q., Dejneka, N. S., Cohen, D. R., Krasnoperova, N. V., Lem, J., Maguire, A. M., Dudus, L., Fisher, K. J., and Bennett, J. (2001) AAV-mediated delivery of ciliary neurotrophic factor prolongs photoreceptor survival in the rhodopsin knockout mouse. *Mol Ther* **3**, 241-248
194. Tao, W., Wen, R., Goddard, M. B., Sherman, S. D., O'Rourke, P. J., Stabila, P. F., Bell, W. J., Dean, B. J., Kauper, K. A., Budz, V. A., Tsiaras, W. G., Acland, G. M., Pearce-Kelling, S., Laties, A. M., and Aguirre, G. D. (2002) Encapsulated cell-based delivery of CNTF reduces photoreceptor degeneration in animal models of retinitis pigmentosa. *Invest Ophthalmol Vis Sci* **43**, 3292-3298
195. Thanos, C. G., Bell, W. J., O'Rourke, P., Kauper, K., Sherman, S., Stabila, P., and Tao, W. (2004) Sustained secretion of ciliary neurotrophic factor to the vitreous, using the encapsulated cell therapy-based NT-501 intraocular device. *Tissue engineering* **10**, 1617-1622
196. Sieving, P. A., Caruso, R. C., Tao, W., Coleman, H. R., Thompson, D. J., Fullmer, K. R., and Bush, R. A. (2006) Ciliary neurotrophic factor (CNTF) for human retinal degeneration: phase I trial of CNTF delivered by encapsulated cell intraocular implants. *Proc Natl Acad Sci U S A* **103**, 3896-3901
197. Emerich, D. F., and Thanos, C. G. (2008) NT-501: an ophthalmic implant of polymer-encapsulated ciliary neurotrophic factor-producing cells. *Current opinion in molecular therapeutics* **10**, 506-515
198. Birch, D. G., Weleber, R. G., Duncan, J. L., Jaffe, G. J., Tao, W., and Ciliary Neurotrophic Factor Retinitis Pigmentosa Study, G. (2013) Randomized trial of ciliary neurotrophic factor delivered by encapsulated cell intraocular implants for retinitis pigmentosa. *Am J Ophthalmol* **156**, 283-292 e281
199. Yang, Y., Mohand-Said, S., Danan, A., Simonutti, M., Fontaine, V., Clerin, E., Picaud, S., Leveillard, T., and Sahel, J. A. (2009) Functional cone rescue by RdCVF protein in a dominant model of retinitis pigmentosa. *Mol Ther* **17**, 787-795
200. Byrne, L. C., Lin, Y. J., Lee, T., Schaffer, D. V., and Flannery, J. G. (2015) The expression pattern of systemically injected AAV9 in the developing mouse retina is determined by age. *Mol Ther* **23**, 290-296
201. Ait-Ali, N., Fridlich, R., Millet-Puel, G., Clerin, E., Delalande, F., Jaillard, C., Blond, F., Perrocheau, L., Reichman, S., Byrne, L. C., Olivier-Bandini, A., Bellalou, J., Moyse, E., Bouillaud, F., Nicol, X., Dalkara, D., van Dorsselaer, A., Sahel, J. A., and Leveillard, T. (2015) Rod-derived cone viability factor promotes cone survival by stimulating aerobic glycolysis. *Cell* **161**, 817-832
202. Fernandez-Sanchez, L., Lax, P., Esquivia, G., Martin-Nieto, J., Pinilla, I., and Cuenca, N. (2012) Safranin, a saffron constituent, attenuates retinal degeneration in P23H rats. *PLoS One* **7**, e43074
203. Parfitt, D. A., Aguila, M., McCulley, C. H., Bevilacqua, D., Mendes, H. F., Athanasiou, D., Novoselov, S. S., Kanuga, N., Munro, P. M., Coffey, P. J., Kalmar, B., Greensmith, L., and Cheetham, M. E. (2014) The heat-shock response co-inducer arimoclomol protects against retinal degeneration in rhodopsin retinitis pigmentosa. *Cell death & disease* **5**, e1236
204. Aguila, M., Bevilacqua, D., McCulley, C., Schwarz, N., Athanasiou, D., Kanuga, N., Novoselov, S. S., Lange, C. A., Ali, R. R., Bainbridge, J. W., Gias, C., Coffey, P. J., Garriga, P., and Cheetham, M. E. (2014) Hsp90 inhibition protects against inherited retinal degeneration. *Hum Mol Genet*
205. Vasireddy, V., Chavali, V. R., Joseph, V. T., Kadam, R., Lin, J. H., Jamison, J. A., Kompella, U. B., Reddy, G. B., and Ayyagari, R. (2011) Rescue of photoreceptor degeneration by curcumin in transgenic rats with P23H rhodopsin mutation. *PLoS One* **6**, e21193

206. Fernandez-Sanchez, L., Lax, P., Isiegas, C., Ayuso, E., Ruiz, J. M., de la Villa, P., Bosch, F., de la Rosa, E. J., and Cuenca, N. (2012) Proinsulin slows retinal degeneration and vision loss in the P23H rat model of retinitis pigmentosa. *Hum Gene Ther* **23**, 1290-1300
207. Lax, P., Esquivia, G., Altavilla, C., and Cuenca, N. (2014) Neuroprotective effects of the cannabinoid agonist HU210 on retinal degeneration. *Exp Eye Res* **120**, 175-185
208. Gorbatyuk, M. S., Knox, T., LaVail, M. M., Gorbatyuk, O. S., Noorwez, S. M., Hauswirth, W. W., Lin, J. H., Muzyczka, N., and Lewin, A. S. (2010) Restoration of visual function in P23H rhodopsin transgenic rats by gene delivery of BiP/Grp78. *Proc Natl Acad Sci U S A* **107**, 5961-5966
209. Clemson, C. M., Tzekov, R., Krebs, M., Checchi, J. M., Bigelow, C., and Kaushal, S. (2011) Therapeutic potential of valproic acid for retinitis pigmentosa. *The British journal of ophthalmology* **95**, 89-93
210. Sandberg, M. A., Rosner, B., Weigel-DiFranco, C., and Berson, E. L. (2011) Lack of scientific rationale for use of valproic acid for retinitis pigmentosa. *The British journal of ophthalmology* **95**, 744
211. Nagel, G., Szellas, T., Huhn, W., Kateriya, S., Adeishvili, N., Berthold, P., Ollig, D., Hegemann, P., and Bamberg, E. (2003) Channelrhodopsin-2, a directly light-gated cation-selective membrane channel. *Proc Natl Acad Sci U S A* **100**, 13940-13945
212. Bi, A., Cui, J., Ma, Y. P., Olshevskaya, E., Pu, M., Dizhoor, A. M., and Pan, Z. H. (2006) Ectopic expression of a microbial-type rhodopsin restores visual responses in mice with photoreceptor degeneration. *Neuron* **50**, 23-33
213. Lagali, P. S., Balya, D., Awatramani, G. B., Munch, T. A., Kim, D. S., Busskamp, V., Cepko, C. L., and Roska, B. (2008) Light-activated channels targeted to ON bipolar cells restore visual function in retinal degeneration. *Nature neuroscience* **11**, 667-675
214. Doroudchi, M. M., Greenberg, K. P., Liu, J., Silka, K. A., Boyden, E. S., Lockridge, J. A., Arman, A. C., Janani, R., Boye, S. E., Boye, S. L., Gordon, G. M., Matteo, B. C., Sampath, A. P., Hauswirth, W. W., and Horsager, A. (2011) Virally delivered channelrhodopsin-2 safely and effectively restores visual function in multiple mouse models of blindness. *Mol Ther* **19**, 1220-1229
215. Mace, E., Caplette, R., Marre, O., Sengupta, A., Chaffiol, A., Barbe, P., Desrosiers, M., Bamberg, E., Sahel, J. A., Picaud, S., Duebel, J., and Dalkara, D. (2014) Targeting Channelrhodopsin-2 to ON-bipolar Cells With Vitreally Administered AAV Restores ON and OFF Visual Responses in Blind Mice. *Mol Ther*
216. Kleinlogel, S., Feldbauer, K., Dempski, R. E., Fotis, H., Wood, P. G., Bamann, C., and Bamberg, E. (2011) Ultra light-sensitive and fast neuronal activation with the Ca(2)+-permeable channelrhodopsin CatCh. *Nature neuroscience* **14**, 513-518
217. Lin, J. Y., Knutsen, P. M., Muller, A., Kleinfeld, D., and Tsien, R. Y. (2013) ReaChR: a red-shifted variant of channelrhodopsin enables deep transcranial optogenetic excitation. *Nature neuroscience* **16**, 1499-1508
218. Busskamp, V., Duebel, J., Balya, D., Fradot, M., Viney, T. J., Siegert, S., Groner, A. C., Cabuy, E., Forster, V., Seeliger, M., Biel, M., Humphries, P., Paques, M., Mohand-Said, S., Trono, D., Deisseroth, K., Sahel, J. A., Picaud, S., and Roska, B. (2010) Genetic reactivation of cone photoreceptors restores visual responses in retinitis pigmentosa. *Science* **329**, 413-417
219. Lane, F. J., Huyck, M. H., and Troyk, P. (2011) Looking ahead: planning for the first human intracortical visual prosthesis by using pilot data from focus groups of potential users. *Disability and rehabilitation. Assistive technology* **6**, 139-147
220. Ahuja, A. K., Dorn, J. D., Caspi, A., McMahon, M. J., Dagnelie, G., Dacruz, L., Stanga, P., Humayun, M. S., Greenberg, R. J., and Argus, I. I. S. G. (2011) Blind subjects implanted with the Argus II retinal prosthesis are able to improve performance in a spatial-motor task. *The British journal of ophthalmology* **95**, 539-543
221. Zrenner, E., Bartz-Schmidt, K. U., Benav, H., Besch, D., Bruckmann, A., Gabel, V. P., Gekeler, F., Greppmaier, U., Harscher, A., Kibbel, S., Koch, J., Kusnyerik, A., Peters, T., Stingl, K., Sachs, H., Stett, A., Szurman, P., Wilhelm, B., and Wilke, R. (2011) Subretinal electronic chips allow blind patients to read letters and combine them to words. *Proceedings. Biological sciences / The Royal Society* **278**, 1489-1497

222. Luo, Y. H., Davagnanam, I., and dacCuz, L. (2013) MRI brain scans in two patients with the argus II retinal prosthesis. *Ophthalmology* **120**, 1711-1711 e1718
223. Humayun, M. S., Weiland, J. D., Fujii, G. Y., Greenberg, R., Williamson, R., Little, J., Mech, B., Cimmarusti, V., Van Boemel, G., Dagnelie, G., and de Juan, E. (2003) Visual perception in a blind subject with a chronic microelectronic retinal prosthesis. *Vision Res* **43**, 2573-2581
224. Humayun, M. S., Dorn, J. D., da Cruz, L., Dagnelie, G., Sahel, J. A., Stanga, P. E., Cideciyan, A. V., Duncan, J. L., Elliott, D., Filley, E., Ho, A. C., Santos, A., Safran, A. B., Ardit, A., Del Priore, L. V., Greenberg, R. J., and Argus, I. I. S. G. (2012) Interim results from the international trial of Second Sight's visual prosthesis. *Ophthalmology* **119**, 779-788
225. da Cruz, L., Coley, B. F., Dorn, J., Merlini, F., Filley, E., Christopher, P., Chen, F. K., Wuyyuru, V., Sahel, J., Stanga, P., Humayun, M., Greenberg, R. J., Dagnelie, G., and Argus, I. I. S. G. (2013) The Argus II epiretinal prosthesis system allows letter and word reading and long-term function in patients with profound vision loss. *The British journal of ophthalmology* **97**, 632-636
226. Stingl, K., Bartz-Schmidt, K. U., Besch, D., Braun, A., Bruckmann, A., Gekeler, F., Greppmaier, U., Hipp, S., Hortdorfer, G., Kernstock, C., Koitschev, A., Kusnyerik, A., Sachs, H., Schatz, A., Stingl, K. T., Peters, T., Wilhelm, B., and Zrenner, E. (2013) Artificial vision with wirelessly powered subretinal electronic implant alpha-IMS. *Proceedings. Biological sciences / The Royal Society* **280**, 20130077
227. MacLaren, R. E., Pearson, R. A., MacNeil, A., Douglas, R. H., Salt, T. E., Akimoto, M., Swaroop, A., Sowden, J. C., and Ali, R. R. (2006) Retinal repair by transplantation of photoreceptor precursors. *Nature* **444**, 203-207
228. Gonzalez-Cordero, A., West, E. L., Pearson, R. A., Duran, Y., Carvalho, L. S., Chu, C. J., Naeem, A., Blackford, S. J., Georgiadis, A., Lakowski, J., Hubank, M., Smith, A. J., Bainbridge, J. W., Sowden, J. C., and Ali, R. R. (2013) Photoreceptor precursors derived from three-dimensional embryonic stem cell cultures integrate and mature within adult degenerate retina. *Nature biotechnology* **31**, 741-747
229. Hiram, Y., Osakada, F., Takahashi, K., Okita, K., Yamanaka, S., Ikeda, H., Yoshimura, N., and Takahashi, M. (2009) Generation of retinal cells from mouse and human induced pluripotent stem cells. *Neurosci Lett* **458**, 126-131
230. Osakada, F., Ikeda, H., Mandai, M., Wataya, T., Watanabe, K., Yoshimura, N., Akaike, A., Sasai, Y., and Takahashi, M. (2008) Toward the generation of rod and cone photoreceptors from mouse, monkey and human embryonic stem cells. *Nature biotechnology* **26**, 215-224
231. West, E. L., Pearson, R. A., MacLaren, R. E., Sowden, J. C., and Ali, R. R. (2009) Cell transplantation strategies for retinal repair. *Progress in brain research* **175**, 3-21
232. Orhan, E., Dalkara, D., Neulle, M., Lechavue, C., Michiels, C., Picaud, S., Leveillard, T., Sahel, J. A., Naash, M. I., Lavail, M. M., Zeitz, C., and Audo, I. (2015) Genotypic and phenotypic characterization of P23H line 1 rat model. *PLoS One* **10**, e0127319
233. Cao, Y., Posokhova, E., and Martemyanov, K. A. (2011) TRPM1 forms complexes with nyctalopin in vivo and accumulates in postsynaptic compartment of ON-bipolar neurons in mGluR6-dependent manner. *J Neurosci* **31**, 11521-11526
234. Grosse, S., Huot, N., Mahiet, C., Arnould, S., Barradeau, S., Clerre, D. L., Chion-Sotinel, I., Jacquemarcq, C., Chapellier, B., Ergani, A., Desseaux, C., Cedrone, F., Conseiller, E., Paques, F., Labetoulle, M., and Smith, J. (2011) Meganuclease-mediated Inhibition of HSV1 Infection in Cultured Cells. *Mol Ther* **19**, 694-702
235. Arnould, S., Chames, P., Perez, C., Lacroix, E., Duclert, A., Epinat, J. C., Stricher, F., Petit, A. S., Patin, A., Guillier, S., Rolland, S., Prieto, J., Blanco, F. J., Bravo, J., Montoya, G., Serrano, L., Duchateau, P., and Paques, F. (2006) Engineering of large numbers of highly specific homing endonucleases that induce recombination on novel DNA targets. *Journal of molecular biology* **355**, 443-458
236. Grizot, S., Smith, J., Daboussi, F., Prieto, J., Redondo, P., Merino, N., Villate, M., Thomas, S., Lemaire, L., Montoya, G., Blanco, F. J., Paques, F., and Duchateau, P. (2009) Efficient targeting of a SCID gene by an engineered single-chain homing endonuclease. *Nucleic acids research* **37**, 5405-5419

237. Dupuy, A., Valton, J., Leduc, S., Armier, J., Galetto, R., Gouble, A., Lebuhotel, C., Stary, A., Paques, F., Duchateau, P., Sarasin, A., and Daboussi, F. (2013) Targeted gene therapy of xeroderma pigmentosum cells using meganuclease and TALEN. *PLoS One* **8**, e78678
238. Roger, J., Brajeul, V., Thomasseau, S., Hienola, A., Sahel, J. A., Guillonnet, X., and Goureau, O. (2006) Involvement of Pleiotrophin in CNTF-mediated differentiation of the late retinal progenitor cells. *Developmental biology* **298**, 527-539
239. Matsuda, T., and Cepko, C. L. (2007) Controlled expression of transgenes introduced by in vivo electroporation. *Proc Natl Acad Sci U S A* **104**, 1027-1032
240. Delacote, F., Perez, C., Guyot, V., Duhamel, M., Rochon, C., Ollivier, N., Macmaster, R., Silva, G. H., Paques, F., Daboussi, F., and Duchateau, P. (2013) High frequency targeted mutagenesis using engineered endonucleases and DNA-end processing enzymes. *PLoS One* **8**, e53217
241. LaVail, M. M. Retinal Degeneration Rat Model Resource. Availability of P23H and S334ter Mutant Rhodopsin Transgenic Rats and RCS Inbred and Congenic Strains.
242. Pang, J. J., Dai, X., Boye, S. E., Barone, I., Boye, S. L., Mao, S., Everhart, D., Dinculescu, A., Liu, L., Umino, Y., Lei, B., Chang, B., Barlow, R., Strettoi, E., and Hauswirth, W. W. (2011) Long-term retinal function and structure rescue using capsid mutant AAV8 vector in the rd10 mouse, a model of recessive retinitis pigmentosa. *Mol Ther* **19**, 234-242
243. Dalkara, D., Byrne, L. C., Lee, T., Hoffmann, N. V., Schaffer, D. V., and Flannery, J. G. (2012) Enhanced gene delivery to the neonatal retina through systemic administration of tyrosine-mutated AAV9. *Gene Ther* **19**, 176-181
244. Takahashi, K., and Yamanaka, S. (2006) Induction of pluripotent stem cells from mouse embryonic and adult fibroblast cultures by defined factors. *Cell* **126**, 663-676
245. Peachey, N. S., Ray, T. A., Florijn, R., Rowe, L. B., Sjoerdsma, T., Contreras-Alcantara, S., Baba, K., Tosini, G., Pozdeyev, N., Iuvone, P. M., Bojang, P., Jr., Pearing, J. N., Simonsz, H. J., van Genderen, M., Birch, D. G., Traboulsi, E. I., Dorfman, A., Lopez, I., Ren, H., Goldberg, A. F., Nishina, P. M., Lachapelle, P., McCall, M. A., Koenekoop, R. K., Bergen, A. A., Kamermans, M., and Gregg, R. G. (2012) GPR179 is required for depolarizing bipolar cell function and is mutated in autosomal-recessive complete congenital stationary night blindness. *Am J Hum Genet* **90**, 331-339
246. Orlandi, C., Posokhova, E., Masuho, I., Ray, T. A., Hasan, N., Gregg, R. G., and Martemyanov, K. A. (2012) GPR158/179 regulate G protein signaling by controlling localization and activity of the RGS7 complexes. *The Journal of cell biology* **197**, 711-719
247. Audo, I., Bujakowska, K., Orhan, E., Poloschek, C. M., Defoort-Dhellemmes, S., Drumare, I., Kohl, S., Luu, T. D., Lecompte, O., Zrenner, E., Lancelot, M. E., Antonio, A., Germain, A., Michiels, C., Audier, C., Letexier, M., Saraiva, J. P., Leroy, B. P., Munier, F. L., Mohand-Said, S., Lorenz, B., Friedburg, C., Preising, M., Kellner, U., Renner, A. B., Moskova-Doumanova, V., Berger, W., Wissinger, B., Hamel, C. P., Schorderet, D. F., De Baere, E., Sharon, D., Banin, E., Jacobson, S. G., Bonneau, D., Zanlonghi, X., Le Meur, G., Casteels, I., Koenekoop, R., Long, V. W., Meire, F., Prescott, K., de Ravel, T., Simmons, I., Nguyen, H., Dollfus, H., Poch, O., Leveillard, T., Nguyen-Ba-Charvet, K., Sahel, J. A., Bhattacharya, S. S., and Zeitze, C. (2012) Whole-exome sequencing identifies mutations in GPR179 leading to autosomal-recessive complete congenital stationary night blindness. *Am J Hum Genet* **90**, 321-330
248. Shim, H., Wang, C. T., Chen, Y. L., Chau, V. Q., Fu, K. G., Yang, J., McQuiston, A. R., Fisher, R. A., and Chen, C. K. (2012) Defective retinal depolarizing bipolar cells in regulators of G protein signaling (RGS) 7 and 11 double null mice. *J Biol Chem* **287**, 14873-14879
249. Chang, B., Hurd, R., Wang, J., and Nishina, P. (2013) Survey of common eye diseases in laboratory mouse strains. *Invest Ophthalmol Vis Sci* **54**, 4974-4981
250. Neuille, M., Morgans, C. W., Orhan, E., Michiels, C., Sahel, J. A., Audo, I., Duvoisin, R., and Zeitze, C. (2014) LRIT3 is essential to localize TRPM1 to the dendritic tips of depolarizing bipolar cells and may play a role in cone synapse formation. *European Journal of Neuroscience*
251. Mattapallil, M. J., Wawrousek, E. F., Chan, C. C., Zhao, H., Roychoudhury, J., Ferguson, T. A., and Caspi, R. R. (2012) The Rd8 mutation of the *Crb1* gene is present in vendor lines of

- C57BL/6N mice and embryonic stem cells, and confounds ocular induced mutant phenotypes. *Invest Ophthalmol Vis Sci* **53**, 2921-2927
252. Chen, S., Oikonomou, G., Chiu, C. N., Niles, B. J., Liu, J., Lee, D. A., Antoshechkin, I., and Prober, D. A. (2013) A large-scale in vivo analysis reveals that TALENs are significantly more mutagenic than ZFNs generated using context-dependent assembly. *Nucleic acids research*
 253. Davidson, M. K., Lindsey, J. R., and Davis, J. K. (1987) Requirements and selection of an animal model. *Israel journal of medical sciences* **23**, 551-555
 254. Jeon, C. J., Strettoi, E., and Masland, R. H. (1998) The major cell populations of the mouse retina. *J Neurosci* **18**, 8936-8946
 255. Swaroop, A., Kim, D., and Forrest, D. (2010) Transcriptional regulation of photoreceptor development and homeostasis in the mammalian retina. *Nature reviews. Neuroscience* **11**, 563-576
 256. Orlandi, C., Cao, Y., and Martemyanov, K. A. (2013) Orphan receptor GPR179 forms macromolecular complexes with components of metabotropic signaling cascade in retina ON-bipolar neurons. *Invest Ophthalmol Vis Sci* **54**, 7153-7161
 257. Klooster, J., van Genderen, M. M., Yu, M., Florijn, R. J., Riemsdag, F. C., Bergen, A. A., Gregg, R. G., Peachey, N. S., and Kamermans, M. (2013) Ultrastructural localization of GPR179 and the impact of mutant forms on retinal function in CSNB1 patients and a mouse model. *Invest Ophthalmol Vis Sci* **54**, 6973-6981
 258. Ray, T. A., Heath, K. M., Hasan, N., Noel, J. M., Samuels, I. S., Martemyanov, K. A., Peachey, N. S., McCall, M. A., and Gregg, R. G. (2014) GPR179 is required for high sensitivity of the mGluR6 signaling cascade in depolarizing bipolar cells. *J Neurosci* **34**, 6334-6343
 259. Vouillot, L., Thelie, A., and Pollet, N. (2015) Comparison of T7E1 and surveyor mismatch cleavage assays to detect mutations triggered by engineered nucleases. *G3* **5**, 407-415
 260. Daboussi, F., Zaslavskiy, M., Poirot, L., Loperfido, M., Gouble, A., Guyot, V., Leduc, S., Galetto, R., Grizot, S., Oficjalska, D., Perez, C., Delacote, F., Dupuy, A., Chion-Sotinel, I., Le Clerre, D., Lebuhotel, C., Danos, O., Lemaire, F., Oussedik, K., Cedrone, F., Epinat, J. C., Smith, J., Yanez-Munoz, R. J., Dickson, G., Popplewell, L., Koo, T., VandenDriessche, T., Chuah, M. K., Duclert, A., Duchateau, P., and Paques, F. (2012) Chromosomal context and epigenetic mechanisms control the efficacy of genome editing by rare-cutting designer endonucleases. *Nucleic acids research* **40**, 6367-6379
 261. Valton, J., Daboussi, F., Leduc, S., Molina, R., Redondo, P., Macmaster, R., Montoya, G., and Duchateau, P. (2012) 5'-Cytosine-phosphoguanine (CpG) methylation impacts the activity of natural and engineered meganucleases. *J Biol Chem* **287**, 30139-30150
 262. Treisman, J. E., Morabito, M. A., and Barnstable, C. J. (1988) Opsin expression in the rat retina is developmentally regulated by transcriptional activation. *Molecular and cellular biology* **8**, 1570-1579
 263. Byrne, L. C., Ozturk, B. E., Lee, T., Fortuny, C., Visel, M., Dalkara, D., Schaffer, D. V., and Flannery, J. G. (2014) Retinoschisin gene therapy in photoreceptors, Muller glia or all retinal cells in the *Rs1h*^{-/-} mouse. *Gene Ther* **21**, 585-592
 264. Gupta, R. M., and Musunuru, K. (2014) Expanding the genetic editing tool kit: ZFNs, TALENs, and CRISPR-Cas9. *The Journal of clinical investigation* **124**, 4154-4161
 265. Tsai, S. Q., Wyvekens, N., Khayter, C., Foden, J. A., Thapar, V., Reyon, D., Goodwin, M. J., Aryee, M. J., and Joung, J. K. (2014) Dimeric CRISPR RNA-guided FokI nucleases for highly specific genome editing. *Nature biotechnology* **32**, 569-576
 266. Guilinger, J. P., Thompson, D. B., and Liu, D. R. (2014) Fusion of catalytically inactive Cas9 to FokI nuclease improves the specificity of genome modification. *Nature biotechnology* **32**, 577-582
 267. Ran, F. A., Hsu, P. D., Lin, C. Y., Gootenberg, J. S., Konermann, S., Trevino, A. E., Scott, D. A., Inoue, A., Matoba, S., Zhang, Y., and Zhang, F. (2013) Double nicking by RNA-guided CRISPR Cas9 for enhanced genome editing specificity. *Cell* **154**, 1380-1389

De l'identification de gènes candidats et leur caractérisation fonctionnelle à l'apport d'une preuve de concept dans le cas d'une thérapie génique par édition génomique dans les maladies génétiques rétiniennes stationnaires ou progressives.

La rétine est un tissu spécialisé dans le traitement de l'information visuelle par l'intermédiaire des photorécepteurs, cônes et bâtonnets, et des neurones de deuxième ordre, les cellules bipolaires et les cellules ganglionnaires dont les axones forment le nerf optique. Notre groupe s'intéresse à élucider les mécanismes génétiques impliqués dans les maladies rares stationnaires, comme dans la cécité nocturne congénitale stationnaire (CNCS), ou progressives comme dans la dystrophie de type bâtonnet-cône (DBC). Cette thèse apporte de nombreuses connaissances sur la physiologie rétinienne. D'une part, nous avons identifié GPR179, un nouveau gène impliqué dans la CNCS complète, étudié la localisation de la protéine et la physiopathologie des protéines mutantes. Nous avons également créé et caractérisé fonctionnellement un nouveau modèle souris invalidé pour *GPR179* qui nous a permis de mieux approcher la première synapse rétinienne entre les photorécepteurs et les cellules bipolaires adjacentes. D'autre part, nous avons caractérisé le génotype et le phénotype de l'un des modèles les plus utilisés de la DBC, le rat P23H. Nous avons ensuite développé une approche d'édition génomique pour invalider les mutants *RHO* ayant un effet dominant négatif en testant *in vitro*, *ex vivo* et *in vivo* les meganucleases, TALEN (Transcription Activator-Like Effector Nuclease) puis le système CRISPR/Cas9 (clustered regularly interspaced short palindromic repeats/CRISPR associated protein 9).

Mots-clefs : rétine, GPR179, rhodopsine, édition génomique, endonucléases, thérapie génique

From gene identification and functional characterization to genome editing approaches for inherited retinal disorders.

The first steps in vision occur in the retina when rod and cone photoreceptors transform light into a biochemical signal, which gets processed by bipolar cells, ganglion cells and finally by the brain. Our group investigates genetic causes and mechanisms involved in inherited stationary and progressive retinal diseases as congenital stationary night blindness (CSNB), and rod-cone dystrophy (RCD), also called retinitis pigmentosa. This thesis gives several insights on the retinal physiology. On one hand, we identified *GPR179*, a new gene mutated in complete CSNB, studied the localization and the physiopathology of missense and splice-site mutations. We also delivered a new knock-out mouse model which we functionally characterized, and studied *GPR179* partners to provide a better understanding of the first visual synapse between photoreceptors and ON-bipolar cells. On the other hand, we genotypically and phenotypically characterized one of the most popular RCD model, the P23H rat model. There is currently no treatment for RCD and different therapeutic strategies are under investigation. We wanted to deliver the basis for a genome editing approach for *RHO* mutations, acting as a dominant negative effect, which cannot be addressed by current gene replacement strategies. We opened the field by performing *in vitro*, *ex vivo* and *in vivo* genome editing experiments using meganucleases, TALEN (Transcription Activator-Like Effector Nuclease) and finally CRISPR/Cas9 system (clustered regularly interspaced short palindromic repeats/CRISPR associated protein 9) and revealed how challenging the setting of genome editing strategies was.

Keywords: retina, GPR179, rhodopsin, genome editing, endonucleases, gene therapy